STATUS OF KINASES IN VIRAL AND BACTERIAL CO-INFECTIONS

Ph.D. Thesis

By

CHARU SONKAR

Roll no. 1601271003

DEPARTMENT OF BIOSCIENCES AND BIOMEDICAL ENGINEERING

INDIAN INSTITUTE OF TECHNOLOGY INDORE

April 2021

STATUS OF KINASES IN VIRAL AND BACTERIAL CO-INFECTIONS

Ph.D. Thesis

By

CHARU SONKAR

Roll no. 1601271003

DEPARTMENT OF BIOSCIENCES AND BIOMEDICAL ENGINEERING

INDIAN INSTITUTE OF TECHNOLOGY INDORE

April 2021

INDIAN INSTITUTE OF TECHNOLOGY INDORE

CANDIDATE'S DECLARATION

I hereby certify that the work which is being presented in the thesis entitled **STATUSOF KINASES IN VIRAL AND BACTERIAL CO-INFECTIONS** in the partial fulfilment of the requirements for the award of the degree of **DOCTOR OFPHILOSOPHY** and submitted in the **DEPARTMENT OF BIOSCIENCES AND BIOMEDICAL ENGINEERING, Indian Institute of Technology Indore**, is an authentic record of my work carried out during the period from December 2016 to April 2021 under the supervision of Dr. Hem Chandra Jha, Assistant Professor, BSBE, IIT Indore. The matter presented in this thesis has not been submitted by me for the award of anyother degree of this or any other institute.

22 April 2021

Signature of the student with date

(CHARU SONKAR)

This is to certify that the above statement made by the candidate is correct to the best ofmy/our knowledge.

22/4/2021

Signature of Thesis Supervisor with date

(Dr. HEM CHANDRA JHA)

CHARU SONKAR has successfully given his/her PhD. Oral Examination held on **9/9/2021**

Signature of Chairperson (OEB), Date: 09/09/2021

Signature of External Examiner, Date: 09/09/2021

Signature(s) of ThesisSupervisor(s) Date: 09/09/2021

Signature of PSPC Member #1, Date: 09/09/2021

Signature of PSPC Member #2 Date: 09/09/2021

ORAL EXAMINATION BOARD

Name and Affiliation of the Examiners	Signature with date
1. Prof. S.E. Hasnain, External Examiner	09/09/2021
2. Prof. S. Mukhopadhyay, PSPC member	09/09/21
3. Dr. S.K. Vishvakarma, PSPC member	09/09/2021
4. Dr. H.C. Jha, Supervisor	9/9/2021
5. Dr. Rajesh Kumar, Chairman(OEB)	9/9/2021

9/9/2021

(Signature of Chairman, PhD ORAL EXAMINATION BOARD with date)

P.V. Kodgire 13/09/2021

(Signature of Convener, DPGC with date)

* *Oral examination be scheduled only one week after thesis is sent to the members of the oral board.*

For Office Use Only

Course Units: CPI:

The candidate has met all the requireements for the award of the PhD degree and be issued provisional Degree after submission of Hard bound copies of the Thesis and the No Dues Certficate.

Date: Deputy / Assistant Registrar (Academic)

Page 2 | 2

INDIAN INSTITUTE OF TECHNOLOGY INDORE

CERTIFICATE

This is to certify that the research work embodied in this thesis entitled **"Status of Kinases in Viral and Bacterial Co-Infections"** submitted to the Indian Institute of Technology Indore (IITI) by **Ms. Charu Sonkar** is for the award of the degree of Doctor of Philosophy. This work reported herein is original and has not been submitted so far, in part or full, for any other degree or diploma of any other University.

Signature

Dr. Hem Chandra Jha

Thesis Supervisor

ACKNOWLEDGEMENTS

First and foremost, I would like to thank God, the Almighty, for His showers of blessings throughout my work to complete the research successfully.

I want to express my sincere gratitude to my supervisor **Dr. Hem Chandra Jha**, for providing me with this excellent opportunity to pursue a PhD in the field of virology and cancer biology. His valuable guidance and knowledge helped me to complete this journey successfully. He has helped me to remain streamlined during the tenure of my research work. He has provided me with several opportunities to learn various techniques and advised me to learn things even from my mistakes. I would like to pay sincere thanks for his inexhaustible patience during my academic writing correction phase. Without his coherent and illuminating instruction, this thesis would not have reached its present form.

I wish to express my sincere gratitude to **Prof. Neelesh Kumar Jain**, Acting Director, Indian Institute of Technology, Indore, to extend all the facilities and allow me to be a part of this esteemed organization. Further, I would like to thank my PSPC members, **Dr. Santosh Kumar Vishvakarma and Prof. Suman Mukhopadhyay,** for their valuable suggestions and support during different phases of my research. I humbly acknowledge the Head and DPGC Convener, Discipline of BSBE, for their constant support through my research endeavours. I extend my sincere thanks to all faculty members of BSBE for helping me gain new insight into my research through the various courses taught to me during the course work. I particularly extend my heartfelt gratitude to Dr. Pawan Kumar for his insightful suggestions and his extended help with computational studies.

I am thankful to **Mr. Arif Patel, Dr. Kumar Gaurav and Mr. Murphy B Ganveer** (Deputy manager) for their gentle help and support for the smooth functioning of lab instruments and other academic tasks. I must thank **Dr. Ravinder** for helping me conduct my confocal microscopy experiments. I extend my thanks to **Mr. Tapesh Parihar** (Manager, Academics) for extending their timely help in all aspects. I take this opportunity to extend my thanks to the library staff and technical staff of IIT Indore for their help during my research work.

Nevertheless, my labmates have helped to make this journey easier and for creating

a research conducive environment. I am happy to extend my heartfelt gratitude to **Ms. Nidhi Varshney,** Dr. Tarun Prakash Verma, **Ms. Annu Rani and Mr. Buddhadev Baral** for being friendly, motivating, kind and supportive juniors and for always extending help to me. I am thankful to **Dharmendra Kashyap, Omkar Indari and Deeksha Tiwari** for being good colleagues. Special thanks to, Ms. Monika Jain for her spirited discussions, guidance and sisterly love that kept my morale up. I extend my gratitude to **Dr. Pramod Kumar Gavel** for his constant help and guidance. I personally want to thank my friends at IIT, **Mena Krishnan, Ankit Jaiswal, Anubhav Tamrakar, Sajjan Rajpoot, Navpreet Kaur, Nirali Pandya and Saumya Jaiswal** for being excellent companions and stress buster friends. I would also extend my gratitude to **Dr. Eshan Khan and Dr. Arun Verma** for making the environment conducive and productive through their constant support.

Words are short to express my gratitude to the source of my life, my parents. My motivation throughout life is my mother, **Mrs. Renu Sonkar** and my father **Mr. Rajendra Sonkar** have showered their unconditional love and affection to me in all circumstances of life. Without them, I would never be able to reach where I am today. Words cannot express my gratitude towards my sister **Ms. Chanchal Sonkar** for providing constant support, guidance, help and being motivating, kind through all the phases of my life. I would not have started this journey of Ph.D. or being able to complete it without her. I cannot thank enough my younger sister Ms. Shreya Sonkar, for being a stress buster and constant moral support in my life.

Last but not the least, I would like to thank the almighty for granting me the health and strength to undertake this research task and enabling me to accomplish it successfully

CHARU SONKAR

This Thesis is

Dedicated to

My Beloved Family

Charu Sonkar

SYNOPSIS

Gastric cancer (GC) ranks fifth as the most common cancer and the second leading cause of death in the world. There are approximately more than 1,000,000 newly diagnosed cases and 738,000 deaths every year due to GC. It has been estimated that 17.8 % of cancers are caused by infectious agents out of which 5.5% of cancer are caused by *Helicobacter pylori* (*H. pylori*). In the case of GC, *H. pylori* contribute to more than 60% of cases and Epstein Barr Virus (EBV) is associated with around 10% of cases.

Infectious agents associated with GC are *H. pylori*, EBV and human cytomegalovirus (HCMV). *H. pylori* and EBV have been classified as type I carcinogens according to the International Agency for Research on Cancer (IARC). *H. pylori* are most frequently found in the inner lining of the stomach. However, to date, the specific mechanism through which *H. pylori* induces GC is still unknown. EBV is another etiologic agent known to contribute to GC development. EBV-associated GC (EBVaGC) is a characteristic subtype of GC which shows distinct clinicopathological features. HCMV is assumed to be an oncomodulator virus that infects tumour cells and increases their malignancy. There is evidence that supports its role in the development of gastric adenocarcinoma at an early stage. Hence there is a need for a more profound understanding of molecular mechanisms to determine effective therapeutic targets. To understand the role of *H. pylori* and EBV in GC they are sequentially elaborated.

H. pylori play a vital role in the development of various gastro-duodenal diseases. Usually, healthy microflora produces a bacteriocin-like inhibitory protein that inhibits *H. pylori* growth. The number of *H. pylori* may increase due to loss in healthy microflora. Subsequently, it leads to the production of gastric acid, followed by ulceration. Some strains of *H. pylori* are virulent, and host factors may also be responsible for disease progression. Additionally, other bacteria that are acid-tolerant might also reside at the infection site within ulcers and thus enhance the problem caused by *H. pylori*. Importantly, many virulent strains of *H. pylori* harbour numerous adhesins (BabA/B, SabA, AlpA/B, OipA and HopZ) and the cag

(cytotoxin-associated genes) pathogenicity island encoding a type IV secretion system (T4SS). A tight bacterial contact with the host cell may get established by the adhesins. Moreover, a bacterial effector protein like CagA is delivered into host cells through this secretion system. A study also mentioned that *H. pylori* colonization might also depend on the alteration of mucosal epithelial apoptosis by chronic inflammation. Surprisingly, the relation between various *H. pylori* serotypes, their growth alone, or with gastric epithelial microenvironment to the possible occurrence in GC has not been evaluated to date. Investigation of *H. pylori* strains for their growth, and subsequent host cell transformation ability may open better understanding in this domain. Hence, it is necessary to evaluate the growth pattern of various clinical isolates of *H. pylori* and their response to treatment with commercially available oral rinses/solutions. Further, *H. pylori* show a high level of intra- species genetic diversity where strain-specific features are critical for the progression of GC. If *H. pylori* infection remains untreated, it colonizes the stomach and can persevere lifelong. The driving factors which turn *H. pylori* into pathogenic bacteria are poorly known. Also, it is well known that kinases play a role as pivotal regulators in epigenetic modulation in various diseases, including cancer. Recent studies have suggested that *H. pylori* infection leads to the up-regulation of tyrosine kinase, MAPK cascade, PDK1, AKT3, SRC, FYN, YES, and mTOR, and dysregulation of non-receptor tyrosine kinase in cancer progression.

Moreover, the discovery of EBV, the first human virus associated with cancer, clearly showed the oncogenic potential of microorganisms. Most of the human cancers (15-20%) are associated with a viral infection, and EBV is recognized as one of the contributors to Gastric cancer (GC) (9% of all GC). The exact mechanism of EBV as an oncogenic agent in GC is poorly understood. The EBV is associated with several lymphoid and epithelial cancers and is considered an active oncogenic agent in GC progression [8]. In the EBV associated GC, host genes such as JAK2, MET, FGFR2, BRAF, RAF, EPHA4, PAK1, PAK2, EPHB6, ERBB4, ERBB2, and ITK are up-regulated. In contrast, FGFR4 and ROR2 genes are down-regulated in GC. Another challenging aspect is the coinfection of EBV with *H. pylori* that has

been reported to cause aggressive GC. Thereby, it is imperative to develop a coinfection model for investigating the progression of GC, which can be used to test the potential role of protein kinases, which is one of the hallmarks in all cancers. Since *H. pylori* and EBV have a strong oncogenic role in gastric carcinogenesis. Moreover, it is also known that *H. pylori* infection leads to gastritis which in later stages of life can potentially predispose individuals toward gastric adenocarcinoma. A previous study suggests that dose-dependent *H. pylori* infection produces cytotoxic factors, (ammonia) involved in gastric mucosal injury and plays an important role in cancer progression. Further, EBV associated gastric carcinoma comprises almost 10% of the total GC cases. Higher loads of EBV have been found in gastric biopsy tissues suggesting its significant role in GC progression. Higher EBV load is also a risk factor for various other cancers. The role of pathogen burden in *H. pylori* and EBV co-infected GC need to be studied.

On the other side, Corona Virus Disease 2019 (COVID-19) was caused by a novel coronavirus (2019-nCoV) that emerged in December 2019. Later, it was formally named as severe acute respiratory syndrome virus 2 (SARS-CoV-2) by the International Committee on Taxonomy of Viruses (ICTV). Now it has become a global pandemic. Further, cancer patients are considered as the most susceptible group in this (COVID-19) pandemic and the GC patients pose a significant challenge for the treatment. To date, the clinical characteristics of GC patients who are infected with COVID-19 are remotely known. Moreover, the presence of ACE2, a SARS-CoV-2 receptor is also observed in gastric mucosa and GI tract cells, which may be considered as a vulnerable site for SARS-CoV-2 infection. The lasting presence of the virus in gastric mucosa indicates the possibility of gastric glandular epithelial cells as a vulnerable site of the virus. Hence, the treatment of GC patients with COVID-19 is concerning. Therefore, there is an urgent need to find medicines that can treat both COVID-19 and GC which can result in less drug resistance and more effective treatment. Such a target molecule can be kinase. As several kinase pathways are considered as a gold target for anti-cancer therapies therefore they might play a pivotal role in SARS-CoV-2 infection and replication. Therefore, kinase mediated study is necessary for developing potent therapeutic

targets for COVID-19 patients suffering from GC.

LIST OF PUBLICATIONS

- **Sonkar C**., Verma T., Chatterji D., Jain A.K., Jha H.C. (2020), Status of kinases in Epstein-Barr virus and *Helicobacter pylori* Coinfection in gastric Cancer cells. BMC Cancer, 20, 925 (DOI: 10.1186/s12885-020- 07377-0)
- **Sonkar C**., Kashyap D., Varshney N., Baral B., Jha H.C. (2020), Impact of Gastrointestinal Symptoms in COVID-19: A Molecular Approach, SN Compr Clin Med,1–12, (DOI: 10.1007/s42399-020-00619-z).
- Kashyap D., Baral B., Vermin T.P., **Sonkar C**., Chatterji D., Jain A.K. (2020), Oral rinses in growth inhibition and treatment of *Helicobacter pylori* infection. BMC Microbiol, 20, 45 (DOI: 10.1186/s12866-020-01728-4.)
- MISP book chapter: **Sonkar C**., Jha H.C. (2019), Diagnosis of tumorigenesis and cancer, In Machine Intelligence and Signal Analysis, Springer, Singapore, 633-643 (ISBN)
- **Sonkar C**., Doharey P.K., Rathod A.S., Singh V., Kashyap D., Sahoo A., Mittal N., Sharma B., Jha H.C. (2021), Repurposing of Gastric Cancer drugs against COVID-19, Comput Biol Med, 137:104826-104826.
- **Sonkar C**., Varshney N., Koganti S., Jha H.C. (2021), Kinases and therapeutics in pathogen mediated Gastric Cancer. (Manuscript under revision)
- **Sonkar C**., Baral B., Varshney N., Rani A., Verma T.P., Jha, H.C. (2021),
- Evaluation of kinases with differential doses of *H. pylori* and EBV in gastric cancer cells, Pathog Dis. (manuscript submitted)
- Jakhmola S., Indari O., Kashyap D., Varshney N., Rani A., **Sonkar C.** (2020), Recent updates on COVID-19: A holistic review. Heliyon, 6, e05706 (DOI: 10.1016/j.heliyon. 2020.e05706.)

List of Content

	expression	

List of Figure

List of Table

Acronym

S.No.	Abbreviated Form	Acronym
1	Gastric cancer	GC
2	Helicobacter pylori	H.
3	Epstein Barr virus	EBV
4	B-Raf proto-oncogene, serine/threonine kinase	BRAF1
5	Interleukin-2-inducible T-cell kinase	ITK
6	Tyrosine kinase 2	TYK2
7	Tyrosine-protein kinase Fyn	FYN
8	p21 protein (Cdc42/Rac)-activated kinase 1	PAK1
9	p21 protein (Cdc42/Rac)-activated kinase 2	PAK2
10	pyruvate dehydrogenase kinase1	PDK1
11	Ephrin type-A receptor 4 precursor12	EPHA4
12	Ephrin type-B receptor 6 precursor14	EPHB6
13	AKT Serine/Threonine Kinase 3	AKT3
14	Proto-oncogene tyrosine-protein kinase Sarcoma	SRC
15	the cellular homolog of the Yamaguchi sarcoma virus oncogene	YES
16	The mechanistic target of rapamycin	mTOR
17	Janus kinase 2	JAK2
18	Hepatocyte growth factor receptor	MET
19	Fibroblast Growth Factor Receptor 4	FGFR2
20	Raf-1 proto-oncogene, serine/threonine kinase	Raf
21	Fibroblast Growth Factor Receptor 4	FGFR4
22	Receptor Tyrosine Kinase Like Orphan Receptor 2	ROR2
23	Erb-B2 Receptor Tyrosine Kinase 4	ERBB4
24	Erb-B2 Receptor Tyrosine Kinase 2	ERBB2
25	Adhesins associated protein A	AlpA
26	Blood group antigen-binding adhesin A	BabA

27	Bcl-2 homologous antagonist/killer	BAK
28	Apoptosis regulator Bcl-2	BCL-2
29	BH3-interacting domain death agonist	BID
30	Cytotoxin associated gene A	CagA
31	Cyclin D1	CCND1
32	Caudal type homeobox 2	CDX2
33	Colony Forming Unit	CFU
34	FAS-associated death domain	FADD
35	Human Gastric Biopsy	HB
36	Human Gastric Juice	HJ
37	Hope family outer protein	Hop
38	Matrix Metallopeptidase 7	MMP7
39	Phorbol-12-myristate-13-acetateinduced protein 1	NOXA
40	Optical Density	OD
41	Outer membrane-associated protein	Oip
42	Phosphatidylinositol 3,4,5-trisphosphate 3-phosphatase and dual-specificity protein phosphatase	PTEN
43	Bcl-2-binding component 3	PUMA
44	Sialic acid-binding adhesion	SabA
45	Human cytomegalovirus	HCMV
46	Receptor tyrosine kinases	RTK
47	Non-receptor tyrosine kinases	nRTK
48	Phosphatidylinositol 3-kinase	(PI3K)/Akt
49	Inhibitors of apoptosis	IAPs
50	fucosylated lewisb	Ieb
51	Receptor Protein Tyrosine Phosphatase	RPTP
52	Src homology region 2	SHP2
53	Coiled-Coil Domain Containing 151	CCDC151

54	Cholinergic Receptor Nicotinic Beta 2 Subunit	CHRNB2
55	Guanosine Monophosphate Reductase 2	GMPR2
56	Hepatoma-derived growth factor-related protein 2 isoforms 1	HDGFRP2
57	V-Set And Transmembrane Domain Containing 2 Like	VSTM2L
58	Cytotoxin-associated genes pathogenicity island	CagPAI
58	Phosphatidylinositol 4,5-bisphosphate 3-kinase catalytic subunit alpha isoform	PIK3CA
59	Latent membrane proteins	LMP
60	Jun/Activator protein 1	AP-1
61	Human epidermal growth factor receptor 2	HER2
62	Cytomegalovirus latency-associated transcripts	CLTs
63	Ubiquitin-specific protease USP7	HAUSP
64	Concordant methylation of multiple genes/loci	CIMP
65	Zinc finger E-box-binding homeobox 1	ZEB1
66	AT-rich interactive domain-containing protein 1A	ARID1A

Symbol

S.No.	Abbreviated form	Symbol
1	Seconds	s
2	Hour	h
3	Microlitre	µL
4	Micro-molar	µM
5	Colony Forming Unit	CFU
6	Degree centigrade	oC
7	Milli litre	ml
8	Nanometre	Nm
9	Milli gram	Mg
10	Millimolar	mM
11	Minutes	Min
12	Nanogram	Ng
13	Nanomolar	nM
14	Nanosecond	NS
15	Base pair	Bp
16	Weight	W
17	Volume	V
18	Polymerase chain reaction	PCR
19	Micro gram	µM
20	Dulbecco's Modified Eagle's medium	DMEM
21	Dimethyl sulphoxide	DMSO
23	Green fluorescent protein	GFP
24	Reverse Transcriptase PCR RT-	PCR

CHAPTER 1

INTRODUCTION

Helicobacter pylori (*H. pylori*) play a vital role in the development of various gastro-duodenal diseases (Yamaoka, 2010). Usually, healthy microflora produces a bacteriocin-like inhibitory protein that inhibits *H. pylori* growth (Ishihara et al., 2006). The number of *H. pylori* may increase due to loss in healthy microflora. Subsequently, it leads to the production of gastric acid, followed by ulceration ("Pathogenesis of *Helicobacter pylori* Infection Clinical Microbiology Reviews," n.d.). Some strains of *H. pylori* are virulent, and host factors may also be responsible for disease progression (Bravo, Hoare, Soto, Valenzuela, & Quest, 2018). Additionally, other bacteria that are acid-tolerant might also reside at the infection site within ulcers and thus enhance the problem caused by *H. pylori* (S. Mishra, 2013). Worldwide, *H. pylori* have been classified according to the population genetics tool (STRUCTURE) developed by Pritchard et al. (Porras-Hurtado et al., 2013; Pritchard, Stephens, Rosenberg, & Donnelly, 2000). Broadly, they represent geographical areas and named as: hpEurope, hpSahul, hpEastAsia, hpAsia2, hpNEAfrica, hpAfrica1 and hpAfrica2 (Moodley et al., 2012). Also, there is a large variability in the occurrence of GC worldwide (Crew & Neugut, 2006). Asian countries such as South Korea, China, and Japan have a high incidence of GC (Pourhoseingholi, Vahedi, & Baghestani, 2015). India is a low-risk country for GC; however, it may be attributed to underreporting (Sharma & Radhakrishnan, 2011). There lies a lacuna in the epidemiological studies and reporting from small towns and villages, which represents a large part of the Indian population (Sankaranarayanan, Ramadas, & Qiao, 2014). *H. pylori* seroprevalence in the adult population of developing countries varies from 55 to 92%. In contrary to this, the seroprevalence of *H. pylori* in Chinese and Japanese adults is 44 and 55%, respectively (K. Singh & Ghoshal, 2006). The primary manifestation of *H. pylori* in India is the duodenal ulcer, which is a major concern (GRAHAM, LU, & YAMAOKA, 2009). A study suggested that 56% of *H. pylori* infection contributes to the leading cause of GC (Ghoshal et al., 2008). Therefore, a comprehensive study

of *H. pylori* strains and their pathogenic properties is crucial in the Indian scenario. *H. pylori* may be transmitted through an oral-oral or oro-faecal route, and thus oral cavity may act as its possible reservoir (Gebara et al., 2006). Its presence in the oral cavity is seldom eliminated by *H. pylori* eradication therapy (Yee, 2016). Moreover, the oral site may act as a source for reinfection, which is found to be as high as 60% in Indian subjects (Anand, Kamath, & Anil, 2014; Chugh, 2008, p.). Hence, its eradication from the oral microenvironment is essential (Anand, Nandakumar, & Shenoy, 2006; Zarić et al., 2009). Several antimicrobial (e.g., bisbiguanides, metal ions, phenols, and quaternary ammonium compounds) and antiplaque agents (e.g., surfactants and essential oils) in the form of toothpaste and mouth rinses have been formulated (Marsh, 2010). Antiplaque agents destroy bacterial biofilm, which prevents adherence and growth of bacteria, while antimicrobial agents inhibit the growth or kill the target bacteria (Baehni & Takeuchi, 2003). Importantly, many virulent strains of *H. pylori* harbour numerous adhesins (BabA/B, SabA, AlpA/B, OipA, and HopZ) and the cag (cytotoxin-associated genes) pathogenicity island encoding a type IV secretion system (T4SS) (Backert, Clyne, & Tegtmeyer, 2011). A tight bacterial contact with the host cell may get established by the adhesins (Amieva & El–Omar, 2008). Moreover, bacterial effector proteins like CagA are delivered into host cells through this secretion system (Backert, Tegtmeyer, & Fischer, 2015). A study also mentioned that *H. pylori* colonization might also depend on the alteration of mucosal epithelial apoptosis by chronic inflammation (Shirin & Moss, 1998). Surprisingly, the relation between various *H. pylori* serotypes, their growth alone, or with gastric epithelial microenvironment to the possible occurrence in GC has not been evaluated to date. Investigation of *H. pylori* strains for their growth, and subsequent host cell transformation ability may open better understanding in this domain.

Globally, about 1 in 6 deaths occur due to cancer with GC being the third leading cause of cancer-related deaths. Despite primary management which consists of surgical resection followed by radiation therapy and chemotherapy, it is poorly prognosticated (Van Cutsem, Sagaert, Topal, Haustermans, & Prenen, 2016). The delay in the detection of GC leads to frequent relapse and metastasis. Hence, it is

imperative to find the serendipitous prognostic markers, which may be helpful in the early diagnosis of GC. The crucial link between GC and *H. pylori* is well established (F. Wang, Meng, Wang, & Qiao, 2014). *H. pylori* are considered a type I carcinogen in GC (Prabhu, Amrapurkar, & Amrapurkar, 1995). *H. pylori* show a high level of intra- species genetic diversity where strain-specific features are critical for the progression of GC (Cover, 2016). If *H. pylori* infection remains untreated, it colonizes the stomach and can persevere lifelong. The driving factors which turn *H. pylori* into pathogenic bacteria are poorly known (Dong & Cui, 2019). Recent studies suggested that *H. pylori* infection leads to the up-regulation of tyrosine kinase, MAPK cascade, PDK1, AKT3, SRC, FYN, YES, and mTOR, and dysregulation of non-receptor tyrosine kinase in cancer progression (Biology et al., 2014; Y. Chen, Wang, Li, Xu, & Zhang, 2006; Hatakeyama, 2009; Y. G. Xie et al., 2016).

Finally, the discovery of EBV, the first human virus associated with cancer, clearly showed the oncogenic potential of microorganisms (Esau, 2017). Most of the human cancers (15-20%) are associated with a viral infection, and EBV is recognized as one of the contributors in GC (9% of all GC) (Morales- Sanchez & Fuentes-Panana, 2016). The exact mechanism of EBV as an oncogenic agent in GC is poorly understood. The EBV is associated with several lymphoid and epithelial cancers and is considered an active oncogenic agent in GC progression (Matsusaka et al., 2011). In the EBV associated GC, host genes such as JAK2, MET, FGFR2, BRAF, RAF, EPHA4, PAK1, PAK2, EPHB6, ERBB4, ERBB2, and ITK are up-regulated (Clinical, Significance, Kinases, & Cancer, n.d.; C. Gao, Ma, Pang, & Xie, 2014; Lin et al., 2000a; J. Liu et al., 2017; Miyazaki et al., 2013; Raimondi & Falasca, 2011; Xu, Gong, Qian, Song, & Liu, 2018). In contrast, FGFR4 and ROR2 genes are down-regulated in GC (Yan, Du, Yao, & Liu, 2016; Ye, Jiang, Li, Wang, & Han, 2016). In Asian countries, the incidence of EBV positive persons developing GC is rapidly increasing (6-10% approximately). Moreover, western and central Asian countries have a considerably higher frequency of EBV positive cases (Sousa, Pinto-Correia, Medeiros, & Dinis-Ribeiro, 2008). The incidence of GC can vary up to approximately ten-fold depending on the geographic region

which implies that genetic or environmental factors can affect carcinogenesis (Zali, Rezaei-Tavirani, & Azodi, 2011). Exposure to biological and chemical carcinogens, such as *H. pylori*, EBV, nitrosamines, and oxidants, can lead to DNA damage and mutation of gastric epithelial cells (Toh & Wilson, 2020). These mutations alter the expression of oncogenes and tumour suppressor genes, resulting in cancer progression (Lodish et al., 2000). The oncogenic protein involves kinases that induce transformation through either inappropriate or excessive phosphorylation of target proteins (Sefton, 1985). Many of the kinases have been found to play a role in tumorigenesis through transmembrane, cytoplasmic, and nuclear signalling, cell-cycle control, and regulation of apoptosis (Tsintarakis & Zafiropoulos, 2017). Hence, screening and targeting oncogenic kinases are rapidly becoming a part of a personalized strategy for the treatment of cancer (Awad et al., 2019). Additionally, investigation of genes associated with host kinase and the aforementioned pathogen is necessary to understand the dynamic progression of GC. Since it is known that *H. pylori* and EBV have a strong oncogenic role in gastric carcinogenesis (Murai et al., 2007). Thereby, it is imperative to develop a coinfection model for investigating the progression of GC, which can be used to test the potential role of protein kinases, which is one of the hallmarks in all cancers. Further, a previous study suggests that dose-dependent *H. pylori* infection produces cytotoxic factors, (ammonia) involved in gastric mucosal injury (Mobley, Mendz, & Hazell, 2001) and plays an important role in cancer progression (Bamoulid et al., 2017; Lahner, Carabotti, & Annibale, 2018). Further, EBV-associated gastric carcinoma comprises almost 10% of the total GC cases (Iizasa, Nanbo, Nishikawa, Jinushi, & Yoshiyama, 2012; Takada, 2000). Higher loads of EBV have been found in gastric biopsy tissues suggesting its significant role in GC progression (Nakayama et al., 2019). Higher EBV load is also a risk factor for various other cancers (Mazurek et al., 2020a; Nilsson, Forslund, Andersson, Lindstedt, & Greiff, 2019). Therefore, the role of pathogen burden in *H. pylori* and EBV co-infected GC need to be studied.

Corona Virus Disease 2019 (COVID-19) caused by a novel coronavirus (2019-nCoV) emerged in December 2019 (Y. Gao et al., 2020; Jakhmola, Indari, Baral,

et al., 2020). Later, it was formally named as severe acute respiratory syndrome virus 2 (SARS-CoV-2) by the International Committee on Taxonomy of Viruses (ICTV). Now it has become a global pandemic. SARS-CoV-2 belongs to the betacoronavirus genus, Nidovirales order and is closely related to severe acute respiratory syndrome coronavirus (SARS-CoV). This virus displays human to human transmission who are in close contact through airdpolets, hence WHO declared it as worldwide public health emergency (N. Zhu et al., 2020). The cumulative number of globally reported cases exceeds 180 million and the number of global deaths is almost 4 million million (Weekly Epidemiological Update on COVID-19 - 29 June 2021, n.d.).

To date, no precise treatment is available for COVID-19 associated diseases.

Importantly, cancer patients are among the most susceptible group in this (COVID-19) pandemic and the GC patients pose a significant challenge for the treatment (Moujaess, Kourie, & Ghosn, 2020). GC itself is a global health problem, each year over 1 million people are diagnosed with GC worldwide To date, the clinical characteristics of GC patients who are infected with COVID-19 are remotely known (L. Zhang et al., 2020). The presence of ACE2, a SARS- CoV-2 receptor is also observed in gastric mucosa and GI tract cells, which may be considered as a vulnerable site for SARS-CoV-2 infection (Mao et al., 2020; Sonkar, Kashyap, Varshney, Baral, & Jha, 2020). The lasting presence of the virus in gastric mucosa shows the possibility of gastric glandular epithelial cells as a site of the virus infection (Cheung et al., 2020; Mao et al., 2020). Therefore, there is an urgent need to find out GC medicines that can also target COVID-19.

Coronavirus uses RNA- dependent RNA polymerase (RdRp) for the transcription of their genes and replication of their genome (Snijder, Decroly, & Ziebuhr, 2016). Coronavirus replication is functional by the non-structural proteins (nsps) which are encoded by open reading frame (orf) 1a and 1b which translates nsps into polyproteins (Beg & Athar, 2020; Laha et al., 2020). Further, this polyprotein undergoes maturation through proteolysis to form polymerase complex. The SARS-CoV-2 polymerase complex comprises an nsp12 subunit which is connected with the nsp7-nsp8 heterodimer and nsp8 subunit at a distinct binding site (Peng et

al., 2020). This nsp12 is the catalytic subunit that has RdRp activity of its own. Though its polymerase efficiency is quite low (Subissi, Posthuma, et al., 2014). It has been reported that the active site of nsp12 binds to the first turn of RNA and arbitrates the RdRp activity (Hillen et al., 2020). It plays the central role in the replication of the virus with the help of two co-factors namely nsp7 and nsp8. Furthermore, it possesses the nucleotidyltransferase activity due to presence of nidovirus RdRp-associated nucleotidyltransferase (NiRAN) domain, which has an atypical kinase-like fold with GTP and UTP binding efficiency (Kirchdoerfer & Ward, 2019). Interestingly, in SARS-CoV, significant portions of NiRAN domains were missing (Kirchdoerfer & Ward, 2019). Hence, it was intriguing to analyze the kinase activity of the nsp12 protein-containing NiRAN domain.

In another study, kinases are deemed as a master regulator for SARS-CoV-2 viral growth, repair, and other cellular functions. Reports suggest when SARS- CoV-2 enters the host cell, cell division halts, and inflammation pathways get activated through tentacles like structure (filopodia) which ultimately helps the virus to spread to neighbouring cells. Thus the host cell becomes a virus factory (Bouhaddou et al., 2020). Therefore, we hypothesized that many FDA approved kinases inhibitors may hinder the life cycle of SARS-CoV-2. About 30 kinase inhibitors have been characterized in terms of antiviral potential, affecting viral entry metabolism and replication (Weisberg et al., 2020). Similarly, many kinases are found to be over-expressed in cancer also leading to uncontrolled growth in the cells. Furthermore, various kinase inhibitors have been found effective against these kinases. Both cancer and virus alter the cellular machinery which is mostly regulated by kinases (Bagga & Bouchard, 2014). However, to the best of our knowledge, this is the first study of kinase inhibitors for COVID-19 concerning GC.

Arteriviruses are positive-stranded RNA viruses which can infect mammals. They can cause disease associated with respiratory distress syndrome, lethal haemorrhagic fever or abortion (Snijder et al., 2013). In arterivirus, it is well documented that self-GMPylation/UMPylation activities of a NiRAN-RdRp are considered to generate a transient state primed for transferring nucleoside

monophosphate (NMP) to unknown viral or cellular biopolymers. In SARS-CoV-2 also, nsp12 (NiRAN-RdRp) also has Mn2+dependent NMPylation activity (Slanina et al., 2021). This NMPylation activity catalyses the transfer of a single NMP to the cognate nsp9. Both NiRAN activity and nsp9 NMPylation have an pivotal role in coronavirus replication (Slanina et al., 2021). Characteristics like the singular phyletic association with nidoviruses and its genetic segregation with the RdRp make NiRAN a plausible key regulator enzyme of nidoviruses (Lehmann et al., 2015). Moreover, it also possesses kinase-like folds in SARS-CoV-2. Hence, targeting NiRAN-RdRp becomes a favourable target for both SARS-CoV-2 and GC.

Through this study, we can target the gene which are highly expressed in GC and which can be targeted against SARS-CoV-2 also. Hence, this inhibition of genes could prevent the drug resistance caused by the use of different drugs. NIRAN-RdRp domain would help to identify specific kinase responsible for GC as a comorbidity of COVID-19. Further, this study would also aid in determining COVID-19 comorbidity-specific therapeutics and reducing drug-induced complications in the host. Considering these observations objectives were designed, which are as follows:

Objective 1: This study was designed to evaluate the growth pattern of various clinical isolates of *H. pylori* and their response to treatment with commercially available oral rinses/solutions. The study also includes the evaluation of tumour suppressor and proto-oncogene status in gastric epithelial cells as a response to treated and untreated isolates of *H. pylori*.

Objective 2: This study intends to show the association of EBV and *H. pylori* (coinfection model) in GC through kinase protein. Given the above, the present study was conducted to demonstrate the coinfection of EBV and *H. pylori* in AGS cell line for GC progression and to determines the morphological changes after coinfection. Further, the aim was to evaluate the expression of the kinases in coinfection and to study the probable apoptotic pathway involved in the co-infected GC.

Objective 3: In the current study, we tried to demonstrate the pathogenicity in

gastric cancer cells through *H. pylori* infection followed by co-infection of EBV. The vice-versa situation where the EBV-infection was followed by *H. pylori* co-infection in the AGS cell line for GC was also assessed. To be more specific, we have attempted to evaluate the role of pathogen burden and the synergy of pathogens on kinases which are crucial factors for cancer development. To the best of our knowledge, the current manuscript is the first report based on the association of pathogens load (EBV and *H. pylori*) with GC through various kinase proteins.

Objective 4: In this study by the use of bioinformatics approaches we proposed that nsp12 or RdRp of SARS-CoV-2 possess the kinase-like folds and are involved in the phosphotransferase catalysis. We also report the docking of some known kinase inhibitors which are used against kinases and also dysregulated in GC. Further, we performed the MMGBSA and simulation of four compounds which gave the best binding energies and optimal ADMET properties during our investigation. This study intends to provide the medicine/compounds which can be used to treat GC patients infected with COVID-19.

Chapter 2

Review of Literature

2.1 Kinases and therapeutics in pathogen mediated Gastric Cancer

The human kinome consists of 535 protein kinases and about 90 of these protein kinases belong to the family of tyrosine kinases. Phosphorylation is among important mechanisms for regulating various cellular functions namely proliferation, cell cycle, apoptosis, motility, growth, differentiation, among others. Deregulation of kinase activity can lead to drastic changes in cellular processes. Further, these deregulated kinases are often oncogenic and found to play important role in the survival and spread of cancer cells (Cicenas, Zalyte, Bairoch, & Gaudet, 2018). Kinases are involved in cancer through various ways namely: misregulated expression and/or amplification, aberrant phosphorylation, mutation, chromosomal translocation, and epigenetic regulation. Further, this can be sub-classified into receptor tyrosine kinases (RTK) and non-receptor tyrosine kinases (nRTK). There are reports which suggest the upregulation of several RTKs and nRTKs in GC (Chichirau, Diechler, Posselt, & Wessler, 2019). There are a few proposed molecular markers and signatures of GC which include phosphatidylinositol 3-kinase (PI3K)/Akt, Nuclear factor-kappa B (NFκB), inhibitors of apoptosis (IAPs), and B-Cell CLL/Lymphoma 2 (Bcl-2) family proteins are highly expressed in GC, hence being associated with the development of GC (Fig. 2.1.1) (Kamran et al., 2017).

GC ranks fifth as the most common cancer and the second leading cause of death in the world. There are approximately more than 1,000,000 newly diagnosed cases and 738,000 deaths every year due to GC (Sitarz et al., 2018; Thrift & El-Serag, 2020). It has been estimated that 17.8 % of cancers are caused by infectious agents out of which 5.5% of cancer are caused by *H. pylori*. In the case of GC, *H. pylori* contribute to more than 60% of cases, and Epstein Barr Virus (EBV) is associated with around 10% of cases (Correa & Piazuelo, 2011; S. Singh & Jha, 2017).

Infectious agents associated with GC are *H. pylori*, EBV, and human cytomegalovirus (HCMV) (Fig. 2.1). *H. pylori* and EBV have been classified as type I carcinogens according to the International Agency for Research on Cancer (IARC) (D. Liu et al., 2020). *H. pylori* are most frequently found in the inner lining of the stomach (Díaz, Valenzuela Valderrama, Bravo, & Quest, 2018). However, to date, the specific mechanism through which *H. pylori* induces GC is still unknown. EBV is another etiologic agent known to contribute to GC development (Eichelberg et al., 2019; Kashyap et al., 2020). EBV-associated GC (EBVaGC) is a characteristic subtype of GC which shows distinct clinic pathological features (J. Yu et al., 2017). HCMV is assumed to be an oncomodulator virus that infects tumour cells and increases their malignancy (Fig 2.1.1). There is evidence that supports its role in the development of gastric adenocarcinoma at an early stage (Fattahi, Nikbakhsh, et al., 2018). Hence there is a need for a more profound understanding of molecular mechanisms to determine effective therapeutic targets. This review provides brief information about common kinase used by these organisms, thus targeting them could prevent drug resistance and its associated GC. We have also provided updated information about the therapeutics used against these kinases. Therefore, our review presents a holistic view of kinases and therapeutics involved in GC concerning *H. pylori*, HCMV and EBV.

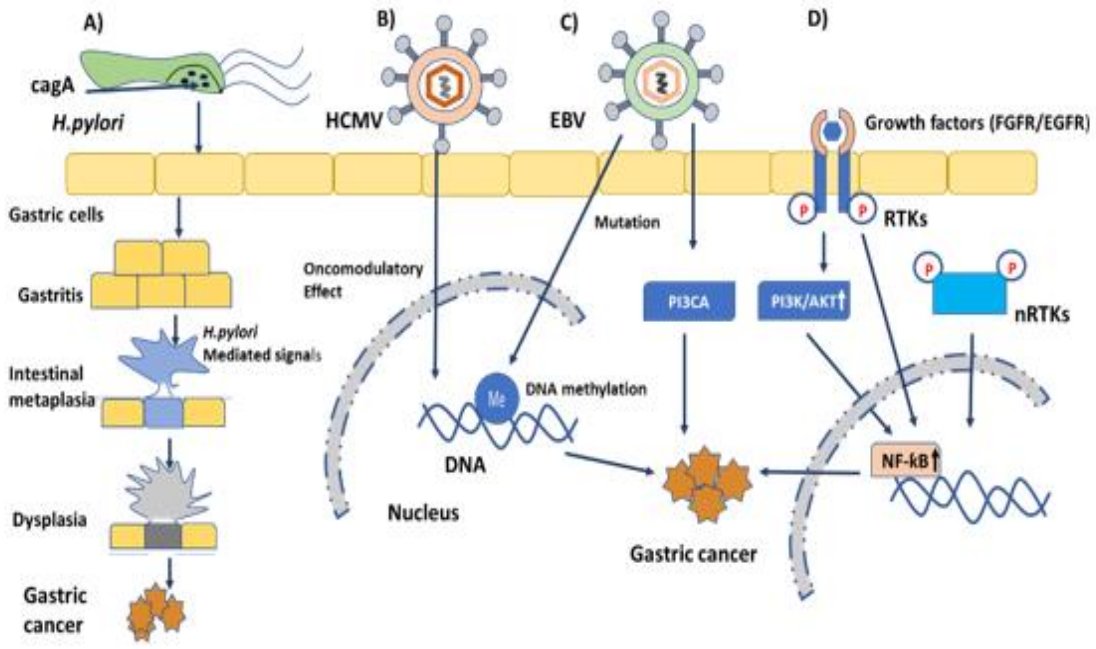

Fig 2.1.1: A diagrammatic representation of gastric cancer and its causes. A) Discusses the stages of GC caused by *H. pylori*. B) HCMV mediated GC C) EBV mediated GC D) kinases mediated GC

2.1.1 Helicobacter pylori

H. pylori is spiral-shaped gram-negative bacteria, first isolated by Barry Marshall and Robin Warren about 30 years ago in the human stomach (Falush, 2003). *H. pylori* can colonize the gastric mucosa for several years and it is strongly associated with chronic, diffuse, superficial gastritis of the fundus and antrum (Nomura et al., 1991). The susceptibility of an individual depends on *H. pylori* virulence, environmental factors, the genetic susceptibility of the host, and the reactivity of the host immune system. Despite the host immune response, *H. pylori* infection can be difficult to eradicate (Chmiela, Karwowska, Gonciarz, Allushi, & Stączek, 2017). Also, the majority of *H. pylori* strains express virulence factors that affect host cell signalling pathways. The virulence factor includes blood group antigen-binding adhesin A (BabA), Vacuolating Cytotoxin A (VacA), and Cytotoxin associated gene A (CagA) gene which has been considered as a risk factor for the disease outcome in certain populations. Further, it has several outer membrane

proteins like alpA, alpB, homB, hopZ, oipA, and sabA (Yılmaz & Koruk Özer, 2019). They are involved in the adherence of the bacteria to the gastric epithelial cells. BabA is one of the outer membrane proteins of *H. pylori* that can bind to the fucosylated lewisb (leb) blood group (Ilver et al., 1998). It helps in the adherence of *H. pylori* to gastric epithelial cells; therefore, it prevents bacteria from peristalsis and gastric emptying (Kable et al., 2017). The fundamental mechanism remains imprecise and the coordination of the BabA receptor during interaction of *H. pylori* with gastric epithelium is to be further studied. One of the most extensively studied toxins produced by *H. pylori* is the VacA, named because it can cause "vacuole" like membrane vesicles in the cytoplasm of gastric cells (Bernard et al., 1997). VacA is considered to be important for *H. pylori* colonization and is known to contribute to gastric adenocarcinoma (Foegeding, Caston, McClain, Ohi, & Cover, 2016). Several studies suggest that VacA can induce apoptosis by the mitochondrial pathway. However, it can also directly lead to the release of cytochrome c release from mitochondria which suggests the involvement of other pathways as well which lead to cell death (P. Zhu et al., 2017). Further, several other reports suggest that VacA can bind to multiple cell-surface components, namely Receptor Protein Tyrosine Phosphatase (RPTP)β, RPTPα, various lipids, the epidermal growth factor (EGF) receptor, and heparan sulfate. However, determining which binding interaction with VacA and the related signalling that causes cellular alteration is yet to be studied (Cover & Blanke, 2005).

Reports suggest that highly virulent *H. pylori* strains contain the cytotoxin-associated genes pathogenicity island (cagPAI). This cagPAI is of 40 kb region and contains 31 genes that encode components of a type IV secretion system. Further, it is involved in CagA translocation and the host's inflammatory response (Šterbenc, Jarc, Poljak, & Homan, 2019). Importantly, intracellular CagA acts as a "master key" or "picklock", which evolved during evolution to hijack key host cell signal transduction functions.

2.1.1.1 Kinases involved in *H. pylori* mediated Gastric cancer

A variety of serine/threonine and tyrosine kinases controls most of the eukaryotic

signalling pathway. There are only a few main targets of CagA, which control key checkpoints of eukaryotic signalling. Here the signal transmission by translocated CagA and *H. pylori* on multiple kinases can manipulate the selection of fundamental processes in the human gastric epithelium such as cell adhesion, polarity, proliferation, apoptosis, inflammation, and cell cycle progression (Table 1). As CagA is phosphorylated by Proto-oncogene tyrosine-protein kinase (Src), it binds to Src homology region 2 (SHP2) and activates the extracellular signal-regulated kinase 1/2 (ERK1/2) pathway, leading to conformation changes like cell proliferation and differentiation (Fig. 2.2). This activation occurs without phosphorylation of tyrosine residues (Richardson et al., 2009). This phosphorylation can stimulate transcription factor NF-κB (Alm & Trust, 1999; J.-F. Tomb et al., 1997). CagA also has CRPIA (conserved repeat responsible for phosphorylation-independent activity) which leads to interaction with hepatocyte growth factor, scatter factor receptor c-Met in phosphorylation independent manner which is known for its involvement in invasive tumour growth. Further, it leads to association with phospholipase Cγ (PLCγ) which leads to activation of (PI3K)/Akt signalling. It also leads to the activation of β-catenin and NF-κB signalling which results in cell proliferation and inflammation (S.-Y. Chen, Zhang, & Duan, 2016). Several reports suggest that *H. pylori* can activate the p38 mitogen-activated protein kinase (MAPK) signalling pathway which can result in increased expression of the COX-2 gene. However, inhibiting p38 MAPK cannot completely inhibit COX-2 (Xuan Liu et al., 2017, p. 30). COX-2 enzymes stimulate the GC cells to induce the expression of VEGF which is an angiogenic growth factor through unknown mechanisms (N. Liu et al., 2016). Several other genes like Tumour protein P53 (TP53) were upregulated and Coiled-Coil Domain Containing 151 (CCDC151), Cholinergic Receptor Nicotinic Beta 2 Subunit (CHRNB2), Guanosine Monophosphate Reductase 2 (GMPR2), Hepatoma-derived growth factor-related protein 2 isoform 1 (HDGFRP2), and V-Set And Transmembrane Domain Containing 2 Like (VSTM2L) were found to be down-regulated in *H. pylori*-positive GC group. Furthermore, the Hippo signalling pathway is also assumed to have a pivotal role in *H. pylori*-associated GC (Y. Hu et al., 2018). Hence, targeting

the aforementioned genes and thorough investigation is still needed to decipher potent targets through cag A signalling.

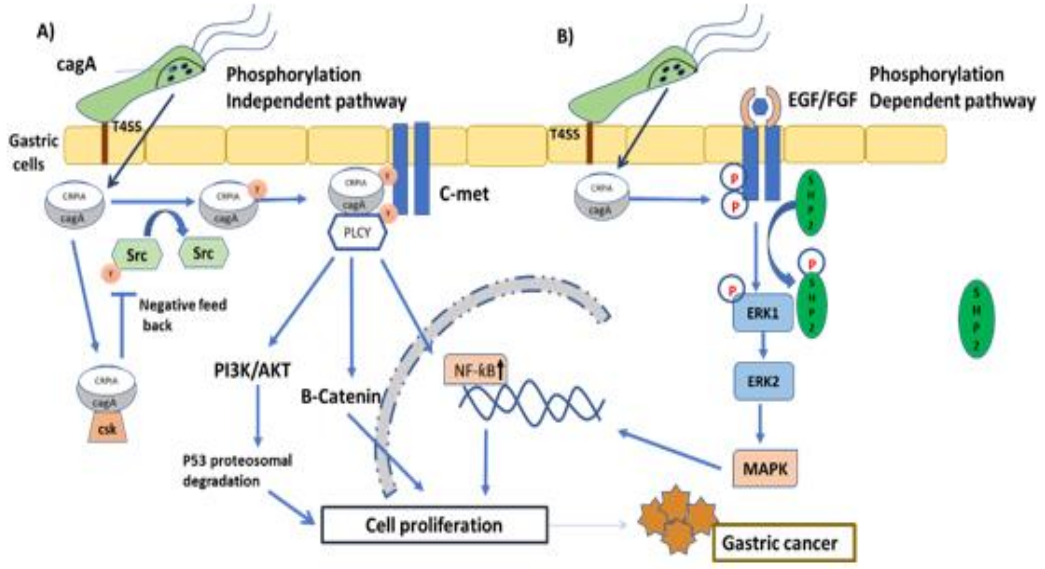

Fig 2.1.2: Phosphorylation-dependent and independent pathway through CagA

2.1.2 Epstein Barr virus

EBV is a gamma herpes virus that has infected nearly 90% of the world population (Sasaki et al., 2019). The EBV is a double-stranded DNA genome that is approximately 184 kb in length, and it expresses about 80 proteins and 46 functional small untranslated RNAs. These proteins may be involved in viral replication or synthesis of viral particles during the lytic cycle. Each extra-chromosomal viral DNA in the cells has six nuclear antigens namely EBNAs 1, 2, 3A, 3B, 3C, and -LP, and three latent membrane proteins namely LMPs 1, 2A, and 2B (Jha et al., 2016; Young et al., 2007). It has also been reported that when DNA tumour viruses get access into the cell which prevents the virus from completing its life cycle, it enters latent phase and expresses oncogenic viral genes (Banerjee et al., 2013; Jha et al., 2015). This could be true for EBV also in the development of gastric carcinoma, and the NK and T cell lymphomas. Thus, if EBV genes and their partners of human genes/pathways are recognized. Then, they may act as key interactive players in EBV related GC pathogenesis (R. Zhang et al., 2017).

2.1.2.1 Kinases engaged in EBV associated Gastric cancer

In EBVaGC, EBV establishes type I latency which expresses EBNA1, LMP2 proteins but does not express LMP1 protein. Further BARF1 proteins are also secreted in type I latency (Fukayama, 2010). EBVaGC is the outcome of the monoclonal proliferation of EBV-infected cells (Sasaki et al., 2019). EBVaGC shows distinct characteristics such as DNA hypermethylation, recurrent phosphatidylinositol 4,5-bisphosphate 3-kinase catalytic subunit alpha isoform (PIK3CA) mutations, overexpression of PDL1/2, and immune cell signalling activation (Kang, Baek, Kang, Baek, & Kim, 2019). According to TCGA DNA methylation is high in EBV positive tumours when compared to other cancers. (Bass et al., 2014; Matsusaka, Funata, Fukayama, & Kaneda, 2014). When these EBV-positive tumours were assayed they displayed hypermethylation of CDKN2A (p16INK4A) promoter, but they did contain hypermethylation of MutL homolog 1 (MLH1) which is characteristic of MSI- associated Concordant methylation of multiple genes/loci (CIMP) (Geddert, Hausen, Gabbert, & Sarbia, 2010). Genes that contain promoter hypermethylation are most distinctively silenced in EBV-positive GC. There are certain upregulated and down-regulated host genes during EBVaGC tumorigenesis. The upregulated genes are Zinc finger E-box-binding homeobox 1 (ZEB1), PeBOW, BCL-2, Cyclin D1, Indian hedgehog homolog (IHH) (Table 2.1.1). These genes are involved in enabling a longer latency period of EBV in the cell, anti-apoptosis, cell cycle progression, and snail protein expression respectively. The down-regulated genes are Somatostatin Receptor 1 (SSTR1), Phosphatase and tensin homolog (PTEN), AT-rich interactive domain-containing protein 1A (ARID1A), and CDKN2A (Table 2.1.1). These genes are involved in the loss of apoptosis, activation of the PI3K pathway, enhanced lymphovascular invasion, and uncontrolled cell proliferation (Naseem et al., 2018). PD-L1 is a glycoprotein that interacts with the programmed cell death 1 (PD-1) receptor that is mostly expressed on the surface of infiltrating cytotoxic T cells (CTLs). PD-L1 expression can be impaired by the activation of signalling pathways like the JAK/STAT, PI3K/protein kinase B (Akt)/mammalian target of rapamycin (mTOR), MEK/ERK, and Jun/Activator protein 1 (AP-1) pathways. These

pathways can act independently or can act in a synchronized manner to control PD-L1 expression, at the mRNA and protein level. Thus participating in the promotion of gastric carcinogenesis (Miliotis & Slack, 2020). Further, the kinases JAK2, mesenchymal-epithelial transition factor (Met), fibroblast growth factor receptor 2 (FGFR2), BRAF, RAF, EPH Receptor A4 (EPHA4), P21 (RAC1) Activated Kinase (PAK) PAK1, PAK2, Erb-B2 Receptor Tyrosine Kinase (ERBB) ERBB4, ERBB2, and inducible T-cell kinase (ITK) were found to be up-regulated in EBVaGC (Sonkar, Verma, Chatterji, Jain, & Jha, 2020). Targeted therapies for human epidermal growth factor receptor 2 (HER2), Met, FGFR2, and EGFR2 have already been developed.

Out of several latent genes, EBV nuclear antigen-1 (EBNA-1) is expressed in EBVaGC and all EBV infected cancers. EBNA1 can interact with two different host proteins which are used in the regulation of PML, CK2 kinase, and the ubiquitin-specific protease USP7 (HAUSP) (Sivachandran et al., 2010). LMP2A was found to be in 50% of EBVaGC cases. Further, this initiates the transformation process by PI3K/Akt pathway and also inhibits TGFβ1-induced apoptosis. This provides EBV- infected cells with a clonal selection advantage during tumour development (Fukuda & Longnecker, 2004, 2007). Hino et al. found that to prevent EBV-infected cells from serum deprivation, LMP2A activates the NF-κB-survivin which in turn play important role in the progression of EBV-infected GC (Hino et al., 2008). Another enzyme namely Cyclooxygenase-2 (COX-2) plays an important role in EBVaGC. COX-2 is an inducible isoenzyme of cyclooxygenase which in response to inflammatory stimuli or growth factors catalyzes the formation of prostaglandin E2 (PGE2). COX-2 induction can lead to upregulation of Akt which results in the promotion of angiogenesis and reduction of E-cadherin which can increase the invasiveness of the cancer cells. Hence EBV downregulates COX-2 expression via TRAF2 and ERK signal pathway in EBVaGC (Qi et al., 2019, p. 2).

Table 2.1.1: Genes involved in gastric cancer modulated by different pathogens along with their mechanism of tumorigenesis

Gene	Mechanism of tumorigenesis	Pathogen	Reference
ZEB1	Inhibits latent to lytic switch of EBV, enabling a longer latency duration Initiates epithelial-to-mesenchymal transition	EBV *H. pylori* HCMV	(Baud et al., 2013; Teo, Chen, Huang, & Chan, 2017; J. Zhao et al., 2013)
PIK3CA	Increases cell proliferation and survival by activating downstream PI3K/Akt pathway	EBV *H. pylori* HCMV	(Am, J, Z, & G, 2019; Servetas, Bridge, & Merrell, 2016; Sunakawa & Lenz, 2015)
PeBOW	A protein complex that enhances cell survival and ribosome biogenesis	EBV	(X. Wang et al., 2016)
PD-1/2	Suppresses immune surveillance and facilitate tumor development	EBV HCMV	(Schönrich & Raftery, 2019, p. 1; Sunakawa & Lenz, 2015)
JAK2	Stimulates cell proliferation, survival and differentiation	EBV *H. pylori*	(Judd et al., 2014; Sunakawa & Lenz, 2015)
Bcl-2	Anti-apoptotic protein	EBV *H. pylori* HCMV	(W. Chen et al., 2015; Gryko et al., 2014; Li et al., 2010)
Cyclin D1	Allows cell cycle progression through the G1phase	EBV *H. pylori*	(Hirata et al., 2001; Li et al., 2010)
IHH	Increases metastatic potential through angiogenesis, Snail protein expression, as well as a decrease in E-cadherin and tight junctions	EBV	(Yau, Tang, & Yu, 2014)
SSTR1	Expression is decreased by eight-fold in EBVaGC, allowing cell proliferation, loss of apoptosis and invasion SSTR-1 was downregulated upon *H. pylori* infection	EBV, *H. pylori*	(J. Zhao et al., 2013, p.)
PTEN	Loss of this tumour suppressor leads to PI3K/Akt pathway activation, and increased cell growth, angiogenesis, migration, loss of cell adhesion, and cell cycle regulation	EBV *H. pylori*	(Servetas et al., 2016; Sunakawa & Lenz, 2015)
ARID1A	Loss leads to enhanced tumour migration and lymphovascular invasion through downregulation of e-cadherin	EBV	(Sunakawa & Lenz, 2015)
P16	Loss leads to uncontrolled cell growth and may induce expression of thymidine phosphorylase, which facilitates tumour angiogenic activity	EBV	(Yau et al., 2014)

2.1.3 The synergy between *H. pylori* and EBV causing gastric cancer

Over the last couple of years, several studies have hypothesized that *H. pylori* and EBV can be linked with gastric carcinogenesis. But the studies based on coinfection are limited (Cárdenas-Mondragón et al., 2013; Dávila-Collado, Jarquín-Durán, Dong, & Espinoza, 2020; Pandey, Jha, Shukla, Shirley, & Robertson, 2018a). EBV and *H. pylori* both induce severe inflammatory responses. The study in which co-infected patients have increased inflammatory lesions as compared to patients infected with either EBV or *H. pylori* (Cárdenas-Mondragón et al., 2013). Furthermore, premalignant lesions and intestinal-type of GC are often associated with EBV positivity in *H. pylori*-positive GC (Cárdenas-Mondragón et al., 2013). Thus, EBV synergy with *H. pylori* inducing additive inflammatory response and enhanced inflammation. Moreover, both pathogens are correlated to the activation of MAP kinases and NF-kb oncogenic pathways in GC cell lines (Byun, Park, Lim, & Kim, 2016; XueQiao Liu & Cohen, 2016; Mohr et al., 2014; Pena- Ponce, Jimenez, Hansen, Solnick, & Miller, 2017). Co-infection of EBV can impede the host response to *H. pylori*. The virulence factor of *H. pylori* (CagA) interacts with host protein SHP 1, causing dephosphorylation and inactivation of the bacterial protein. Thus, SHP 1 halts the oncogenic activity of CagA. However, the host SHP-1 gene is also methylated by EBV coinfection. Further, in GC this infection can cause the silencing of miRNA and exosomes which indicates the collective effect of EBV could increase the oncogenic ability of *H. pylori* (Saju et al., 2016). It has also been reported that ITK, TYK2, FYN kinase was enhanced in gastric cancer cells (Sonkar, Verma, et al., 2020). Therefore, targeting signalling would be a promising strategy for therapeutics.

2.1.4 Human cytomegalovirus

HCMV is a member of the human herpesvirus family. It is a double-stranded DNA genome of over 230 kb and encodes approximately 180 proteins is known to induce chronic inflammation. It is known to affect 30–100% of normal adults which could result in life-long latent. During the latent stage, it is known to encode a viral protein

which includes LUNA, UL133-UL138 locus, US28, UL111A, and the cytomegalovirus latency-associated transcripts (CLTs) (Del Moral-Hernández et al., 2019; Sinclair, 2008; Slobedman et al., 2010). Many of its biological responses support chronic inflammation, leukocyte dysfunction, angiogenesis, and wound healing (Soroceanu & Cobbs, 2011). Further, it is also known for its association with several cancers such as prostate cancer, leukaemia, colorectal cancer, and breast cancer. However, its association with gastrointestinal disorders is meekly studied (Liang Zhang et al., 2017). Entry of the virus occurs by interaction with several glycoproteins such as gB, gH, gL, gO, and UL128–131 (Chan, Nogalski, & Yurochko, 2009). According to reports, gB also interacts with PDGFR-α (Y. Wu et al., 2017). However, its potential function of PDGFR-α ability in binding with gB or in a viral entry is still controversial (Chan et al., 2009). Based on the variable region of the viral surface gB gene. HCMV is divided into five genotypes. It has also been stated that genotype gB2 is prevalent in the gastrointestinal tract thus recognized as the first site of HCMV infection (Mohebbi et al., 2020). Furthermore, a higher amount of HCMV DNA is found in GC tissues and it is also correlated with lymphatic metastasis. HCMV can play an oncogenic role through dysregulating Wnt–β-catenin signalling and promote GC development (Fattahi, Kosari-Monfared, et al., 2018). CTNNBIP1 (β-catenin interacting protein 1) gene which functions as tumour suppressor gene is an antagonist of Wnt signalling and binds to the β-catenin molecules. Further its downregulation is linked to tumour grade and is assumed to be regulated by HCMV and EBV (Kosari-Monfared et al., 2019). Out of the latent genes expressed by HCMV UL136 was found in GC tissues and it is also known to activate IL6/STAT3. IL-6 is known to activate JAK1, JAK2 and TYK2 kinases. Hence targeting IL6/STAT3 can be a potent therapeutic target for HCMV mediated GC (Shi et al., 2020). UL138 is generally expressed in almost all tumour tissue. However, it was found to induce apoptosis in GC cells with an increase in the cleavage of apoptotic proteins caspase-3 (cas-3), caspase-9 (cas-9) and reduction of an anti-apoptotic protein Bcl-2. Further, it can also bind with heat shock protein-70 (HSP-70) along with many cancer-related proteins inhibit gastric tumour progression (W. Chen et al., 2015). Hence in-depth knowledge of signalling

in HCMV latent genes can prove promising targets for therapeutic for HCMV mediated tumour progression. Although kinases are considered to be a potential target, to the best of our knowledge no study related to kinases is done in HCMV mediated GC.

2.1.5 Common kinases between HCMV, EBV, and *H. pylori*-associated gastric cancer

JAK/STAT signalling is a key regulator of gene expression and immune response. JAK3/TYK2 levels are found to be considerably upregulated in stomach adenocarcinoma (STAD) (Meng, Ding, Yu, & Li, 2020, p. 2). The first recognized member of a family of non-receptor kinases is TYK2. TYK2 acts as a heterodimeric cytokine receptor complex that consists of four distinct TYK2-associated receptor chains namely IFNAR1, IL-12Rβ1, IL-10R2, and IL-13Rα1 (Wöss, Simonović, Strobl, Macho-Maschler, & Müller, 2019, p. 2). Its second receptor chain is linked either with JAK1 or JAK2, which has a signal-transducing chain containing STAT docking sites. Generally, upon receptor-complex activation, these sites are phosphorylated by JAKs. TYK2 also associates with the gp130 receptor chain. However, there is no evidence that gp130-utilizing cytokines rely on TYK2 for signal transduction (Wöss et al., 2019, p. 2). TYK2 is the common kinase found in HCMV, EBV, and *H. pylori*-associated GC (Fig 2.1.3). Hence targeting TYK2 can prove an efficient therapeutic target for GC caused by all the pathogens. This could also prevent drug resistance in GC patients. To the best of our knowledge TYK2 inhibitors are not yet used for the treatment of GC.

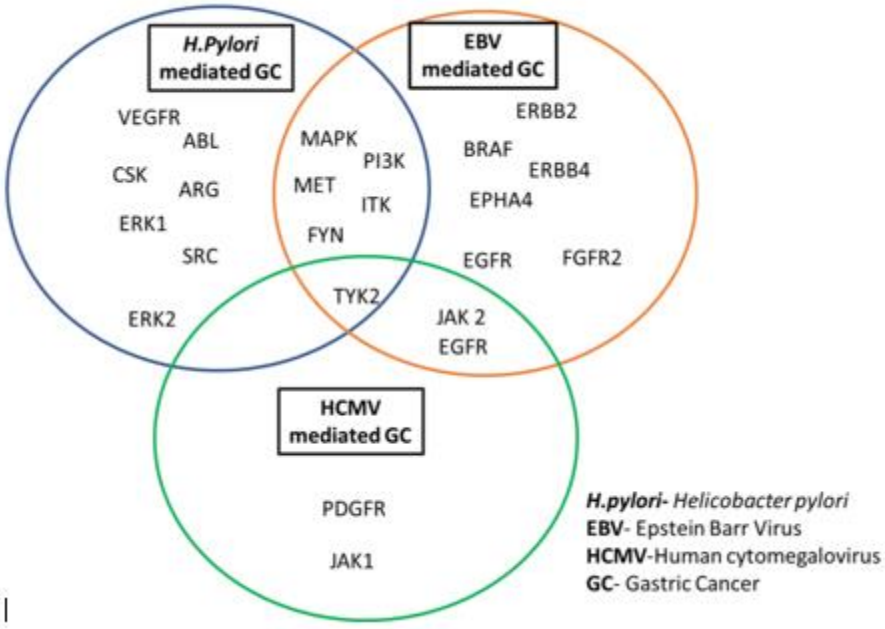

Fig 2.1.3: Venn diagram showing common kinases in *H. pylori*, EBV, and HCMV associated gastric cancer. Kinase used by *H. pylori*, EBV, and HCMV for causing gastric cancer has been mentioned. Further common kinases of the aforementioned pathogens are also illustrated.

2.1.6 Therapeutics targeting the common kinase

The common kinase found in *H. pylori* and EBV mediated GC are PI3K, Met, MAPK, FYN, and ITK. Further common kinase between EBV, HCMV, and *H. pylori*, EBV, and HCMV mediated GC are JAK2 and EGFR and TYK2 respectively (Fig 3). These kinases and their respective drugs are sequentially discussed.

The PI3K/AKT/mTOR pathway coordinates vital cellular functions such as proliferation, metabolism, cell growth, and angiogenesis. This pathway is commonly activated in many human cancers (Yap, Bjerke, Clarke, & Workman, 2015). Studies have shown that PI3KCB, PI3KCA, mTOR, and AKT1 are amplified in GC cell lines and this pathway is triggered in up to 60% of GC patients, substantiate the therapeutic susceptibility of the pathway (Lang et al., 2007). An

ongoing phase II trial tests the activity of the AKT inhibitor ipatasertib (GDC-0068) along with modified FOLFOX6 chemotherapy in advanced GC patients (Table. 2.1.2) (Genentech, Inc., 2020). A phase I trial that evaluates the safety of the isoform-specific PI3K inhibitor BYL719 in combination with the HSP90 inhibitor AUY922 in participants of advanced GC conceal PI3K mutation or ERBB2 amplification is recently completed (Table. 2) (Novartis Pharmaceuticals, 2020). Met receptor is found to be overexpressed in 2-23% of GC and associated with poor prognosis (Ang, Yong, & Tan, 2016). The first-in-human trial inspecting AMG-337 potency in patients with c-Met amplified GC showing constant antitumor response is underway (Amgen, 2016). Another ongoing phase II study of AMG-337 in Met-overexpressed GC (Amgen, 2017). Moreover, another phase I/II trial will check the efficacy of AMG-337 along with leucovorin calcium, fluorouracil, and oxaliplatin for the treatment of advanced GC patients (Table. 2) (Hong et al., 2019). Several studies have shown the involvement of ERK /MAPK pathways which is known to play role in cell motility in GC as well as in normal epithelia. Further, it is also known to regulate the activity of Matric metalloproteases (MMPs) which further influence cell migration and invasiveness. It is also the common kinase found in *H. pylori* and EBV mediated GC. Doxycycline is also known to participate in various processes namely induction of apoptosis, reversion of EMT, blockade of G1-S cycle, stabilization of p53 and p21, regulation of cell adhesion and migration, modulation of the ROS/ASK1/JNK pathway. It is further known to inhibit the ERK/MAP pathway both at transcriptional and protein levels (Table. 2.1.2) (Magnelli et al., 2020). According to Cui et.al, it was found that ITK was highly expressive both in the early recurrent group and in diffusal types of GC. Hence this could be used as a prognostic marker of GC (Cui et al., 2020). Pazopanib is a novel oral multitargeted tyrosine kinase inhibitor with a wide range of activities that are mediated through the VEGF receptor (VEGFR) types 1, 2, and 3, platelet-derived growth factor receptors α and β, ITK and stem cell factor receptor (c-kit), however, this inhibitor is used in renal cell carcinoma (Table. 2.1.2) (Pottier et al., 2020). The JAK pathway has usually been targeted for myeloproliferative and inflammatory disorders, however recently it also has been expanded to solid

tumours. Concerning gastrointestinal malignancies, ruxolitinib which is a JAK1 and JAK2 inhibitor, when combined with capecitabine and regorafenib is currently under evaluation in pancreatic and colorectal cancer respectively (Table. 2.1.2) (Fontana & Smyth, 2016). Tyrosine-kinase receptors are pivotal molecules in signalling pathways that result in the growth and differentiation of normal cells. Abnormal expression of tyrosine kinases is due to abnormal phosphorylation of tyrosine in GC (Lin et al., 2000b). Although to the best of knowledge TYK2 drug is not available for GC. However, Nifuroxazide, which was primarily identified as a treatment drug for diarrhoea is found to show effective inhibition of multiple myeloma cell survival by suppressing JAK2 and TYK2 directly (Table. 2.1.2) (Nelson et al., 2008).

Table 2.1.2: Therapeutics against gastric cancer targets and their association with GC

Kinase gene	Kinase inhibitor	*H. pylori* mediated GC	EBV associated GC	HCMV associated GC	Reference
ERBB2/ Her2	Trastuzumab		+		(Croxtall & McKeage, 2010; Wen et al., 2015)
VEGFR	Ramucirumab	+			(Ang et al., 2016; Vennepureddy, Singh, Rastogi, Atallah, & Terjanian, 2017)]
EGFR	lapatinib+ capecitabine and oxaliplatin		+	+	(Hecht et al., 2016)
FGFR	AZD4547, dovitinib, ponatinib		+		(Deng et al., 2012; Gozgit et al., 2012; Katoh, 2016; L. Xie et al., 2013)
AKT	ipatasertib	+	+		(Genentech, Inc., 2020)
PI3K	BYL719 +AUY922	+	+		(Novartis Pharmaceuticals, 2020)
Met	AMG-337	+	+		(Amgen, 2016, 2017, p. 2)

JAK2	Ruxolitinib, Tofacitinib		+	+	(Bhullar et al., 2018)
ITK	Pazopanib	+	+		(Pottier et al., 2020)
Src	Bosutinib, Dasatinib, Ponatinib, Vandetanib	+			(Bhullar et al., 2018)
MAPK	Doxycycline	+	+		(Magnelli et al., 2020)
JAK2	Ruxolitinib		+	+	(Fontana & Smyth, 2016)
TYK2	Nifuroxazide	+	+	+	(Nelson et al., 2008)

2.1.7 Conclusion

Although HCMV, EBV, and *H. pylori*-related GCs are diversified into different categories, the stomach is an organ in which multiple microorganisms coexist and are responsible for disease progression. Although the underlying mechanism is partially suggested the synergistic oncogenic effects of two or more infectious agents remain to be further explored. Kinase receptors are among the most frequently altered oncogenes in GC, rendering them key disease biomarkers and attractive drug targets. Some targets like AKT, c-Met and Her-2 can be potent targets for inhibiting GC. There are also some common kinases and signalling pathways used by the aforementioned pathogens which may result in an efficient therapeutic target and can also prevent drug resistance in GC patients. Thus, a comprehensive study compiling the kinases as a therapeutic target in pathogen-mediated gastric cancer is essential.

2.2 Impact of Gastrointestinal symptoms in COVID-19: A molecular approach

COVID-19 caused by novel SARS-CoV-2 is known to arrive from Wuhan wet market as an etiological agent leading to a global pandemic (2019-2020) (Jin et al., 2020). According to WHO as of 17th Sept 2020, this infection has more than 29 million active cases and about 0.58 million reported deaths in the form of viral pneumonia and affecting about 214 countries worldwide ("WHO Coronavirus Disease (COVID-19) Dashboard," n.d.). The pandemic of novel coronavirus is a great challenge because of the exponential increase in patients, rate of infectivity, scarcity of resources, poor prognosis of disease, and ambiguity regarding disease

pathogenesis (Endeman, van der Zee, van Genderen, van den Akker, & Gommers, 2020).

Furthermore, SARS-CoV-2 is known to attack the lower respiratory system and cause viral pneumonia; however, it may also affect the gastrointestinal system [4]. Reports suggest that patients infected with nCoV showing digestive symptoms like diarrhoea, vomiting may be among presenting features of the disease [5]. However, the prognosis of COVID-19 patients with gastrointestinal symptoms are mostly unknown. In about 50% of COVID-19 cases, there is the presence of SARS-CoV-2 in faecal samples and its viral RNA has also been identified in intestinal mucosa suggesting that the GI tract may be a probable route of infection [6]. Based on the studies in SARS-CoV- 2, its receptor (ACE2) is known to be a critical component of gastric mucosa and gastrointestinal cells as well, due to which gastric mucosa or gastrointestinal tract may be considered as a vulnerable site for SARS-CoV-2 infection [7, 8]. The lasting presence of the virus in gastric mucosa may indicate the possibility of gastric glandular epithelial cells as an incubation site of the virus. This can be further consolidated by the presence of viral nucleocapsid protein in the cytoplasm of the gastrointestinal tract days after its clearance from respiratory sputum [9].

Since this virus arises from the family of Coronaviridae, it belongs to the betacoronavirus genera. Moreover, the collectively known host receptor utilized by the SARS-CoV-2 is ACE2, sialic acids, and CD147 for the host cell infection [10–12]. Human leukocyte antigen (HLA) is an antigen-presenting factor for viral peptides and may be prioritized for the development of a vaccine against SARS-CoV-2 [13]. Both sialic acids and HLA are known to be important for *H. pylori* mediated gastritis and GC respectively [14, 15]. Thus, they played an important role in causing gastrointestinal symptoms associated with COVID-19. With the emergence of the gastrointestinal tract as an important site for SARS-CoV-2 pathogenesis. A possible mechanism of viral interaction and pathology is not yet completely known. In this review, we summarize the association of gastrointestinal disorders with SARS-CoV-2, their association from the other coronaviruses along

with the receptors which play a crucial role in facilitating the virus entry. Briefly, we also highlighted the gut microbe association in enhancing the infection, potential targets used as therapeutics, and drugs that can be repurposed for the COVID-19 patients with gastric co-morbidities. This article highlights potential diagnostic approaches like RDT and LC-MS for sensitive and specific identification of viral proteins. Taken all together, this article reviews the epidemiology, probable receptors and puts forward the tentative ideas of the therapeutic targets, their drugs, and diagnostic tool for COVID-19 with the gastrointestinal aspect of the disease.

2.2.1 Coronavirus and gastrointestinal symptoms: a long-back association

The coronaviruses comprise large, enveloped, positive-stranded RNA viruses. Coronavirus caused a broad spectrum of diseases in animals and humans [16]. Human coronaviruses (HCoV) can be classified into two serogroups with HCoV-229E and HCoV-NL63 included in serogroup one and HCoV-OC43 and HCoV-HKU1 falling in serogroup 2 [17]. The first two human coronaviruses, HCoV-229E, and HCoV-OC43 are correlated with upper respiratory tract infections. Further, HCoV-OC43 and HCoV-HKU1 cause gastrointestinal symptoms such as diarrhoea, vomiting, nausea, and abdominal pain in up to 57% and 38% of infected people respectively [18, 19]. Therefore, gastrointestinal symptoms can be treated as evident as respiratory symptoms in coronavirus colds, often designated “gastric flu”.

Another coronavirus, Severe Acute Respiratory Virus (SARS) which is also well known to affect the gut. Although infection results in diffuse alveolar damage, the changes in the gut are more precise which may include transmigration of intestinal bacteria and more lipopolysaccharide (LPS) permeability in the intestine. LPS causes an increase in the production of tumour necrosis factor (TNF), interleukin-1 (IL-1), and IL-6, thus resulting in aggravation of disease [20]. Further, studies showed by Leung et al, SARS replication in the cells of the small and large intestine of patients with an accumulation of higher viral titer inside the endoplasmic reticulum (ER) and viral particles might leave from the apical membrane of the

enterocytes. While, the report suggests that there is only minimal disruption of intestinal cells caused by the virus despite the tropism, thus, diarrhoea associated with SARS infection may be more related to proteins or toxins produced during viral replication than malabsorption or inflammation [21].

Middle East respiratory syndrome coronavirus (MERS-CoV), another virus of the coronaviridae family, is known to cause human respiratory infections and gastrointestinal symptoms. Zhou et al, illustrated that intestinal organoids and human primary intestinal epithelial cells were immensely susceptible to MERS-CoV and can sustain vigorous viral replication [22]. Apart from the respiratory tract, the human alimentary tract may be analyzed as a potential site for viral entry. Enteric viruses (adenovirus, rotavirus) and some non-enteric viruses (adenovirus A12) can bypass the physical barriers and infect susceptible cells in the alimentary tract [23]. The gastrointestinal symptoms are generally seen in most human coronaviruses [24]. So far, seven human coronaviruses have been known as the causative agents of mild or severe respiratory infections.

2.2.2 Epidemiology and Gastric disorder as a clinical predictor of SARS-CoV-2

SARS-CoV-2 shows the most common symptoms of the disease include pneumonia along with cough, sore throat, myalgia diarrhoea, nausea, vomiting, and fatigue [25, 26]. In adults, the most common symptoms are anorexia (39.9%-50.2%), and diarrhoea (2%-49.5%) while children suffered most from vomiting (6.5%-66.7%). Furthermore, 34.3% of COVID-19 patients are having digestive symptoms that contribute to their delayed recovery, unlike the remaining patients who recover early [27]. Since, the incubation time of a virus can range from 1-24 days, screening the patients becomes a tough task to handle [27, 28]. Moreover, several reports showed that viral RNA was detected in stool samples from 48.1% patients-even in stool collected after the respiratory samples tested negative [27, 29]. This suggests that the virus utilized the faecal-oral route for its transmission. Additional evidence of the association of SARS-CoV-2 and gut came when it was found in the endoscopy sample of a COVID-19 patient [9]. Wang et.al. has cultured the SARS-CoV-2 from four different patients' stool samples and found live virions

in two samples through microscopy [30]. Although, there are also reports that viruses are transmitted through fomites [31]. However, more research is required to confirm if this virus is viable in the stool and also to analyze the level of transmission through the faecal-oral route [32].

Importantly, multiple studies have found that the susceptible population for COVID-19 includes elderly mostly >70 years of age, individuals with underlying disease, or weakened immune systems [33]. Further, in a meta-analysis by Men and colleagues, 10% of patients were showing only gastrointestinal features upon infection. This may be due to delayed diagnosis which may lead to potential problems in the patient and the person who comes in contact with the patient. Another study suggests that about 3% of COVID- 19 cases showed only digestive symptoms and no respiratory symptoms [8, 34]. *H. pylori* are a well-established gastrointestinal pathogen associated with multiple gastric disorders like chronic gastritis and gastric cancer. According to reports SARS-CoV-2 and *H. pylori*, infection is more likely to occur in patients with blood group A. Thus, increases the risk of gastrointestinal infection [35]. Further, the patient having a history of *H. pylori* infection may become more susceptible to oral-faecal route transmission.

Nearly one-fifth of COVID-19 patients have reported gastrointestinal symptoms [36]. About 70% of patients with viral RNA shedding through the gastrointestinal tract were reported which lasted for about 10 weeks after the symptom onset [31]. Pathophysiological reports have suggested that no considerable damage was observed in the mucosal epithelium of the oesophagus, stomach, and duodenum tissues. However, major infiltration of lymphocytes is observed in the squamous epithelium of lamina propria of the stomach, duodenum, and rectum which may cause abdominal pain [37]. Further, abdominal pain is highly associated with COVID-19 severity along with nausea and vomiting which are comparatively less frequent. Considering the association of gut anomalies and its association with COVID-19 some of the symptoms like abdominal pain and diarrhoea can also be considered as COVID-19 symptoms or can be used as clinical predictors [36].

2.2.3 Receptor-mediated signalling with gastrointestinal disorders

It is well established that ACE2 is a receptor for SARS-CoV-2. Moreover, sialic acid, CD147 can also act as a receptor [10, 38]. However, the human coronavirus HKU1 and OC43 include human leukocyte antigen (HLA) as its attachment factor and sialic acid as its receptor respectively [39, 40]. In SARS-CoV-2 too HLA may present the viral peptides [41]. Moreover, another study by Ming et al, 2020 on COVID-19 patients from Wuhan has reported that there is an increased level of neutrophil, Interleukin-6 (IL-6), chemokine's IP-10, MCP-1, MIP-1A, tumor necrosis factor-alpha (TNFα), and less expression of lymphocytes [42, 43]. Here we precisely explain the downstream signalling from the aforementioned factors concerning gastrointestinal disorders and COVID-19 taking SARS-CoV as a reference.

ACE2 is largely found in the gastrointestinal tract [44]. The messenger RNA of the ACE2 receptor is highly expressed and stabilized by neutral amino acid transporter B0AT1 (SLC6A19) in the gastrointestinal system [45]. SARS- CoV-2 utilizes spike protein for binding to its receptor ACE2, upon binding the plasma membrane fusion occurs and releases viral RNA. Furthermore, viral RNA is detected as a pathogen-associated molecular pattern (PAMP's) by pattern recognition receptor (mostly toll-like receptor) [46]. The RNA released is recognized by the viral RNA receptor retinoic-acid inducible gene I (RIG-I), cytosolic receptor melanoma differentiation-associated gene5 (MDA5), nucleotidyltransferase cyclic GMP-AMP synthase (cGAS), and stimulator of interferon genes (STING) [40, 47]. Further, this binding recruits TIR-domain-containing adaptor protein along with mitochondrial antiviral-signalling protein (MAVS) and induces downstream signalling which includes activation of nuclear factor-κB (NF-κB), interferon (IFN), and series of pro-inflammatory (IL-6) and antiviral cytokines (Fig. 2.2.1) [48, 49]. This viral entry can also be through endocytosis by clathrin-dependent or independent pathway which may be used as a mechanism to avoid host detection (Fig. 2.2.1) [50, 51]. The upregulation of RIG-I and MDA-5 mediated through retinoic acid-inducible gene I-like receptors (RLRs) and toll-like receptors are also associated with gastric adenocarcinoma cells [52]. The role of ACE is controversial, it is known to have a significant role in gastric ulcer healing and can be related to virus-mediated

diarrhoea [53]. Hence studying ACE2 related signalling with gastric disorders and SARS-CoV-2 would provide better insight in determining therapeutic targets.

Reports suggest that through in-silico analysis of viral peptides of major histocompatibility complex class I gene (MHC) ([HLA] A, B, C), HLA may present highly conserved SARS-CoV-2 peptides which suggest its ability to activate cross-protective T-cell mediated immunity. These findings suggest that the severity of SARS-CoV-2 may be affected by the genetic variability of [HLA] A, B, and C [54]. Downregulation of HLA is a probable cause for poor prognosis in gastric as well as oesophageal cancer. Though epigenetic and oncogenic studies of HLA are still ambiguous, reports suggest that MAPK and AKT (HER2) signalling regulates the expression of HLA in gastric and oesophagal cancer [55]. Considering the importance of HLA and MAPK in the signalling pathway they appear to be important targets for therapeutic use.

Sialic acid which is responsible for regulating various physiological and pathological processes is composed of a diversified family of acidic sugar [56]. This can be used for the internalization of bacteria like *H. pylori* in gastric mucosa through sialic acid-binding adhesin (SabA) for subsequent persistence of infection. *H. pylori* infection is considered a crucial risk factor in gastric carcinogenesis where only a subset of individuals develops tumours [57]. In healthy conditions, gastric mucosa mostly expresses neutral fucosylated glycans whose glycophenotype is modified by *H. pylori* infection which leads to overexpression of β3-N-acetylglucosaminyltransferase-5 (β3GnT5) which is followed by increased biosynthesis of sialyl-Lewis x [58]. This increased biosynthesis of sialyl-Lewis x further leads to a successful strengthening of gastric epithelial attachment to *H. pylori* for efficient colonization, hence increasing the risk of gastric disorder. It has also been found that high levels of α 2,3 sialic acid residues were linked to GC cell invasion and metastasis [59]. Thus, the role of sialic acid in gastric comorbidities is evident, however; its role in SARS-CoV-2 is also emerging. The SARS-CoV-2 has very high infectivity due to its structure which contains various groups of terminal sialic acid [60, 61]. According to Menicagli et.al., one of the hypotheses states that sialic acid strengthens the capacity of diffusion which relies on the varied

number of glycoproteins present on the COVID-19 capsule [62]. Additionally, there are certain sialic acids present on the host cell surface which act as additional receptors for binding sites of the S protein of SARS-CoV-2 [63]. Hence, playing a role in the pathogenicity and epidemiology of the associated disease [63].

CD147 also known as Basigin or EMMPRIN is a transmembrane glycoprotein is known to bind to the spike protein of SARS-CoV-2 and mediate virus invasion and infection to other cells [11, 38]. Recently a research team by Zhinan et al after conducting surface Plasmon resonance analysis and competitive inhibition experiment found that CD147 anti- body competitively inhibited binding of CD147 and S protein [64]. Hence, it can be the potent target for therapeutics for COVID-19 patients. Moreover, CD147 is required for malaria parasite, Plasmodium falciparum invasion, which can explain the infection of SARS-CoV-2 in red blood cells [65]. However, it is also associated with gastric cancer invasion, metastasis and might be utilized for prognosis and indicator of tumour recurrence [66].

Increased level of IL-6 is often related to respiratory failure and acute respiratory distress syndrome (ARDS). It plays a crucial role in aggravating cytokine storms in COVID-19. It mainly follows two pathways cis and trans. In cis IL-6 binds with membrane-bound IL-6 receptor (mIL-6R) and gp130 which activates Janus kinases (JAKs) and signal transducer and activator of transcription 3 (STAT3) pathway. This JAK/ STAT3 pathway then activates innate and acquired immunity causing cytokine release syndrome (CRS). In the trans pathway, IL-6 binds to its soluble receptor (sIL-6R) which again activates JAK-STAT3 signalling. Further, it leads to the secretion of vascular endothelial growth factor (VEGF), monocyte chemoattractant protein–1 (MCP-1), IL-8, and reduced E-cadherin expression on endothelial cells hence aggravating cytokine storm [67]. IL-6 R can also be used as a prognostic marker in gastric cancer. Hence IL-6 can be a potent therapeutic target for COVID-19 patients suffering from gastric cancer [68].

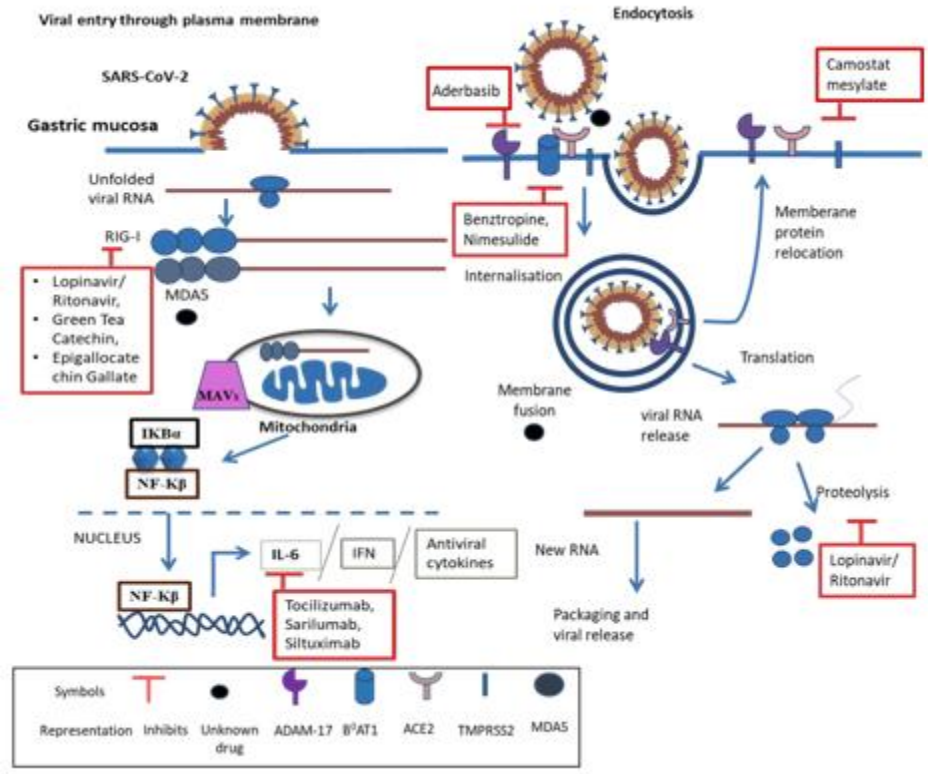

Fig 2.2.1: Potential colliding targets, their signalling, and inhibitors: SARS- CoV-2 RNA enters the cells through plasma membrane and endocytosis followed by recognition by RIG-I and MDA5 which binds to MAVs. Further, which leads to the secretion of IL-6, IFN, and antiviral cytokines. Moreover, commercially available drugs and targets with no known drugs have also been shown. Here ACE2, TMPRSS2, RIG-I, MDA5, IL-6, and ADAM-
17 may serve as important targets concerning gastric disorder as well.

2.2.4 Potential colliding targets and associated drugs

The potential targets like ACE-2, TMPRSS2, Cathepsin L/B, CD147, STING, RIG-I, MDA5, P38 MAPK, ADAM-17, sialic acid B0AT1, and IL-6 along with drugs can be used as therapeutics in COVID-19 and associated gastrointestinal disorders have been briefly explained.

SARS-CoV-2 spike protein binds to the ACE-2 receptor which may cause activation of p38 mitogen-activated protein kinase (MAPK), upregulate ADAM-17, and stimulate ROS formation [69, 70]. The Spike-ACE-2 complex

is proteolytically processed by type 2 transmembrane protease (TMPRSS2) at its S1/S2 junction to release the S2 subunit, which further facilitates viral and cell membrane fusion [71, 72]. Hence to facilitate virus entry TMPRSS2 and cathepsin L/B primes the S-protein of SARS-CoV-2 [71]. The commercially available drug for TMPRSS2 is Camostat Mesylate and Nafamostat (Table 2.2.1), which is a clinically proven protease inhibitor and it can also improve reflux esophagitis, Dyspepsia and inhibit SARS-CoV-2 infection [73–76]. Cathepsin L/B which also plays a crucial role in gastric cancer can be inhibited by cysteine protease inhibitor E64d (Table 2.2.1) [71, 77]. CD147 helps in P. falciparum invasion by binding to reticulocyte-binding protein 5 (Rh5) [78]. CD147 can also bind to the spike protein of SARS-CoV-2 for entry into the host cell [11, 38]. Targeting CD147 through the meplazumab monoclonal antibody could be a possible potential therapy against COVID-19 disease (Table 2.2.1) [79].

STING (stimulator of interferon (IFN) genes is encoded by TMEM173) and is considered as a key adaptor molecule that links to the identification of cytosolic DNA leading to the production of IFNs and NFkB. STING can also identify infections by some RNA viruses. Some arguments suggest the polymorphisms of the STING pathway could be involved in the pathogenesis of COVID-19 [80]. It is also reported that decreased STING is associated with poor prognosis of gastric cancer patients (Table 2.2.1) [81]. RIG-I precisely identifies the intracellular double-stranded viral RNA bearing 5′ triphosphate and invites molecules to activate antiviral signalling [82]. Hence antiviral drugs would be useful to target its activity such as Lopinavir in combination with ritonavir, along with the natural products like Green Tea Catechin, Epigallocatechin Gallate is also been found to be effective [83]. Though the administration of Lopinavir /Ritonavir is often associated with drug-related diarrhoea [84, 85]. Green Tea Catechin is considered a beneficial and effective way to prevent gastrointestinal disorders (Table 2.2.1) [86].

Sialic acid also plays a key role in eradicating *H. pylori* infection by inhibiting ROS production and NF-kB activation [87]. Hence sialic acid-mediated inhibitors may provide potent treatment to patients. Soluble macromolecules containing sialic acid can act as decoy receptors and competitively inhibit the receptor-binding such as

α2-macroglobulin, Umifenovir, and other natural inhibitors include eggwhite which can be useful in COVID-19 patients having gastric disorders (Table 2.2.1) [87, 88]. B0AT1 is an amino acid transporter, the abbreviation of major apical neutral amino acid transport system B0 and it belongs to the solute carrier family 6 (SLC6A19) [89]. It is the major Na+- dependent transporter for neutral amino acids in the small intestine and kidney [89]. The approved drug for B0AT1 inhibitor is Nimesulide (cyclooxygenase inhibitor) and Benztropine (Table 2.2.1) [90]. Increased secretion of pro-inflammatory cytokines like Interleukin-6 (IL-6) is a common factor in patients with gastritis and SARS-CoV-2 infection. IL-6 is a pro-inflammatory cytokine is linked to increased inflammation in chronic acute gastritis [91, 92]. IL-6 may act as a prognostic marker for gastric cancer and a potential biomarker for COVID-19 progression [68, 93]. Hence, Tocilizumab and Sarilumab is an FDA-approved drug that is an interleukin-6 receptor antagonist that can be a potent therapeutic drug (Table 2.2.1) [94, 95]. Siltuximab is a monoclonal antibody against IL-6 (Table 2.2.1) [96].

Table 2.2.1: Potential colliding targets and probable drugs with their phase I/II/III trials with their activity

Target	Gastrointestinal Disorder Association	Drug/phaseI/II-(PI) Phase I/III-(PII)	Drug Activity	References
ACE2	Gastric ulcer healing, Virus mediated diarrhea	PII- APN01	ACE2 inhibitor	[7,10,44,53,69-70]
TMPRSS 2	Dyspepsia, Reflux Esophagitis	Camostat Mesylate PII-NCT04352400 PII-nafamostat	Protease Inhibitor	[71-76]
RIG-I	*H. pylori* Infection, Gastric Adenocarcinoma	Lopinavir/Ritonavir, Green Tea Catechin, Epigallocatechin Gallate PI-NCT03065023	Protease Inhibitor	[47,82-86]
MDA5	Gastric Adenocarcinoma			[47]
[HLA]A	Gastric cancer, oesophagal cancer	Not known commercial drug available		[13-15,41,54-55]

Sialic acid-containing	*H. pylori* Infection	Egg whites		[10-12,14, 39,56-63,87, 88][84]
ADAM-17	Gastric acid secretion	Aderbasib (INCB7839)	ADAM-17/TACE inhibitor	[69-70,129, 130]
P38 MAPK	Gastric Cancer	PI-Ralimetinib (LY2228820)	P38 MAPK inhibitor	[69,70], [130, 131]
B^0AT1 (SLC6A19)		Benztropine, Nimesulide	B^0AT1 Inhibitor, Cyclooxygenase Inhibitor	[45,89,90]
IL-6	Chronic gastritis	Tocilizumab, Sarilumab	Interleukin-6 receptor antagonist	[20,39,42,43,48,49,67,68,91-96]
CD147	Gastric cancer	(PII) NCT04275245/ Meplazumab	anti-CD147 antibody	[11,38,64-66,78,79]

2.2.5 Gut dysbiosis: interaction of microbiota with SARS-CoV-2

The human gut consists of 1014 microorganisms like bacteria, fungi, archaebacteria, and viruses [97]. These gut microbiomes have an important role in maintaining the health of the individual. The microbiomes and host have a symbiotic association in that the earlier gets food and shelter and in turn, helps the latter in regulating physiological functioning like dietary digestion, and imparting protective immunity against pathogens [98]. Alterations of gut microbiota known as “gut dysbiosis” which is associated with several diseases and disorders such as type 2 diabetes, IBD, cardiovascular disease, and depression [99–101]. Moreover, the COVID-19 treatment regime includes sets of drugs that have negative impacts on different organelles and may cause gut dysbiosis also [102].

Intriguingly, pulmonary health is also affected through a vital cross-talk between the lungs and the gut microbiota known as the “gut-lung axis” [103]. This axis is bidirectional, i.e., microbial metabolites and the endotoxins can modulate the lung through blood, and during inflammation in the lung, it affects the gut microbiota [104]. This interdependency boosts a striking possibility that SARS-CoV-2 may

affect the gut microbiota. Numerous reports have pointed out that alteration in the composition of the gut microbiota is correlated with respiratory infections [105]. Moreover, severe clinical outcomes in SARS-CoV-2 infected patients are associated with immune compromisation and ageing. Therefore, it is tempting to speculate the probable cross-talk between the gut microbiota and the lung in COVID-19 which may further influence the clinical manifestation.

One hypothesis regarding gut dysbiosis is microbiomes' impacts on cytokines. Type II interferon (interferon-γ) is one such cytokine that plays important role in antiviral responses [106]. Furthermore, microbial metabolic processes in the gut strongly impact the production of cytokines [98]. Generally, the microbiota can enhance chronic phase protein and interferon signalling in lung cells to protect them from viral infection [107]. However, in the case of SARS-CoV-2 infection, the body's response to infection changes the scenario. Occasionally, COVID-19 patients' immune response against the virus results in a cytokine storm ultimately leading to hyper-inflammation and multi-organ failure [108, 109]. So far, a cytokine profile associated with COVID-19 severity has been characterized by increased interferon-γ inducible protein as well as many other cytokines. There is a lack of clinical evidence supporting the modulation of the gut microbiota that may have therapeutic value in COVID-19 patients, subjected to further research. From the current understanding, it can be speculated that the host cytokine molecular pathways, microbiota components. in association with cytokine responses can be used as novel microbiome-based therapeutic approaches for SARS-CoV-2 infection [110].

2.2.6 Diagnostic approaches

Due to the growing COVID-19 pandemic, there is a shortage of molecular testing capacity. Therefore, there is a need for a new point of care immunodiagnostic tests for fast and accurate testing of the disease. However, they can only be used for research purposes and cannot be used for clinical decision-making. There are 2 types of new point-of-care immunodiagnostic tests for antigen detection and host antibody detection.

2.2.6.1 Rapid diagnostic tests based on antigen detection

COVID-19 virus proteins (antigens) present in a sample infected person are detected by Rapid diagnostic test (RDT). If the concentration of target antigen is sufficient in the sample, the specific antibodies fixed to a paper strip enclosed in a plastic casing will bind to the target protein. This will generate a visually detectable signal, usually within 30 minutes. Actively replicating a virus expresses the antigen; hence this test can be used for early detection of infection. However, the tests depend on various factors such as virus concentration, quality of the sample, and precise formulation of reagents. Hence, its accuracy for the SARS-CoV-2 virus can range from 34% to 80% [111].

2.2.6.2 Rapid diagnostic tests based on host antibody detection

This RDT detects the antibodies present in the blood of the patients believed to be infected COVID-19 with body produced in response to the infection [112]. The strength of antibodies produced depends on various factors such as the severity of disease, age, nutritional status, and certain medications against infections like HIV [113]. Further, mostly antibodies are produced in the second week of infection or may be generated in the recovery state of patients. However, one of the drawbacks of this test is that it may provide false-positive results by interacting with antibodies generated for other infections [111].

2.2.6.3 Proteomics of SARS-CoV-2 infected host cells reveals their potential targeted therapy

The reaction towards the SARS-CoV-2 outbreak through expeditious, fast, and specific testing is widely recognized as critical. Nowadays mostly qRT-PCR based methods are used for the testing of SARS-CoV-2. While, the non-MS (mass spectrometry) methods such as enzyme-linked immunosorbent assays (ELISAs), western blots, and protein arrays depend on antibodies that were more successful during the outbreak of SARS-CoV in 2003 [114, 115]. Considering the immense variability in antibody production, the Liquid Chromatography coupled to Mass Spectrometry (LCMS) is an alternative attractive diagnostic approach for the identification of small molecules such as peptides and proteins in clinical settings with consistent results [116, 117].

These techniques measure the quantity of intact or proteolytically digested proteins

with specificity, speed, sensitivity, and resolution up to the femtogram [118]. Most of the LCMS techniques recruit tandem MS [119]. Furthermore, the measurement of fragment ions that are formed in tandem MS has its clinical significance due to its higher specificity and lesser chances of false-positive results [120]. Ihling et. al, identified the SARS-CoV-2 virus nucleoproteins from diluted gargle solution of COVID-19 patients through the precipitation of protein followed by the proteolytic digestion through MS [121]. Study shows that the expression of ACE-2 receptor is high in heart tissue through the tandem-MS via Tandem Mass Tag (TMT)-labelling and correlated with the higher heart failure. Bojkova et al, have isolated the SARS-CoV-2 and infected the human Caco-2 cell line which is a human colon epithelial cells, and used proteome and translatome mass spectrometry to perform the cellular response [122]. Further, they were identified as the key casualties of the host cell retaliation to infection. The above finding revealed the potential key molecules as a drug target for the SARS-CoV-2 infection [122].

2.2.6.4 One dimensional and two-dimensional liquid chromatography ESI/MS and quantification of virions

Although, it is easy to identify the genome sequences of SARS-CoV the recognition of protein is difficult. Two different structural proteins such as spike and nucleocapsid that are encoded by SARS-CoV were identified by Krokhin et al. through the MS technique [123]. Intriguingly, Zeng et al, first time identified the four structural protein as well as cytosol and nucleus fractions of SARS-CoV infected Vero E6 cells and also from the crude virion with the shotgun strategy with 2D-LC-MS/MS followed by ESI-MS/MS or by one-dimensional electrophoresis followed by ESI-MS/MS [124]. Post-translational modifications (PTMs) of viral proteins interfere with host cell signalling, cellular machinery hijacking, and enhancing infectivity [125]. Thus, viruses like influenza, SARS-CoV, and SARS-CoV-2 utilizes these PTM for enhancing the replication of their genome and for virion production. Moreover, the novel phosphorylation of structural proteins of SARS-CoV has been identified by this approach [126]. Heavy glycosylation of spikes may facilitate viral attachment, membrane fusion and critically stimulate the host immune response. There are about 22 potential N-glycosylation sites in the S1

and S2 subunits of spike proteins. Shajahan et al, mapped the glycosylation sites of spike protein subunits S1 and S2 which are expressed on human cells through resolution MS [127]. Moreover, they have quantitatively characterized the N-glycosylation sites. Intriguingly, they have observed the unpredicted O-glycosylation modifications on the RBD domain of the S1 subunit, spike protein. This is the first report where they have shown O-glycosylation on the S1 subunit. Thus, this study might play their role in vaccine development through elucidation of the glycan attachment on spike protein of SARS-CoV-2

(Fig 2.2.2) [127]. The limitations of LCMS in its medical setup, complex matrices, trace level analytes, and time-consuming sample preparations [128].

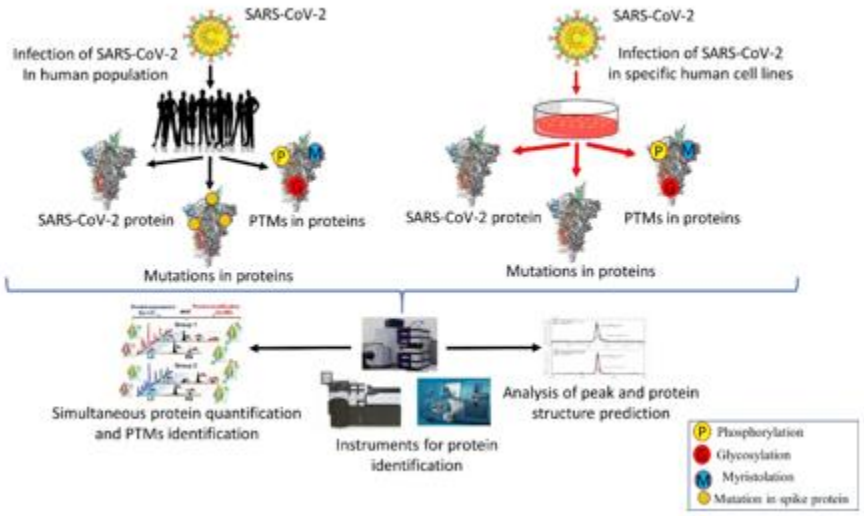

Fig 2.2.2: Flow diagram: Analysis of SARS-CoV-2 proteins, mutations and post-translational modifications through LCMS followed by ESI/MS for effective therapeutics

2.2.7 Conclusion

We conclude that SARS-CoV-2 is a causative agent of COVID-19 and its association with the GI tract is well known from earlier coronaviruses leaving a long-lasting impact on patients. The severity will increase in patients having GI disorders. The attribute of gastrointestinal symptoms existing in COVID-19 is more subtle than the respiratory symptoms hence they are easily ignored. However, during the entire course of COVID-19, patients might have only gastrointestinal

symptoms and may shed the virus in faeces, even though their respiratory samples test negative. Thus it is pivotal to observe these gastrointestinal symptoms with caution in the early stage of COVID-19. Further, dynamic monitoring of the digestive system and cytokines are also required during clinical practice to decrease the chances of complications and mortality of COVID-19 patients. Moreover, the detection of SARS-CoV-2 in faecal samples is essential for clinicalpractice along with routine testing, particularly for patients with atypical symptoms before leaving the hospital to confirm viral clearance. The ACE2 receptor is ubiquitously found on the surface of the GI tract, thus it is a potential replication site for SARS-CoV-2. Another receptor sialic acid is used by SARS-CoV-2 for its entry and HLA as its attachment factor. We have mentioned several potential targets that could be used as possible therapeutics. COVID-19 patients have suffered from hyper-inflammation due to which gut microbes will further exacerbate the infection. In addition to inflammation, the current treatment regimens can also negatively affect gut microbiota and cause digestive complications. We have also aimed to provide insight techniques like RDT, LC-MS which can be used for diagnosis and target the viral proteins with high sensitivity. Hence, this review intends to provide comprehensive information on SARS-CoV-2 concerning GI disorders.

Chapter 3

Materials and methods

3.1 Patient recruitment

The endoscopic procedure was performed after getting informed written consent from the patients. The protocol for the present study was approved by the ethical committee of the Indian Institute of Technology Indore, as well as Choithram Hospital Indore, and all procedures were performed by following the revised declaration of Helsinki 2000. Before collection of the sample written consent of the participants was obtained in a consent form. We collected only Rapid Urease Test (RUT) positive 14 biopsies (male = 9 and female = 5) and 11 gastric juice (male = 6, female = 5) samples from gastritis patients (Table 1). Patients undergoing antibiotic treatment against *H. pylori* were excluded from sampling. For further processing, biopsy samples were immediately placed in a microcentrifuge tube containing Brucella broth (BD- DIFCO, USA) with 20% glucose (Hi-Media, Mumbai, India), while gastric juice was collected in a sterile 15 ml centrifuge tube. Samples were transported to IIT Indore in ice.

3.2 Culturing, Isolation and identification of *H. pylori* from clinical samples

The biopsy samples were homogenized by using a glass rod. One loopful of the homogenous sample was streaked on Columbia agar plate (Hi-Media, Mumbai, India) containing the *H. pylori* selective antibiotics, (5 mg/L cefsulodin,10 mg/L vancomycin, 5 mg/L amphotericin B, 5 mg/L trimethoprim, and 10% defibrinated blood, BD-DIFCO, USA). The plates were incubated in a microaerophilic chamber (Whitley DG 250) containing specific growth conditions (i.e., 85% N2, 10% CO2, and 5% O2) at 37 °C. The same procedure was followed for gastric juice samples, and the colonial growth was observed for the next 3–4 days. *H. pylori* isolated from biopsy and gastric juice samples were named HB and HJ, respectively, followed by a number representing the sequence of sampling. In the present study, we also used I10 as a reference *H. pylori* strain, which was kindly gifted by Dr. Ashish Kumar

Mukhopadhyay from the National Institute of Cholera and Enteric Diseases (NICED) Kolkata. A point-sized colony was identified and used for the Gram staining. The colony was screened through morphological similarities with *H. pylori*.

3.2.1 Culture of clinical isolates in liquid and solid growth medium

A single colony was picked from the Columbia agar plate of each sample and inoculated in brain heart infusion media (BD-DIFCO, USA), containing 10% Fetal Bovine Serum (FBS; BIOWEST, South America origin) with 3X *H. pylori* selective antibiotics in a snap cap tube (BD, Cat. No. 352001). Simultaneously, it was also streaked on a BHI agar plate containing the same concentration of FBS and antibiotics. Both broth and plate were incubated in a similar growth condition, as described above.

3.2.2 Growth curve

The isolated *H. pylori* strains were analyzed for the growth pattern until 24 h. In brief, the isolates were cultured in a 14 ml round bottom snap cap tube (BD) in biological duplicates by setting initial OD600 0.05, which correspond to approximately 80 million CFU per ml (Gryko et al., 2014, p. 2). Further, they were incubated in the microaerophilic chamber, as mentioned above. 150 µl grown culture was placed in duplicate in 96 well flat-bottom plates, and OD was recorded at 600 nm (Synergy H1 Hybrid Multi-Mode Reader, BioTek). The final OD value was normalized with media as a negative control.

3.2.3 Culturing of *H. pylori* for co-infection studies

For the one co-infection study, two clinically isolated bacterial strains were considered; HB1 (human biopsy sample#1), HJ9 (Human gastric juice sample#9), and one reference strain I10. Moreover, for another co-infection study where the aim was to investigate the effect of pathogen loads in AGS cells only I10 was used. The *H. pylori* bacteria were grown in selective media in a 14 ml round bottom snap cap tube (BD). They were then incubated in the microaerophilic chamber for 72 h. Subsequently, 150 µl of grown culture was placed in duplicate in 96 well flat-bottom plates, and optical density (OD) was recorded at 600 nm. An optical density of 0.3 at 600 nm represents 500 million CFU/ mL (G. Kim et al., 2016). The final

OD value was normalized with media as a negative control (Gryko et al., 2014; Kashyap et al., 2020). The number of bacterial cells per ml (CFU/mL) of culture was evaluated according to the final OD, and the required volume of the bacterial culture for infection was then calculated. For coinfection studies with different bacterial isolates, MOI 100 was used. However, for investigation of pathogen loads in co-infection MOI of *H. pylori* bacteria, I10 was taken as 100, 200 and 500.

3.2.4 DNA isolation

H. pylori culture was harvested in phosphate-buffered saline for DNA extraction at OD600nm of 0.2–0.6. The pelleted cells were suspended in extraction solution (10 mM Tris pH 8.0, 15mM NaCl, 10mM EDTA, 0.5% SDS) and kept at 55 °C for 1 h. Proteinase K (Thermo fisher scientific, Gujarat, India) solution (20 mg/ml) was added (1 mg/ ml), and samples were incubated overnight at 37 °C. RNAse-A (Hi-Media, Mumbai, India) was added (0.1 mg/ ml) to the solution and kept at 37 °C for 1 h. The DNA was then extracted with the phenol-chloroform-isoamyl-alcohol method, as reported previously (Youle & Strasser, 2008, p. 2).

3.2.5 PCR detection

H. pylori DNA samples were amplified by Platinum™ Taq DNA Polymerase (Invitrogen, Carlsbad, CA). The reaction volume for PCR was 50 µL (50mM KCl, 1.5mM MgCl2, 200mM dNTPs, 10mM Tris-HCl (pH = 8.3), 10 pmol primer, 2.5 units Taq polymerase and 100 ng of DNA template). 16 s rRNA specific forward primer 5′ CTGGAGAGACTAAGCCCTCC 3′ and reverse primer 5′ ATTACTGACGCTGATTGCGC 3′ respectively were used for amplification (product size − 110 bp). The amplification was carried out with initial denaturation at 95 °C for 7 min, followed by 40 cycles of denaturation, annealing, extension, and a final extension at 94 °C for 2 min, 55°C for 30 s, 72 °C for 30 s and 72 °C for 10 min respectively. Analysis of the amplified products were done by gel electrophoresis using 2.5% agarose gel and stained with 0.5 µg/ml ethidium bromide. Product size was confirmed by using a 50-bp DNA ladder (Hi-Media, Mumbai, India). The image of gel was acquired on a gel documentation system (ImageQuant LAS 4000, GE Healthcare Life Sciences).

3.3 Oral rinses

Five different commercially available mouthwash solutions were purchased from local pharmacy store and were assigned names A, B, C, D & E. Mouthwash A contains cetylpyridinium chloride 0.075% w/w, mouthwash B contains chlorhexidine (0.2% w/v), mouthwash C contains naturally derived clove oil (0.1 mg/gm) (cloves extracts), mouthwash D contains thymol (thyme) 0.064%, methyl salicylate (wintergreen) 0.06% and eucalyptol (eucalyptus) 0.092%, and mouthwash E contains 2% w/v povidone-iodine.

3.3.1 Confirmation of the active component of oral rinses through LC-MS

Mass and spectral analysis were done by Bruker Daltonik, Benchtop, High-Performance Electrospray Ionization Quadrupole time-of-flight LC-MS spectrometer designed for estimation of an exact mass of the components present in mouthwash solutions. The bactericidal function of cetyl-pyridinium chloride (CPC) or 1-hexadecyl pyridinium chloride or chlorhexidine gluconate (CHG), clove oil, menthol/thymol, and povidone/iodine is well known and used in various antibacterial products like mouthwashes, throat sprays, nasal sprays.

3.3.2 *H. pylori* growth inhibition by oral rinses

Povidone-iodine (2%) was diluted in water (1:1), while other mouthwashes were used in provided concentrations. A fixed number of *H. pylori* (6 × 107) were incubated with 1 ml of all mouthwashes for 30 s, 10 s, and 5 s, followed by centrifugation at 3000 rpm for 5 min. The control group was left untreated. Pellets were suspended in 0.5 ml of BHI media containing 10% FBS and selective antibiotics followed by incubation in microaerophilic conditions, as mentioned above. 150 µl of culture was taken in each well in duplicates in a flat bottom 96 well plate and optical density was recorded at 600 nm (Synergy H1 microplate reader, Biotek) at 0, 6, 12, 18, and 24 h time points, and the growth curve was plotted.

3.3.3 Densitometry of *H. pylori* growth on BHI agar plate

A plate densitometry study on a BHI agar plate was performed to validate the growth pattern in the liquid medium. To check the growth of *H. pylori* (HB1, HB5, HJ9, HB14, and I10) on BHI agar plate, 1X107 bacteria were taken (OD600 0.3

represents 500 million CFU per ml) (Gryko et al., 2014) and suspended in 100 µL of BHI broth and then spread by using glass spreader. Further, images of plates were obtained at 0, 6, 12, and 24 h, and data were analyzed by measuring the mean grey value using Image J software (NIH) (Fig. 2c). In addition to this, the growth of bacteria on a BHI agar plate after 30 s solution treatment was also determined. 0.5X107 bacteria were taken and subjected to centrifugation at 3000 rpm for 5 min. The supernatant was discarded, and the pellet was treated with 333 µL of the selected oral rinses (A, B, C, D, and E) for 30 s. The treatment was stopped by centrifugation at 3000 rpm for 5 min, and the supernatant was discarded. The pellets were suspended in 50 µL of BHI broth and spread in half of the plate and incubated in a microaerophilic condition followed by taking an image at various time intervals. We have shown representative images of *H. pylori* growth on BHI plates. Further, for better understanding, we calculated the fold change in growth, and the obtained data were plotted into graphs.

3.3.4 RNA isolation and gene expression study through qRTPCR

Fixed number (6X107 CFU per ml) of *H. pylori* isolates (I10, HJ9, HB14, HB1) were treated with 1 ml of oral rinse for 30 s and 5 s. Here, oral rinse A was excluded from the cell culture study because of alcoholic constituents. Further, *H. pylori* isolates were incubated with AGS cells under specific conditions (5% CO2, 37 °C) for 12 h. At the 12 h time point, the pellet was collected by centrifugation (1600 rpm for 5 min) and washed twice with PBS. Total RNA was isolated by using Ribozol reagent (VWR™ Cat No. N580) as per the manufacturer's instruction. The cDNA was synthesized using the PrimeScript 1st strand cDNA Synthesis Kit (Takara, Cat No. RR820Q) according to the manufacturer's instruction. Quantitative real-time PCR (qRT- PCR) analysis was performed using the AriaMx Real-Time PCR System (Agilent technologies 5301 Stevens Creek Blvd Santa Clara, CA 95051 USA), for assessment of gastric cancer marker genes (CCND1, CDX2, PTEN, and MMP7), pathogen-associated genes (CagA, BabA, and 16 s rRNA) (Table 3.3.4.1) and, apoptotic genes (FADD, APAF1, BID, BAK, NOXA, PUMA and BCL-2) (Table 3.3.4.2)

Table 3.3.4.1: List of primers for gastric cancer markers and pathogen-

associated genes

Gene name	Forward primer	Reverse primer
CCND1	TGTGCCACAGATGTGAAGTT	CTTGGGGTCCATGTTCTGCT
CDX-2	GCAGCCAAGTGAAAACCAGG	TCTCAGAGAGCCCCAGCG
PTEN	ACCCACCACAGCTAGAACTT	GGGAATAGTTACTCCCTTTTTGTC
MMP7	AGTGGTCACCTACAGGATCG	ATCTCCTCCGACCTGTCC
16 s RNA (*H. pylori*)	CTGGAGAGACTAAGCCCTCC	ATTACTGACGCTGATTGCGC
GAPDH	TGCACCACCAACTGCTTAG	GATGCAGGGATGATGTTC
CagA	GCCATCATGTTTTAGGCTACC	GACGCCCTAGGGAATGATC
BabA	GATCAACGCGGCGGTAGG	CCGTTCAAAGAACAAGTGATGG

Table 3.3.4.2: List of primers for apoptotic genes used in the study

Gene name	Forward Primer	Reverse Primer
PARP1	GGCGATCTTGGACCGAGTAG	AGCTTCCCGAGAGTCAGGAT
APAF1	CTTGCTGCCCTTCTCCATGA	TTGCGAAGCATCAGAATGCG
FASR	CCTGCCAAGAAGGGAAGGAG	TTTGGTGCAAGGGTCACAGT
BID	CTGCAGGCCTACCCTAGAGA	GTGTGACTGGCCACCTTCTT
BIK	ACCTGGACCCTATGGAGGAC	CTGAGGCTCACGTCCATCTC
BIM	CTTCCATGAGGCAGGATGAA	TCCAATACGCCGCAACYCYY
BAX	CATGGGCTGGACATTGGACT	AAAGATGGTCACGGTCTGCC
NOXA	CAAGAACGCTCAACCGAGCC	GCCGGAAGTTCAGTTTGTCTC
FAS	GGACCCTCCTACCTCTGGTT	GCCACCCCAAGTTAGATCTGG
FADD	CACCAAGATCGACAGCATCG	AGATTCTCAGTGACTCCCGC
BAK	GGTTTTCCGCAGCTACGTTT	TAGCGTCGGTTGATGTCGTC
PUMA	GAGCCCGTAGAGGGCCTG	TACTGTGCGTTGAGGTCGTC
BCL-2	CATGTGTGTGGAGAGCGTCA	CATGTAAAGCCAGCCTCCGT
CASPAS9	TGCTCAGACCAGAGATTCGC	TCTTTCTGCTCGACATCACCAA

3.3.5 Ethidium bromide and acridine orange (EB/AO) assay

EB/AO dual staining was performed for the assessment of the apoptotic, necrotic, and live cells after infection with oral rinses treated *H. pylori*. The experiment was performed in duplicates, and the image was acquired by confocal microscopy (Olympus IX83) at 10X with 3X zoom-in triplicates. The working concentration of acridine orange and ethidium bromide was 100 µg/ml each (Blanchard & Nedrud, 2012).

3.4 Animal cell cultures

Adenocarcinoma gastric (AGS) cell line was procured from National Centre for Cell Science (NCCS), Pune, India. The cells were grown in Dulbecco's modified Eagle's medium (DMEM; Himedia, Mumbai, India) supplemented with 10% fetal bovine serum (FBS; BIOWEST, South America origin), 1% penicillin-streptomycin (Himedia, Mumbai, India). Infectious EBV was produced by transfection of BAC-EBV-GFPWT into HEK-293T (human embryonic kidney cell) cells, selection followed by chemical induction. We received the transfected HEK293T EBV BAC as a gift from the University of Pennsylvania, USA, which were further cultured in the lab. Cultured HEK 293T EBV BAC were induced for five days with 20 ng/ml tetradecanoyl phorbol acetate (TPA) and 3 mM butyric acid (Sigma-Aldrich Corp., St. Louis, MO). The supernatant from cell culture was collected and treated with DNAse. The viruses were concentrated by ultracentrifugation 23,500×g at 4°C for 1 h 30 min and quantified through qRT-PCR (Halder et al., 2009; Pandey, Jha, Shukla, Shirley, & Robertson, 2018b; Shukla, Jha, El-Naccache, & Robertson, 2016). The infective dose of EBV was determined by infecting 25×104 AGS cells seeded in 6 well plates with 0, 25, 50, 75, 100, and 125 µl of the isolated virus. It was followed by isolation of mRNA, preparation of cDNA, and RT-qPCR for detection of EBNA-1. EBNA1 oncoprotein is the only viral protein expressed in all forms of latency during EBV infection (Boudreault, Armero, Scott, Perreault, & Bisaillon, 2019, p. 1). We confirmed the presence of EBV in the AGS cells through RT-qPCR. RT-qPCR is a recognized method for determining multiplicity of infection which has been used in other studies as well, and thus we used this method to determine the titer value(Coleman et al., 2015; Shannon-Lowe et al., 2009). We found that the infective dose resulting in high expression of EBNA-1 was 100 µl which corresponds to 20 MOI (Heawchaiyaphum et al., 2020; Lay et al., 2010).

3.5 Coinfection of EBV and *H. pylori*

AGS cells (25×104) were seeded in 6 well plates followed by *H. pylori* infection through transwell inserts of 0.45 µm at MOI of 100. After 6-8 h, transwell was removed, and the cells were infected with EBV at an infective dose of 100 µl. This was followed by centrifugation at 2000 rpm for 20 min followed by re-insertion of

the transwell insert. This setup was then incubated for variou ed the same without the use of a transwell. The graphical representation s time intervals. For the direct infection approach, the rest of the protocol remain of the experiments performed in the project is shown in Fig 3.7.1, which depicts the procedure of direct and indirect coinfection in the cells, which were followed by other experiments like RT-qPCR. After 12, 24, and 36 h, cells were scrapped through a cell lifter and centrifuged at 3000 rpm for 5 min to get the pellet.

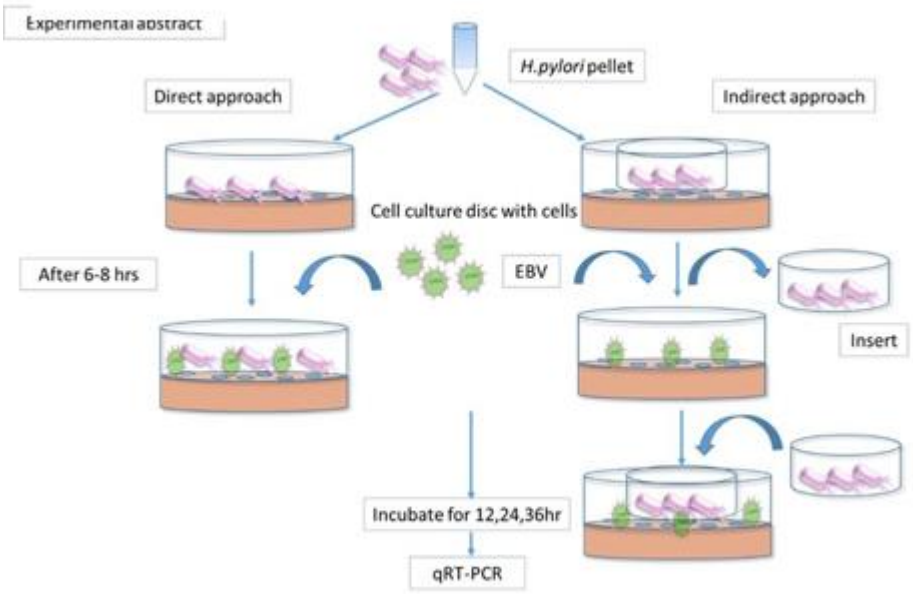

Table 3.5.2.1. List of primers of kinase genes used in the study

Gene name	Forward primer	Reverse primer
EPHB6	ATGAAGTGCCCTCTGCTGTC	CTGCCTGGTCATAGTAGCGG
MAPK1	AACAGGCCCATCTTTCCAGG	CCAGAGCTTTGGAGTCAGCA
SRC	ACATCCCCAGCAACTACGTG	CAGTAGGCACCTTTCGTGGT
AKT3	ACCGCACACGTTTCTATGGT	TTCATGGTGGCTGCATCTGT
JAK2	TGGGGTTTTCTGGTGCCTTT	TAGAGGGTCATACCGGCACA
PAK1	ACAGGAGGTGGCCATTAAGC	CACAGCTGCAATTTGGCCTT
PAK2	ATTGGACAAGGGGCTTCTGG	CCACATCAGTGAGTGACCCC
ERBB2	CGCTGAACAATACCACCCCT	GCCAGCTGGTTGTTCTTGTG
FGFR2	CCAACTGCACCAACGAACTG	ACTGTTCGAGAGGTTGGCTG
METMET	GTCCTGCAGTCAATGCCTCT	GTCAGCCTTGTCCCTCCTTC
PDK1	AAGTTCATGTCACGCTGGGT	GCATCTGTCCCGTAACCCTC
ROR2	ACGTACGCATGGAACTGTGT	CGGCACATGCAAACCAAGAA
ERBB4	ACAGGGGGCAAACAGTTTCA	AGCCCACCAATTACTCCAGC
FYN	CTCAGCACTACCCCAGCTTC	AGGTCCCCGTATGAGACGAA
ITK	ATTATCTACGCACCCAGCGG	ATGCCCTCACACACATCCAG
TYK2	CCCATGGCTTGGAAGATGGT	ACTCAGCTTGATGAAGGGGC
YES 1	GCTCCTGAAGCTGCACTGTA	GCATCCTGTATCCTCGCTCC
EPHA4	AAGGCTATCGGTTACCCCCT	CTTCAAGCTGTTGGGGTTGC
MERTK	GCCCCATCAGTAGCACCTTT	TGCACGTAGCATTGTGGACT
TYRO3	CAAACTGCCTGTCAAGTGGC	CCCGCCAATGAGGTAGTTGT
BRAF	AGAGGCGTCCTTAGCAGAGA	ATCGGTCTCGTTGCCCAAAT
MTOR	TCGCTGAAGTCACACAGACC	CTTTGGCATATGCTCGGCAC
RAF1	AATCAGCCTCACCTTCAGCC	AAAGAGCCTGACCCAATCCG
FGFR4	GAGTCTCGTGATGGAGAGCG	AGTTATAGCGGATGCTGCCC

3.5.1 Scratch assay

Cells were seeded into a 6-well plate and continuously cultured to 100% confluency to form a monolayer. A single-line wound was formed by scratching the cell monolayer with a 1000 μL pipet tip. The cell monolayer was washed with PBS to remove debris. Cells were infected according to the IDD and EDD approach and images were taken at 0 h of I10 infection, 0 h of EBV infection (6 h after I10 infection), and 12hr after co-infection. The wound was imaged under a light microscope (Olympus) and the wound area was quantified by using ImageJ software.

3.6 Immunofluorescence analyses

IF analysis was used to assess ITK expression in the cells in EDD and IDD setup.

25×104 cells were seeded on glass coverslips in 6-well plates. After EDD and IDD infection cells were incubated for 12 h. Then, cells were washed three times in PBS fixed in 4% paraformaldehyde for 30 min and washed once in PBS. Cells were treated with 0.25% Triton X-100 for 30 min followed by a PBS wash. Further, cells were blocked with 1% BSA for 1h and then washed three times in PBS. Thereafter, cells were incubated with specific primary antibodies ITK (1:150; Invitrogen Thermo Fisher, USA) for 2 h at RT. After two times PBS washes, cells were incubated with anti-mouse IgG F(ab')2 fragment Alexa fluor 488 conjugate (1:1000; Cell signalling technology, USA) and DAPI (1:50; G-Biosciences, India). Coverslips were then mounted on the clean slide for visualization. The confocal laser scanning microscopy (CLSM) was performed using a Multiphoton laser (FV1200MPE, IX83 Model, Olympus).

3.7 Statistical analysis

The analysis and quantification of the experimental setup were done through Image J and Graph Pad Prism software version 6, respectively. Biological triplicate was required for each experiment. Quantitative data were shown as mean ± SD. Difference comparisons between groups were analyzed with an independent t-test or ANOVA. In all analyses, $p < 0.05$ was seen as the significant level.

3.8 Data source

The protein sequence of SARS-CoV-2-RNA dependent RNA polymerase (PDB ID:7BTF) was downloaded from the RCSB protein data bank. The first 400 amino acids from 934 amino acids were used for analysis. The criteria for selection of 1-400 amino acids from the full-length sequence of SARS-CoV-2-RdRp was according to existing literature, as this N-terminal part of the RdRp contains NiRAN domain (Neogi et al., 2020; Peng et al., 2020). The trimmed N-terminal 400 amino acids of protein SARS-CoV-2-RdRp was first checked for the stability on the ProSA web server (Wiederstein & Sippl, 2007). Further, this SARS-CoV-2-RdRp (N-terminal 400 amino acids) was used for all our docking and simulation studies.

3.9 Active site prediction using CASTp

Further, Binding pockets and the probable ligand-binding residues over the SARS-

CoV-2-RdRp-NiRAN domain protein were identified using CASTp 3.0 software with default probe radius of 1.4 Å was kept constant. CASTp 3.0 utilizes computational geometry algorithms consisting of Delaunay triangulation, alpha shape, and discrete flow (Tian, Chen, Lei, Zhao, & Liang, 2018). The software measured the volume and surface areas (SA) of the computed cavities using a solvent accessible surface model (Richards' surface) and the molecular surface model (Connolly's surface) and provided the outcome in decreasing order of binding pocket volume and areas. Also, the output was visualized using discovery studio software.

3.10 Molecular docking using AutoDock 4.2

Blind docking of 16 compounds were performed using AutoDock 4.2 to check the binding of our compounds at the CASTp predicted active site. The protein structure of the SARS-CoV-RdRp-NiRAN domain (1-400 amino acids) already prepared in PyMol was used for the docking studies. Further for grid generation and docking, we edited as well as prepared protein using autodock 4.2 suite. Removal of water, the addition of polar hydrogens, the addition of Kollman charges were done. Protein and ligands both were edited and prepared and saved in. pdbqt format. Then grid box was generated using the Graphical Interface program AutoDock Tools (ADT). Grid was prepared using the Autogrid and the grid size was set to 50 × 50 × 50 xyz points with a grid spacing of 1.000 Å and the grid centre was designated at dimensions (x, y, and z): 120.047, 116.829, and 99.308. After grid preparation it was saved as gpf format, the default docking parameters (Genetic algorithm for search and Lamarkian 4.2 for output) were selected and saved as .dpf format. After that Autogrid and Autodock were run followed by result analysis. Further, the docking result was analyzed for conformation with the best dock score and the complex was further visualized using discovery studio.

3.11 ADMET properties prediction

The 12 inhibitors with the highest docking scores and minimum binding energies were analyzed for their pharmacokinetic properties such as Absorption, Distribution, Metabolism, Elimination, and Toxicity (ADMET), and drug-likeness. A freely accessible SwissADME webserver was used to evaluate ADMET such as

probable hydrogen bonding atoms; human Oral Absorption (where less than 25% is considered poor and above 80% is considered good); QP 18 LogS (Predicted aqueous solubility of the compounds, the acceptable range is -6.0 to -0.5) and the IC50 values for the obstruction of the human Ether-a-go-go-Related Gene (hERG) K+ channels (where less than -5 is considered satisfactory) (Lipinski, 2004; Sato, Yuki, Ogura, & Honma, 2018). Predicting Small-Molecule Pharmacokinetic and Toxicity Properties Using Graph-Based Signatures (pkCSM) were used to analyze Lipinski's rule of five, various pharmacokinetic properties, and drug likeliness.

3.12 Redocking using Glide Schrodinger 2019-2

To validate the docking study done by AutoDock4.2, we have revalidated through Glide v8.3, Schrodinger, LLC, New York, NY, 2019-2. First ligands and protein were prepared and then docking was performed.

3.12.1 Ligand preparation

Energy minimization of all the 16 compounds were done using the OPLS-2005 force field (LigPrep, Glide-v8.3 Schrodinger, LLC, New York, NY, 2019-2). Further ligands were processed using the LigPrep module a part of the Schrodinger suite which can generate different types of structures from each input structure with various tautomers, ionization states, ring conformations, and stereochemical characteristics (Shan, Klepeis, Eastwood, Dror, & Shaw, 2005).

3.12.2 Protein and grid preparation

SARS-CoV-2-RdRp-NiRAN domain was used for protein preparation using the protein preparation wizard of Maestro program v10.2, a part of the Schrodinger suite (Schrodinger, LLC, New York, NY, 2019-2). Default parameters (missing atoms update, optimization, and minimization) were used to prepare the protein/receptor. The grid box was created using receptor grid generation program Glide v8.3, Schrodinger, LLC, New York, NY, 2019-2 (Halgren et al., 2004). Grid was generated after optimization and minimization of protein and the dimensions of the inner box were kept X=20, Y=20, Z=20, and dimensions of the outer box were as kept X=36, Y=36, Z=36 around 5 A° of the residues predicted by CASTp in the cavity.

3.12.3 Molecular docking

Flexible docking was performed using Glide v8.3, Schrodinger 2019-2 to evaluate the docking score, glide score and glide e-model of all the prepared ligands against the SARS-CoV-2-RdRp- NiRAN domain using Glide v8.3, Schrodinger 2019-2.

Different conformations of the ligands were allowed to interact and generate docking score, glide score, and glide e-mode with protein. Best conformation of ligand based on docking score was evaluated against the SARS-CoV-2-RdRp-NiRAN domain. Docking score is a collective scoring of term consists of Vander Waals energy, Coulomb energy, lipophilic term, hydrogen bond term, metal-binding term, rewards, and penalties.

Docking results were evaluated based on the scoring function given by Glide G-score, which can be represented as:

Where in the formula: this, Lipo = hydrophobic interactions, Metal = metal binding, BuryP = buried polar group penalty, RotB = penalty for freezing rotatable bonds and Site = polar interactions existing in the active site represented.

3.13 Molecular mechanics-generalized born surface area (MMGBSA)

After docking the compounds which have the best docking scores and suitable ADMET properties were selected for Prime molecular mechanics-generalized born surface area (MMGBSA). The structure of receptor and ligand complex which were obtained from molecular docking were used for the MMGBSA study. MMGBSA is useful for the determination of the ligand binding energy calculation (Prime, version 2.1, Schrodinger, LLC, New York, 2011). Minimizations of the receptor and ligand complex poses were done using the local optimization feature in the Prime. OPLS-2005 is the force field used in the Generalized-Born/Surface Area continuum solvent model for the calculation of the energies of the complexes. Ligand strain energy was also calculated during the MMGBSA.

3.14 Molecular dynamics simulation study

In this study, MD simulations were done using Desmond a module of the Schrodinger suite to evaluate the stability of the protein-ligand complex. Protein-ligand RMSD, root mean square fluctuation (RMSF), and protein-ligand contacts. Bar graphs were analyzed to assess the stability and conformational behaviour of

the protein-ligand complex along with the entire 100 ns simulation.

3.14.1 System building

System building of the complex was done using System builder, desmond, Schrodinger, LLC, New York, NY, 2019-1. As the solvent model, the TIP3P water model was used. For the neutralization and stabilization of the solution system (Gupta et al., 2020), we used the default parameters of recalculating the addition of ions and salt addition (0.15 M of NaCl) in an orthorhombic solvent box of dimensions (the distance of 10 × 10 × 10 Å and angle of 90 ×90 × 90 degrees) to cover the complex completely and provide the environment for Molecular dynamics simulation.

3.14.2 Molecular Dynamic simulation

MD simulation was performed using Desmond, Schrodinger, LLC, New York, NY, 2019-1. Molecular dynamics simulation of the complex was performed after the system-building of the SARS-CoV-2-RdRp-NiRAN domain-ligand complex was completed. The build system of the complex was loaded for MD simulation each for 100 ns. All the parameters like recording interval (ps), energy, trajectory, NPT (temperature- 300 K, pressure = 1.01325 bar) were followed as the default value, and checkpoint interval of the simulation was kept at 240.06 ps (Aduri et al., 2019; Chaudhary, Singh, Varadwaj, & Mani, 2020). Each of the simulations was performed for 100 ns.

Chapter 4

Results

4.1 Oral rinses in growth inhibition and treatment of *Helicobacter pylori* infection

4.1.1 Gastric biopsy and juice collection from gastritis patients for isolation of *H. pylori*

To date, there are no *H. pylori* isolates reported from central India to the best of our knowledge. Moreover, isolates from northern and southern India have been listed in previous reports (Kauser et al., 2005). *H. pylori* were successfully isolated from five out of 14 biopsy samples and four out of 11 juice samples (Table 4.1.1). After observation in antibiotic selective media, Gram staining was performed on all isolates (Fig 4.1.1). Further, three clinical isolates from biopsies and one from juice were subjected for the amplification of *H. pylori* (16 s rRNA) through qRT-PCR. Additionally, validation of the clinical isolates was confirmed through nucleotide sequencing (data not shown). Furthermore, the growth of bacteria may be attributed to its pathogenic ability; hence we have studied the growth pattern of the isolated *H. pylori* and compared it with the reference strain (I10).

Table 4.1.1: Gastric biopsy and juice collection from gastritis patients

S. No	Sample HB	HJ	Sex	RUT status	Grown sample	
1	√	√	F	+	HB1	HJ1
2	√	√	M	+	-	-
3	√	√	M	+	-	-
4	√	×	M	+	HB4	-
5	√	×	M	+	HB5	-
6	√	×	M	+	-	-
7	√	√	M	+	-	-
8	√	√	F	+	-	-
9	√	√	F	+	-	HJ9
10	√	√	M	+	HB10	HJ10
11	√	√	M	+	-	-
12	√	√	M	+	-	-
13	√	√	F	+	-	-
14	√	√	F	+	HB14	HJ14

HB- Gastric biopsy, HJ- Gastric juice

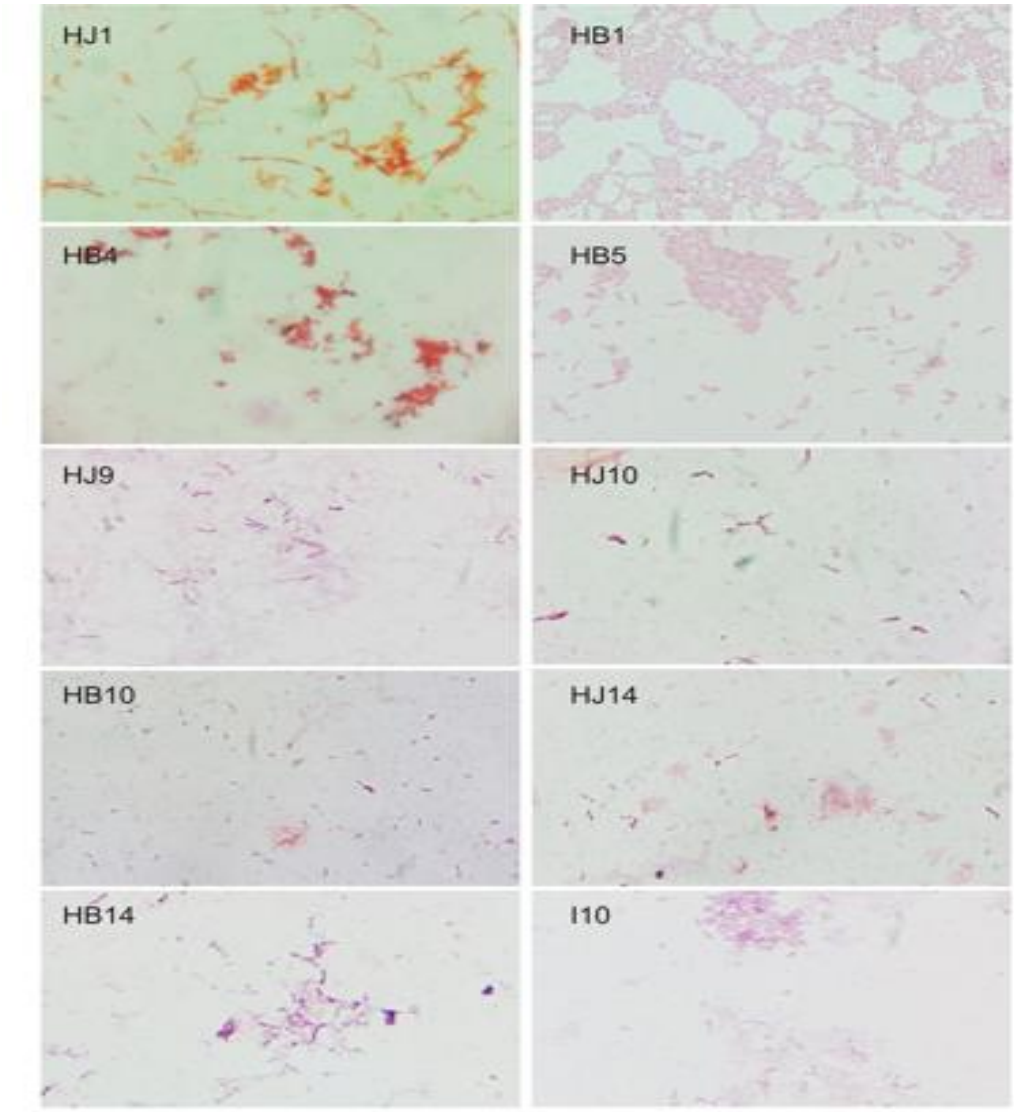

Fig 4.1.1: Identification of bacteria through Gram staining. Gram staining of different clinical isolates of *H. pylori*, namely, I10, HJ9, HB10, HJ10, HB14, HJ14, HB1, HJ1, HB4, and HB5 were showing typical gram-negative bacteria

4.1.2 The growth pattern of different clinical isolates of *H. pylori*

The growth curve of confirmed strains of *H. pylori* was determined by recording OD at 600 nm at various time points (0, 2, 6, 12, 18, and 24 h) and a the curve was plotted (Fig 4.1.2 a). Our results revealed that the growth of two clinical strains, namely HB1 and HB5 was significantly faster ($p < 0.05$) compared to the other seven clinical and one reference strain (I10). Interestingly, HB1 and HB5 have similar while not identical growth patterns at all examined time points (Fig. 4.1.2a).

It is also fascinating that the growth pattern of HB1 and HJ1 was quite different, even though they were isolated from the same patient (Fig 4.1.2a). Moreover, other clinical strains (HB4, HJ9, HJ10, HB10, HJ14, and HB14) shows a similar growth pattern as I10 until 24 h. To better understand the growth pattern of isolated *H. pylori*, graphs were plotted in the form of a bar chart at all recorded time points (0, 2, 6, 12, 18, and 24 h) and were compared with the reference strain (I10) (Fig .4.1.2b). Three to five folds faster growth was observed in HB1 and HB5 compared to I10 at 2 h, and further, it increased up to 24 h (Fig 4.1.2b). Moreover, isolates such as HJ1, HB10, and HB14 were showing moderately higher growth (3 to 5 folds) compared to reference strain I10 from 6 h onwards (Fig 4.1.2b). Importantly, the growth of HB1 and HB5 was steadily increasing up to 18 h. Hence, our study reflected two fast-growing strains (HB1 and HB5) compared to other clinical isolates HJ1, HB4, HJ9, HJ10, HB10, HB14, HJ14, and reference strain I10 (Fig 4.1.2b).

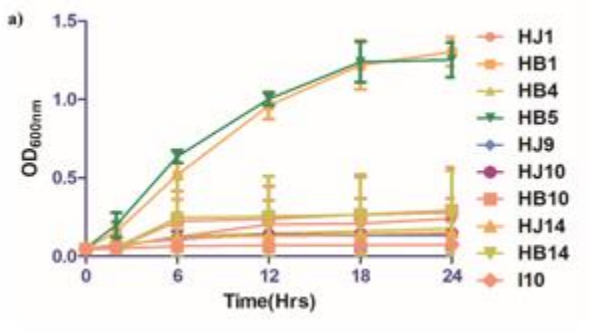

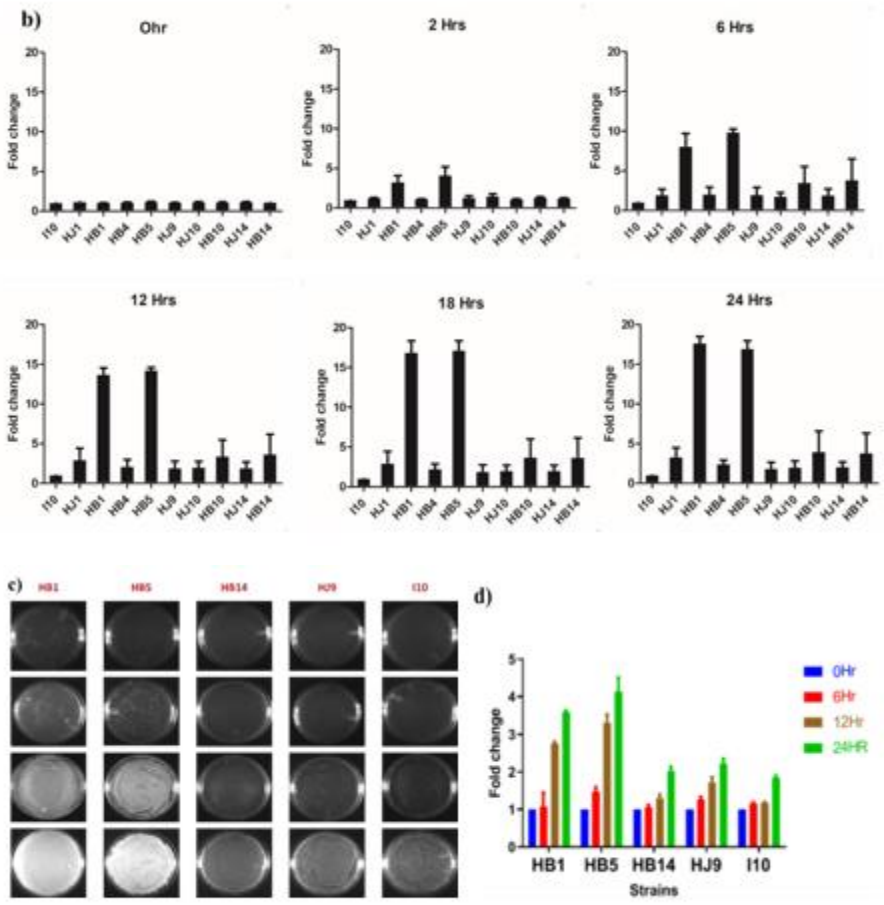

Fig 4.1.2: Growth pattern of isolated *H. pylori* strains. a) The growth pattern of clinical isolates (HJ1, HB1, HB4, HB5, HJ9, HJ10, HB10, HJ14, HB14) and reference strain (I10) under specific microaerophilic conditions assessed at 0, 6, 12, 18, and 24 h. The data are the mean ± SD (n = 4) of two independent experiments with technical replicates. b: Graphs are plotted for relative growth in comparison to I10 at 0, 2, 6, 12, 18, and 24 h. c Plate densitometry image of selected *H. pylori* isolate HB1 (lane first); HB5 (lane second); HB14 (lane third); HJ9 (lane fourth); and I10 (lane fifth) are showing growth till 24 h. The experiment is performed in duplicates, and the representative images are shown. d Fold change was calculated in comparison to 0 h.

4.1.3 Confirmation of active component of oral rinses through LC-MS

The active components in the oral rinses of A, B, C, D, and E were reconfirmed through LCMS at the Sophisticated Instrument Centre facility at IIT Indore (Fig 4.1.3). The results validate the presence of labelled active components in them. We have got exact mass spectra at 304.5, 253, 205.1, 212.1, and 102.12 for CPC, chlorhexidine, clove oil, thymol, and povidone/iodine respectively (Fig 4.1.3). Further, to evaluate the efficacy of selected oral rinses *H. pylori* growth analysis after treatment was performed.

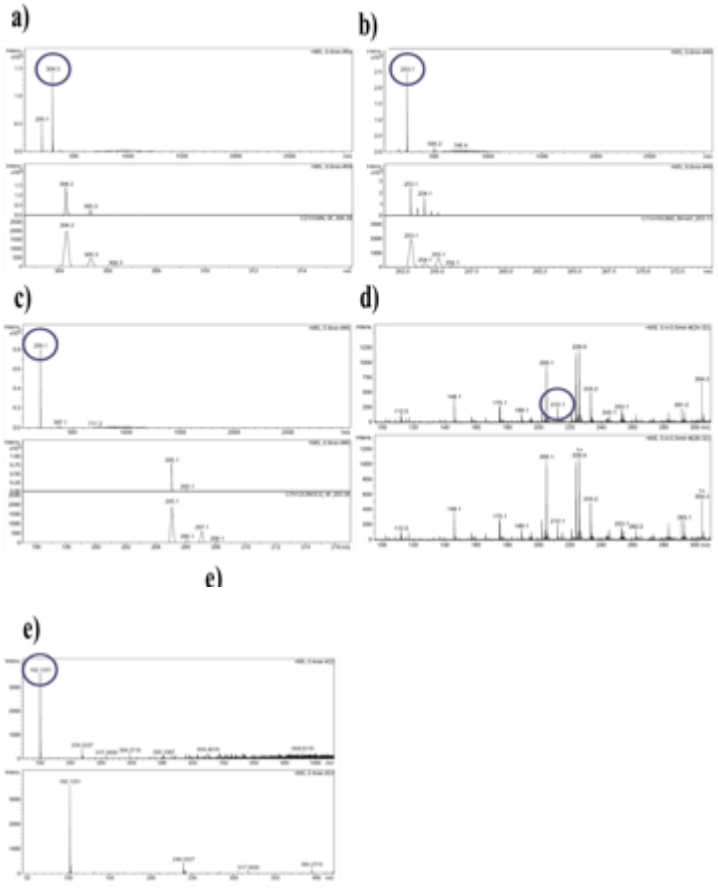

Fig 4.1.3: Confirmation of chemical plaque control agents through LCMS

4.1.4 The growth pattern of selected clinical isolates of *H. pylori* after treatment with oral rinses

All chosen oral solutions recommend 30 s oral rinsing for effective plaque control. Further, our two fast-growing (HB1 and HB5), two slow-growing (HJ9 and HB14), and a reference strain (I10) were selected for this experiment (Fig 4.1.4a, b, c, d).

Interestingly, we observed that oral rinses A and C were not able to stop the growth of fast-growing strain after 30 s treatment (Fig 4.1.4a). Although, the growth of fast-growing strain was again increased after 2 h post-treatment with solution A and C while solution B, D, and E were able to inhibit the growth until 24 h post-treatment. We have found that solution A was least efficient in the control of HB1 growth followed by C. The substantial growth of HB1 was observed from 6 h onwards when treated with solution A and 12 h post-treatment when treated with oral rinse C (Fig 4.1.4c). Moreover, the growth of another fast-growing strain, HB5, treated with oral rinses A and C, was suppressed until only 2 h (Fig 4.1.4c). There was considerable growth of HB5; 6 h onwards with A, and C treatment. Importantly, oral rinses B, D, and E were able to suppress the growth of HB1 and HB5 until 24 h in this study (Fig 4.1.4a, c). Additionally, slow-growing strains such as HJ9 and HB14 were not able to grow until 12 h with all used oral solutions (Fig 4.1.4b). However, these strains start growing from 12 h onwards when treated with solution C (Fig 4.1.4b). Notably, our reference strain, I10, has not shown any growth after treatment with all oral rinses until 24h (Fig 4.1.4b, d). In all these experiments, we have used untreated strains as positive controls and culture media as negative control. A combination of effective oral rinses was used to evaluate their efficacy on treatment for a shorter duration.

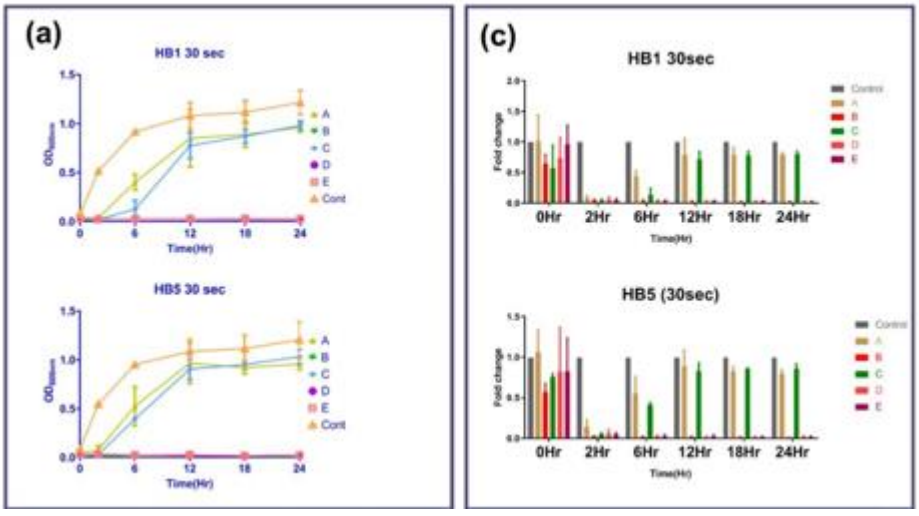

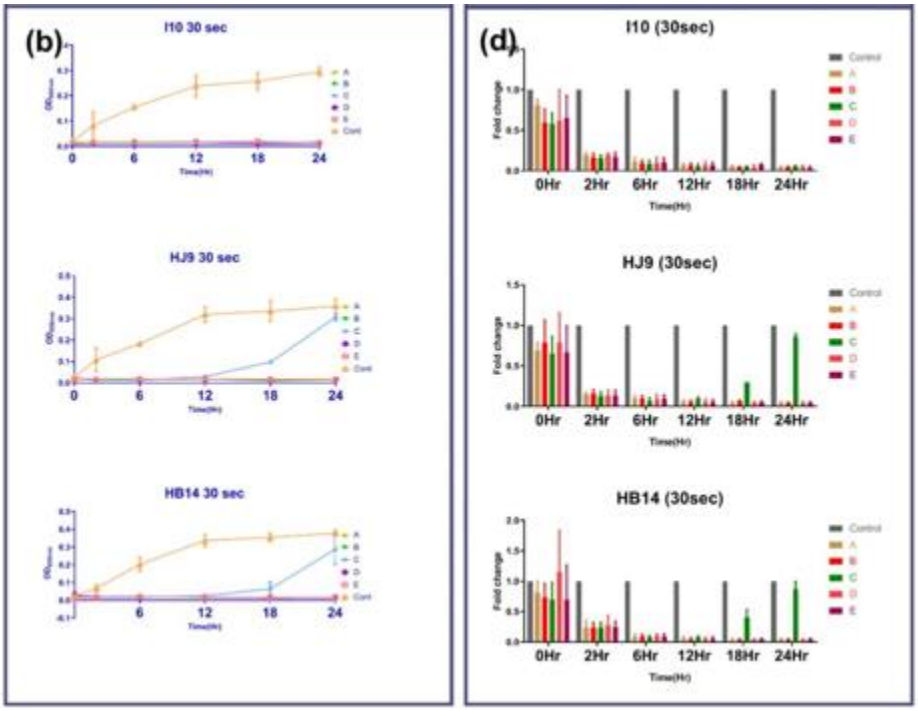

Fig 4.1.4: Growth pattern of *H. pylori* isolates after treatment with oral rinses for 30 s. Treatment of oral rinses A, B, C, D, and E) was given to 6X107 of *H. pylori* for 30 s, and growth was observed until 24 h compared to untreated control. Graphs reflect the growth of (a) fast (HB1 and HB5) and (b) slow-growing (HJ9, HB14, and I10) isolates. Relative growth of (c) fast (HB1 and HB5) (d) slow-growing (I10, HJ9, and HB14) was estimated compared to untreated control. The data are the mean ± SD of two independent experiments with technical replicate (n = 4, mean ± SD)

4.1.4.1 Selective oral rinses are restricting *H. pylori* growth even at shorter exposure

Oral rinse B, D, and E were found to be effective in controlling the growth of slow as well as fast-growing strains at 30 s treatment. Hence, we investigated the effect of these selected solutions, alone (B, D, and E) and in combination, (BD, BE, DE, and BDE) for a shorter duration of treatment (5 s) compared to recommended 30 s (Fig. 4.1.4.1a, b). Even the 5 s treatment to fast-growing *H. pylori* isolates with all efficacious oral rinses alone and in combination were able to restrict the growth until 2 h (Fig 4.1.4.1a, c). Surprisingly, data recorded 6 h posttreatment were demonstrating the growth of HB1 and HB5 with D, E, and their combinations.

Importantly, all groups in which solution B is included show to be restricting the growth of HB1 and HB5 (Fig 4.1.4.1a, c). Interestingly, the growth of slow-growing strains HJ9, HB14, and reference strain I10, completely abolished with all the above solution combinations till 24 h (Fig 4.1.4.1b). Moreover, when we treated these oral rinses for 10 s alone and in combination, a similar pattern was established as with 30 s (Fig. 4.1.4.2).

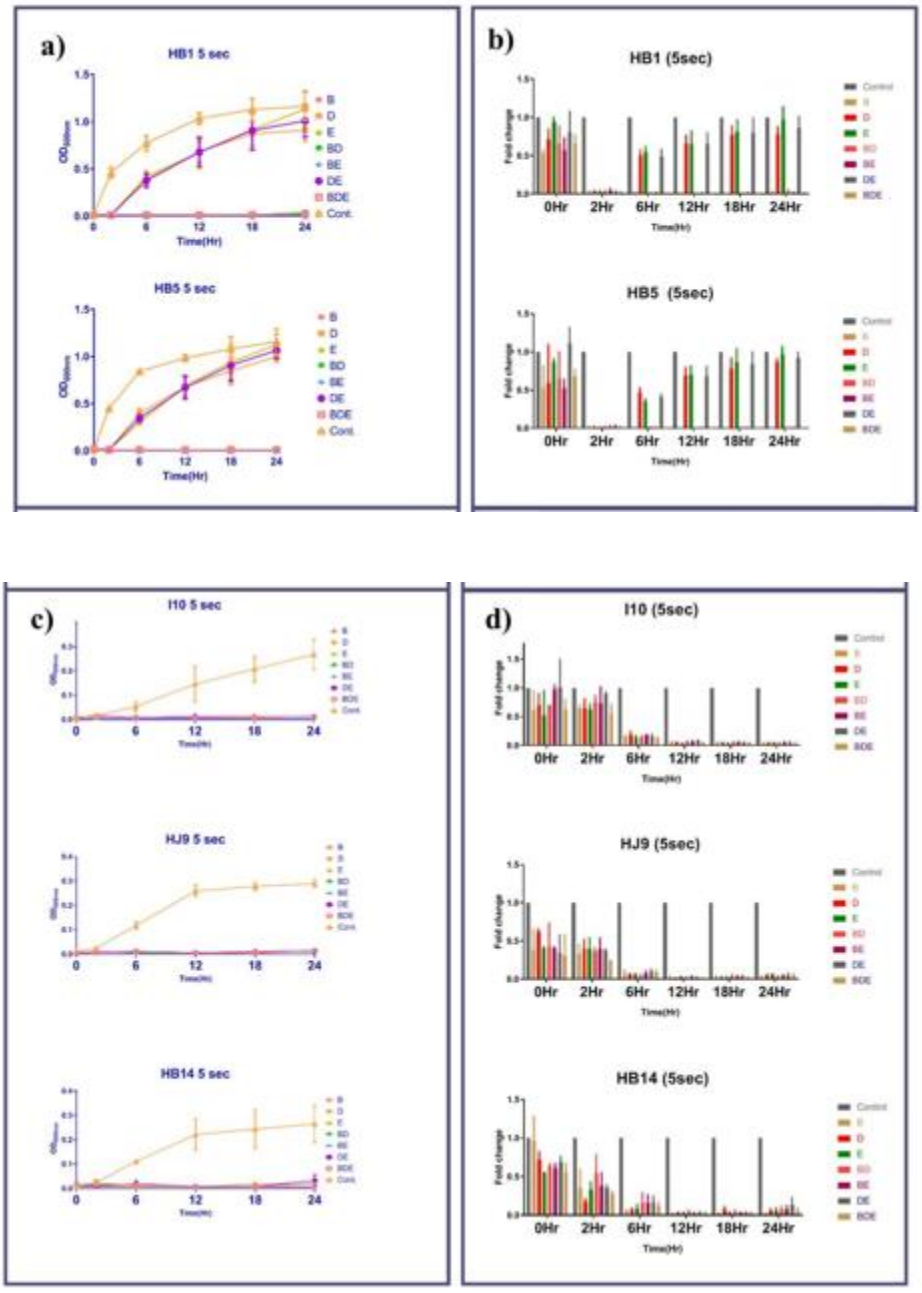

Fig 4.1.4.1: Treatment with selected oral rinses for a shorter duration. 6X107 of *H.*

pylori were treated with selected oral rinse alone and in combination (B, D, E, BD, BE, DE, and BDE) for 5 s. Growth was observed until 24 h in comparison to untreated control. Growth curve of (a) fast-growing isolates (HB1 and HB5) and (b) slow-growing isolates (HJ9, HB14, and I10). Relative growth of fast HB1 and HB5 (c) and in of slow-growing I10, HJ9, and HB14

(d) compared to untreated control. The data are the mean ± SD of two independent experiments with technical replicate (n = 4, mean ± SD)

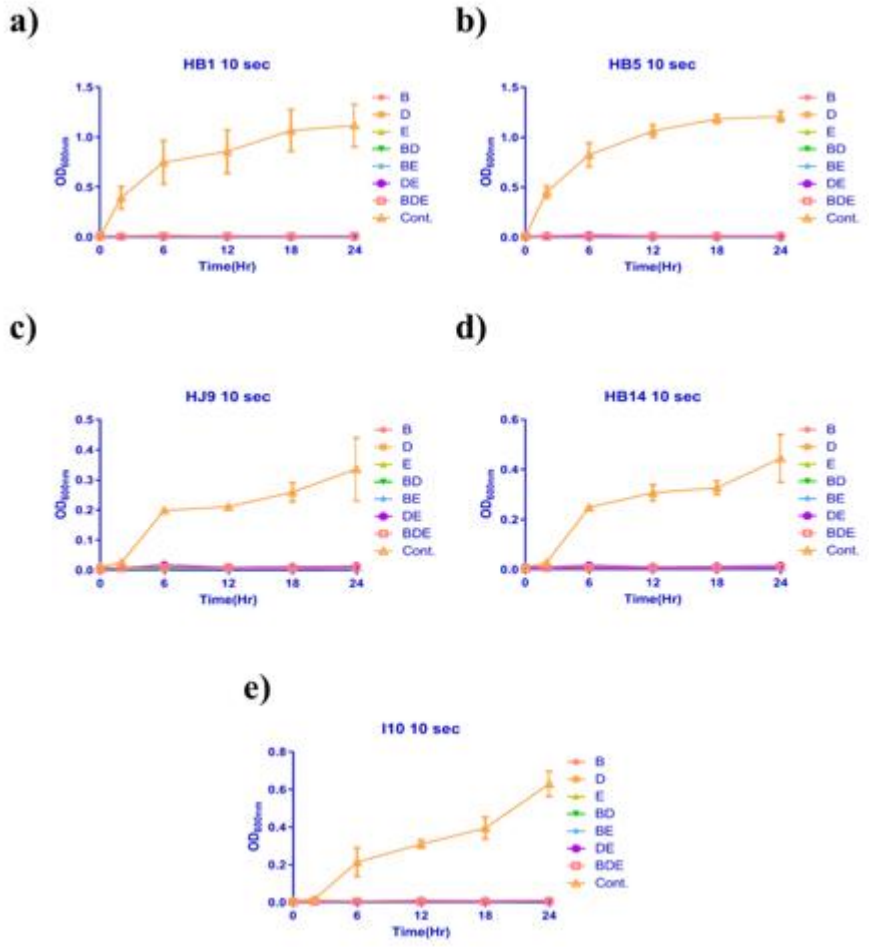

Fig 4.1.4.2: Growth pattern of *H. pylori* isolates after treatment of solutions for 10 s.

4.1.4.2 The growthpattern of *H. pylori* after oral rinses treatment on BHI agar plate

In addition to solution treatment in liquid culture, we further evaluated the growth pattern of *H. pylori* isolates on a BHI agar plate after 30 s treatment with the

selected oral rinse solution. Representative pictures of the solution-treated *H. pylori* strains are shown in Fig 4.1.4.3 a, b, c, d, and e. The images were quantified using Image J software (NIH), and graphs were plotted (Fig 4.1.4.2 f, g, h, i, j). As expected, solution treatment of C was ineffective, and *H. pylori* growth was observed in the case of fast-growing HB1 and HB5 after 12 h (Fig 4.1.4.3 a, b, f, g). Moreover, we also witnessed growth after 24 h for slow-growing strains (I10, HJ9, and HB14). Surprisingly, no growth was observed in the case of oral rinse A treatment in all the strains, contrary to the growth in liquid culture (Fig 4.1.4.3). Again, as expected, no growth was detected after treatment with oral rinses B, D, and E at all the recorded time points. The solutions inhibit the *H. pylori* growth differentially; hence further, investigation of the known gastric cancer markers and *H. pylori* genes to assess the effect of oral rinses on its pathogenicity.

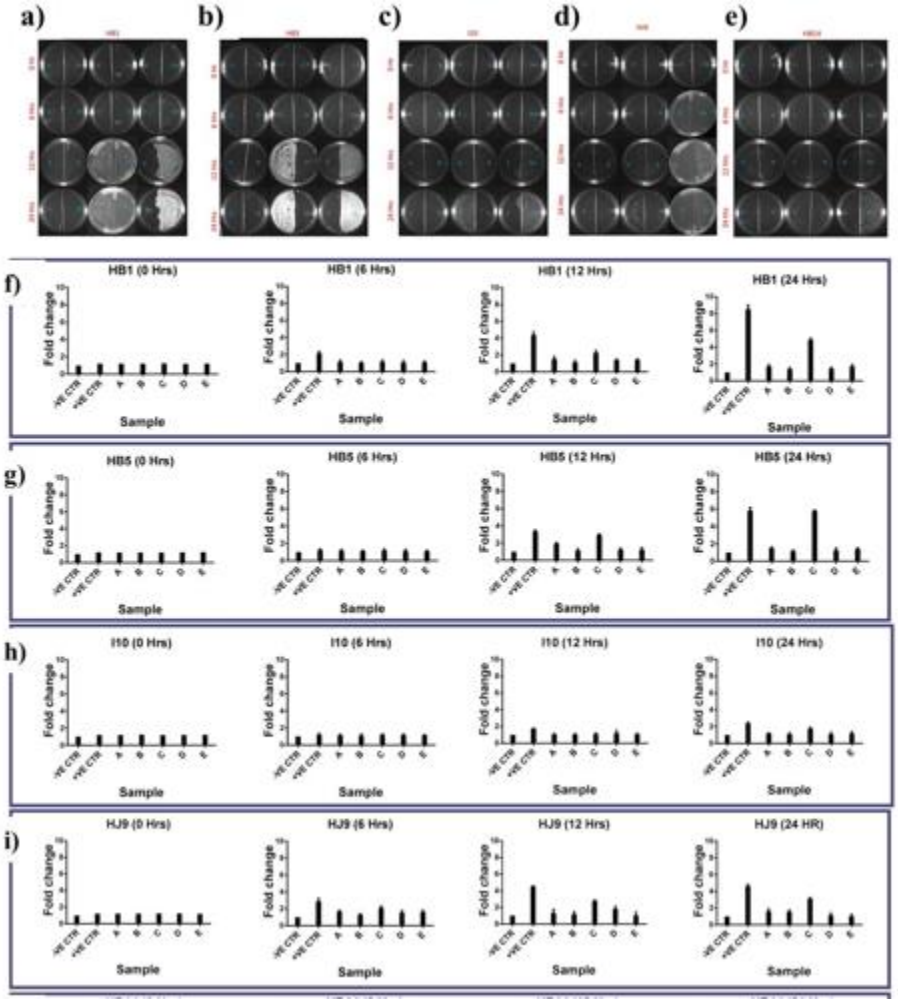

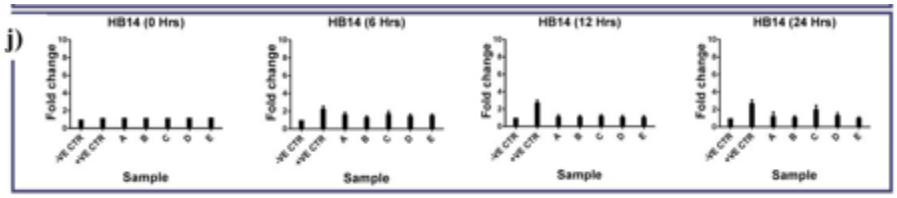

Fig 4.1.4.3: Plate densitometry of *H. pylori* after treatment with oral rinses. Oral rinses treatment of A, B, C, D, and E was given to 1X107 *H. pylori*, followed by spreading on half of the BHI Agar plate. Representative images showing growth of (a) HB1, (b) HB5, (c) I10 (d) HJ9, and (e) HB14 till 24 h Relative growth was estimated for fast-growing isolates (f) HB1 and (g) HB5; and slow-growing isolates (h) I10, (i) HJ9, and (j) HB14. Blank plates were considered as negative control and untreated isolates as a positive control. The data are the mean ± SD of two independent experiments with technical replicate (n = 4, mean ± SD)

4.1.5 Gene profiling of specific gastric cancer marker and *H. pylori* after oral rinse treatment

Expression of *H. pylori* genes, namely 16s rRNA, Cag A, and Bab A, were investigated in this experiment. Additionally, reported GC markers such as CCND1, CDX2, PTEN, and MMP7 were also included (Canales et al., 2017; Kauser et al., 2005; Shirin & Moss, 1998). A mixed expression profile was observed on treatment with oral rinses (B, C, D, and E) for 5 s in the I10 strain. On treatment with solution B, *H. pylori* genes (16 s rRNA, CagA, and BabA) and GC markers (CCND1, PTEN, and MMP7) were down-regulated. However, expression was higher in CDX2 with 5 s treatment to *H. pylori*, followed by 12 h incubation with gastric epithelial cells. *H. pylori* genes, 16 s rRNA, and Cag A are down-regulated with the treatment of C and E (except HJ9) while Bab A was down-regulated with C (Fig 4.1.5c, e). Moreover, PTEN and MMP7 were down-regulated with oral rinse solutions B, C, and E (Fig 4.1.5k, m). Interestingly, 30 s treatment to I10 was able to abolish the expression of 16s rRNA; CagA; and BabA with solution B; B, C, D, and E; and B, C, and E, respectively (Fig 4.1.5b). Our results also revealed that expression of CDX2; and MMP7 were higher with solutions C, D, E; B, C, and D respectively with the 30 s treatment at 12 h time point (Fig 4.1.5j, n). Similarly, when we treated another slow-growing strain HJ9 for 5 s with oral

rinses followed by incubation with AGS. Strikingly a mixed response in gene expression profiling. In the case of PTEN; and MMP7, the expression is moderately enhanced with solutions C, D, and E; B, C, and D, respectively. Whereas solution B and E were able to diminish the expression of PTEN and MMP7, respectively (Fig 4.15l, n). 30 s treatment of oral rinse B to the same strain followed by incubation shows slight downregulation in the expression of 16 s rRNA, CagA, BabA, CCND1, CDX2, and PTEN, however, the expression of MMP7 was an exception (Fig 4.1.5). Further, when we treated HB14, another slow-growing strain, for 5 s with oral rinses solution followed by incubation with AGS, CagA, BabA, CCND1, CDX2, and MMP7 was considerably down-regulated with solution B (Fig 4.1.5). Additionally, CCND1, CDX2, and MMP7 were minimally expressed with the treatment of B, C, and E, while PTEN is downregulated with E (Fig 4.15). Moreover, treatment of HB14 for 30 s and incubation with AGS, also leads to the downregulation of CCND1, CDX2, and PTEN with C, D, and E, while expression of MMP7 was unregulated with C, D, and E (Fig 4.1.5n). However, CagA was abolished with B, C, and D (Fig 4.1.5). Furthermore, results reflect different gene expression profiles with the treatment of 5 and 30 s in fast-growing strain HB1 (Fig 4.1.5). Expression of CagA; and BabA were down-regulated with the treatment of B, D, and E; and B, C, D, and E, respectively (Fig 4.1.5c, e). Whereas the expression of CCND1; CDX2; and MMP7 were enhanced with B, C, D, and E; E; and B, respectively (Fig 4.1.5g, i, m). Treatment for 30 s to HB1 shows a minimal expression of CagA with solution B, C, and D, while; MMP7 was up-regulated with all the oral rinses (Fig 4.1.5d, n). Induction of apoptosis in the cancer cell is one of the widely used treatment regimens against cancer (J. qiang Guo, Li, & Guo, 2017). Hence we have assessed apoptotic pathways that may be induced after growth inhibition of *H. pylori* due to the treatment of oral rinses.

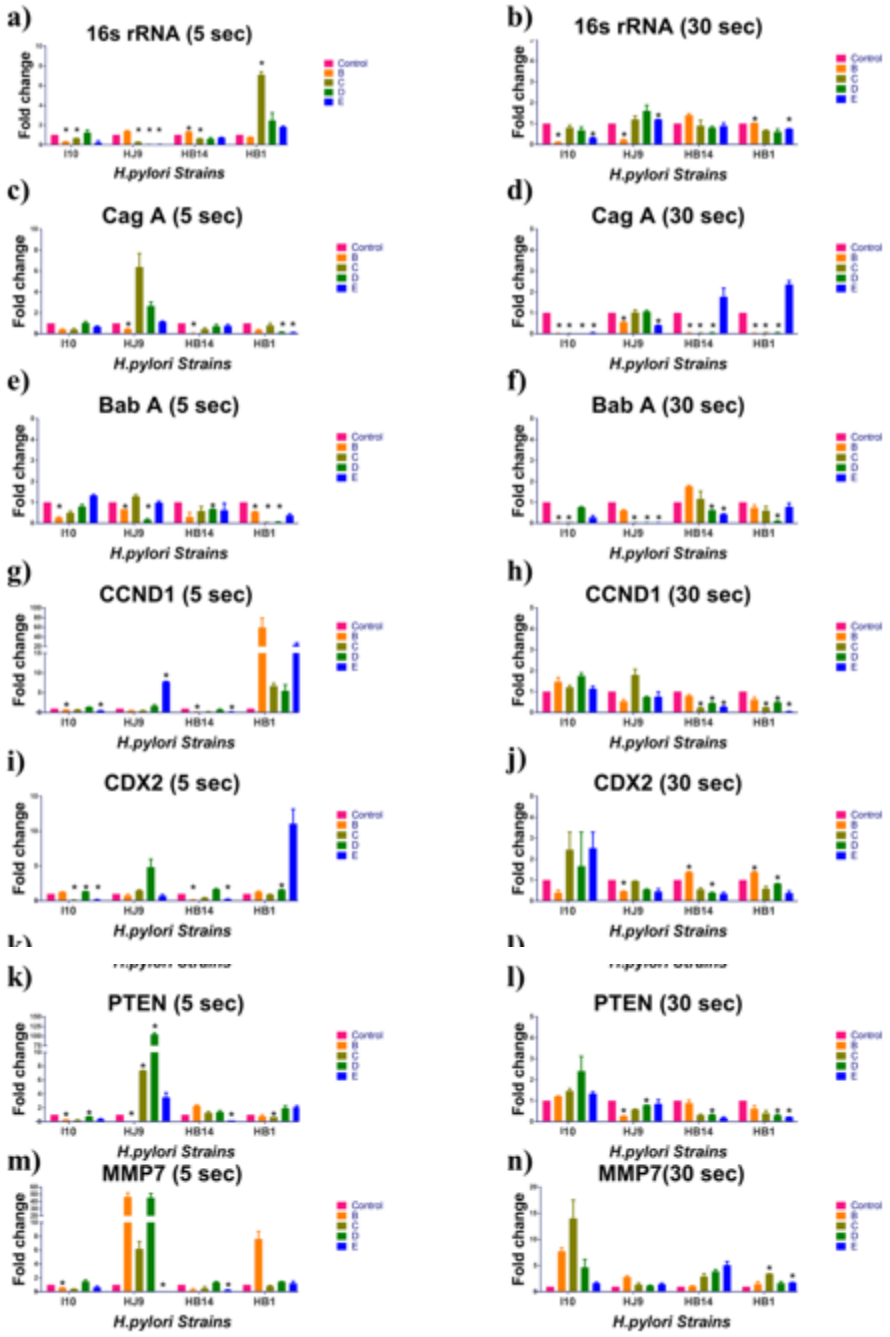

Fig 4.1.5: Investigation of *H. pylori* and gastric cancer genes: Treatment of solution was given to 6X107 of H.ylori and incubated with 0.5X106 AGS cell for 12 h. RNA was isolated, and transcript level was determined by qRTPCR. Experiments were performed in duplicates. Expression of 16 s rRNA (a, b); CagA (c, d); BabA (e, f); CCND1 (g, h); CDX2 (i, j); PTEN (k, l); MMP7 (m,

n) was evaluated on 5 and 30 s treatment respectively. AGS cells infected with wild

type *H. pylori* were treated as the control in this study

4.1.6 Status of apoptotic gene expression

Earlier studies have classified cells as live, apoptotic, and necrotic after EB/AO staining (Ogden et al., 2010). We investigated these cells (live, apoptotic, and necrotic) on infection with *H. pylori* treated with oral rinses for 30 s (Fig 4.1.6). Additionally, the evaluation of apoptotic pathways, such as intrinsic/extrinsic/independent, was performed after treatment of *H. pylori* isolates with these solutions for 5 and 30 s through qRT-PCR (Fig 4.1.7). 5 s exposure of solution D in I10 strain was able to enhance the expression of APAF1, BID, and BAK (Fig 4.1.7c, e, g). Interestingly, I10 treated with solution C and incubated with AGS cells were able to suppress all studied apoptotic genes (Fig 4.1.7). Whereas, other solutions were not able to change the expression patterns of these genes considerably. Furthermore, 30 s treatment of I10 and incubation with AGS cells show a different pattern (Fig 4.1.7). I10 treated with solution B was able to reduce the expression of all the selected genes except FADD (Fig 4.1.7). However, treatment with solution D and E were slightly enhancing the expression of all pro-apoptotic genes (Fig 4.1.7). Furthermore, when we applied these solutions for 5 s on HJ9 and incubated with AGS cells, an upsurge in APAF1 expression, while BCL-2 was found down-regulated except in solution D (Fig 4.1.7c, m). Surprisingly, 30 s treatment of HJ9 reflected a varied gene expression compared to 5 s. Oral rinse C, D, and E with 30 s exposure were able to up-regulate all apoptotic genes except NOXA and PUMA (Fig 4.1.7). However, the expression of anti-apoptotic BCL-2 was reduced with oral rinse B (Fig 4.1.7n). Application of these oral rinses for 5 s on HB14 followed by incubation with AGS cells demonstrated that oral rinse D up-regulates all pro-apoptotic genes (Fig 4.1.7). Interestingly, treatment with B was able to enhance extrinsic apoptotic regulator FADD and reduce the expression of all used intrinsic markers. It also diminished the expression of BCL-2 (Fig 4.1.7), fascinatingly, all apoptotic markers except PUMA were considerably down-regulated with the 30 s treatment of solution D (Fig 4.1.7). Moreover, the expression of FADD, APAF1, and BAK, were also reduced with solution E (Fig 4.1.7b, d, f). Furthermore, in the case of fast-growing strain, HB1,

solution C, and E were slightly up-regulating the expression of FADD, APAF1, BID, and BAK (Fig

4.1.7 a, c, e). In addition to this, solution B-treated cells were able to upregulate FADD, APAF1, BID, and NOXA (Fig 4.1.7a, c, g, k). Treatment of solution C for 30 s to the same strain showed up-regulation of FADD, BID, and PUMA (Fig 4.1.7b, h, j). In contrary to this, slight up-regulation was observed for BCL-2 in all used solutions.

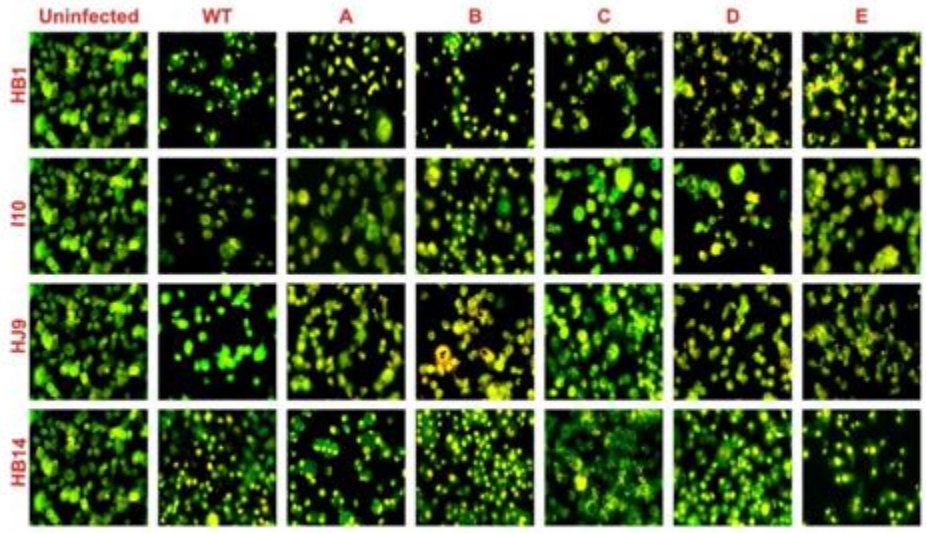

Fig 4.1.6: EB/AO dual staining assay. 0.25 ×106 AGS cells were plated in 6 well plates and infected with 30 s oral rinse solution (a, b, c, d, and e) treated and wild type (WT) *H. pylori* isolates. Furthermore, 12 h post-infection, the cells were stained with EB/AO solution, and images were acquired. (a) HB1,
(b) I10, (c) HJ9, and (d) HB14 infected and uninfected AGS cells

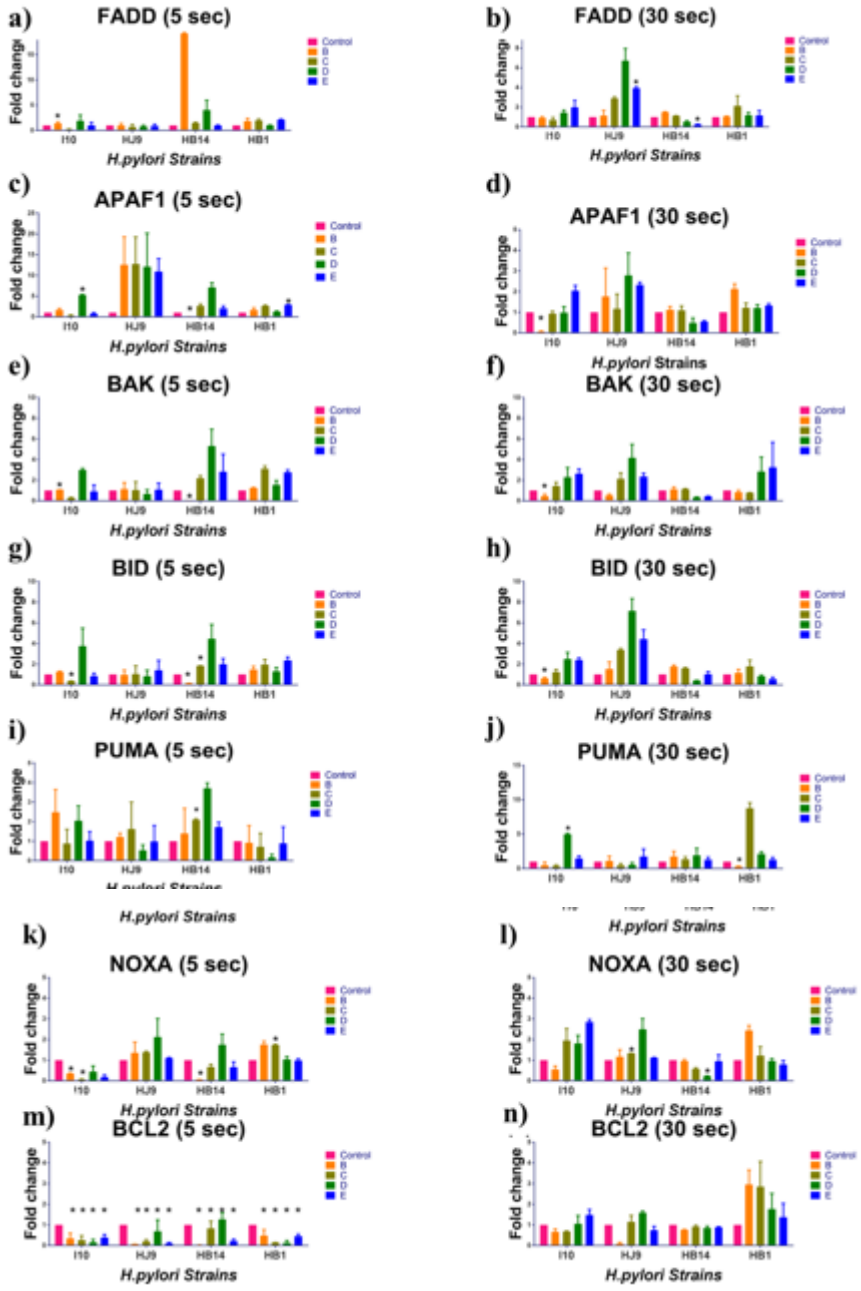

Fig 4.1.7: Status of apoptosis-related genes. Treatment of solution was given to 6X107 of *H. pylori* and incubated with 0.5X106 AGS cell for 12 h. RNA was isolated, and the transcript level was determined by qRTPCR. Experiments were performed in duplicates. Expression of (a, b) FADD; (c, d) APAF1; (e, f) BAK; (g, h) BID; (i, j) PUMA; (k, l) NOXA; and (m, n) BCL-2 was assessed after treatment for 5 and 30 s respectively. The data are the mean ± SEM of two independent experiments with technical replicate (n = 4)

4.2 Status of kinases in Epstein-Barr virus and *Helicobacter pylori* Coinfection in Gastric Cancer Cells

4.2.1 Isolation and characterization of *H. pylori* isolates

We have successfully extracted five isolates of *H. pylori* from gastric biopsy and gastric juices, namely, HB1, HB10, HJ1, HJ9, and HB14, which was followed by Gram staining, where I10 was used as reference strain (Fig. 4.2.1.1). Genomic DNA isolation was performed and a 16s RNA primer was used for the screening of the bacteria along with reference strain (Fig. 4.2.1.2). Among the five isolates, two isolates were selected for further experiments. The reference strain I10, along with two isolated strains of the *H. pylori* isolates HB1 and HJ9, were used for further experiments. The PCR was performed using *H. pylori* strains' genomic DNA as a template to amplify 16 s rRNA genes, with a product size of 110 bp (Fig. 4.2.1.3).

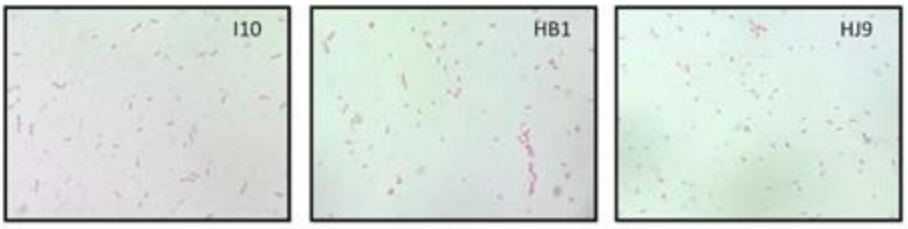

Fig 4.2.1.1: Gram's staining of *H. pylori* strain: Gram's staining of *H. pylori* strain I10 and isolates HB1, HJ9 respectively

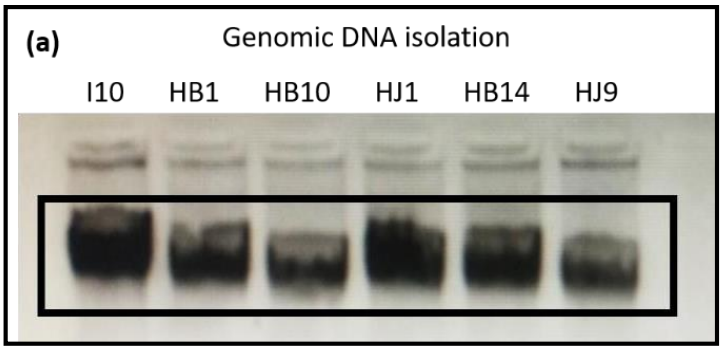

Fig 4.2.1.2: Genomic DNA isolation for samples: *H. pylori* isolates were obtained through genomic isolation for samples I10, HB1, HB10, HJ1, HB14, and HJ9.

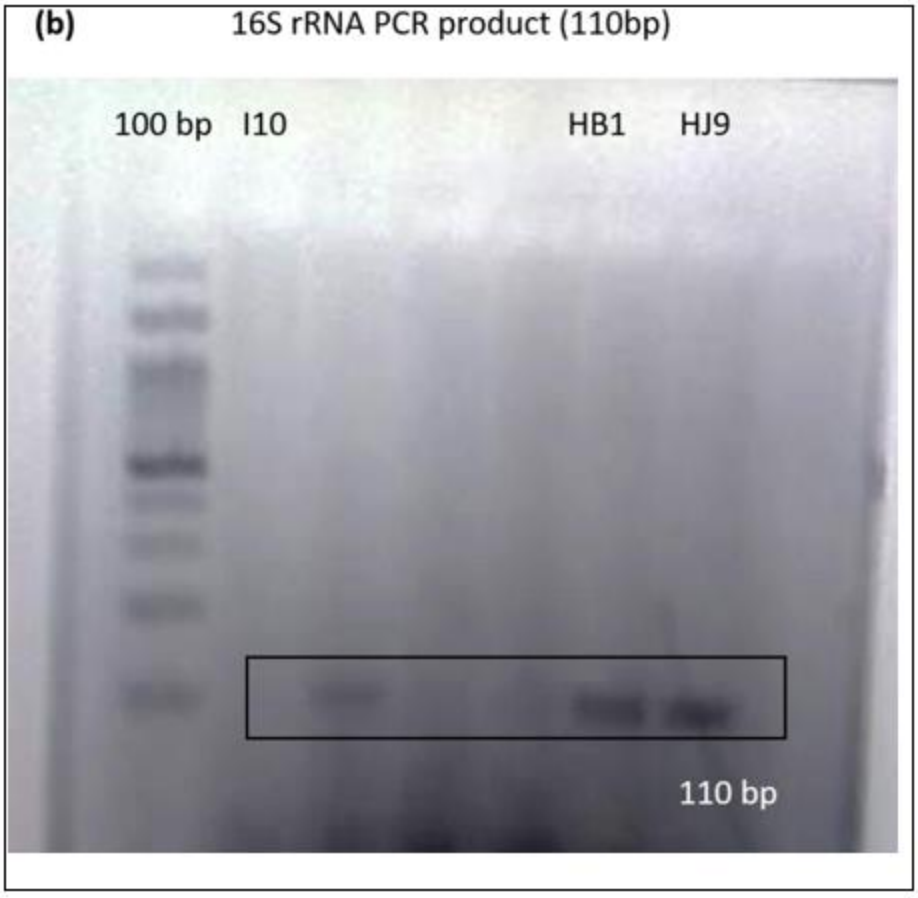

Fig 4.2.1.3: 16s PCR product of samples: 16s PCR product size of 110bp was obtained for I10, HB1, and HJ9, respectively.

4.2.2 *H. pylori* and EBV coinfection leads to morphological changes

Previous studies have shown that morphological and phenotypic changes can be detected in virus-infected cells (Foglieni et al., 2005). These cells acquire a characteristic elongated cell shape with an invasive phenotype that contributes to tumour invasion and metastasis (Safari & Jodeiry Zaer, 2017). Our data shows that similar morphological changes such as elongated tapering ends were observed in AGS infected *H. pylori* at 24 h (Selbach et al., 2003). Our results show that tapering ends of co-infected cells were found to be more elongated as compared to those seen in uninfected cells (Fig. 4.2.2.1 A I, 4.2.2.1A II). Interestingly, the co-infected AGS showed morphological changes even after 12 h of incubation, which may reflect the positive synergistic effect of EBV and *H. pylori* in cell proliferation.

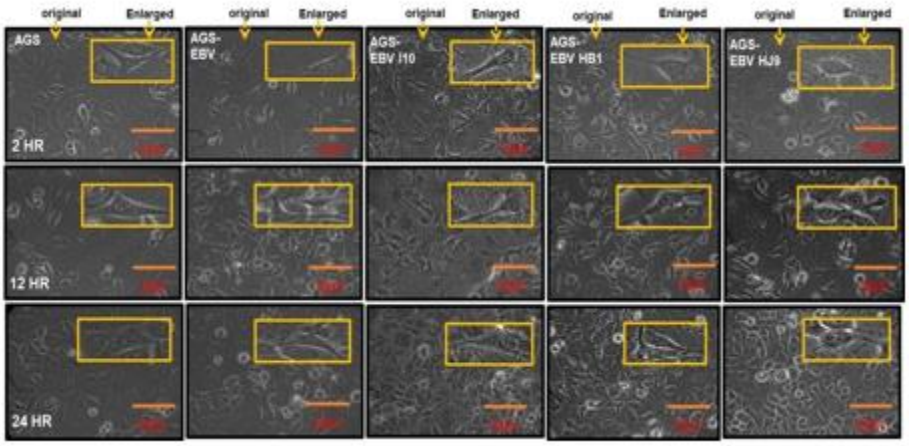

Fig. 4.2.2.1 A I: *H. pylori* and EBV co-infection lead to morphological changes. AGS cells were infected with EBV and then AGS cells were infected with EBV and *H. pylori* I10, HB1, HJ9 respectively. Changes in the number of cells and morphological changes were observed at 2 h, 12 h, and 24 h where the insert image shows the enlarged image of morphological changes.

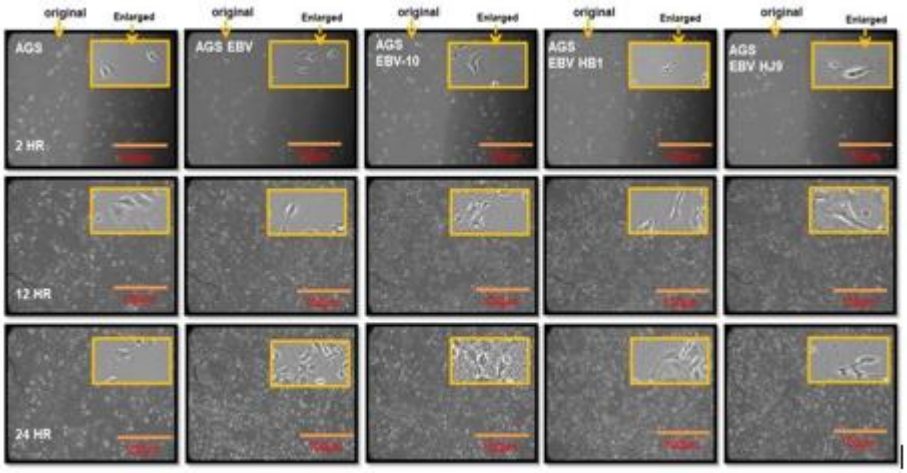

Fig 4.2.2.1A II: *H. pylori* and EBV co-infection lead to morphological changes: AGS cells were infected with EBV and then AGS cells were infected with EBV and *H. pylori* I10, HB1, HJ9 respectively. Changes in the number of cells and morphological changes were observed at 2 h, 12 h, and 24 h where the insert image shows the enlarged image of morphological changes.

The elongations in tapering ends were quantified by confocal laser scanning microscopy using DAPI stain at various time intervals such as 12, 24, 36, and 48 h, respectively (Fig. 4.2.2.1 B I). The analysis and quantification of the experimental

setup were done through Image J and Graph Pad Prism software, respectively (Fig. 4.2.2.1 B III). Our results asseverate that the maximum length projection appears at 12 h post-infection (Fig. 4.2.2.1 B II). The lengths of the sharp end of co-infected cells were measured to estimate the effect of EBV on AGS cells at 12 h incubation. Our data shows that an approximately 10 fold increase in the tapering end length was observed in comparison with the control, which suggests that EBV has a positive effect on cell growth and migration (Fig. 2B).

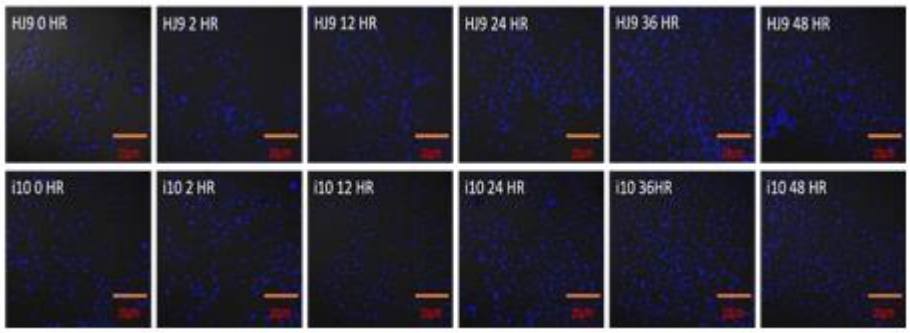

Fig 4.2.2.1 B I: *H. pylori*-infected AGS cells stained with DAPI: AGS cells were infected with I10, HJ9, and stained with DAPI and at 0, 2, 12, 24, 36, and 48 h cell length was measured through ImageJ software.

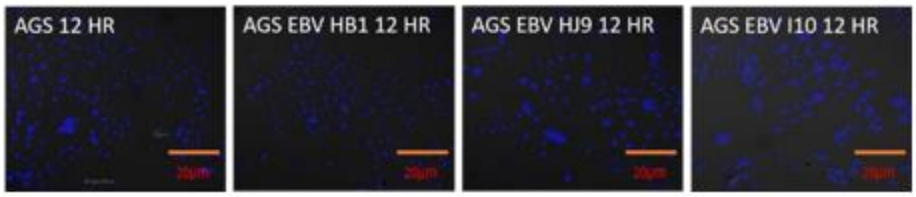

Fig 4.2.2.1 B II: Cell length measurement at 12 h: AGS cells were then infected with I10, HJ9 followed by infection with EBV in each infected cell, and cell length was measured at 12 h through image J software.

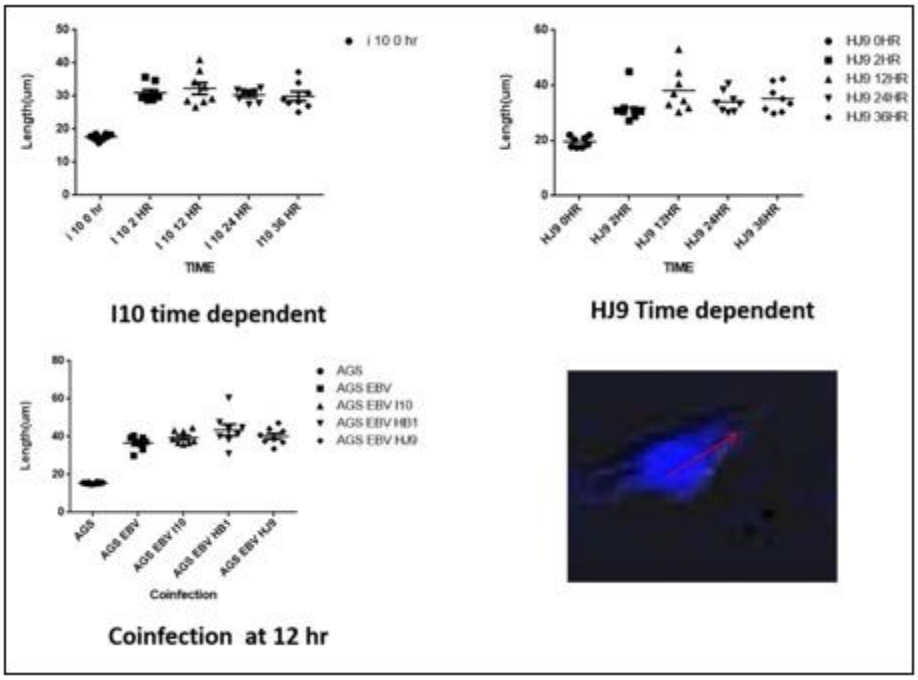

Fig 4.2.2.1 B III: Quantification of extended length was done for all experiments through Graph Pad Prism software. The single-cell DAPI stained picture of the cell determines the way the cell length is measured through the software. The arrow depicts the measurement of the cell length.

4.2.3 Effect of coinfection on cell proliferation

Previous studies have suggested that EBV and *H. pylori* both may promote cell proliferation by inducing morphological changes (Roose, Polevoy, Clevers, & Embo, 1998; Selbach, Moese, Backert, Jungblut, & Meyer, 2004). The cell proliferation assay shows a decrease in cell number when cells were infected with EBV alone. However, an increase in cell proliferation is observed when EBV infection is followed by a bacterial infection (Fig 4.2.3). Hence, our finding suggests that bacteria may provide a positive thrust for cell proliferation. In comparison with control, the cells co-infected with HJ9 showed an approximately 2 fold increase in cell proliferation at 12 h. However, in HB1 co-infected cells, no significant change in proliferation was observed till 24 h. The positive effect of bacterial co-infection on the growth of cells is strain-dependent, and it can affect the proliferation in a time-dependent manner. Interestingly, the cell number increases significantly when AGS cells are infected with EBV alone or co-infected

with *H. pylori* and EBV when compared to un-infected AGS cells.

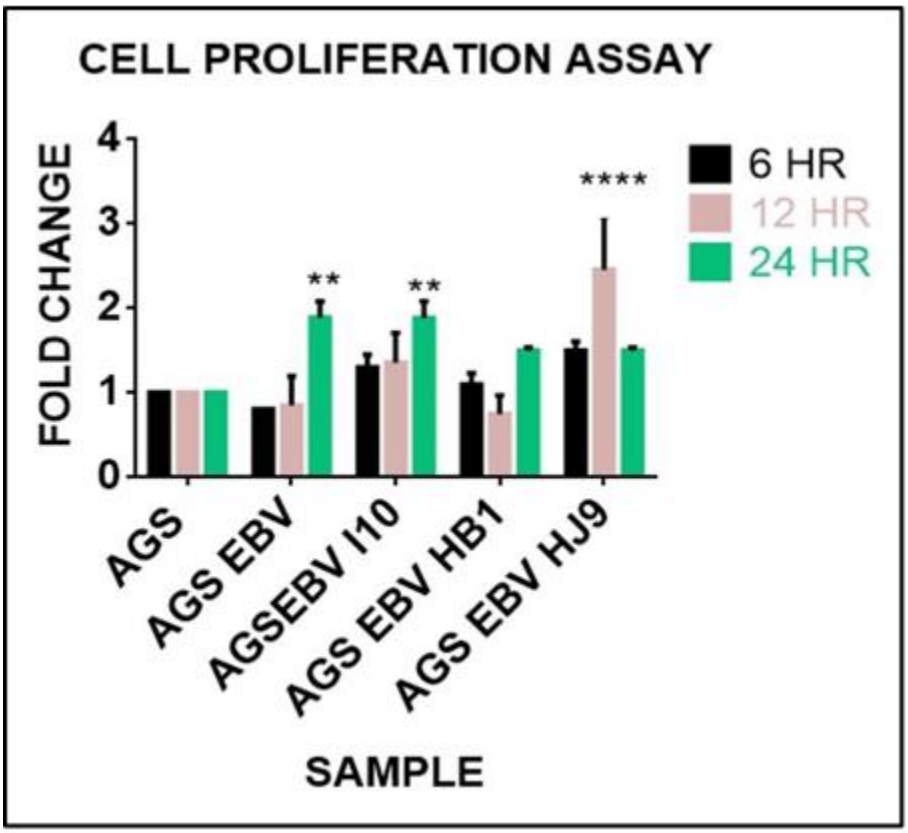

Fig 4.2.3: Effect of co-infection in cell proliferation. Cell proliferation of AGS is calculated when treated with EBV and AGS-EBV with different strains of bacteria I10, HB1, and HJ9 respectively at different time points of 6, 12, and 24 h. The results are shown as the mean SD of three independent experiments where *p<0.05, **p<0.001, ****p<0.0001 analyzed through Two-way Anova.

4.2.4 Assessment of kinase expression through a secretory and adhesive mechanism of bacteria

To evaluate differential expressions of several kinases, both direct and indirect infection methods were used (Pandey et al., 2018b). In the indirect approach, the effect of proteins secreted from bacteria was assessed; and in the direct approach, the kinases that are mostly affected by adherence were evaluated. Here, we tried to investigate the kinases of secretory and adherence pathways of *H. pylori* to get an insight into the underlying strategy which involves the cooperation of *H. pylori* in EBV-driven proliferation of gastric epithelial cells. Hence, already developed *H.*

pylori and EBV coinfection model was used for AGS human gastric epithelial cells. This model would give us access to investigate the effect of molecules secreted by *H. pylori*. Hence, we used the 0.45 µm insert, which has been used for a similar purpose in the previous reports (Basque, Chénard, Chailler, & Ménard, 2001; Pandey et al., 2018b). As the effect of adherence of *H. pylori* to gastric mucosa through CagA is linked to the severity of gastritis, it was intriguing to compare the effect of secretory proteins and adherence of bacteria in gastric cells infected with EBV (Bodger & Crabtree, 1998; N. Kim et al., 2002; Oleastro & Ménard, 2013).

All 24 kinases were screened based on their presence in GC either infected with *H. pylori* or EBV alone. Their gene expressions were evaluated at a time interval of 12, 24, and 36 h, respectively. Out of 24 genes, eight genes showed considerable changes in gene expression, which are BRAF1, ITK, TYK2, FYN, PAK1, PAK2, PDK1, and EPHB6. Among the eight genes, four genes showed significant changes in expression, which were ITK, FYN, TYK2, and EPHB6. Reports suggest a high expression of ITK, FYN, and TYK2 in GC, whereas EPHB6 showed reduced expression in GC (Kwok, Backert, Schwarz, Berger, & Meyer, 2002; Slavova, Buhr, & Bennani-baiti, 2016). According to our experimental data, TYK2 and EPHB6 transcripts were enhanced by the indirect coinfection approach, whereas the other two genes, like FYN and ITK, were observed to be up-regulated in the direct coinfection approach (Fig 4.2.4).

In the direct approach at 12 h incubation, ITK was found to be significantly down-regulated in AGS cells co-infected with EBV-I10, EBV-HB1, and EBV- HJ9 compared to controls at 12 h time point. Interestingly, ITK was slightly down-regulated in AGS-EBV compared to control AGS cells. However, there is a slight down-regulation of the ITK gene in AGS-EBV infected cells in comparison with AGS (Fig 4.2.4.1 A.1). Additionally, the FYN gene transcript showed non-significant changes in AGS-EBV and EBV-I10. However, FYN levels were considerably up-regulated in EBV-HB1 and EBV-HJ9 (Fig 4.2.4.1 A.2). Noticeably, FYN expression was 2.5-fold higher. Hence, in comparison to AGS within EBV-I10, EBV-HB1 and EBV-HJ9 showed about 2.5-fold increases in expression in FYN when compared to controls. Further, the TYK2 gene transcript

showed down-regulation in AGS-EBV and EBV-HB1 while showed enhanced up-regulation in EBV-I10 and EBV-HJ9 (Fig 4.2.4.1 A.3). The EPHB6 gene transcript showed more than 6-fold was up-regulated by AGS-EBV and EBV-HB1, while, coinfection groups such as EBV-I10 and EBV-HJ9 showed more than 2.5-fold and 10-fold enhanced expression, respectively (Fig 4.2.4.1 A.4). Therefore, based on the gene expression profiling, it is clear that TYK2 and EPHB6 may have a pivotal role in early prognosis and pathway determination.

Furthermore, at a 24 h time point, ITK expression does not vary significantly in AGS-EBV and EBV-HB1, while considerable down-regulation was observed showing a mild and significant decrease in expression in EBV-I10 and EBV-HJ9, respectively (Fig 4.2.4.1 B 1). However, FYN expression showed a 2.5 to a 60,000-fold increase in expression of AGS-EBV and EBV- HJ9, respectively. Additionally, EBV-HB1 showed a slight increase in expression, whereas EBV-I10 showed no remarkable changes in gene expression in comparison to AGS (Fig 4.2.4.1 B 2). The TYK2 expression was significantly reduced in both EBV-I10 and EBV-HJ9 while showing no noticeable changes in AGS-EBV and EBV-HB1 (Fig 4.2.4.1 B 3). The EPHB6 expression level was found to be detected mildly and significantly less in EBV-HB1 and EBV-HJ9, respectively, while no changes were observed in the expression of EPHB6 in AGS-EBV and EBV-I10 respectively (Fig 4.2.4.1 B 4). Importantly, there were no significant changes observed at 36 h in these cells (Fig 4.2.4.1 C).

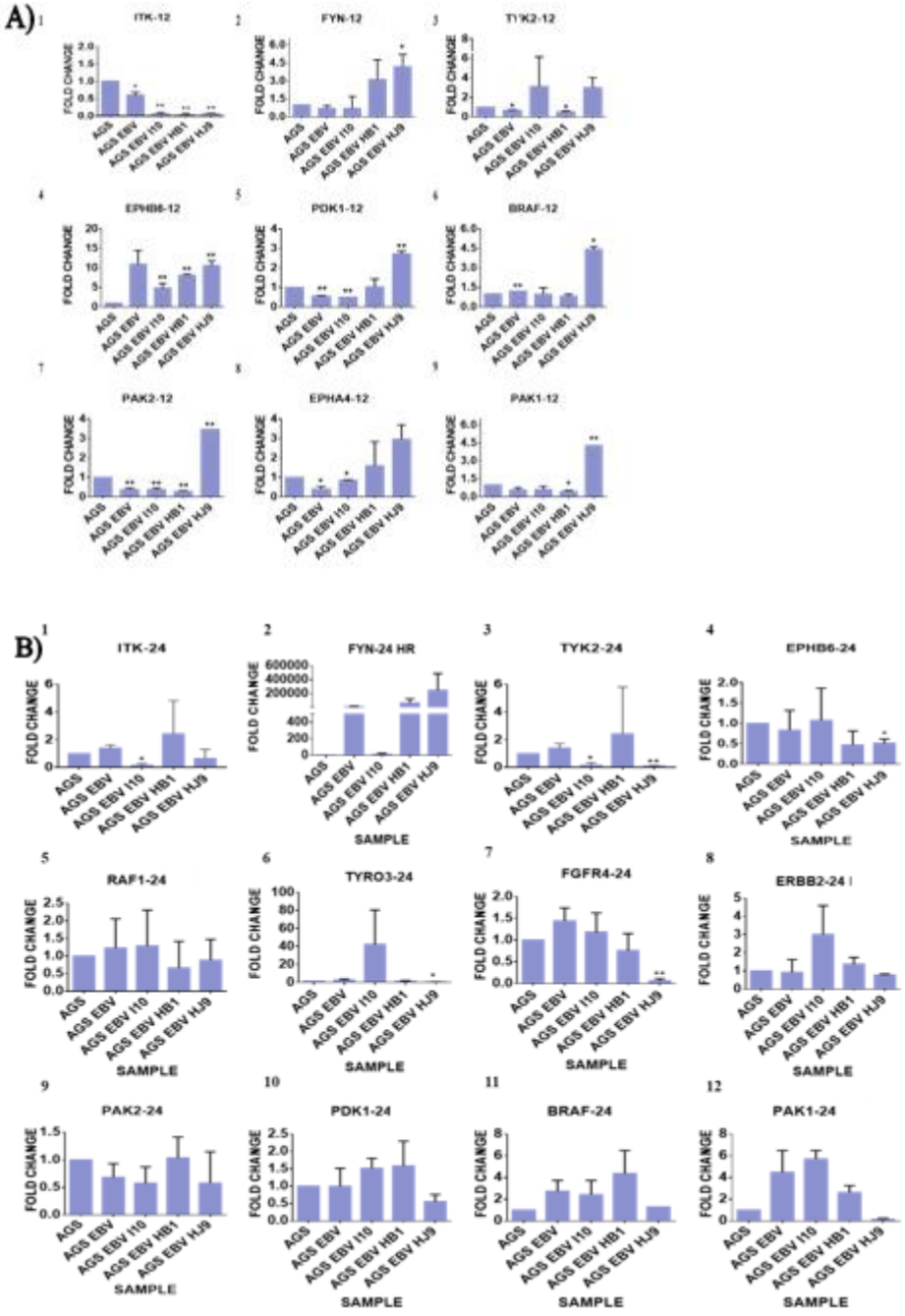
A)
ITK-12
FYN-12
TYK2-12
EPHB6-12
PDK1-12
BRAF-12
PAK2-12
EPHA4-12
PAK1-12
FOLD CHANGE
AGS
AGS EBV
AGS EBV I10
AGS EBV HB1
AGS EBV HJ9
B)
ITK-24
FYN-24 HR
TYK2-24
EPHB6-24
RAF1-24
TYRO3-24
FGFR4-24
ERBB2-24
PAK2-24
PDK1-24
BRAF-24
PAK1-24
FOLD CHANGE
SAMPLE

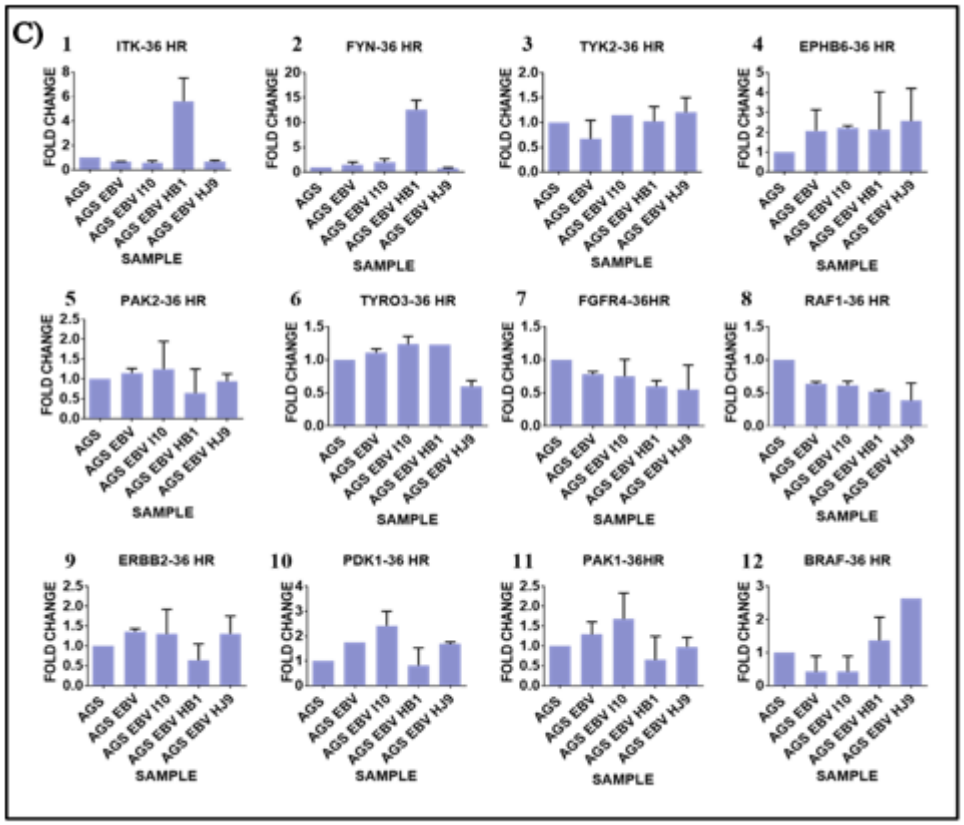

Fig 4.2.4.1: Assessment of kinase expression adhesive mechanism of bacteria. Gene's expressions were shown with the direct and indirect approach at different time points. A, B, C at 12, 24, and 36 h respectively. Where "-" indicates experiment performed without insert i.e direct approach.

In the indirect approach at 12 h, ITK and FYN expression were significantly increased from about 6-10-fold and 10-50 folds in EBV-I10 and EBV-HJ9, respectively (Fig 4.2.4.2 A 1, A 2). In comparison, these genes showed no significant changes in AGS-EBV and EBV-I10. However, the TYK2 gene showed a significant decrease in the expression of EBV-HJ9 and EBV-HB1, while no considerable changes were observed in AGS-EBV and EBV-I10 (Fig 4.2.4.2 A 3). The EPHB6 gene transcript showed a more than 10fold increase in AGS-EBV and EBV-HJ9, and more than 6-fold increases in EBV-I10 and EBV-HB1 (Fig 4.2.4.2 A 4). ITK gene expression at 24 h showed more than 10,000-to-50,000-fold increases in EBV-HB1 and AGS-EBV, respectively, whereas 20-fold increases is observed in EBV-HJ9 (Fig 4.2.4.2 B 1). In the FYN gene, no significant changes

were observed in AGS-EBV, while more than 2.5-, 10-, and 20-fold increase in expression were observed in EBV-HJ9, EBV-I10, and EBV–HB1, respectively (Fig 4.2.4.2 B 2). The TYK2 gene expression decreased mildly, in AGS-EBV, and no changes were found in EBV-I10, while a significant increase is observed in EBV-HB1 and EBV-HJ9 (Fig 4.2.4.2 B 3). EPHB6 gene showed approx. A 20-fold increase in the expression in AGS-EBV and approx. 2.5-fold increase in EBV- HJ9, EBV- I10, and EBV-HB1, respectively (Fig 4.2.4.2 B 4). In 36 h, the ITK gene showed more than 6, 10, a 250-fold increase in AGS-EBV, EBV-I10, EBV- HB1, respectively, and a significant decrease in EBV-HJ9 (Fig 4.2.4.2 C1). The FYN gene transcript showed 17,000, 20, 250, 4-fold increased expression in AGS-EBV, EBV-I10, EBV-HB1, and EBV-HJ9, respectively (Fig 4.2.4.2 C 2). The TYK2 gene showed no significant changes in any sample (Fig 4.2.4.2 C 3). EPHB6 gene showed an increase in expression of the transcript, with 6, 17, 28, and 30fold in AGS-EBV, EBV-10, EBV-HB1, and EBV-HJ9,
respectively (Fig 4.2.4.2 C 4). Hence, our findings suggest that two or more mechanisms may be involved in these experiments.

A)

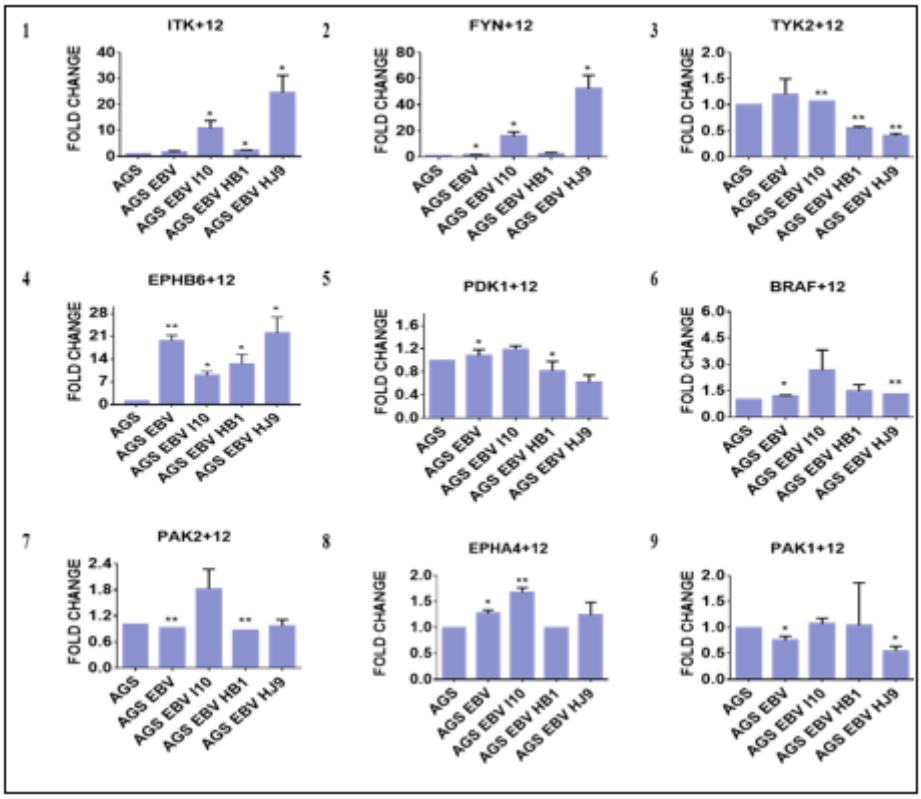
1
ITK+12
2
FYN+12
3
TYK2+12
4
EPHB6+12
5
PDK1+12
6
BRAF+12
7
PAK2+12
8
EPHA4+12
9
PAK1+12
FOLD CHANGE
AGS
AGS EBV
AGS EBV I10
AGS EBV HB1
AGS EBV HJ9

B)

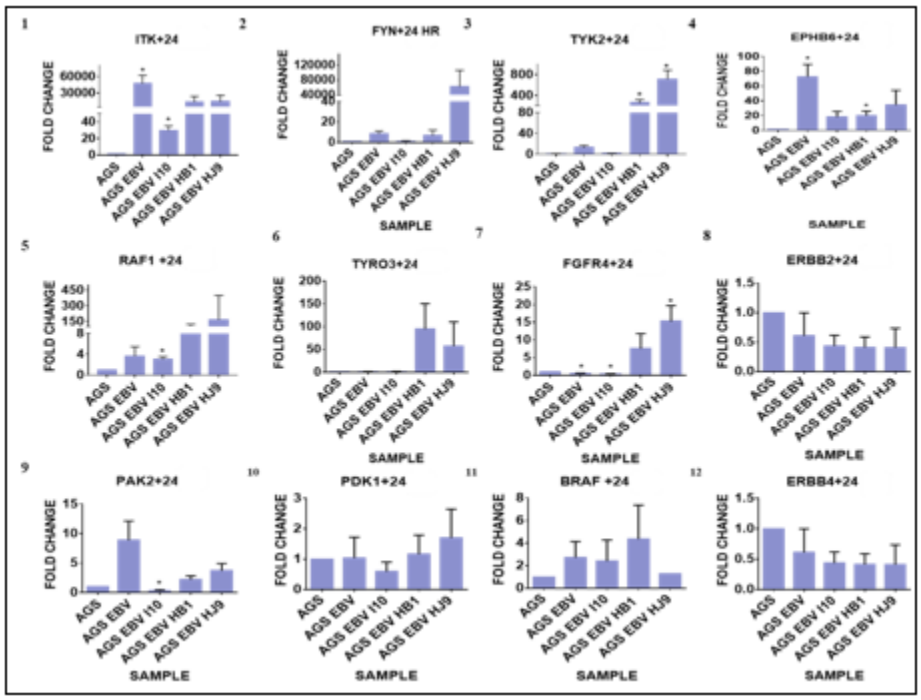
1
ITK+24
2
FYN+24 HR
3
TYK2+24
4
EPHB6+24
5
RAF1 +24
6
TYRO3+24
7
FGFR4+24
8
ERBB2+24
9
PAK2+24
10
PDK1+24
11
BRAF +24
12
ERBB4+24
FOLD CHANGE
SAMPLE
AGS
AGS EBV
AGS EBV I10
AGS EBV HB1
AGS EBV HJ9

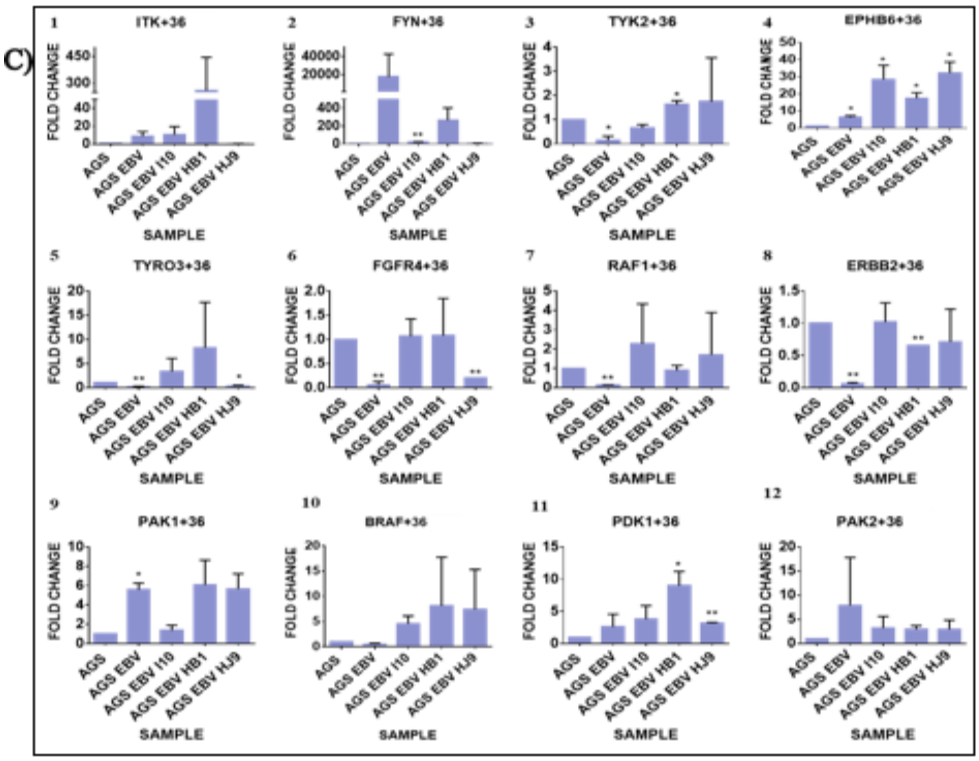

Fig.4.2.4.2: Assessment of kinase expression through the secretory mechanism of bacteria. Gene's expressions were shown indirect approach at different time points. A, B, C at 12, 24, and 36 h respectively. Where "+" indicated experiment performed with insert i.e indirect approach

4.2.5 Investigation of apoptotic markers in co-infected gastric epithelial cell lines

It is well reported that apoptotic genes are altered with *H. pylori* and EBV infection in gastric epithelial cell lines individually; however, studies on the effect of coinfection on apoptotic genes have been modest (Shinozaki-Ushiku, Kunita, & Fukayama, 2015). Therefore, to identify the apoptotic genes crucial during coinfection, twelve apoptotic genes were studied that were specific for GC, whose primers have been listed in (Table 3.5.4.2.) (J. qiang Guo et al., 2017). Their expression levels were evaluated at a time interval of 12 and 24 h of incubation. However, to determine the early apoptotic marker, 12 h was chosen as a time point to proceed with the further investigation of gene expression. The apoptotic genes such as APAF, BIK, FASL, and BAX were found to be significantly down-

regulated at 24 h, which implies their potential role in cell proliferation (Fig 4.2.5).

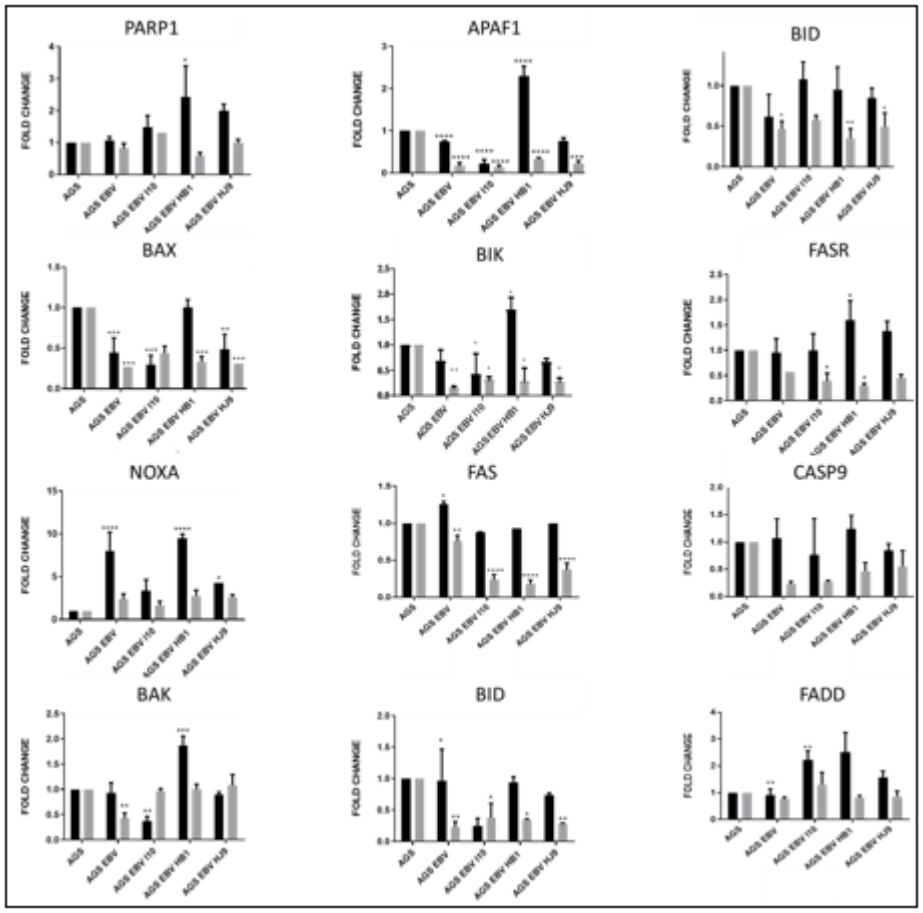

Fig 4.2.5: Investigation of apoptotic markers in co-infected gastric epithelial cell lines: Gene expression expressions of apoptotic genes were assessed at 12 h and 24 h apoptosis after co-infection of AGS with bacteria and virus. The results are shown as the mean SD of three independent experiments where *p<0.05, **p<0.001, ****p<0.0001 analyzed through Two-way Anova.

4.3 Effect of differential *H. pylori* and EBV load on the gastric cancer cells

4.3.1 Assessment of the effect of pathogen load on kinase expression

To check the effect of pathogen load on AGS, we investigated the various kinases through qPCR which are commonly found to be upregulated in gastric cancer. Two different approaches were used for giving the infection to AGS cells. The first approach was I10 dose-dependent manner (IDD) in which *H. pylori* (I10) dose was given with MOI 100, 200, and 500 and another approach was the EBV dose-

dependent manner (EDD) in which EBV doses of 50, 100, and 150 µl were used. A total of 8 kinases were screened based on their presence in GC either infected with *H. pylori* or EBV alone. Their gene expressions were evaluated at time intervals of 12 and 24 h. An interleukin-2- inducible T-cell kinase (ITK) and Tyrosine-protein kinase Fyn (FYN) both belong to receptor tyrosine kinase. Various reports have suggested that there is a higher expression of ITK and FYN in GC (Liersch-Löhn, Slavova, Buhr, & Bennani-Baiti, 2016; Lin et al., 2000b). Similar expressions were obtained in our results in which both ITK and FYN were showing significant upregulation (p- 0.002) with MOI 200 in IDD at 12 h when compared to control AGS (Fig. 4.3.1A I & II). ITK was found to be considerably overexpressed in coinfected AGS cells with EBV-I10/100, EBV-I10/200, and EBV-I10/500 compared to control (AGS). Interestingly, ITK was about 10-15 folds upregulated in AGS-EBV and EBV-I10/100 compared to control AGS cells. Further, there is about significant upregulation of the ITK gene in EBV-I10/200 and EBV-I10/500 infected AGS cells (p- < 0.01) in comparison with AGS control respectively. However, in the EDD approach, both kinases were significantly upregulated at the dose of 150 µl at 12 h (p- < 0.01) (Fig. 4.3.1B I & II). In 24 h, FYN was significantly upregulated in AGS I10 EBV 100 in comparison with AGS control. And ITK was significantly upregulated in AGS I10 EBV 150 in comparison with AGS control (Fig. 4.3.2B I & II) whereas both were found to be elevated in AGS-EBV in IDD at 24 hr (Supplementary Fig. 4.3.2A I & II).

BRAF1 (v-raf murine sarcoma viral oncogene homolog B1) is a serine/threonine kinase which is found to be upregulated in GC. In both IDD and EDD approaches, BRAF1 is upregulated by ~1 fold as compared to control AGS at 12 h (Fig. 4.3.1 AIII & BIII) and 24 h (Fig. 4.3.2 AIII & BIII). EPHA4 (Ephrin type-A receptor 4) is utilized by both EBV and *H. pylori* as a receptor. In the IDD approach both at 12 (Fig. 4.3.1 AIV) and 24 h (Fig. 4.3.2 AIV), the expression of EPHA4 was significantly upregulated (p- < 0.01 and p- < 0.05 respectively) in AGS-EBV as compared to control (AGS). In the EDD method, the expression of the gene was upregulated in AGS I10 EBV

100 in comparison to AGS at 12 h (Fig. 4.3.1 B IV) and AGS I10 EBV 150 24 h

(Fig. 4.3.2 B IV). PAK1 and PAK2 are serine/threonine kinases that have a role in modulating focal adhesions. In the case of IDD, these genes were significantly upregulated in AGS EBV I10/200 and AGS EBV I10/500 respectively at 12 h (p-value- 0.005 & 0.01 respectively) (Fig. 4.3.1 A V & VI). PAK2 was significantly downregulated in AGS EBV as compared to control (p-<0.01) at 12 h (Fig. 4.3.1 A V) whereas the opposite expression was observed at 24 h (p-0.01) (Fig. 4.3.2 A V). Similarly, PAK1 was significantly downregulated in AGS EBV I10/100 in comparison to control (p-0.01) at 12 h (Fig. 4.3.1 A VI) and vice-versa at 24 h (p-0.003) (Fig. 4.3.2 A VI). In the EDD approach, PAK2 was overexpressed in AGS I10 EBV150 and significantly downregulated in AGS I10 and AGS I10 EBV 50 and AGS I10 EBV 100 as compared to AGS (p-value - 0.003 & 0.01& 0.01 respectively) at 12 h (Fig. 4.3.1 B V). The gene expression was showing significant downregulation in the case of AGS I10 EBV/150 (p-value- 0.001) and significant upregulation in AGS I10 EBV 50 (p-value - 0.003) at 24 h (Fig. 4.3.2 A V). PAK1 was upregulated in AGS I10 EBV 50 and downregulated in AGS I10, AGS I10 EBV100 and EBV150 in comparison to control at 12 h (Fig. 4.3.1 B VI) whereas it was significantly upregulated in AGS I10 EBV50, EBV 100 and EBV150 (p- < 0.01 and p- < 0.05 respectively) in expression pattern at 24 h (Fig. 4.3.2 A VI).

TYK2 is a non-receptor tyrosine kinase 2 was upregulated in all infection and coinfection scenarios of IDD at 12 h (Fig. 4.3.1A VII) while at 24 h the gene was significantly overexpressed in the case of AGS EBV I10/100 in comparison to control (p- 0.04) and opposite expression pattern was seen in case of AGS EBV, AGS EBV I10/200 and AGS EBV I10/500 (p- < 0.01, 0.005 & 0.01) (Fig. 4.3.2 A VII). On the other hand, in the EDD mode of infection, the gene expression was found to be elevated AGS I10 EBV 50 (p- < 0.05) and AGS I10 EBV150 (p- < 0.05) as compared to control at 12 (Fig. 4.3.1 B VII) and AGS I10 EBV 100 was upregulated in 24 h (Fig. 4.3.2 B VII). PDK1 also known as pyruvate dehydrogenase kinase 1 plays an important role in fatty acid metabolism. In the case of IDD, the gene expression was significantly downregulated in AGS EBV and AGS EBV I10/100 as compared to AGS (p-0.01 & 0.001) while overexpressed

in AGS EBV I10/200 and I10/500 (p-0.01) at 12 h (Fig. 4.3.1A VIII). Furthermore, at 24 h ~ 0.5-1-fold increase in expression was observed in all doses of I10 in comparison to control (Fig. 4.3.2 A VIII). In the EDD approach, PDK1 was overexpressed at 12 h in AGS I10 EBV/50 coinfection cases as compared to AGS (Fig. 4.3.1 B VIII) while at 24 h the gene was significantly down expressed in all doses of EBV in comparison to control (p-value- 0.001, 0.02 & 0.0003) and considerably increased in AGS I10 as compared to control (Fig. 4.3.2 B VIII).

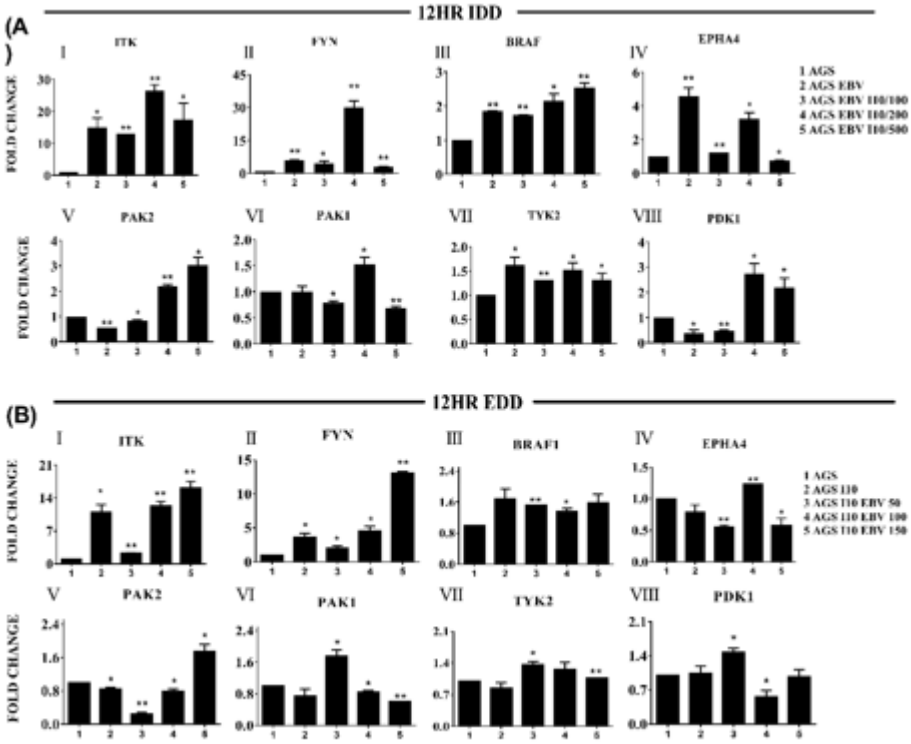

Fig 4.3.1 Assessment of pathogen burden on kinase expression. Gene expression of BRAF1, ITK, TYK2, EPHA4, PAK1, PAK2, PDK1, and FYN
was shown with different MOI of *H. pylori* I10 and different doses of EBV at 12 h. (A) I10 dose-dependent experiment (IDD) where MOI of *H. pylori* I10 was 100, 200, and 500 and (B) EBV dose-dependent experiment (EDD) where the dose of EBV was 50, 100, and 150 µl. The results are shown as the mean ± SD of three independent experiments where *p<0.05 and **p<0.01 were analyzed through unpaired t-test.

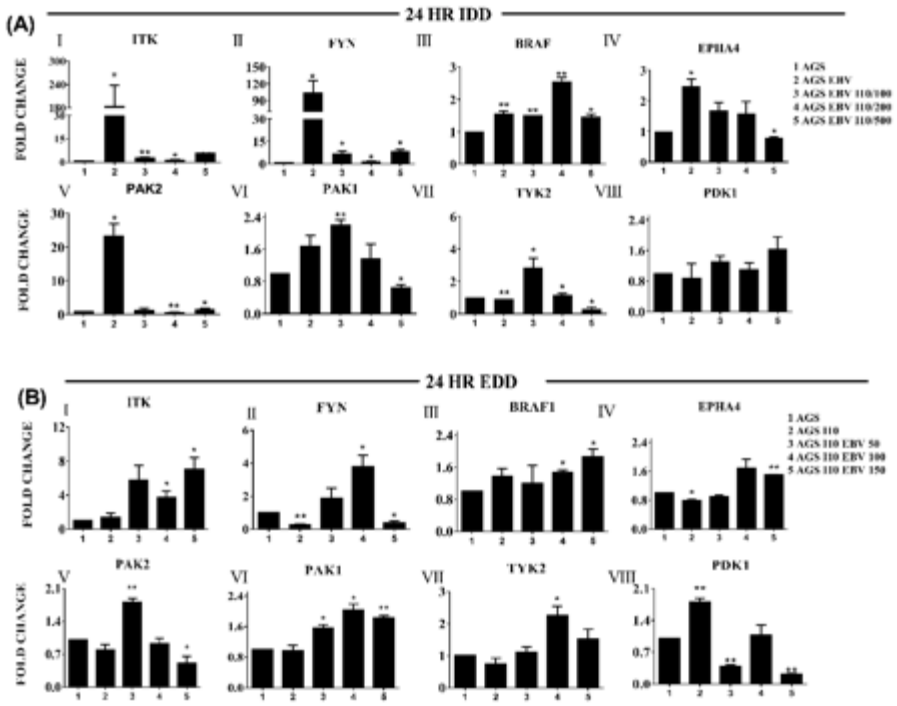

Fig 4.3.2: Assessment of the effect of pathogen load on kinase expression at 24 h. Gene expression of BRAF1, ITK, TYK2, EPHA4, PAK1, PAK2, PDK1, and FYN was shown with different MOI of *H. pylori* I10 and different doses of EBV at 24 h. (A) I10 dose-dependent experiment (IDD) where MOI of *H. pylori* I10 was 100, 200 and 500 and (B) EBV dose-dependent experiment (EDD) where the dose of EBV was 50, 100 and 150 µl. The results are shown as the mean ± SD of three independent experiments where *p<0.05 and **p<0.01 were analyzed through unpaired t-test.

4.3.2 EBV and *H. pylori* co-infection induce cell proliferation

The unwanted proliferation of the cell is one of the key features in cancer development. We have performed a cell proliferation assay by trypan blue to check the role of pathogen load in the proliferation of AGS cells. In the IDD approach, the highest cell count was observed with EBV I10/200 at both 6 and 12 h post-infection (Fig 4.3.3 A and B). However, the increase was significant only at 12 h post-infection compared to the uninfected AGS (p-0.02). With the EDD approach, the highest cell count was found with the I10 EBV-150 dose in both the time points (Fig 4.3.3 C and D). In this approach also the difference in cell count was highly

significant at the 12 h time point compared to the control (p-0.006).

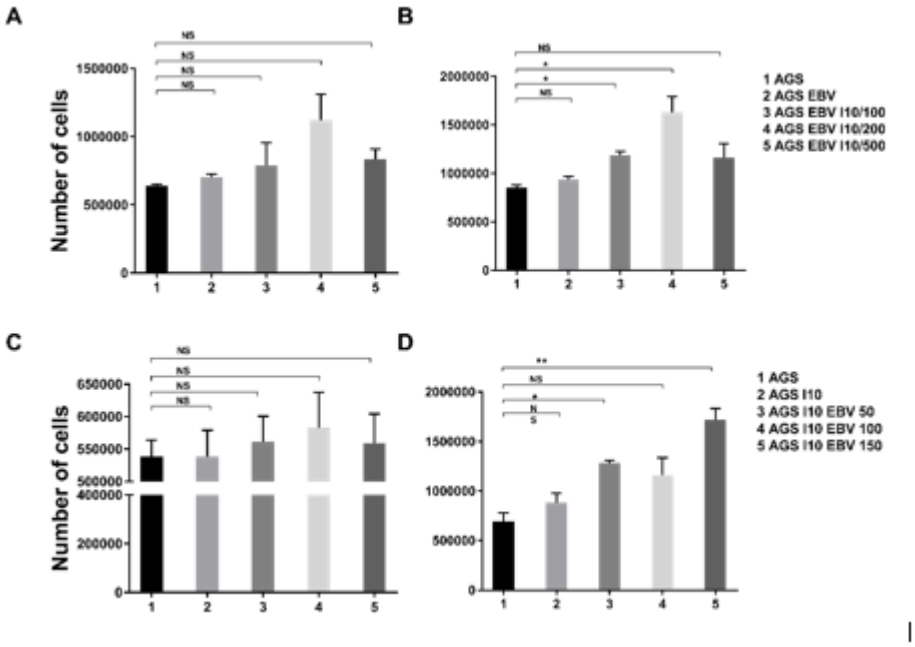

Fig 4.3.3: Dose-dependent *H. pylori* and EBV coinfection increase the cell proliferation in AGS cells: (A) Measurement of cell proliferation in IDD compared to increase in the number of cells uninfected AGS cells after 6 hr.

(B) Measurement of cell proliferation in IDD compared to uninfected AGS cells after 12 h. (C) Measurement of cell proliferation in EDD compared to uninfected AGS cells after 6 h. (D) Measurement of cell proliferation in EDD compared to uninfected AGS cells after 12 h.

4.3.3. Decrease wound area in a dose-dependent manner

We have also checked the cell migration ability by scratch wound assay and the migration of cells was expressed as % wound area. Interestingly in all the combinations of the IDD approach, the decrease in wound area was significant (p-<0.01) at EBV 0 h and 12 h post-I10-EBV coinfection compared to 0 h I10 infection (Fig 4.3.4 A i and ii). The smallest wound area was found with EBV

I10/200 (Fig 4.3.4 A i and ii). In the EDD approach, the wound was smallest in I10 EBV150 at 12 h time point compared to the 0 hr (Fig 4.3.4 B i and ii). The decrease in wound area was significant in all the infections and co-infections at 12 h time point ($p<0.01$). The results of cell proliferation and wound closure assay were

similar to the expression pattern of ITK and FYN in both the IDD and EDD approach at 12 h time point.

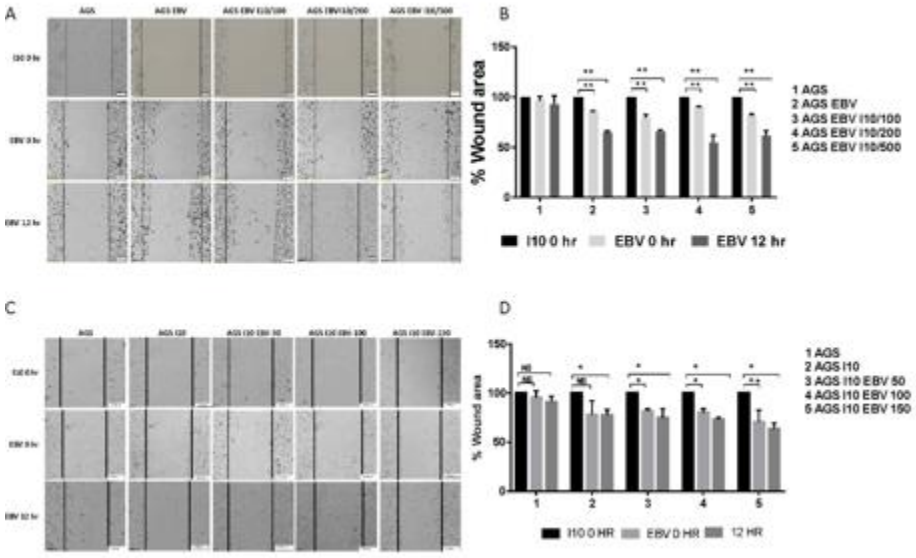

Fig 4.3.4: Investigation of cell migration in various doses of *H. pylori* and EBV in AGS cells (A) Representative image of scratch wound assay IDD co- infection. The first panel shows the 0 h I10 infection. The second panel shows 0 h EBV and the third shows 12 h post-infection for uninfected, EBV, EBV I10/100, EBV I10/200, and EBV I10/500. (B) Graphical representation of % of wound area in 0 h I10 infection and 12 h IDD co-infections. (C) Representative image of scratch wound assay EDD co-infection. The first panel shows the 0 h I10 infection. The second panel shows 0 h EBV and the third shows 12 h post-infection for, I10, I10 EBV-50, I10 EBV-100, and I10 EBV-200 compared to uninfected AGS. (D) Graphical representation of % of wound area in I10 0 h and 12 h EDD co-infections.

4.3.4 Evaluation of ITK expression in IDD and EDD through immunofluorescence assay

The altered level of ITK was observed in both experimental setups (IDD and EDD). Expression of ITK was found significantly increased ($p<0.01$) for infected samples of AGS EBV and AGS EBV I10/200 compared to uninfected AGS in IDD, (Fig. 4.3.5 A and B). ITK expression in AGS I10, AGS I10 EBV 50, AGS I10 EBV 100, AGS I10 EBV 150 doses was significantly higher ($p<0.01$) compared to uninfected AGS in EDD (Fig. 4.3.5 C and D).

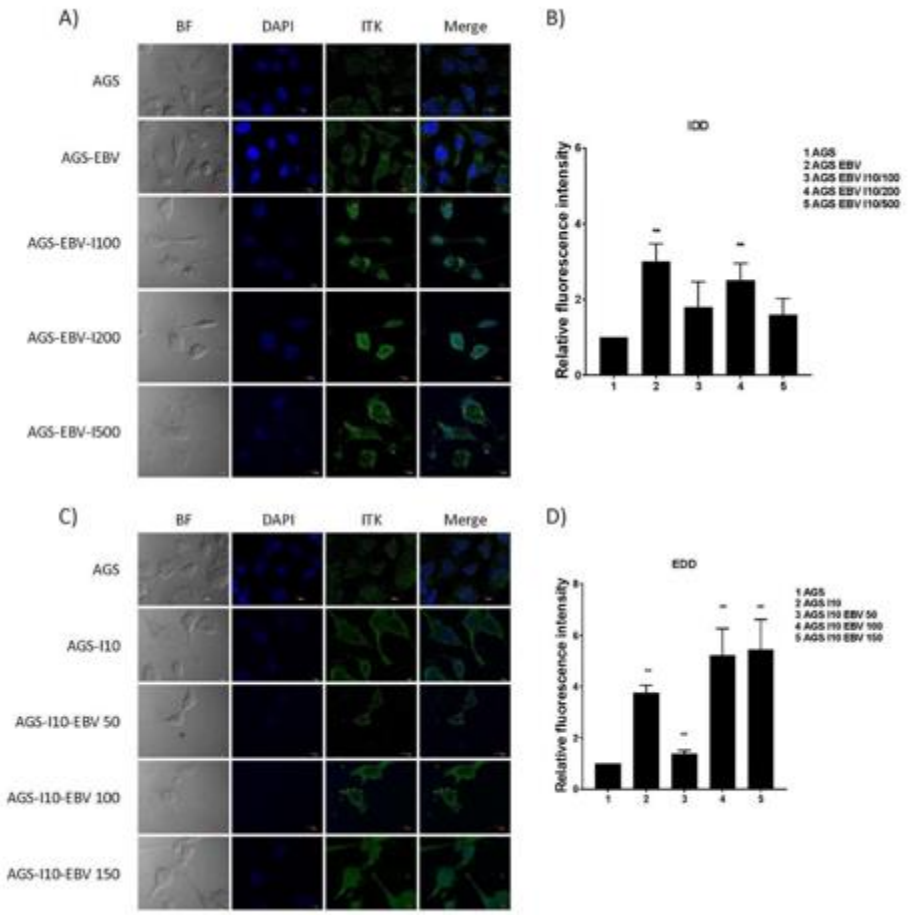

Fig 4.3.5: Evaluation of ITK expression in IDD and EDD through immunofluorescence assay: The representative image shows protein expression of ITK in AGS cells by I10 dose-dependent experiment (IDD) and EBV dose-dependent (EDD).co-infection at 12 h, which was detected by immunofluorescence assays (60x). (A) AGS, AGS EBV, AGS EBV I10/100, AGS EBV I10/200, AGS EBV I10/500 co-infection setup was used for IDD.

(B) The fold change of immunofluorescence for IDD was evaluated through graph pad prism (C) AGS, AGS I10, AGS I10 EBV50, AGS I10 EBV100, AGS I10 EBV 150 co-infection setup was used for EDD. (D) The fold change of immunofluorescence for EDD was evaluated through graph pad prism. DAPI was used to stain cells, ITK antibody was used to detect ITK in the cells. Further, the images were captured with confocal microscopy. The results are shown as the mean SD of three independent experiments where *$p<0.05$ and **$p<0.001$ were analyzed

through unpaired t-test through graph pad prism.

4.4 Repurposing of Gastric Cancer drugs against COVID-19

A set of non-structural proteins control the replication machinery of coronavirus (nsps) which are encoded by open reading frame 1a (ORF1a) and 1ab in its genome. Both the ORFs are translated as a single polypeptide chain which undergoes proteolytic cleavage to generate multiple proteins that assemble to form a multi-subunit polymerase complex (Ziebuhr, 2005). Further, this complex mediates viral genome transcription and replication. RNA-dependent RNA polymerase (RdRp) is one of the most multipurpose enzymes of retroviruses. This is an important enzyme for the replication of the genome and translation. The main cofactor of this complex is the catalytic subunit nsp12/RdRp (Pandeya, Ganeshpurkar, & Mishra, 2020). The nsp12 subunit can conduct the polymerase reaction but with very low efficiency, whereas nsp7 and nsp8 cofactors remarkably stimulates its polymerase activity (Subissi, Imbert, et al., 2014). Furthermore, nsp12 is known to have an N-terminal extension that possesses a kinase-like fold, possibly nidovirus RdRp-associated nucleotidyltransferase (NiRAN) (Kirchdoerfer & Ward, 2019). The NiRAN and the interface domains approximately span over residues 51- 398 amino acids of the SARS-Cov2-RdRp polypeptide sequence (Neogi et al., 2020; Peng et al., 2020). Moreover, to study the kinase activity of the RdRp along with NiRAN activity, this domain was trimmed from 1 to 400 amino acids (Fig 4.4.1). Its conserved amino acids, active site, and binding pockets are also stated in Table 4.4.1.

The trimmed protein structure of the SARS-CoV-2-RdRp-NiRAN domain (1-400 amino acids) was run on the ProSA web server to check their stability and structure validation (Wiederstein & Sippl, 2007). Recognition of errors and validation of the model quality of protein structure is a major part of the 3D model preparation. In our study, we used ProSA web server which is frequently used for the 3D model validation. This server calculates overall quality scores for a specific input structure. For a good protein model, this score should be within the range. If the score is out of range the structure may have error. In our case, we got the Z-Score -7.16 which is within range and shows the model is of good quality (Wiederstein &

Sippl, 2007). A plot of residues scores of a native protein structure also generated during ProSA run, which represents local model quality. This plot shows local model quality by plotting energies as a function of amino acid sequence position. Generally, positive values represent to problematic or erroneous parts of the input structure. In our case most of the residues are correspond to negative values which showed that the quality of our model is quite good.

As per our analysis through CASTp on the SARS-CoV-2-RdRp-NiRAN domain, we got our putative active sites in pocket 3. Out of mentioned amino acids, 6 amino acids (Asp36, Lys73, Asp126, Asp218, Phe219, and Asp221) showed stable interactions during molecular docking through Glide v8.3 Schrodinger, LLC software code. While no stable protein-ligand interactions were found with the residues of pockets 1, 2, 4 and 5. Importantly, all the 16 compounds interacted with the residues of pocket 3. Therefore, pocket 3 was predicted as our real active site.

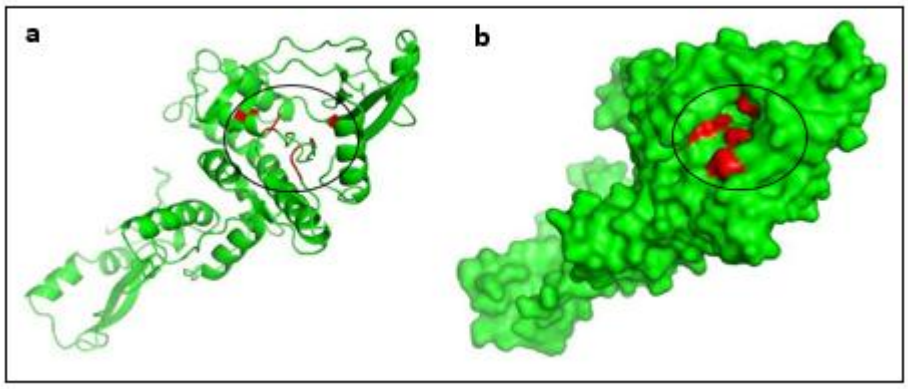

Fig 4.4.1: Structural representation of SARS-CoV2-RdRp-NiRAN domain (PDB ID: 7BTF). Figures generated on PyMol. (a) Green colour cartoon representation. (b) green colour solid surface representation showing putative active site residues (Asp36, Lys73, Asp126, Asp218, Phe219, and Asp221) with red colour.

Table 4.4.1: Three-dimensional crystal structure of the molecular target, COVID-19. RdRp protein nsp12 (1-400 a.a) along with its active site and pockets

Sr. no.	PocID	Area (Å2)	Volume (Å3)	Pocket amino acids
1	1	581.745	1114.417	Leu 245, Thr 246, Trp 268, Leu 270, Leu 316, Val 320, Phe 321, Thr 324
2	2	390.342	570.082	Leu 270, Leu 271, Lys 272, Tyr 273, Thr 324, Ser 325, Phe 326, Gly 327, Pro 328, Leu 329, Val 330
3	3	292.687	160.167	Arg 33, Ala 34, Phe 35, Asp 36, Ile 37, Tyr 38, Lys 50, Cys 53, Arg 55, Val 71, Lys 73, His 75, Glu 83, Arg 116, Leu 119, Thr 120, Lys 121, Tyr 122, Thr 123, Asp 126, Val 204, Thr 206, Asp 208, Asn 209, Asp 211, Tyr 217, Asp 218, Asp 221
4	4	152.254	95.969	-
5	5	118.289	86.049	Glu 254, Glu 278, Lys 281, Leu 282, Arg 285, Val 320, Phe 321

4.4.1 Molecular docking studies

Recent pathophysiological understanding of SARS-CoV-2 infection stipulates that those infected with the virus could experience cytokine release syndrome (CRS). Further, this CRS is distinguished by elevated interleukin IL-6, IL-2, IL-7, IL-10, etc (Costela-Ruiz, Illescas-Montes, Puerta-Puerta, Ruiz, & Melguizo-Rodríguez, 2020). Hence, the treatment of cytokine storms could play a crucial role in the treatment of severe COVID-19. Several cytokines involved in COVID-19 are mediated by Janus kinases (JAKs) (Luo et al., 2020). ITK is highly expressed in T cells and regulates the activation and function of both CD4+ and CD8+ T cells, including cytokine production and cytotoxic function (McGee, August, & Huang, n.d.). Hence JAKs and ITK inhibition present a potent therapeutic strategy against COVID-19.

4.4.1.1. Molecular docking studies using Autodock 4.2

The molecular docking of FDA-approved drugs (for JAKs and other kinases) against the SARS-CoV-2-RdRp-NiRAN domain (1-400 amino acid) was performed with the help of software AutoDock 4.2. Further, the binding affinity of

the drugs was chosen based on the lowest RMSD value of 0.00. RMSD value 0 represents identical structures and when this value increases, the two structures are considered to be more different (Carugo & Pongor, 2001). Out of 16, 12 compounds were selected, and the remaining four kinases' inhibitors were excluded from the list because they violated the Lipinski rule. These four compounds were erdafitinib (PubChem CID: 67462786), fedratinib (PubChem CID:16722836), saracatinib (PubChem CID: 10302451) and fostamatinib (PubChem CID: 11671467). As erdafitinib and fedratinib had molar refractivity over 130 and molecular weight over 500 g/mol, respectively. Further, saracatinib and fostamatinib had molecular weight of more than 500 g/mol and hydrogen bind acceptor more than 5. The selected 12 compounds were included in our study considering no cut-off value. The binding energy for these compounds were (-7.3 kcal/mol), brepocitinib (-8.7 kcal/mol), decernotinib (-7.9 kcal/mol), fasudil (-7.2 kcal/mol), - filgotinib (-8.0 kcal/mol), GSK2606414 (-8.6 kcal/mol), peficitinib (-7.6 kcal/mol), ruxolitinib (-7.4 kcal/mol) and ibrutinib (-8.8 kcal/mol). Tofacitinib (-6.9 kcal/mol), Upadacitinib (-6.6 kcal/mol) and Pamapimod (-6.9 kcal/mol) (Table 4.4.2). These binding energies indicate the presence of a kinase-like domain in the NiRAN domain of nsp12 of RdRp. The types of interactions and the residues involved in the binding of the compound with the SARS-CoV-2-RdRp-NiRAN domain (1-400 amino acid) are also represented in Table 4.4.2. Also, the 2D and 3D interaction diagrams of the selected 12 kinase inhibitors with the SARS-CoV-2-RdRp-NiRAN domain are represented in Table 4.4.3.

Table 4.4.2: Interactions of COVID-19 nsp12 (1-400) amino acid residues with inhibitors and their binding energies.

Inhibitors	Binding affinity	PubChem-ID	Hydrogen binding interactions	Hydrophobic interactions	Electrostatic interactions
Ibrutinib	-8.8	24821023	ASP A:218	Asp A: 36, Val A:204,	Asp A: 221
Brepocitinib	-8.7	118878093	ASP A:36, SER A:236	Val A:204, Asp A: 218,	Lys A: 50
GSK2606414	-8.6	53469448	ASP A:164	Ile A:37, Phe A: 35,	-
Filgotinib	-8.0	49831257	ASN A:209	Phe A:48	Arg A: 33
Decernotinib	-7.9	59422203	Lys A: 73	Asp A:221, Thr A:206	–
Peficitinib	-7.6	57928403	TYR A:38	Phe A:48, Thr A: 51	–
Fasudil	-7.2	3547		Phe A: 35, Ile A:37,	Lys A: 50,
Baricitinib	-7.3	44205240	Lys A: 73	Phe A: 35	Asp A: 218,
Ruxolitinib	-7.4	25126798	Lys A: 73	Leu A: 247, Tyr A:163,	–
Tofacitinib	-6.9	9926791	ASN A:209, ASP A:218, ASP A:208, ASN A:39	Phe A:134	Lys A: 73
Upadacitinib	-6.6	58557659	ASN A:209	Tyr A:38	_
Pamapimod	-6.5	16220188		Val A:204, Ser A:236,	

Table 4.4.3: Interactions of SARS-CoV-2-RdRp-NiRAN domain amino acid residues with kinase inhibitors, and their 3D and 2D structures

Name	3D structure	2D structure
Baricitinib	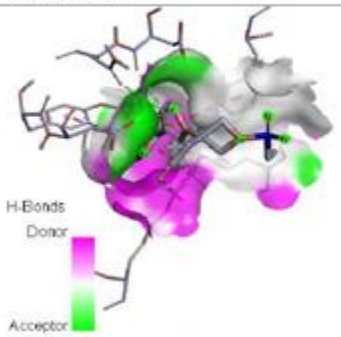	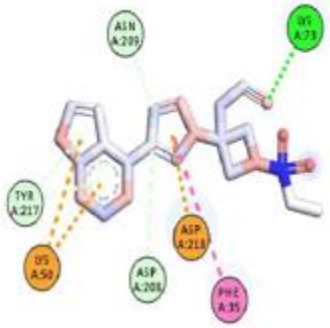
Brepocitinib	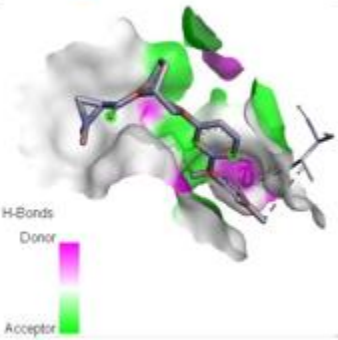	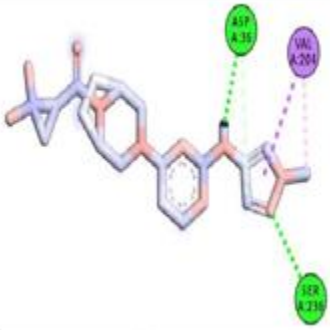
Decernotinib	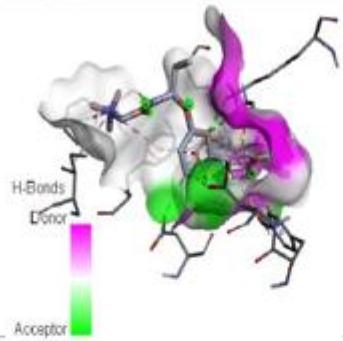	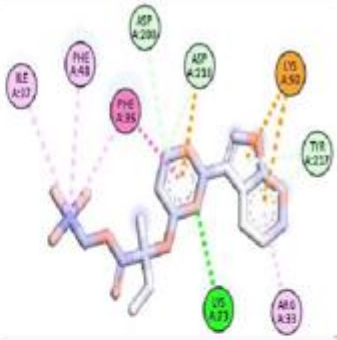
Fasudil	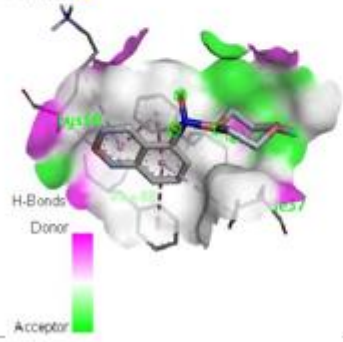	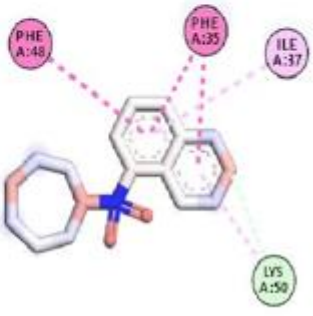

Filgotinib	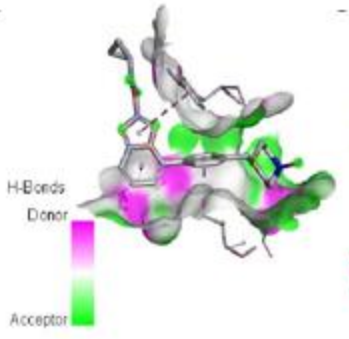	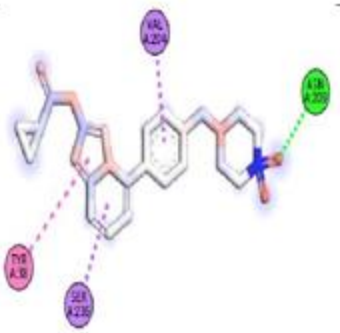
GSK2606414	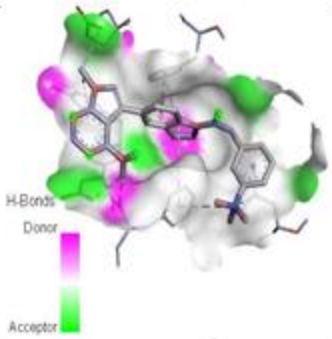	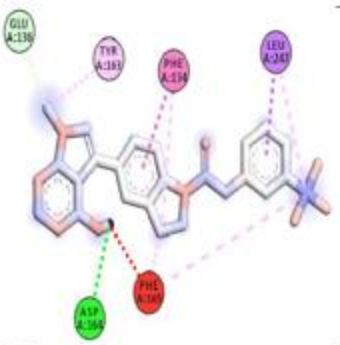
Peficitinib	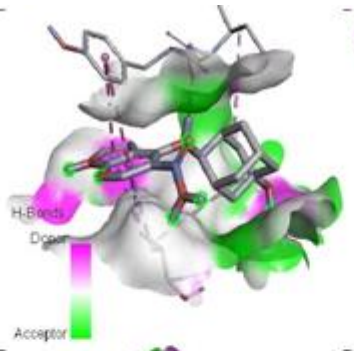	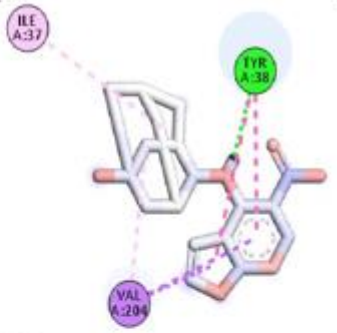
Pamapimod	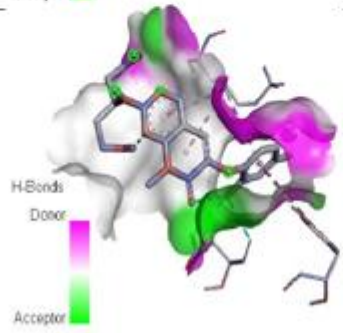	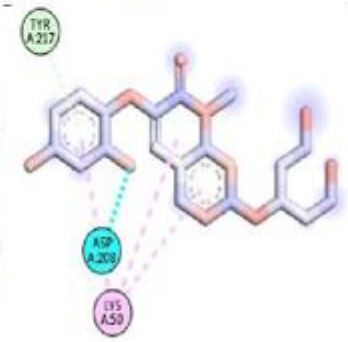

Upadacitinib

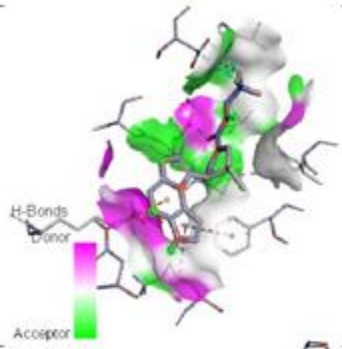

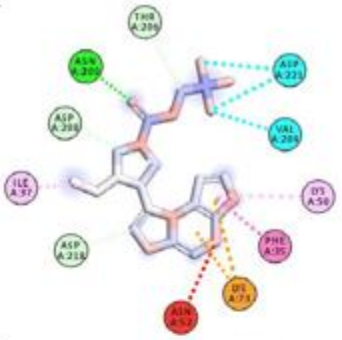

Ruxolitinib

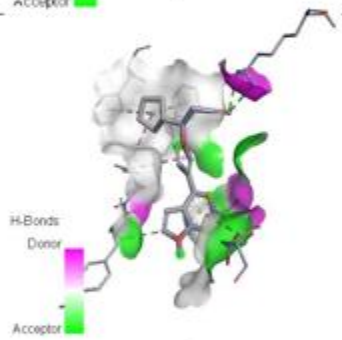

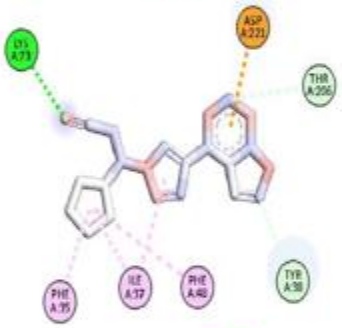

Tofacitinib

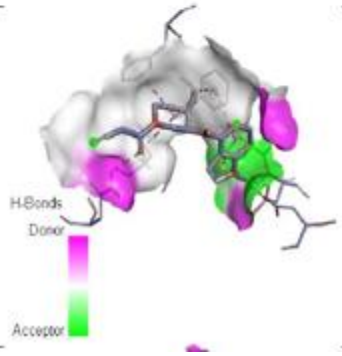

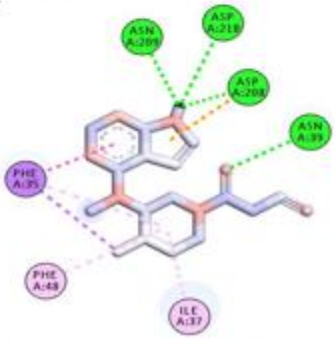

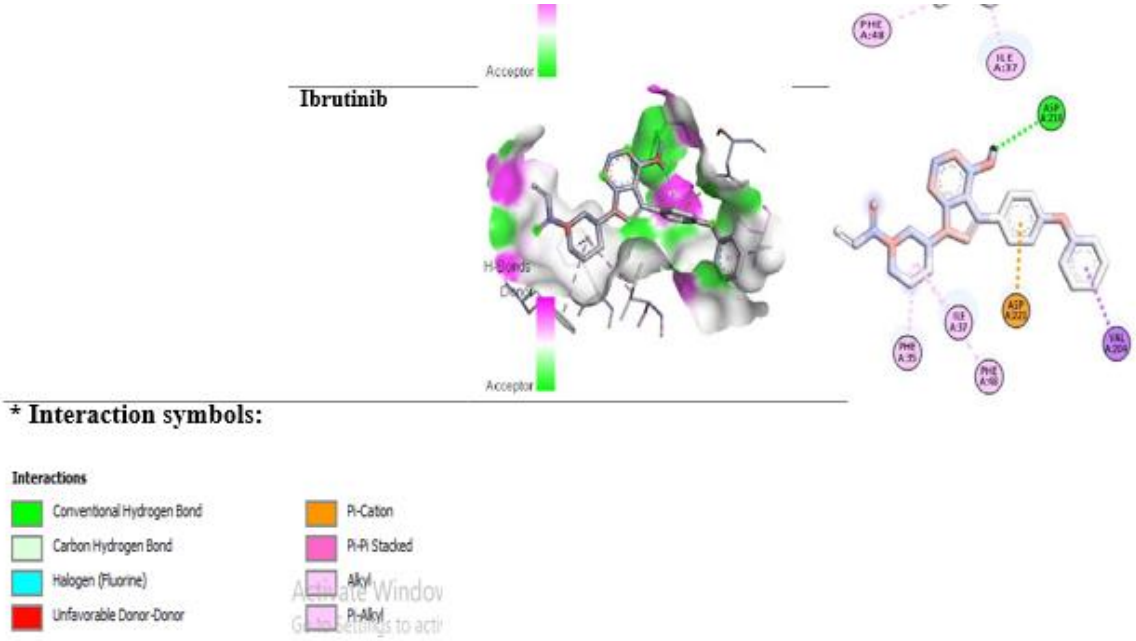

4.4.1.2 Molecular docking studies using Glide Schrodinger suite

Out of twelve compounds, the four best compounds brepocitinib, decernocitinib, filgotinib, and ibrutinib have been selected for further re-docking and MD simulation studies. These compounds have been selected based on their docking score, ADMET properties, and their good history against kinases. Re- docking of these compounds was performed using the Glide module of Schrodinger Suite 2019. 2D and 3D interactions of these compounds with the SARS-CoV-2-RdRp-NiRAN domain were analyzed and figures were generated on the Glide platform of Schrodinger Suite 2019-2. 2D and 3D interaction diagrams are represented in Fig 4.4.3.

In these interactions, we mainly focused on H-bond interactions. The study of Ahmed et al 2020 revealed active sites and the residues involved in the binding of the UTP and GTP within the SARS-CoV-2-RdRp-NiRAN domain (Ahmad et al., 2020). Further, the residues aspartate, glutamate, lysine, and arginine were found making important interaction with the UTP and GTP in the NiRAN domain (Lehmann et al., 2015). It was also revealed that these residues are at the active site and important conserved residues. Through CASTp, the important residues which found to be involved in making the active site were in pocket 3 are Arg33, Phe35,

Asp36, Ile37, Tyr38, Asn39, Lys50, Cys53, Arg55, Val71, Lys73, His75, Glu83, Arg116, Leu119, Thr120, Lys121, Tyr122, Thr123, Val204, Thr206, Asp208, Asn209, Tyr217, Asp218 and Asp221.

In our docking studies, brepocitinib shows strong interactions with the Asp36, Lys73, Asp218, and Asp22. The binding affinity for the brepocitinib was calculated to be -5.543 kcal/mol. In the case of decernocitinib residues Asn209, Asp218, and Asp221 show strong interactions. The binding affinity for the decernocitinib was calculated to be -6.694 kcal/mol. Filgotinib shows main interactions with the residues Asp40, Asp208, and Asp221, and the binding affinity for the complex was calculated to be -4.917 kcal/mol. Similarly, in the case of ibrutinib, the residues which show strong interactions are Asp208, Asp218, and Asp221, and the binding affinity for this complex was calculated to be -6.137 kcal/mol. The docking scores, Glide G- score, and are Glide E-model are represented in Table 4.4.4

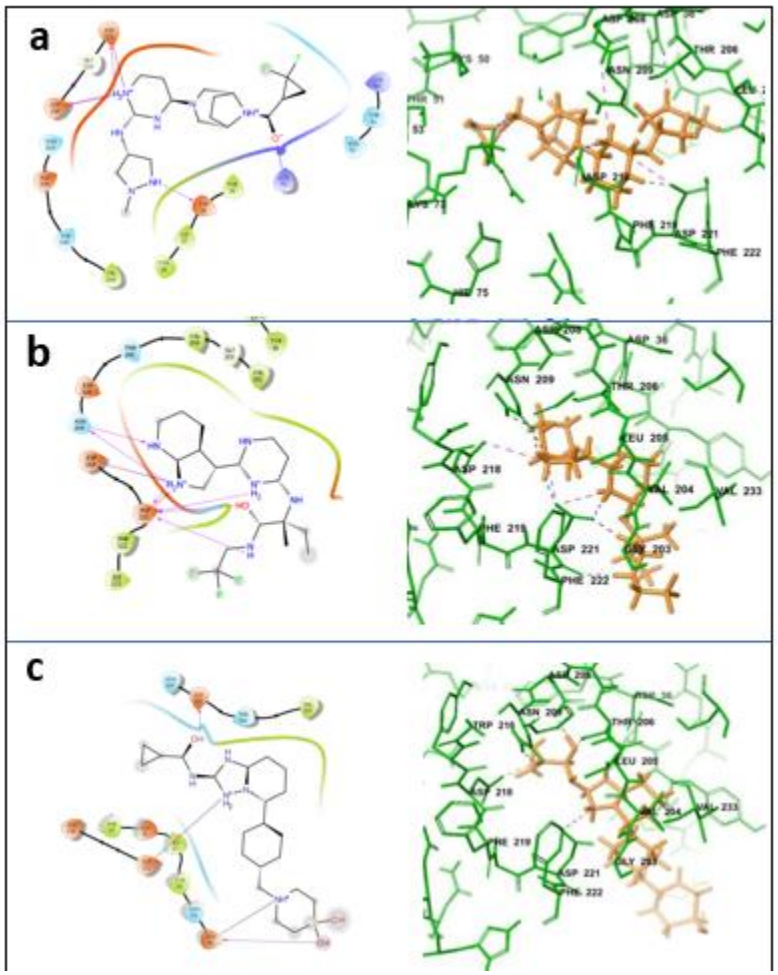

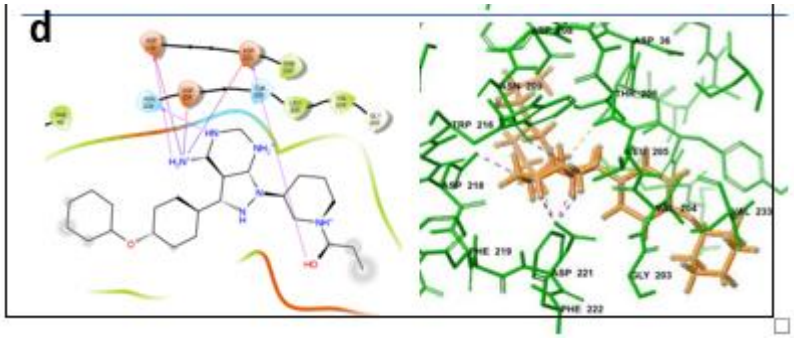

Fig 4.4.2: 2D and 3D interaction diagram of inhibitory compounds with the SARS-CoV2-RdRp-NiRAN domain protein-based Dock; (a) with brepocitinib
(b) with decernocitinib (c) with filgotinib, and (d) ibrutinib are shown here. 2D diagrams were prepared using GLIDE and only H-bond interactions are represented here. In the 3D diagrams, the SARS-CoV2-RdRp-NiRAN domain is presented with thin tubes, residues that directly contact inhibitory compounds are represented in thin stick models.

Table 4.4.4: Molecular docking scores for Brepocitinib, Decernocitinib, Filgotinib, and Ibrutinib against SARS-CoV-2-RdRp-NiRAN domain. Docking performed on Glide, Schrodinger suite.

S.No.	Compound ID/name	Docking Score	Glide G-score	Glide E-model
1	Brepocitinib	- 5.543	- 6.047	- 68.281
2	Decernocitinib	- 6.694	- 6.991	- 75.203
3	Filgotinib	- 4.917	- 4.931	- 60.430
4	Ibrutinib	- 6.137	- 6.704	- 73.405

4.4.2 Drug likeliness

Since the kinase study is already done in the NiRAN domain (Romano et al., 2020), we evaluated the effect of an FDA-approved kinase inhibitor against the kinase which is expressed in both gastric cancer and SARS-CoV-2. Generally, JAK, ITK, Rho-associated kinase, FGFR2, FYN, PERK, TYK2, p38 MAPK, and syk kinase are expressed in GC (Table 4.4.5). For this purpose, 16 kinase inhibitors were selected and screened for drug likeliness through the Lipinski rule using a free web server pkCSM. Out of these 16 kinase inhibitors, 12 inhibitors that showed no

violation of the Lipinski rule were selected for further experiments (Table 4.4.6). The four kinases inhibitors which were excluded from this list were erdafitinib (PubChem CID: 67462786), saracatinib (PubChem CID: 10302451), fostamatinib (PubChem CID:11671467), and fedratinib (PubChem CID:16722836) since they violated the Lipinski rule (Table 4.4.6). As erdafitinib had molar refractivity of more than 130, saracatinib and fostamatinib had molecular weight more than 500 g/mol and hydrogen bind acceptor more than 5. Further, fedratinib also had a molecular weight of more than 500 g/mol.

Table 4.4.5: Kinases expressed in gastric cancer with their PDB-ID and inhibitors

Gene	PDB-ID	Resolution	Kinase inhibitor	Pub chem -ID	Reference
SARS-COV2	6M71 7BTF	2.9 2.95 Å			(Dwivedy et al., 2020)
JAK 1	6SM8 4EHZ	1.85 Å 2.17 Å	Upadacitinib Baricitinib Brepocitinib	58557659 44205240 118878093	(Heijde et al., 2019; Khanna, Chua, Bay, & Baeg, 2015; Nogueira, Puig, & Torres, 2020; Praveen, Chowdary, & Aanandhi, 2020)
JAK 2			Baricitinib	44205240	(Khanna et al., 2015)
JAK			Baricitinib Fedratinib Ruxolitinib Tofacitinib filgotinib peficitinib decernotinib	44205240 16722836 25126798 9926791 49831257 57928403 59422203	(Khanna et al., 2015; Stebbing et al., 2020)
p38 (MAPK	1KV2	2.80 Å	Pamapimod	16220188	(Hill et al., 2008; Magnelli et al., 2020)
Rho-kinase	2F2U	2.40 Å	Fasudil	3547	(Wei, Surma, Shi, Lambert-Cheatham, & Shi, 2016; William et al., 2016)

Syk kinase			fostamatinib	11671467	(H et al., 2005; Kyttaris, 2012; Schwab & Gale (Firm), 2009)
PERK	3QD2	2.81 Å	GSK2606414(crosses blood-brain barrier)	53469448	(Díaz et al., 2018; Mahameed et al., 2019)
TYK2	6OVA	2.50 Å	Brepocitinib	118878093	(Khanna et al., 2015; Nogueira et al., 2020)
ITK			Ibrutinib	24821023	(Lin et al., 2000b; Research, 2013)
FYN			Saracatinib AZD0530	10302451	(Du et al., 2020; Lin et al., 2000b)
FGFR2 kinase	1GJO,1OEC	2.40 Å, 2.40 Å	Erdafitinib	67462786	(de Almeida Carvalho, de Oliveira Sapori Avelar, Haslam, Gill, & Prasad, 2019; Lin et al., 2000b)

Table 4.4.6: Physicochemical properties of the kinase inhibitors and accordance with the rules of drug-likeness

Inhibitors	Molecular weight g/mol	Alogp	Hydrogen bond acceptor	Hydrogen bond donor	Molar Refractivity	No. of rotatable bonds	No. of violations
Baricitinib	371.42	1.0956	7	1	98.51	5	0
Brepocitinib	389.40	1.7885	6	1	105.03	4	0
decernotinib	392.38	3.279	7	3	98.50	6	0
Erdafitinib	446.54	4.1836	6	1	131.48	9	1
Fasudil	291.37	1.2188	5	1	85.48	2	0
Fedratinib	524.68	4.8236	7	3	151.66	11	1
Filgotinib	425.50	1.9752	6	1	118.09	5	0
Fostamatinib	580.46	3.0945	13	4	141.79	10	2
GSK2606414	451.44	4.3681	6	1	123.12	3	0
Peficitinib	326.39	2.0133	3	4	91.62	3	0
Pamapimod	406.38	1.9443	8	3	102.35	8	0
Saracatinib	542.03	3.9395	9	1	151.69	8	2
Upadacitinib	380.37	2.9079	6	2	96.54	3	0
Ruxolitinib	306.37	3.4663	4	1	87.66	4	0
Tofacitinib	312.37	1.5447	4	1	91.20	3	0
Ibrutinib	440.50	4.2173	5	1	131.01	5	0

4.4.3. ADMET evaluation

For selecting appropriate with a good balance of potency along with absorption, distribution, metabolism, excretion, and toxicity (ADMET) analysis was performed using a free web server SwissADME for 12 kinases (Table 4.2.6A and 6B). All the kinase inhibitors showed appropriate human intestinal absorption (HIA), blood-brain barrier (B.B.B.) infiltration. None of the compounds was found carcinogenic. Except for GSK2606414 and upadacitinib, none of the compounds showed AMES toxicity. The results of HIA, B.B.B., LD50 values for the compounds are listed in Table 4.4.7A and 7B.

Table 4.4.7A: ADME/T Properties of 6 different kinase inhibitors

Properties	Brepocitini	Pamapimo	GGSK26064	Filgotini	Fasudi	Ibrutini

	b	d	14	b	l	b
PSA	160.094	163.973	187.027	174.38	118.22	190.873
ALOGP98	1.7885	1.9443	4.3681	1.9752	1.2188	4.2173
Absorption						
Water solubility	-4.097	-3.471	-3.9	-2.549	-2.465	-3.501
Caco2 permeability	1.11	0.448	1.193	1.245	1.405	0.704
Intestinal absorption (human)	95.116	72.992	95.677	82.384	81.002	97.724
Skin Permeability	-2.933	-2.737	-2.738	-2.74	-2.84	-2.735
P-glycoprotein substrate	YES	YES	YES	YES	NO	Yes
P-glycoprotein I inhibitor	NO	YES	YES	YES	NO	Yes
P-glycoprotein II inhibitor	NO	NO	YES	YES	NO	Yes
Distribution						
VDss (human)	0.324	0.16	0.052	0.853	0.242	-0.083
Fraction unbound (human)	0.442	0.127	0.047	0.262	0.313	0.114
BBB permeability	-0.913	-1.622	-0.648	-0.908	-0.133	-0.902
CNS permeability	-3.143	-3.645	-1.858	-2.993	-2.949	-2.431
Metabolism						
CYP2D6 substrate	NO	NO	NO	NO	NO	NO
CYP3A4 substrate	YES	NO	YES	YES	YES	YES
CYP1A2 inhibitor	NO	NO	YES	YES	NO	YES
CYP2C19 inhibitor	NO	NO	YES	NO	NO	YES
CYP2C9 inhibitor	NO	NO	YES	NO	NO	YES
CYP2D6 inhibitor	NO	NO	NO	NO	NO	NO
CYP3A4 inhibitor	NO	NO	YES	YES	NO	YES
Excretion						
Total Clearance	-0.024	0.482	0.105	0.671	0.332	0.601
RenalOCT2 substrate	NO	NO	NO	NO	NO	NO
Toxicity						
AMES toxicity	NO	NO	YES	NO	NO	NO
Max. tolerated dose (human)	-0.551	0.765	-0.155	0.179	0.085	0.373

hERG I inhibitor	NO	NO	NO	NO	NO	NO
hERG II inhibitor	NO	NO	YES	YES	NO	YES
Oral Rat Acute Toxicity (LD50)	2.626	2.424	2.855	2.793	2.783	3.089
Oral Rat Chronic Toxicity (LOAEL)	-0.111	2.437	0.334	0.951	1.223	0.609
Hepatotoxicityty	YES	YES	YES	YES	YES	YES
Skin Sensitisation	NO	NO	NO	NO	NO	NO
T.Pyriformis toxicity	0.298	0.287	0.288	0.286	0.641	0.285
Minnow toxicity	2.554	0.688	-1.579	0.588	1.83	-2.866

4.7 B: ADME/T Properties of 6 different kinase inhibitors

Properties	Baricitinib	Decernotinib	Upadacitinib	Ruxolitinib	Tofacitinib	Peficitinib
PSA	149.888	158.351	152.126	133.732	134.479	139.384
ALOGP98	1.09568	3.279	2.9079	3.46638	1.54478	2.0133
Absorption						
Water solubility	-3.129	-2.969	-2.837	-3.804	-3.526	-3.149
Caco2 permeability	0.266	1.287	0.87	0.919	1.36	0.085
Intestinal absorption (human)	79.532	82.775	89.532	94.108	93.481	87.743
Skin Permeability	-2.766	-2.738	-2.735	-2.803	-3.154	-2.737
P-glycoprotein substrate	Yes	Yes	Yes	NO	NO	NO
P-glycoprotein I inhibitor	NO	NO	NO	NO	NO	NO
P-glycoprotein II inhibitor	NO	NO	NO	NO	NO	NO
Distribution						
VDss (human)	0.059	0.721	0.374	0.667	0.402	0.799
Fraction unbound (human)	0.332	0.194	0.302	0.236	0.41	0.47
BBB permeability	-1.321	-1.414	-1.469	-0.574	-0.752	-1.008
CNS permeability	-3.605	-3.295	-3.491	-2.323	-3.064	-3.869
Metabolism						
CYP2D6 substrate	NO	NO	NO	NO	NO	NO
CYP3A4 substrate	YES	NO	NO	YES	NO	YES

CYP1A2 inhibitor	NO	YES	YES	YES	YES	NO
CYP2C19 inhibitor	NO	NO	NO	YES	NO	NO
CYP2C9 inhibitor	NO	NO	NO	NO	NO	NO
CYP2D6 inhibitor	NO	NO	NO	NO	NO	NO
CYP3A4 inhibitor	NO	NO	NO	NO	NO	NO
Excretion						
Total Clearance	**0.854**	**0.461**	**0.354**	**0.863**	**0.848**	**0.19**
RenalOCT2 substrate	NO	NO	NO	NO	NO	NO
Toxicity						
AMES toxicity	NO	NO	YES	NO	NO	NO
Max. tolerated dose (human)	**-0.111**	**0.349**	**0.708**	**-0.275**	-0.331	**-0.273**
hERG I inhibitor	NO	NO	NO	NO	NO	NO
hERG II inhibitor	YES	YES	YES	NO	NO	NO
Oral Rat Acute Toxicity (LD50)	**2.437**	**2.34**	**2.488**	**2.57**	**2.175**	**2.365**
Oral Rat Chronic Toxicity (LOAEL)	**1.539**	**-0.136**	**0.579**	**0.158**	**0.21**	**0.738**
Hepatotoxicity	YES	YES	YES	YES	YES	**Yes**
Skin Sensitisation	NO	NO	NO	NO	NO	**No**
T.Pyriformis toxicity	**0.296**	**0.288**	**0.285**	**0.364**	**0.34**	**0.285**
Minnow toxicity	**1.769**	**2.223**	**1.473**	**1.348**	**1.944**	**1.417**

4.4.4. Molecular mechanics-generalized born surface area (MMGBSA) MMGBSA study of the selected compounds brepocitinib, decernocitinib, filgocitinib, and ibrutinib was performed with the SARS-CoV-2-RdRp- NiRAN domain and it was observed that all the compounds have a good affinity towards the SARS-CoV-2-RdRp-NiRAN domain (Table 4.2.7). MMGBSA scores for the brepocitinib, decernocitinib, filgocitinib, and ibrutinib were calculated to be -60.1315, -47.6964, -44.1200 and -77.1748, respectively. Among these compounds, ibrutinib showed better affinity as compared to other compounds. The other individual energies of the MMGBSA wiz coulomb, covalent, H bond, solvation, Vander walls were also determined which are given in table 4.4.8

Table 4.4.8: The MM/GBSA binding energy scores and individual contributing energies

Compounds	MMGBSA dG Bind	MMGBSA dG_{Bind} Contribution				
		Coulomb	Covalent	H-bond	solvent GB	vdw
Brepocitinib	-60.1315	-61.7106	3.9950	-4.3891	55.5333	-34.0907
Decernocitinib	-47.6964	-76.8374	14.4035	-3.4601	65.5055	-22.3610
Filgotinib	-44.1200	-59.6305	3.3934	-2.7584	65.9576	-26.1201
Ibrutinib	-77.1748	-167.7890	5.8154	-1.3588	147.4467	-28.3242

4.4.5 Molecular dynamics simulation analysis

Based on the criteria of docking scores, ADMET, and drug likeliness we selected four compounds for the further MD simulation studies. MD simulation studies were performed for the compounds brepocitinib, decernocitinib, filgotinib, and ibrutinib in complex with the SARS-CoV-2- RdRp-NiRAN domain. MD simulations were performed for 100 ns for each complex on the Desmond platform of Schrodinger suite 2019. For each protein-ligand complex , MD simulation was performed (Fig 4.4.5). Post-MD simulation 2D interaction diagram, protein-ligand contact analysis with different types of bonds, RMSD and RMSF analysis were also performed for understanding the stability of the ligand with the protein at the site of interaction during the simulation.

4.4.5.1 SARS-CoV-2-RdRp-NiRAN domain-kinase inhibitors complex analysis

Post-MD simulation 2D interaction diagrams show the interactions of the selected inhibitory compounds with the SARS-CoV-2-RdRp-NiRAN domain (Fig. 4.4.3). The analysis suggested during the simulation, all the selected inhibitory compounds are binding at the same active site. Protein-ligand contacts showing different interaction fractions are represented in figure 4.4.4. H bond occupancy showing the H-bonds throughout the simulations are represented in figures 4.4.6-4.4.9. Root mean square deviation RMSD plots of all these complexes were explained and shown in figure 4.4.5. RMSF of thesemcomplexes were also analyzed and there no considerable fluctuations were observed there.

4.4.5.1.a. (SARS-CoV-2-RdRp-NiRAN domain/Brepocitinib)

Post-MD simulation 2D interactions, in the case of brepocitinib, shows the interactions with Thr51, Lys73, Arg116, Asp208, Asp218, and Asp221. Lys73 and Arg116 donate H-bonds to brepocitinib while Thr51, Asp208, Asp218, and Asp221 receive H bond from brepocitinib. Lys73 and Asp221 make direct H-bond while Thr51, Arg116, Asp208, and Asp218 make H-bond through water molecules. Lys73 and Arg116 make strong H- bond as compared to other residues (Fig 4.4.3a). Protein-ligand contact (SARS-CoV-2-RdRp-NiRAN domain/Brepocitinib) analysis revealed different types of bond formation during the simulation (Fig. 4.4.4a). It was observed that Thr51, Lys73, Arg116, Asp208, Asn209, Asp218, and Asp221 make strong interaction with the brepocitinib. Lys73 and Arg116 make H-bond and water bridges while Asp218 and Asp221 make H-bond, water bridges, and ionic interactions. Thr51 and Asn209 make only water bridges while Asp208 makes water bridges as well as show ionic interaction.

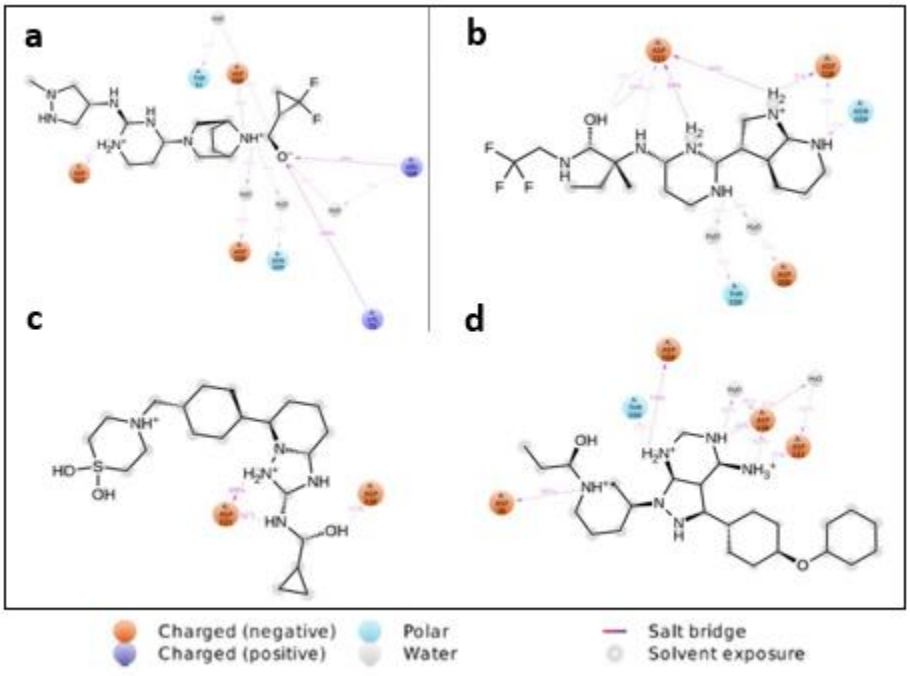

: Post-MD simulations 2D representation of inhibitory compound interactions with the SARS-CoV-2-RdRp-NiRAN domain. Interactions that occur over 20.0% of the

simulation time in the selected trajectory (0.00 through 100 ns) are shown. SARS-CoV-2-RdRp-NiRAN domain showing interaction with (a) brepocitinib (b) decernocitinib (c) filgotinib and (d) ibrutinib. Orange circle: charged (negative), Blue circle: charged (positive), White circle: water and Red circle with bar represents Pi-cation.

Total contact analysis during the entire simulation time of 100 ns shows that maximum contact remained stable till 40 ns after that number of contacts slightly decreases and remain constant till the end of the simulation (Fig 4.4.6a). The timeline representation of contacts shows that Thr51, Lys73, Arg116, and Asp218 make strong interactions throughout the 100 ns of simulation time. While Asp208, Asn209, and Asp221 make interactions around up to 40 nanoseconds of simulation time (Fig 4.4.6b).

RMSD analysis of the SARS-CoV-2-RdRp-NiRAN domain-Brepocitinib complex showed some fluctuation up to 25 ns of simulation after that it became stable till the end of 100 ns of simulation. While ligand RMSD after initial fluctuation of up to 6 ns it becomes stable up to 30 ns. After that, no considerable changes in the ligand RMSD were observed (Fig 4.4.5Aa). RMSD mean for backbone side-chain and ligands were calculated and these were found to be 4.743±0.397Å, 5.665±0.415Å, and 1.588±0.298Å respectively.

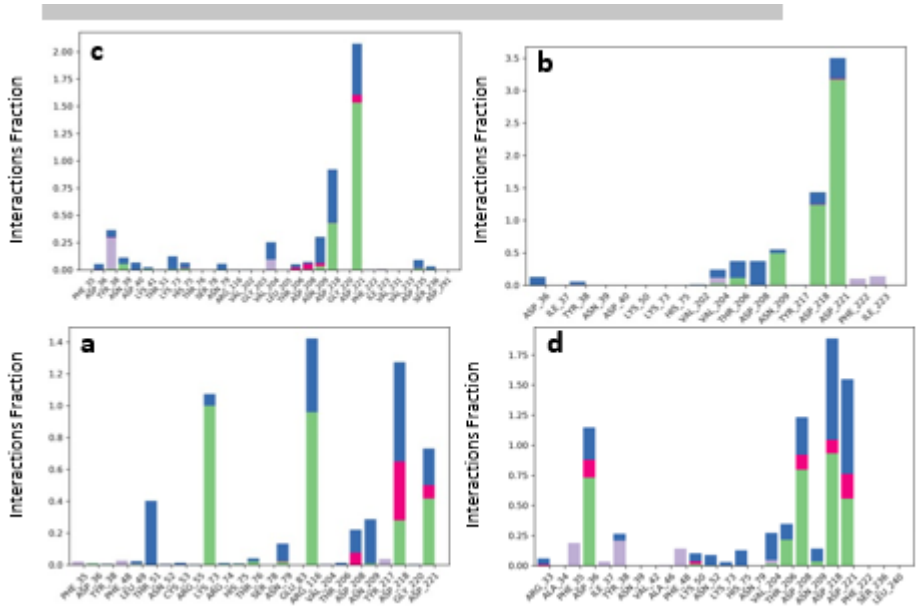

Fig 4.4.4: Protein-ligands contacts histogram representing important interacting residues of SARS-CoV2-RdRp-NiRAN domain with inhibitory compounds during MD simulation. X-axis showing residues and Y-Axis showing interactions fraction. (a) interactions with brepocitinib (b) interactions with decernocitinib (c) interactions with filgotinib (d) interactions with ibrutinib. The green color representing H-bond, violet representing hydrophobic, pink represents ionic, and blue representing water bridges, interactions fraction.

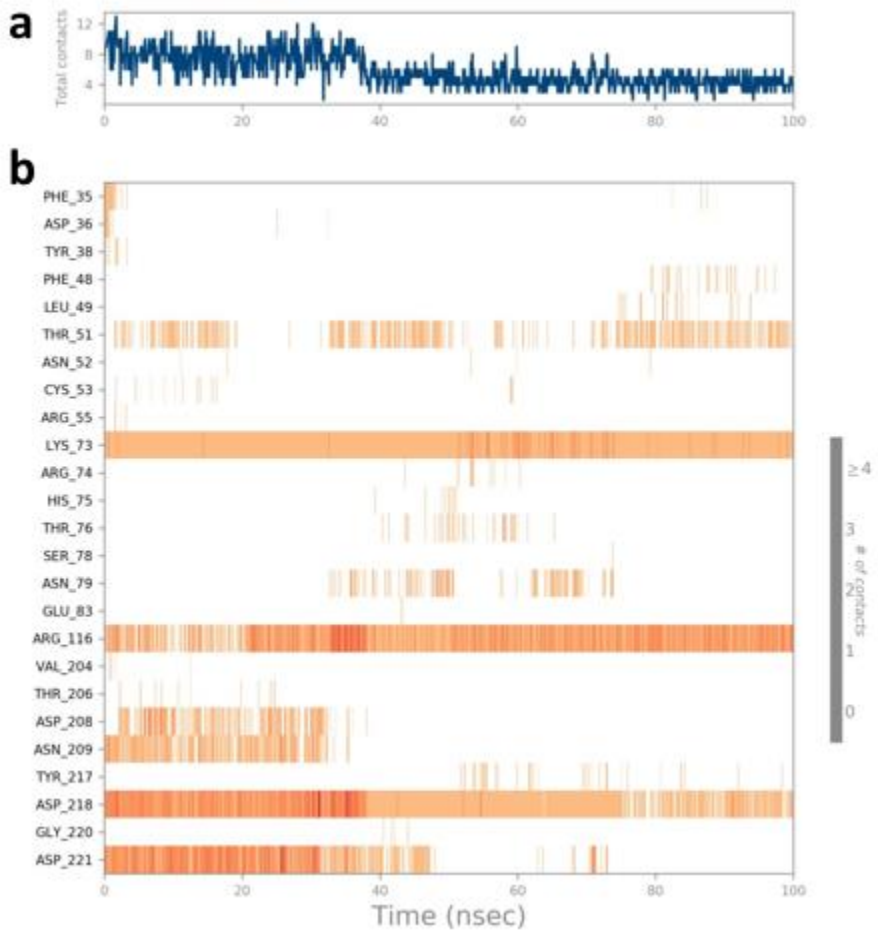

Figure 4.4.6: A timeline representation of the interactions and contacts (H- bonds, Hydrophobic, Ionic, Water bridges). The top panel shows the total number of specific contacts the protein SARS-CoV2-RdRp-NiRAN domain (residues 1-400) makes with the brepocitinib throughout the trajectory. The bottom panel shows which residues interact with the brepocitinib in each trajectory frame. Some

residues make more than one specific contact with the ligand, which is represented by a darker shade of orange, according to the scale to the right of the plot.

4.4.5.1.b. (SARS-CoV-2-RdRp-NiRAN domain/Decernocitinib)

2D interaction diagram after MD simulation showed the interactions of decernocitinib with the SARS-CoV-2-RdRp-NiRAN domain (Fig 4.4.3b). The main interacting residues were Thr206, Asp208, Asp209, Asp218, and Asp221. These were the residues that showed the interaction of more than 20% of the simulation time. Among these residues, only Asn209 donates an H-bond to the decernocitinib while the other residues Thr206, Asp208, Asp218, and Asp221 received H-bond from the decernocitinib.

Histogram of protein-ligand contacts (SARS-CoV-2-RdRp-NiRAN domain-decernocitinib) represents different types of bond interaction fractions (Fig 4.4.4b). The main interacting residues were Val204, Thr206, Asp208, Asn209, Asp218, Asp221, Phe222, and Ile223. Thr206, Asn209, Asp218, and Asp221 showed the direct H-bond interaction and the H-bond through water molecules i.e., called water bridges. Val204 showed hydrophobic and water bridge interaction while Phe222 and Ile223 showed only hydrophobic interactions.

Total contact analysis suggests the total number of specific contacts formed during the simulation. SARS-CoV-2-RdRp-NiRAN domain formed bonds with the ligands. In the case of decernocitinib total contacts remained high up to 50 ns after that it dropped slightly up to 75 ns and after that, it again increased and remained constant till the end of 100 ns of simulation (Fig. 4.4.7a). Fig 4.4.7b represents that which specific residue interact with the ligand in each trajectory frame. In the case of decernocitinib Val204, Thr206, Asp208, Asn209, Asp218, Asp221, and Ile223 made contacts throughout the simulation. Out of these Val204, Asp208, Asn209, and and Ile223 established good interactions whereas Asp218 and Asp221 showed very strong interactions (Fig 4.4.7b).

RMSD graph of the SARS-CoV-2-RdRp-NiRAN domain-decernocitinib complex suggests that fluctuations in the protein RMSD main stable from 5 to20 ns after that the RMSD values increase with simulation time, while fluctuations in the ligand RMSD were observed throughout the simulation time (Fig 4.4.5B.a). The RMSD

mean for backbone side-chain and ligand were calculated to be 4.482±0.888Å, 5.490±0.899Å, 0.961±0.475Å respectively.

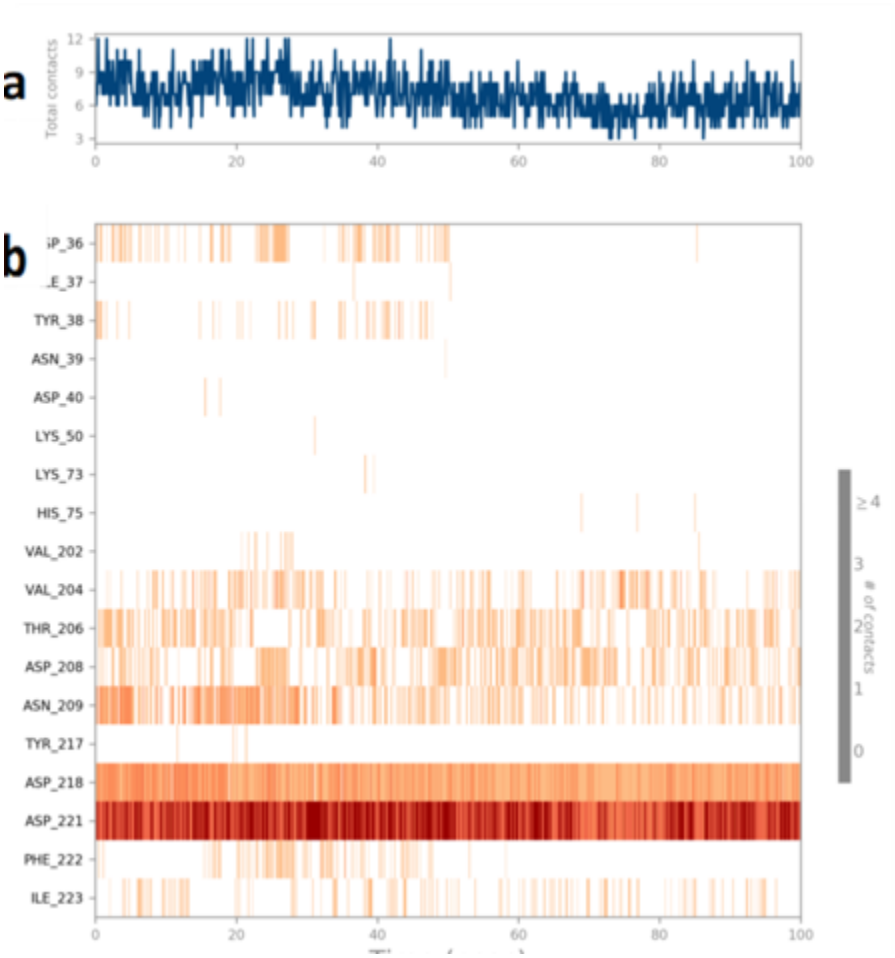

Fig 4.4.7: A timeline representation of the interactions and contacts (H-bonds, Hydrophobic, Ionic, Water bridges). The top panel shows the total number of specific contacts the protein SARS-CoV2-RdRp-NiRAN domain (residues 1- 400) makes with the decernocitinib throughout the trajectory. The bottom panel shows which residues interact with the decernocitinib in each trajectory frame. Some residues make more than one specific contact with the ligand, which is represented by a darker shade of orange, according to the scale to the right of the plot.

4.4.5.1.c. (SARS-CoV-2-RdRp-NiRAN domain/Filgotinib)

Post-MD simulation 2D interaction diagram of SARS-CoV-2-RdRp-NiRAN domain with the filgotinib shows the main interactions with the Asp218 and Asp221. Asp218, and Asp21 both receive the H-bonds from the filgotinib. And these were the only interactions that remained present for more than twenty percent

of simulation time (Fig 4.4.3c).

Histogram of protein-ligand contacts shows that the residues taking part in the interaction of the SARS-CoV-2-RdRp-NiRAN domain with the filgotinib (Fig 4.4.4c), this also represents the bound fractions. The main interacting residues which show considerable effect were Tyr38, Val204, Thr206, Asp208, Asn209, Asp218, and Asp221. Asp218 and Asp221 show strong H-bond interactions also. Asp218 and Asp221 also show water bridges while Asp221 shows ionic interaction. Tyr38 and Val204 showed hydrophobic and water bridge interactions. Asn209 shows H-bond, water bridge, and ionic interactions (Fig 4.4.4c).

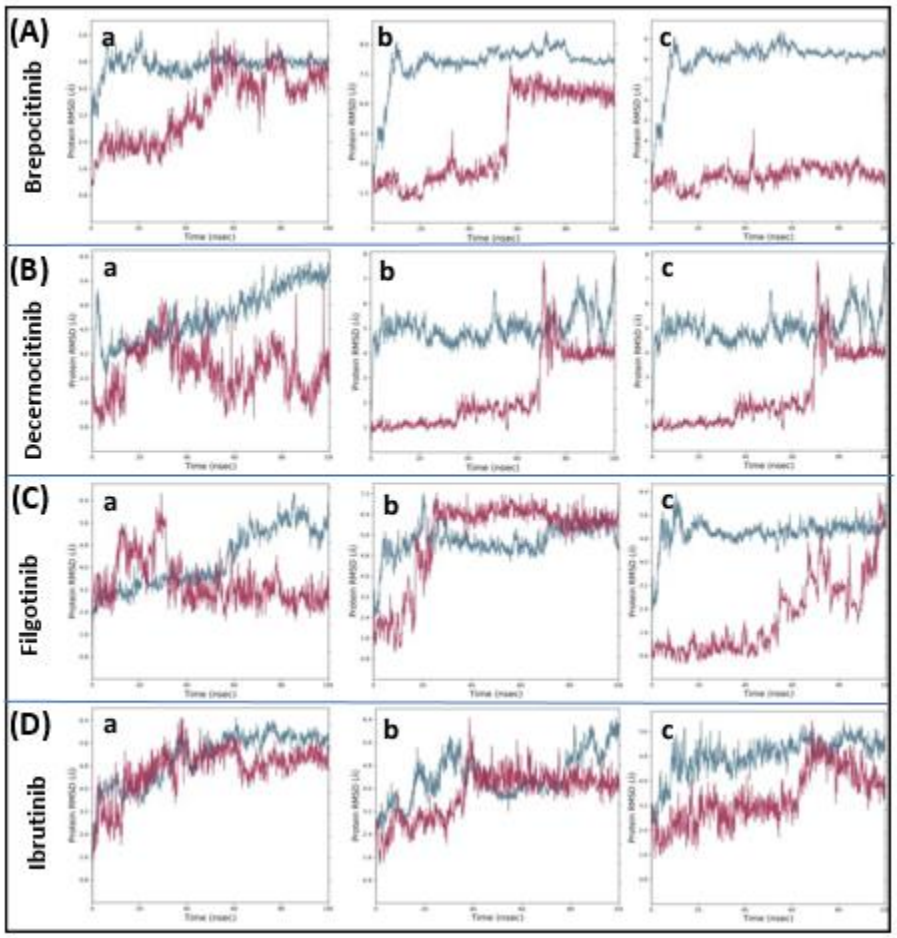

Fig 4.4.5: RMSD results of protein and protein-ligand complexes. The blue graph represents protein RMSD and the maroon graph represents protein- ligand complex RMSD. All the simulations were performed in triplicate and for each complex results are shown in different panels. Panel (A) SARS-CoV- 2-RdRp-NiRAN

domain alone and with brepocitinib in a complex, panel (B) SARS-CoV-2-RdRp-NiRAN domain alone and with decernocitinib in a complex, panel (C) SARS-CoV-2-RdRp-NiRAN domain alone and with filgotinib in complex, and panel (D) SARS-CoV-2-RdRp-NiRAN domain alone and with ibrutinib in the complex.

Total contact analysis during the simulation shows that the highest number of contacts were found during the 12 to 22 ns and 53 to 56 ns and the rest of the simulation time remained constant (Fig 4.4.8a). Supp. Fig 4.4.8b indicates that filgotinib interacts with the Tyr38, Val204, Asn209, Asp218, and
Asp221. Out of these residues, Asp218 and Asp221 show strong interactions while Tyr38, Val204, and Asn209 show good interactions.

RMSD plot of SARS-CoV-2-RdRp-NiRAN domain-filgotinib complex showed stable protein RMSD graph till 50 ns of MD simulation and after that an elevation in the graph was observed. In the case of ligand RMSD up to 38 nanoseconds fluctuations were observed and after that, stability in the RMSD was observed till the end of the simulation (Fig 4.4.5C.a). The RMSD mean for backbone, side-chain, and ligands were calculated to be 4.292±1.034Å, 5.275±1.008Å, and 1.308±0.256Å respectively.

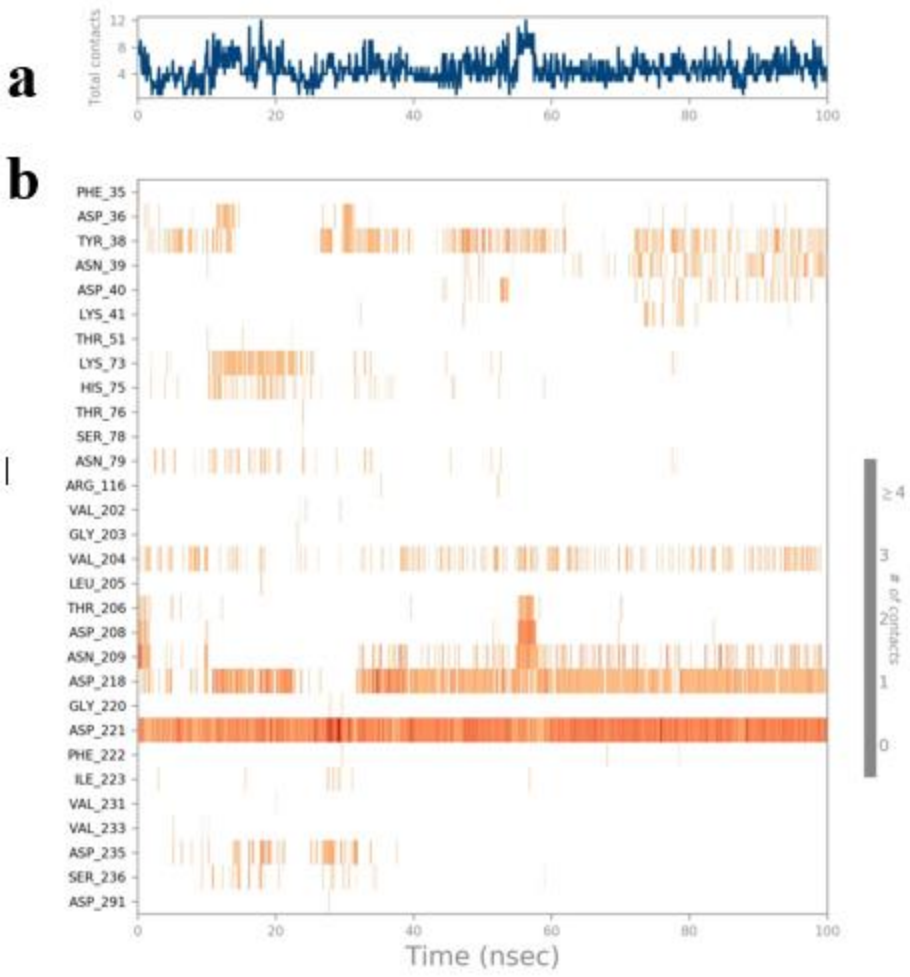

Fig 4.4.8: A timeline representation of the interactions and contacts (H-bonds, Hydrophobic, Ionic, Water bridges). The top panel shows the total number of specific contacts the protein SARS-CoV2-RdRp-NiRAN domain (residues 1- 400) makes with the filgotinib throughout the trajectory. The bottom panel shows which residues interact with the filgotinib in in each trajectory frame. Some residues make more than one specific contact with the ligand, which is represented by a darker shade of orange, according to the scale to the right of the plot.

4.4.5.1.d. (SARS-CoV-2-RdRp-NiRAN domain/Ibrutinib) The 2D interactions diagram after MD simulation showed stable residues for more than 20% of simulation time. Fig 4.4.3d shows the interacting residues of the SARS-CoV-2-RdRp-NiRAN domain with the ibrutinib. The main interacting residues are Asp36, Thr296, Asp208, Asp218, and Asp221. All the residues receive the H-bond

from the ibrutinib, and the residues Asp36, Thr296, and Asp208 displayed direct H-bond while Asp218 and Asp22 made H-bond through water molecules

Histogram of protein-ligand (SARS-CoV-2-RdRp-NiRAN domain with ibrutinib) contacts shows the main interacting residues and bond fractions (Fig 4.4.4d). The main residues of the SARS-CoV-2-RdRp-NiRAN domain which show interaction with the ibrutinib were Asp36, Tyr38, Val204, Thr206, Asp208, Asn209, Asp218, and Asp221. Asp36, Asp208, Asp218, and Asp221 show strong H-bond interactions, as well as these residues also show water bridges and ionic interactions. Thr206 and Asn209 also show H-bond and water bridge interactions. Val204 shows water bridge and hydrophobic interaction (Fig 4.4.4d).

Total contact analysis of the SARS-CoV-2-RdRp-NiRAN domain showed that during the 100 ns of MD simulation maximum number of contacts were observed between 50 to 60 ns and the rest of the time contacts remained almost similar (Fig 4.4.9a). Timeline representation of the contacts shows that Phe35, Asp36, Thr38, Val204, Thr206, Asn209, Asp218, and Asp221 interacted with ligands throughout the simulation. Out of these Asp36, Asp208, Asp218, and Asp221 showed strong interactions as compared to other residues (Fig 4.4.9b).

RMSD plot of the SARS-CoV-2-RdRp-NiRAN domain and ibrutinib is represented in Fig 4.4.5D.a. Protein RMSD becomes stable after 50 ns of simulation similarly, ligand RMSD became stable after 50 ns of simulation. The RMSD mean for backbone side-chain and ligand were calculated to be 5.118±0.893Å, 5.966±0.869Å, and 1.497±0.565Å respectively.

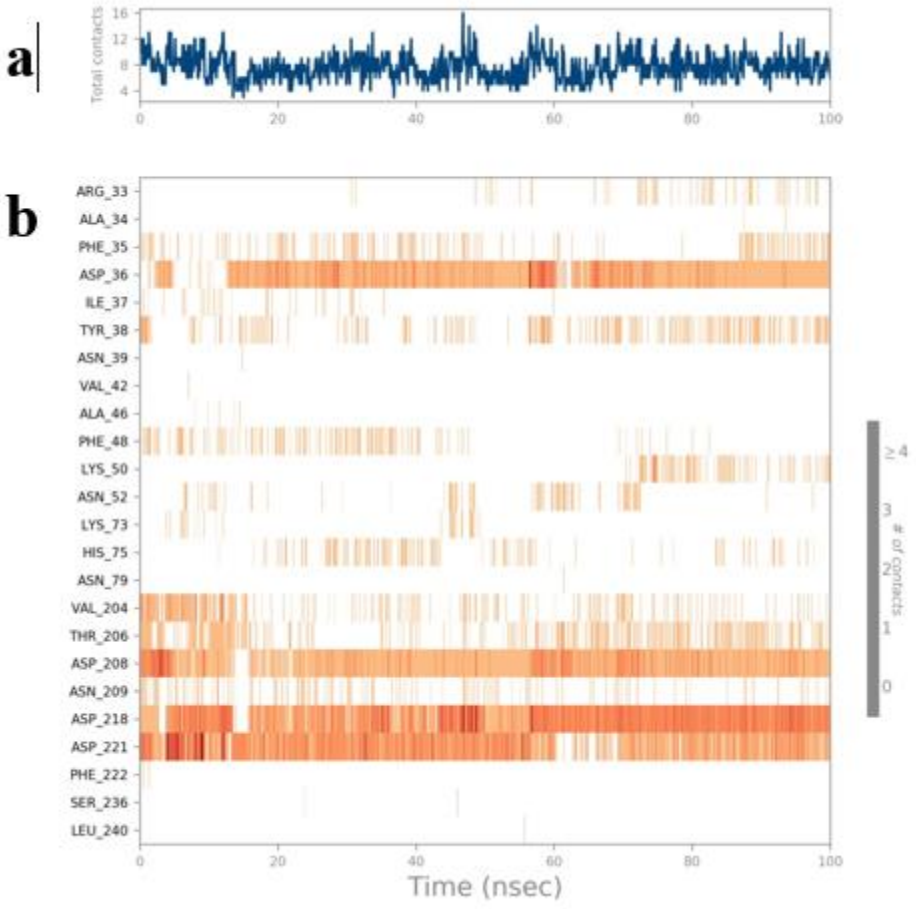

Fig 4.4.9: A timeline representation of the interactions and contacts (H-bonds, Hydrophobic, Ionic, Water bridges). The top panel shows the total number of specific contacts the protein SARS-CoV2-RdRp-NiRAN domain (residues 1- 400) makes with the ibrutinib throughout the trajectory. The bottom panel shows which residues interact with the ibrutinib in each trajectory frame. Some residues make more than one specific contact with the ligand, which is represented by a darker shade of orange, according to the scale to the right of the plot.

CHAPTER 5

DISCUSSION

Various studies suggest an association between *H. pylori* and GC (Yamaoka, 2010). Infection of *H. pylori* in less developed Asian countries like India, Pakistan, Thailand, and Bangladesh is more prevalent than in more developed Asian countries like Japan and China. Interestingly, the occurrence of GC is lower in these less-developed Asian countries compared to Japan and China (K. Singh & Ghoshal, 2006). A similar enigma has been reported from Africa as compared to the Western countries (Sanpui, Chattopadhyay, & Ghosh, 2011). The prevalence of *H. pylori* infection and the occurrence of GC may not appear to be proportionate around the world (Crew & Neugut, 2006). This may be attributed to the variations in the *H. pylori* strain pathogenicity and other associated risk factors for GC. It is essential to understand the discrepancy in *H. pylori* pathogenicity due to geographical and host anatomical locations. In the present study, we were able to demonstrate significantly different growth patterns of isolated *H. pylori* collected from gastric biopsy and juice samples. These findings motivated us to validate the growth pattern of various clinical *H. pylori* isolates through plate densitometry. The *H. pylori* isolation from two different niches of the same person may also lead to a different growth pattern. For the first time, our study revealed that *H. pylori* isolated from the biopsy grow aggressively compared to those isolated from gastric juice of the same subject. For example, HJ1 and HB1; HJ10 and HB10; and HJ14 and HB14 were isolated from two different niches of the same subjects. There was a significant difference in the growth pattern of HJ1 and HB1, which was not much remarkable in the case of HJ10 and HB10, as well as HJ14 and HB14. This finding demonstrates the importance of infection sites and their micro-environment for *H. pylori* dependent disease progression. Similar findings have been reported in pneumococcal infection (Ribble, Goldstein, Norris, & Shellman, 2005). Hence, these results show a specific pattern for the adaptation of *H. pylori*, which may act as a milestone in disease progression and be subjected to further investigation. Earlier, Marshall et al. showed that *H. pylori* eradication resulted in rapid gastric ulcer healing (92% vs. 61%) and a lower relapse rate (21% vs. 84%) than non-

eradication (Hooi et al., 2017). Importantly, resistance to antibiotic treatment is one of the major causes for the development of primary *H. pylori* infection to chronic gastritis and GC (Shenoy & Orihuela, 2016). Studies reported that *H. pylori* isolated from the Indian population are resistant to its specific antibiotics (Ramakrishna, 2006). Additionally, some strains of *H. pylori* are also resistant to triple therapy, which further increases the complication in the eradication procedure (Ansari & Yamaoka, 2018). The transmission mode of *H. pylori* is an oral-oral or oro- faecal route (Datta et al., 2005). Therefore, the oral cavity may serve as a reservoir for *H. pylori* (Gebara et al., 2006). Earlier studies demonstrated that relapse of *H. pylori* infection is mainly due to the presence of its extra-gastric reservoir in the oral compartment (Thyagarajan et al., 2003). Hence, eradication of *H. pylori* in the mouth may help in restricting its transmission and relapse from mouth to stomach (Anand et al., 2006). In our study, the approach is to eliminate *H. pylori* in the oral microenvironment using mouth rinses. It will further help in treating the infection and will enhance the treatment outcome in gastric abnormalities. Various antiplaque and antimicrobial agents are known for inhibiting the growth or killing the target bacteria present in the oral microenvironment. These solutions may consist of chlorhexidine (Salles & Mégraud, 2007), essential oil (Castro-Muñoz et al., 2017), cetylpyridinium chloride (Mathur, Mathur, Srivastava, & Khatri, 2011), povidone-iodine (Marchetti et al., 2011), etc. In our study, we investigated the effect of these oral rinses on *H. pylori* growth and its carcinogenic abilities. Based on differential growth observation of these isolates, we selected two fast (HB1 and HB5) and two slow-growing strains (HJ9 and HB14), along with one reference strain I10, for further study. Oral rinses B, D, and E, were efficient in killing fast-growing strains with 30 s incubation. In contrary to this, oral rinse A and C act as bacteriostatic and inhibit the growth until 2 h. Additionally, in the case of slow-growing strains (HJ9 and HB14), all used solutions except C are useful, while, solution C act as bacteriostatic for up to 12 h. Interestingly, all used oral rinses were found to be efficient in killing reference strain I10, which has been grown for a long time in laboratory conditions. To understand the pathogenic islands of various clinical isolates, there is a need for further investigation of differential oral rinse

response in clinical isolate vs. reference strain even though their growth patterns are similar. To further validate the above experiment, plate densitometry was performed. It was observed that the growth of fast-growing strains (HB1 and HB5) with the treatment of solution C was detected at 12 h in comparison to 6 h of untreated. However, in liquid culture growth was observed at 6 h compared to 2 h in untreated. The growth of isolated strains (HJ1, HB4, HJ9, HB10, HJ10, HB14, and HJ14) was similar to the reference strain I10, whereas, HB1 and HB5 show about 15-fold higher growth after 12 h. These fast-growing strains reflect higher growth at 2 and 6 h by 4 and 9 folds, respectively. Importantly, the growth of HB1 and HB5, which was observed with solution A treatment in liquid culture, was not visible in the plate densitometry. Moreover, the growth of wild-type fast-growing strains could be detected within 2 h in liquid culture compared to 6 h in plate densitometry. The use of oral rinses is a common practice, while prolonged and repetitive use of these oral rinses has adverse effects on the users (D. Hu, Li, Sreenivasan, & DeVizio, 2009; Roopashri, Jayanthi, & Guruprasad, 2011). A study conducted by McGaw & Belch shows negligible toxicity associated with the use of chlorhexidine mouth rinses through radiolabeling methods (Rath & Singh, 2013). However, such studies were conducted in the 1980s; hence, further investigations with modern detection techniques are needed in long-term follow-up. Research on povidone-iodine, reveals that it can cause acute renal failure, mainly when absorbed through mucosal surfaces (McGaw & Belch, 1985; Patel, Gallagher, & Chapple, 2018). Even diluted solutions of povidone-iodine (0.1 to 20%) are toxic to human fibroblasts, granulocytes, and monocytes (Béji et al., 2006). Toxicity of another solution, cetyl pyridinium chloride, is noticed with vomiting, diarrhoea, and abdominal pain. Ingestion of this solution in concentrated form may produce burns of the mouth, pharynx, and oesophagus (Gautam & Gautam, 2018). Additionally, hemorrhagic GI tract necrosis and peritonitis have also been reported (Gautam & Gautam, 2018). Prolonged exposure to common constituents of oral rinses like essential oils, menthol, thymol can act as potential allergens in various ethnical races (Balin & Pratt, 2002). Moreover, some manufacturers produce alcohol-based mouthwashes, which can cause complications like irritation of oral mucosa and

maybe hazardous if ingested accidentally during pregnancy (Antignac, Nohynek, Re, Clouzeau, & Toutain, 2011). One of our focuses in this study was to reduce the time of exposure to minimize the possibility of toxicity caused by these solutions. To achieve our goal, we performed the 5 s treatment and compared it with the 30 s treatment of *H. pylori* isolates. We selected those oral rinses which were efficient in the 30 s treatment in combinations and alone. As expected, the growth of slow-growing strains (I10, HJ9, and HB14) was controlled through all used oral rinses at 5 s incubation. However, only solution B and its combination seem to be potent for all *H. pylori* strains. Strikingly, oral rinses D and E, which were potent on 30 s treatment, have not shown comparable results with fast-growing strains. The high efficacy of solution B may be attributed to its sizeable dicationic molecule (Chlorhexidine), which can adsorb onto negatively charged bacterial cell walls (Antignac et al., 2011). This increases the permeability of the inner membrane and leads to the leakage of low molecular weight components. At 0.2% concentration, this damage is permanent and hence acts as a bactericidal agent (Antignac et al., 2011). The Cag pathogenicity island (cag-PAI) is one of the major virulence determinants of *H. pylori*. Irrespective of the growth pattern variation in isolated *H. pylori* strains, a significant downregulation of the CagA gene was observed with solution B. Also, prolonged exposure to solution C and D to I10, HB14, and HB1 diminish the expression of CagA. Here Cag A expression imitates the growth of *H. pylori* after solution B treatment. EB/AO staining has been used as a gold standard to differentiate between live, apoptotic (early/late), and necrotic cells. We observed that *H. pylori* treated with solution B and incubated with AGS shows more cells in the late apoptotic stage. While with solution C, D, and E treatment, cells are either in the early apoptotic stage or live. This reflects that solution B is the most effective among all the studied oral rinses. To understand the growth arrest of *H. pylori* through used oral rinses, we have mapped several mechanisms of cell death, mainly apoptosis and necrosis. Interestingly, extrinsic apoptotic marker FADD is slightly enhanced in slow-growing strain HJ9 and HB14 with selective oral rinses. Although, studies suggest that FADD is expressed on the surface of cytotoxic T lymphocytes (CTLs) and natural killer (NK) cells as part of their armamentarium

against infected or transformed cells (Reisfield et al., 2011). Moreover, markers for the intrinsic pathway, APAF1 show higher expression during shorter exposure of solution B, C, D, and E to HJ9, while the result is not similar for more prolonged exposure. Notably, BID shows selective up-regulation with solution D in slow-growing strains. Studies have demonstrated that both APAF1 and BID belongs to the BCL-2 family and act with the mitochondria-related apoptotic pathway (Mathur et al., 2011; Wilson, Dixit, & Ashkenazi, 2009). However, the expression pattern for BAK, PUMA, and NOXA was not decisive with used oral rinses s for all included *H. pylori* strains. PUMA and NOXA belong to the proapoptotic BH3 only family, which regulates BCL-2 activity (Patwardhan, Beverly, & Siskind, 2016) Interestingly, the anti-apoptotic gene, BCL-2, was noticeably down-regulated in 5 s treatment while not in 30 s with the selected oral rinses. *H. pylori* usually infect during childhood, where its site of residence is the stomach for decades, causing GC, peptic ulcer, and gastritis.

Further, this bacterium is known to infect half of the world population (Montecucco & Rappuoli, 2001). Since we observed the difference in the growth pattern of *H. pylori* isolated from the biopsy compared to those isolated from gastric juice of the same subject. We further wanted to study the effect of adhesion and secretory proteins of *H. pylori* along with combination with EBV. EBV is another pathogen that is a ubiquitous human herpesvirus with oncogenic activity (Iizasa et al., 2012). EBV is known to be associated with 10 % of gastric cancer (Nishikawa et al., 2018). We also wanted to study the effect of co-infection on GC cells. Consistent with previous reports, morphological changes were observed due to bacterial infection, which supports aggressive cell proliferation (Ciufo et al., 2001). CagA + *H. pylori* infection in AGS cells causes a hummingbird phenotype by dephosphorylating of vinculin. Hence, vinculin may be one of the reasons for the morphological changes (Moese et al., 2007). But as the coinfection provides different morphology, there might be other gene involvement as well. This study demonstrates morphological changes in co-infected AGS cells with bacterial infection followed by EBV. In the co-infected cells, the invasive form was observed at 12 h compared to a previous study in which they were observed at 24 h (Stein et al., 2002). These morphological

changes may be associated with the possible role of EBV and *H. pylori* co-infection in early cell transformation in the gastric epithelial cell line. Further, we were able to quantify the tapering ends by infecting the cells with bacteria at different time intervals. After 12 h incubation of co-infected cells, a remarkable elongation of tapering ends of cells was observed. In this study, 12 h seems to be a potential time interval to evaluate the effect of EBV on the cells infected with bacteria. These co-cultured AGS cells with *H. pylori* strains and EBV showed an increased number of humming-bird cells. This phenotype is considered to promote scattering and spreading of cells, which may be important in carcinogenesis (Argent et al., 2004; J. qiang Guo et al., 2017). But to the best of our knowledge, no such study for length quantification is done for this purpose.

Further to demonstrate the differential expression of kinase not only in co-infected cells but also with two different approaches, i.e., with transwell inserts (indirect approach) and without transwell (direct approach) was used. With indirect and direct approaches, we aim to find the most affected kinase at various time intervals of 12, 24, and 36 h, respectively. The TYK2 and EPHB6 gene were found to be up-regulated by adherence of bacteria to the cells in the presence of EBV, whereas secretory proteins of bacteria up- regulate ITK and FYN expression in the presence of EBV. Though, the expression of genes varies with infection of AGS with EBV, EBV-I10, EBV- HB1, and EBV-HJ9, respectively. Moreover, in the direct approach, the ITK gene showed similar down-regulation in the coinfection of AGS with EBV- I10, EBV-HB1, and EBV-HJ9. In contrast, the TYK2 gene showed significant upregulation in comparison to I10 and HJ9 co-infected cells than in infection with EBV or EBV-HB1 only. In 12 h, the EPHB6 gene transcript also showed a significant increase in the expression in all co-infected cells. However, the EPHB6 gene showed the highest expression in EBV-HJ9 co-infected cells. Similar results were observed with the FYN gene at 24 h. Hence, our findings suggest that TYK2, EPHB6, and FYN can be used for an early prognosis for GC. With the Indirect approach, the ITK gene showed a remarkably significant increase in all infections. Whereas, EBV, only infected cells showed the highest expression, in comparison to EBV-I10, EBV-HB1, and EBV-HJ9 whose expression was

significantly increased. An earlier study conducted on breast cancer cells (MCF7) found that FYN gene expression was higher at 24 h (Lee et al., 2018). Moreover, the expression of TYK2 and ITK was overexpressed in gastric tissue samples (C. Wu et al., 2007). EphB6, an Eph receptor that doesn't have tyrosine kinase activity, was reported to be expressed in some human cancers. Ephb6 with APC mutation is found to be overexpressed in colorectal cancer (J. Liu et al., 2017). Also, reports have suggested that these kinases may have a role in gastric cancer progression (Morishita, Gong, & Masaki, 2014). A similar trend was observed in the FYN gene except for expression in EBV-HJ9, which was reduced in comparison with EBV-I10. Though in EPHB6, considerable up-regulation was observed in all. Hence, when the secretory pathway is of *H. pylori* is concerned ITK, FYN, and EPHB6 can be investigated thoroughly for further studies.

Moreover, *H. pylori* consist of various genes that contribute to enhancing its infection, such as T4SS-pilus- localized protein CagA, vacuolation causing secretory protein VacA, and outer membrane protein BabA. CagA+ *H. pylori* strain increases the risk of distal GC as it uses the integrin receptor present on the host's cells for its entry into the cells (Peek & Blaser, 2002). CagA bridges the T4SS to integrin α5 β1 on host cells, which activates the SRC and focal adhesion kinase, which ensures that CagA is phosphorylated at the site of infection (Selbach et al., 2003). VacA is a secretory protein that causes vacuolation in cultured epithelial cells. VacA binds to integrin β2 and blocks interleukin-2 mediated signalling, which causes downregulation of the Ca2+- dependent phosphatase calcineurin and inhibits antigen-dependent proliferation of transformed T cells (Gebert, Fischer, Weiss, Hoffmann, & Haas, 2003). Eventually, *H. pylori* interfere with tyrosine kinase, Crk, GTPase, and MAP kinase signalling leading to peptic ulcer, gastritis, and GC (Brandt et al., 2007). Although the site of the residence of *H. pylori* remains to be within the semi-permeable mucous gel layer of the stomach facing towards the apical surface of gastric epithelial cells, about 20% of the bacteria is known to bind with the epithelium (J. F. Tomb et al., 1997). When genome analysis of *H. pylori* strains was done, a very high proportion of protein-encoding for the open reading frame was identified in the outer and inner membrane of bacterium which

is known as outer membrane proteins (omPs)such as BabA which has a role in increased mucosal inflammation, atrophy and severe gastric injury (Alm et al., 1999; Yamaoka, 2008).

Importantly, apoptosis is a regulatory action taken by the cell for cell replacement and damaged cell removal, which can be characterized by chromatin condensation, cell shrinkage, and the formation of apoptotic bodies (Chandra, Samali, & Orrenius, 2000). This process is the result of the extrinsic pathway as the death receptor and the intrinsic pathway (Sai-qi Wang et al., 2016). The death receptor is located at the cell surface, such as Fas/Fas ligand is induced by extracellular stress. In comparison, the intrinsic pathway is induced mainly through intracellular stress, which is associated with mitochondria, for example, APAF-1 and BCL-2 families (Kale, Osterlund, & Andrews, 2018). To explore the expression of apoptotic genes through the direct approach, we selected nine apoptotic genes that have been associated with GC. Our experiment found that apoptotic genes, namely APAF-1, BIK, FASL, and BAX, were significantly down-regulated at 24 h (Fig. 6). Earlier reports suggested that apoptotic genes like APAF-1, BCL-2, BAX, and Bcl-2 family were found to be up-regulated in gastric cancer tissues (J. qiang Guo et al., 2017; Kale et al., 2018). Experiments performed with *H. pylori* in epithelial cell background also demonstrated the expressional differences for APAF-1, Fas-Fas ligand, and Bcl-2 related genes (BCL-2, BAX, and BAK) genes at 48h (Choi, Kim, Kim, Jung, & Song, 2003). Furthermore, based on the experiments performed in the report, a comprehensive representation of the outcome of experiments is diagrammatically illustrated in Fig. 6. Where the effect of direct and indirect coinfection in kinase and apoptosis-related signalling pathways is diagrammatically represented.

Further, we wanted to study the effect of doses of bacteria and EBV in gastric cancer cells. For the same purpose two modes of infection were used; IDD and EDD, both patterns comprising the uninfected AGS cells which are contemplated as a control. Further, in the IDD approach, EBV infected to AGS cells were also considered as control whereas increasing doses of *H. pylori* (I10) in the order of MOI 100, 200, and 500 were given with the optimal dose of EBV (100). While in

the EDD mode of infection, I10 infection to AGS cells was viewed as control, and increasing doses of EBV in the order of 50, 100, and 150 were given along with the optimal dose of I10 (MOI 100). The initial infection of I10 was given for 6 h in all modes of infection followed by coinfection for 12 h. The authors earlier reported that 12 h post-infection is the suitable time to examine the effect of EBV on *H. pylori*-infected AGS cells. The coinfected AGS cells exhibited an increased number of hummingbird-like phenotypes (Sonkar, Verma, et al., 2020). Further, previous reports also showed that *H. pylori* can inflect expression of various cellular genes associated with inflammation (Niwa et al., n.d.). Moreover, this infection pattern administered a suited niche for EBV-driven proliferation (Sankaran-Walters et al., 2011). Pandey et al., 2018 reported that exposure to *H. pylori* can increase the inflammatory response which aids signalling activities and induce EBV-driven proliferation of gastric epithelial cells (Pandey et al., 2018b). The higher load of pathogens like *H. pylori* and EBV in the host plays an important role in disease pathology and cancer progression (Bamoulid et al., 2017; Lahner et al., 2018). Further higher load of EBV is also considered to be a prognostic marker in nasopharyngeal carcinoma (Mazurek et al., 2020b; Nilsson et al., 2019) suggesting an important role of viral load in cancer progression. With the differential doses of pathogens, we aimed to identify the expression of different kinases which were mainly involved in the regulation of gastric cancer at a time interval of 12 and 24 h. EPHA4 mRNA was found to be overexpressed in several gastric cancer cell lines and gastric cancer tissues (Oki et al., 2008). Further, EBV oncogenic gene LMP1 was known to regulate EPHA4 expression (Y.-C. Huang et al., 2016). Mishra et al., 2015 reported that CagA of *H. pylori* regulates the expression of PAK2, PAK1 which in turn depletes the level of FYN (J. P. Mishra et al., 2015). *H. pylori* infection adds to gastric cancer by modulating the activity of various genes such as PDK1 which is involved in the cell survival signalling pathway (King & Obonyo, 2015).

In our previous study, we reported that secretory proteins of bacteria upregulate the expression of ITK and FYN in the existence of EBV (Sonkar, Verma, et al., 2020; B. Yu et al., 2020). ITK and FYN are important enzymes known to be involved in

different cancers (Y. Liu et al., 2019). While FYN is mainly involved in solid tumour formation (B. Yu et al., 2020), ITK is mainly involved in lymphoproliferative disorders and lymphomas (Y. Liu et al., 2019). It is also known to be phosphorylated in EBV-mediated pathologies (Y. Liu et al., 2019). FYN is also reported to promote metastasis and epithelial-mesenchymal transition in gastric cancer (Jie Yu et al., 2020). Therefore, similar to our previous observation, in the current study, we found increased ITK and FYN expression in dose-dependent *H. pylori* and EBV co-infected gastric cancer cells. Furthermore, TYK2 and ITK were showing higher expression in gastric tissue samples (C. Wu et al., 2007). Moreover, receptor tyrosine kinases are known to be involved in cell cycle regulation and cancer progression. In our previous study, we have found the overexpression of receptor tyrosine kinases, ITK, and FYN in *H. pylori* and EBV coinfected gastric cancer cells (Sonkar, Verma, et al., 2020). Additionally, a study by Yu et. al has also shown the role of FYN in cell proliferation and migration of colon cancer cells [313]. In our study, with higher doses of *H. pylori* and EBV in coinfected AGS cells we have also seen increased cell proliferation and migration. Further, we also observed increased cell proliferation and migration at the same dose where ITK and FYN were overexpressed in both IDD and EDD approaches. To understand further how protein expression of ITK modulates with the coinfection of *H. pylori* and EBV, we have used an immunofluorescence assay. Interestingly, we have found that ITK expression increased as the dose of the pathogen increased. We hypothesized that ITK should undergo nuclear localization as the dose of infection increased. We have obtained a similar type of result in which ITK undergoes nuclear localization in the dose of IDD I10/100 and 200. Intriguingly, we have found an increased expression on this dose at the transcript level also. However, further evaluation is required to understand the mechanism. Further, nuclear translocation was not observed in the case of EDD mode of infection but the increase in the expression was seen as the dose of the virus increased. Similarly, ITK is known to be found in the cytosolic and nuclear environment in the case of T-cells. In human T-cells, ITK nuclear importins include chaperone karyopherin α (Rch1α) and mutation in this chaperone devastates its

nuclear translocation (Kosaka, Felices, & Berg, 2006, p. 2; Perez-Villar, O'Day, Hewgill, Nadler, & Kanner, 2001). In the case of T-cells, ITK plays a vital role in proliferation and differentiation, and it is also known to express in several epithelial cells (Kosaka et al., 2006). We believe ITK plays an important role in cell proliferation and has a role in cancer progression in the long term. We also believe ITK is among the most affected gene by pathogen burden, hence can be targeted not only to determine the synergy of the mentioned pathogens but also a load of pathogens.

Several kinases are involved in the different stages of SARS-CoV-2 infection. This virus is known to enter through its interaction with the ACE2 receptor (Indari, Jakhmola, Manivannan, & Jha, 2021; Jakhmola, Indari, Kashyap, et al., 2020). These kinases also play a pivotal role in GC progression. Through structural similarity analyses using DALI, it was believed that the NiRAN domain of SARS-CoV-2 Nsp12 possesses structural features of kinase-like folds. However, its exact role is still unknown (Romano, Ruggiero, Squeglia, Maga, & Berisio, 2020). Hence, repurposing kinase inhibitors of GC for SARS-CoV-2 could aid in designing comorbidity specific therapeutics and reducing drug-induced complications. Furthermore, to the best of our knowledge, this is the first study of targeting kinase in GC comorbidity of COVID-19. There are many available drugs are recommended for the treatment of COVID-19 under drug repurposing strategy. Drugs like lopinavir, darunavir, arabidol, nafamostat and chloroquine inhibit the viral entry by different mechanisms like inhibiting protease, hemagglutinin fusion machinery by preventing membrane fusion, changing endosomal pH etc. (Choy et al., 2020; De Meyer et al., 2020; Hoffmann et al., 2020; Jang & Rhee, 2020; Liu & Wang, 2020; Vankadari, 2020; Yao et al., 2020; Zhu et al., 2020). Drugs azithromycin and doxycyclin inhibit the IL-6 production while tocilizumab inhibits the release of IL-6 (De Meyer et al., 2020; Sargiacomo et al., 2020; Xu et al., 2020). Ruxolitinib and baricitinib target the Janus-Kinase pathway and inhibit cytokine release (Cantini et al., 2020; Cao et al., 2020). The other repurposing drugs have miscellaneous effects on the viral pathogenesis and inhibit the viral growth by different mechanisms, for instance, ivermectin inhibits the nuclear transport

activity, and statins targets the angiotensin-converting enzyme 2 (Wehbe et al., 2021; Wösten-van Asperen et al., 2011). The remdesivir, the most accepted repurposed drug for the SARS-CoV-2, inhibits the RdRp protein, therefore, inhibits the viral replication (Elfiky, 2020).

In our case, we targeted the SARS-CoV-2- RdRp-NiRAN domain, as this is a very important protein for viral replication. We used gastric cancer kinase inhibitors to target the SARS-CoV-2-RdRp-NiRAN domain because these compounds showed a strong affinity with the active site of the SARS-CoV-2-RdRp-NiRAN domain. Moreover, these inhibitors may also inhibit the kinases involved in viral pathogenesis. The purpose of our study was to identify the inhibitors that can target the SARS-CoV-2-RdRp-NiRAN domain which has a kinase-like domain as well as they can also inhibit the kinases involved in the pathogenesis of SARS-CoV-2 and gastric cancer.

Since these kinases play an important role in GC cells, they become natural therapeutic target that could facilitate the treatment in patients with GC infected with COVID-19. Hence, inhibitors against these kinases were used for the present study. Further, the nsp12 /SARS-CoV-2- RdRp contains the NiRAN domain. The NiRAN and the interface domains span over residues 51- 398 of the SARS-CoV-2 RdRp polypeptide sequence which is proposed to have kinase-like folds. Moreover, corresponding residues which are important for the enzymatic activity of this domain mostly occur in pocket 3 are Phe35, Asp36, Ile37, Tyr38, Asn39, Phe48, Leu49, Lys50, Thr51, Asn52, Arg55, Val71, Lys73, His75, Glu83, Arg116, Leu119, Thr120, Lys121, Tyr122, Thr123, Asp 126, Val204, Thr206, Asp208, Asn209, Tyr217, considered to be strictly conserved across SARS-CoV-2-RdRp, whereas other were present in the active site of the domain (W.-F. Zhang, Stephen, Thériault, Wang, & Lin, 2020).

For the MD simulation studies, four drugs were selected which showed the best binding energy and other docking parameters. These are brepocitinib, decernotinib, filgotinib, and ibrutinib which are further sequentially explained. Brepocitinib is a potent JAK1/TYK 2 inhibitor. JAK pathway, as stated earlier, plays an important role in the intracellular signalling of cytokines for the various intracellular

processes, which is deemed to be pivotal in both normal and pathological conditions (Nogueira et al., 2020). Hence the loss of functions of TYK2 can leads to inhibition of the signalling of several cytokines such as IL-6, IL-10, IL-12, and IL-23. These cytokines are crucial for the pathogenesis of autoimmune disease (Minegishi et al., 2006). Brepocitinib which was formerly known as PF-06700841, is currently under investigation for several autoimmune indications (Gerstenberger et al., 2020). It is known to directly inhibit TYK2-dependent IL-12, IL-23 signalling, and JAK2 dependent signalling which includes T-cells and keratinocytes (Page et al., 2020).
Our docking studies using Glide Schrodinger Suites showed binding of brepocitinib binds at the active site of the SARS- CoV-2-RdRp-NiRAN domain. And it showed strong H-bond interactions with the Asp36, Lys73, Asp218, and Asp221. Post MD simulation 2D interaction diagram showed Thr51, Lys73, Arg116, Asp208, Asn209, Asp218, and Asp221 as main interacting residues that remained stable for more than 20 percent of simulation time. When compared, residues Lys73, Asp218 and Asp221 were found common in both docking and post MD simulation interactions. This suggests that the common bonds were quite strong and remained stable during the MD simulation. Histogram diagram of protein-ligand (SARS-CoV- 2-RdRp-NiRAN domain-brepocitinib) contacts also confirmed the above results along with other types of bond fractions and bonds formed during the simulation. RMSD results also suggest that during the simulation the protein and ligand remained stable because because of the minimal fluctuations observed in the RMSD values.
Decernotinib is also known as VX-509, is a selective inhibitor of JAK3. Decernocitinib showed about 25-120-fold higher with JAK3 in comparison to JAK1, JAK2, and TYK2, in cell-based assays (Genovese, Vollenhoven, Pacheco-Tena, Zhang, & Kinnman, 2016). The four JAK'S namely JAK1, JAK2, JAK3, and TYK2 share common subunits that

are used by small cytokines like IL-2, IL-4, IL-7, IL-9, IL-15, and IL-21. Loss of function of JAK3 or the common gamma chain can have an immense effect on the immune system without affecting other organs. Decernocitinib is used used against

a variety of auto-immune diseases (Gadina, Schwartz, & O'Shea, 2016). So far, this is the only JAK3 inhibitor known which has been evaluated in the clinical studies of rheumatoid arthritis. It is also reported that decernocitinib reduced T-cell mediated pro-inflammatory response and modulates this response in immune-mediated diseases such as collagen-induced arthritis and delayed-type hypersensitivity (Mahajan et al., 2015). Docking studies showed decernocitinib has interactions with the Asn209, Asp218, and Asp221. Post MD simulation 2D interactions results showed strong H-bond interactions of residues Thr206, Asp208, Asn209, Asp218 and Asp221 with decernocitinib. Both docking and the post MD simulation results showed common residues Asn209, Asp218, and Asp221 were common which suggests that these residues made strong interactions during the simulation process. Histogram diagram of protein-ligand (SARS-CoV-2- RdRp-NiRAN domain-decernocitinib) contacts also showed similar results with different bond fractions, mainly H-bond and water bridges were observed here. Minimum fluctuations in the protein RMSD also suggested the stability of the protein-ligand complex during the simulation.

Filgotinib is an oral selective JAK1 inhibitor, which was proved effective and safe in the TORTUGA trial for patients suffering from ankylosing spondylitis, rheumatoid arthritis, Crohn's disease, and psoriatic arthritis. Several phase-III trials have been completed for Filgotinib against these diseases (van der Heijde et al., 2018). Filgotinib inhibits JAK1 for longer duration, this is evident from its pharmacodynamic and pharmacokinetic studies. These studies indicate that filgotinib and its active metabolite contribute to its pharmacodynamic properties (Westhovens et al., 2017). Filgotinib showed approximately 30-fold higher efficacies towards JAK1 than JAK2 in human whole blood assay. Moreover, its metabolite also targets JAK2 with lower potency (Vanhoutte et al., 2017).

Our docking results showed that the filgotinib interacts with the Asp40, Asp208, and Asp221 of the SARS-CoV-2-RdRp-NiRAN domain. Post-MD simulation 2D interaction results showed that the filgotinib has the main interactions with the residues Asp218, and Asp221. This suggested that the Asp221 residue of SARS-CoV-2-RdRp-NiRAN domain showed strongest interaction with filotinib.

Histogram diagram of protein-ligand (SARS-CoV-2-RdRp-NiRAN domain-filgotinib) contact also showed the same results and it also represented the different bond fractions like H-bond, water bridges, and hydrophobic interactions. RMSD results suggested that the protein RMSD remained stable from 5 to 55 ns and the ligand RMSD remained stable from 30 till the end of 100 ns of simulation. RMSD results also suggested that the fluctuations in the RMSD values were minimal, which suggested the stability of the protein-ligand complex during the simulation.

Ibrutinib is an oral bioavailable potent inhibitor for Bruton's tyrosine kinase (BTK) enzyme. . It covalently binds to the 481 amino acid Cysteine inhibits the function of the BTK enzyme. Several preclinical studies have reported that it also inhibits many cellular processes like ERK signalling, NF-κB DNA binding, and tumour cell migration. However, it doesn't affect normal T-cell (Byrd et al., 2013). Various molecular and phenotypic analyses have confirmed that Ibrutinib also irreversibly inhibit interleukin-2-inducible T-cell kinase (ITK) by targeting T-cell. ITK is a potent therapeutic target that contributes to various pathogenesis, autoimmune and neoplastic diseases. Since there is a significant homology between BTK and ITK, through in-silico studies, Ibrutinib is considered as an immunomodulatory inhibitor of both the kinases (Dubovsky et al., 2013). It can also inhibit gastric carcinoma cell growth by targeting BTK as BTK is highly expressed in GC cells and ITK is highly expressed in GC tissues (Lin et al., 2000; Wang et al., 2016).

Although ibrutinib is a very effective drug against GC but with chronic lymphoid leukaemia (CLL) it showed an increased risk for second primary malignancies (SPM) (Bond et al., 2020). However, in patients suffering from GC, ibrutinib is found to have additive inhibitory effects against Bruton's tyrosine kinase (Btk). Btk is a member of the Tec-family non-receptor tyrosine kinases family. It is over-expressed in gastric carcinoma tissues and gastric cancer cells. Its inhibition by ibrutinib impedes the growth of gastric cancer cells and is involved in effective cell killing mediated by inhibition of Btk. Further, it also induced the apoptosis of gastric carcinoma cells and is involved as a chemo-sensitizer for docetaxel (DTX) which is a standard care for gastric carcinoma patients (Wang et al., 2016). Hence, to the best of our knowledge, the side effect is validated only for CLL patients and

it has several beneficial effects on GC.

In our study, ibrutinib showed strong H-bond interactions with the SARS-CoV-2-RdRp-NiRAN domain and made interactions with the residues Asp208, Asn209, Asp218, and Asp221, with all these residues received H- bonds from ibrutinib. Post MD simulation 2D interaction diagram showed the residues which remained stable more than 20 per cent time of the simulation. Residues Asp36, Thr206, Asp208, Asp218, and Asp221 showed H-bond interaction during the 100 ns of MD simulation. The common residues before and after simulation suggested that these residues have strong interactions. Histogram diagram of protein-ligand (SARS-CoV-2-RdRp-NiRAN domain- ibrutinib) contact also confirmed the same result and the bond fractions were also represented. The most important interactions during the simulation were H- bond, water bridges, and ionic interactions. RMSD results of protein-ligand complex (SARS-CoV-2-RdRp-NiRAN domain-ibrutinib) showed that after 40 ns of simulation protein RMSD became stable and similar results were observed with the ligand RMSD. In both, cases fluctuations in the RMSD values were observed minimal, which suggested that during the simulation protein and ligand both remained stable.

The docking scores showed strong affinity of brepocitinib, decernocitinib, filgotinib, and ibrutinib with the SARS-CoV-2-RdRp-NiRAN domain. The MMGBSA study also supported docking interactions. The docking scores for the brepocitinib, decernocitinib, filgotinib, and ibrutinib were calculated to be -5.543, - 6.694, - 4.917, and -6.137 respectively. In this study, it was observed that all four inhibitory compounds have almost the same affinity towards the SARS-CoV-2-RdRp- NiRAN domain. After docking studies MMGBSA studies were performed and the binding energies were calculated for all the four compounds and these were found to be -60.1315, -47.6964, -44.1200, -77.1748, for brepocitinib, decernocitinib, filgotinib, and ibrutinib respectively. Besides this, the individual MMGBSA energies like coulomb, covalent, H bond, solvation, and Vander walls were also calculated which also demonstrated strong affinity of the compounds with the compounds with the SARS-CoV-2-RdRp-NiRAN domain. Thus, MMGBSA study results showed that all the compounds have a strong affinity with the SARS-

CoV-2-RdRp-NiRAN domain.

Nidovirus RdRp like SARS-CoV2-RdRp contains an N-terminal NiRAN domain that is absent in other viral RdRPs. This domain was found essential for some viruses' propagation like the equine arteritis virus and SARS-CoV (Lehmann et al., 2015a). Chen et al 2020 showed the binding of the ADP-Mg2+ with the SARS-CoV-2-RdRp-NiRAN domain (J. Chen et al., 2020). It was observed that the ADP-Mg2+ binds to the NiRAN domain with the residues K73, E83, R116, D208, N209, G214, D218, F219, and F222.In our docking and simulation studies, it was observed that brepocitinib binds to residues Asp36, Lys73, Asp218 and Asp221 at the active site before simulation and during simulation brepocitinib interacted with the residues Arg55, Arg116, Asp218 and Asp221. Further, decernocitinib docking studies showed that the main interacting residues were Asn209, Asp218, and Asp221, while during the simulation the main interacting residues were Asp208, Asn209, Asp218, and Asp221. In the case of filgotinib, the main docking interacting residues were Asp40, Asp208 and Asp221, while during simulation the main interacting residues were Asn209, Asp218, Asp221. Similarly, in case of ibrutinib, the main interacting residues in docking were Asp208, Asn209, Asp218, and Asp221, while during the simulation the main interacting residues were Asp36, Asp208, Asp218, and Asp221. These results suggest that the residues, which are involved in the binding of the ADP-Mg2+ with the SARS-CoV-2-RdRp-NiRAN domain, are also common with the residues that are binding with the studied inhibitor. Further, these results showed that all the inhibitory compounds in our study bound to the same binding pocket where ADP-Mg2+binds with the SARS-CoV-2-RdRp-NiRAN domain. These results strongly suggest that the inhibitors used in the study are binding at the active site. Docking scores and MMGBSA and MD simulation results also confirms that the binding is quite strong. Besides this, the surrounding residues were also common before and after simulation in all the four selected inhibitory compounds. These results also suggest that the compounds are binding at their active site, and not leaving the active site during the simulation. Altogether, we studied effective drugs to aid the eradication of oral *H. pylori*. also, we studied the effect of co-infection of *H. pylori* and EBV on GC cells. We further

investigated the specific doses of these infectious agents causing significant changes in GC cells. We also studied the kinase inhibitors against the COVID-19 nsp12-NIRAN domain to address the GC comorbidity of COVID-19.\

Chapter 6

Conclusion and future scope of the thesis

H. pylori adaptation to different physiological habitats in the host may be responsible for the differences in its growth and pathogenicity. For avoiding the challenges of relapse and antibiotic resistance, we used oral rinses and found that these are effective against CagA expression in *H. pylori*. Some of the variability in outcome can be attributed to different bacterial strain specificity, host susceptibility, and the type of response elicited in the infected host. Further, to explore the effect of physiological habitats in infection of *H. pylori* we used clinical *H. pylori* isolates along with reference strain to find its phenomenal changes in gastric epithelial cells along with EBV. The remarkable effect of coinfection on morphological changes was found to be in 12 h intervals on implementing quantification of tapering ends. This study also demonstrated the kinase and apoptotic genes that might be affected in co-infected cells through direct and indirect approaches. Where ITK, EPHB6, TYK2, and FYN kinase are highly expressed kinase genes and APAF, BIK, FASL, and BAX are the significantly down-regulated apoptotic genes. ITK and TYK2 are receptor tyrosine kinase, which is specifically involved in cellular differentiation, survival, and proliferation and contains the conserved domain of Ig domains. In contrary to this, non-receptor tyrosine kinase-like FYN is essential for enzyme regulation, and substrate identification was found to be up-regulated by direct dual infection.

Further, we explored that a certain dose of pathogens (EBV and *H. pylori*) IDD (MOI-200) and EDD (100 µl)) can lead to an increase in the kinase gene expression such as ITK and FYN. This suggests that EBV and *H. pylori* at certain amounts could act in a synergistic way to increase the proliferation and migration of co-infected cells. Interestingly certain doses of *H. pylori* may also affect the location and expression of ITK. Although, this finding needs further evaluation. Hence, a particular dose of EBV and *H. pylori* could lead to severe gastric cancer progression. Therefore, a thorough study about the load of these pathogens and their interaction is necessary for early prognostic of gastric cancer. Moreover, ITK could act as a potential target to determine the pathogen load and synergistic effect of

infectious agents. However, we do consider that further investigation is needed to draw more consequential results.

Moreover, we propose the drugs against kinases that can be repurposed for the treatment of GC patients who are infected with COVID-19. We propose nine drugs namely baricitinib, brepocitinib, decernotinib, fasudil, filgotinib, GSK2606414, peficitinib, ruxolitinib, and ibrutinib against the kinase genes which are highly expressed in GC can target SARS-CoV-2 nsp-12/RdRp region. These drugs have shown strong binding affinity with the aforementioned SARS-CoV-2 region and eight except GSK2606414 drugs, had no AMES toxicity. Further, these drugs were tested for their ADMET properties and drug likeliness. Out of these drugs, we selected four potent drugs brepocitinib, decernocitinib, filgotinib, and ibrutinib based on their docking and ADMET properties, and performed their redocking, MMGBSA, and MD simulation studies and discussed them in detail. These four drugs showed very good binding affinities with the SARS-CoV-2-RdRp- NiRAN domain. This also suggested that the SARS-CoV-2-RdRp-NiRAN domain may have similar structure and folds as the kinases have. Taken all together since no vaccine has been successful till now for the COVID-19 patients and drug repurposing is among the current achievable choice, thus these drugs can be validated in-vitro and in-vivo before clinical trials. These drugs can be utilized for patients with GC who have been infected with SARS- CoV-2.

However, for future scope, there is a need for a detailed study about the molecular pathways modulated by the oral rinses in bacteria and surrounded host cells. These studies will also open a broad scope to apply various bactericidal combinations for the treatment and eradication of *H. pylori* infection. Further, their downstream interlinked pathway can provide a potential strategy to understand the progression of GC. However, we do consider the fact that the number of strains used that were isolated from the patients is limited, and further investigation is required for drawing a more profound conclusion. Moreover, we do believe that brepocitinib, decernocitinib, filgotinib, and ibrutinib have the potential to target the potential active site of SARS-CoV-2. However, in-vitro and in-vivo studies would be required for drawing more profound conclusions

References

Abedi, F., Rezaee, R., & Karimi, G. (2020). Plausibility of therapeutic effects of Rho kinase inhibitors against Severe Acute Respiratory Syndrome Coronavirus 2 (COVID-19). Pharmacological Research, 156, 104808. https://doi.org/10.1016/j.phrs.2020.104808

Aduri, N. G., Montefiori, M., Khalil, R., Gajhede, M., Jørgensen, F., & Mirza, O. (2019). Molecular Dynamics Simulations Reveal the Proton:Peptide Coupling Mechanism in the Bacterial Proton-Coupled Oligopeptide Transporter YbgH. ACS Omega, 4, 2040–2046. https://doi.org/10.1021/acsomega.8b02131

Ahmad, M., Dwivedy, A., Mariadasse, R., Tiwari, S., Kar, D., Jeyakanthan, J., & Biswal, B. K. (2020). Prediction of Small Molecule Inhibitors Targeting the Severe Acute Respiratory Syndrome Coronavirus-2 RNA-dependent RNA Polymerase. ACS Omega. (world). https://doi.org/10.1021/acsomega.0c02096

Alimova, M., Sidhom, E.-H., Satyam, A., Dvela-Levitt, M., Melanson, M., Chamberlain, B. T., … Greka, A. (2020). A High Content Screen for Mucin-1-Reducing Compounds Identifies Fostamatinib as a Candidate for Rapid Repurposing for Acute Lung Injury during the COVID-19 pandemic. BioRxiv, 2020.06.30.180380. https://doi.org/10.1101/2020.06.30.180380

Alm, R. A., Ling, L. S. L., Moir, D. T., King, B. L., Brown, E. D., Doig, P. C., Trust, T. J. (1999). Genomic-sequence comparison of two unrelated isolates of the human gastric pathogen Helicobacter pylori. Nature, 397(6715), 176–180. https://doi.org/10.1038/16495

Alm, R. A., & Trust, T. J. (1999). Analysis of the genetic diversity of Helicobacter pylori: The tale of two genomes. Journal of Molecular Medicine, 77(12), 834–846.

https://doi.org/10.1007/s001099900067

Am, A., J, M., Z, N.-C., & G, C. (2019). HCMV modulation of cellular PI3K/AKT/mTOR signaling: New opportunities for therapeutic intervention? Antiviral Research, 163, 82–90. https://doi.org/10.1016/j.antiviral.2019.01.009

Amgen. (2016). A Phase 1, First-In-Human Study Evaluating the Safety, Tolerability, and Pharmacokinetics of AMG 337 in Adult Subjects With Advanced Solid Tumors (Clinical Trial Registration No. NCT01253707). clinicaltrials.gov. Retrieved from clinicaltrials.gov website: https://clinicaltrials.gov/ct2/show/NCT01253707

Amgen. (2017). A Multicenter, Phase 2, Single Arm, Two Cohort Study Evaluating the Efficacy, Safety, and Pharmacokinetics of AMG337 in Subjects With MET Amplified Gastric/Gastroesophageal Junction/Esophageal Adenocarcinoma or Other MET Amplified Solid Tumors (Clinical Trial Registration No. NCT02016534). clinicaltrials.gov. Retrieved from clinicaltrials.gov website: https://clinicaltrials.gov/ct2/show/NCT02016534

Amieva, M. R., & El–Omar, E. M. (2008). Host-Bacterial Interactions in *Helicobacter pylori* Infection. Gastroenterology, 134(1), 306–323. https://doi.org/10.1053/j.gastro.2007.11.009

Anand, P. S., Kamath, K. P., & Anil, S. (2014). Role of dental plaque, saliva and periodontal disease in *Helicobacter pylori* infection. World Journal of Gastroenterology : WJG, 20(19),5639–5653. https://doi.org/10.3748/wjg.v20.i19.5639

Anand, P. S., Nandakumar, K., & Shenoy, K. T. (2006). Are Dental Plaque, Poor Oral Hygiene, and Periodontal Disease Associated With *Helicobacter pylori* Infection? Journal of Periodontology, 77(4), 692–698.

https://doi.org/10.1902/jop.2006.050163

Ang, Y. L. E., Yong, W. P., & Tan, P. (2016). Translating gastric cancer genomics into targeted therapies. Critical Reviews in Oncology/Hematology, 100, 141–146. https://doi.org/10.1016/j.critrevonc.2016.02.007

Ansari, S., & Yamaoka, Y. (2018). Current understanding and management of *Helicobacter pylori* infection: An updated appraisal. F1000Research, 7. https://doi.org/10.12688/f1000research.14149.1

Antignac, E., Nohynek, G. J., Re, T., Clouzeau, J., & Toutain, H. (2011). Safety of botanical ingredients in personal care products/cosmetics. Food and Chemical Toxicology, 49(2), 324–341. https://doi.org/10.1016/j.fct.2010.11.022

Aoe, T. (2020). Pathological Aspects of COVID-19 as a Conformational Disease and the Use of Pharmacological Chaperones as a Potential Therapeutic Strategy. Frontiers in Pharmacology, 11. https://doi.org/10.3389/fphar.2020.01095

Argent, R. H., Kidd, M., Owen, R. J., Thomas, R. J., Limb, M. C., & Atherton,

J. C. (2004). Determinants and consequences of different levels of CagA phosphorylation for clinical isolates of Helicobacter pylori. Gastroenterology, 127(2), 514–523. https://doi.org/10.1053/j.gastro.2004.06.006

Awad, M. M., Leonardi, G. C., Kravets, S., Dahlberg, S. E., Drilon, A., Noonan, S. A., Heist, R. S. (2019). Impact of MET inhibitors on survival among patients with non-small cell lung cancer harboring MET exon 14 mutations: A retrospective analysis. Lung Cancer (Amsterdam, Netherlands), 133, 96–102. https://doi.org/10.1016/j.lungcan.2019.05.011

Backert, S., Clyne, M., & Tegtmeyer, N. (2011). Molecular mechanisms of gastric

epithelial cell adhesion and injection of CagA by Helicobacter pylori. Cell Communication and Signaling : CCS, 9, 28. https://doi.org/10.1186/1478- 811X-9-28

Backert, S., Tegtmeyer, N., & Fischer, W. (2015). Composition, structure and function of the *Helicobacter pylori* cag pathogenicity island encoded type IV secretion system. Future Microbiology, 10, 955–965. https://doi.org/10.2217/fmb.15.32

Baehni, P., & Takeuchi, Y. (2003). Anti-plaque agents in the prevention of biofilm-associated oral diseases: Anti-plaque agents. Oral Diseases, 9, 23–29. https://doi.org/10.1034/j.1601-0825.9.s1.5.x

Balin, A. K., & Pratt, L. (2002). Dilute povidone-iodine solutions inhibit human skin fibroblast growth. Dermatologic Surgery: Official Publication for

American Society for Dermatologic Surgery [et Al.], 28(3), 210–214. https://doi.org/10.1046/j.1524-4725.2002.01161.x

Bamoulid, J., Courivaud, C., Coaquette, A., Crépin, T., Carron, C., Gaiffe, E., Ducloux, D. (2017). Late Persistent Positive EBV Viral Load and Risk of Solid Cancer in Kidney Transplant Patients. Transplantation, 101(6), 1473– 1478. https://doi.org/10.1097/TP.0000000000001280

Basque, J.-R., Chénard, M., Chailler, P., & Ménard, D. (2001). Gastric cancer cell lines as models to study human digestive functions. Journal of Cellular Biochemistry, 81(2), 241–251. https://doi.org/10.1002/1097-4644(20010501)81:2<241::AID-JCB1039>3.0.CO;2-B

Bass, A. J., Thorsson, V., Shmulevich, I., Reynolds, S. M., Miller, M., Bernard, B., UNC Lineberger Comprehensive Cancer Center. (2014). Comprehensive

molecular characterization of gastric adenocarcinoma. Nature, 513(7517), 202–209. https://doi.org/10.1038/nature13480

Baud, J., Varon, C., Chabas, S., Chambonnier, L., Darfeuille, F., & Staedel, C. (2013). *Helicobacter pylori* Initiates a Mesenchymal Transition through ZEB1 in Gastric Epithelial Cells. PLoS ONE, 8(4), e60315. https://doi.org/10.1371/journal.pone.0060315

Beg, M. A., & Athar, F. (2020). Anti-HIV and Anti-HCV drugs are the putative inhibitors of RNA-dependent-RNA polymerase activity of NSP12 of the SARS CoV-2 (COVID-19). Pharm Pharmacol Int J, 8(3), 163–172.

Béji, S., Kaaroud, H., Ben Moussa, F., Abderrahim, E., Zghidi, S., Ben Hamida, F., Kheder, A. (2006). Insuffisance rénale aiguë secondaire à lapovidone iodée. La Presse Médicale, 35(1), 61–63. https://doi.org/10.1016/S0755-4982(06)74522-5

Bernard, M. D., Arico', B., Papini, E., Rizzuto, R., Grandi, G., Rappuoli, R., & Montecucco, C. (1997). *Helicobacter pylori* toxin VacA induces vacuole formation by acting in the cell cytosol. Molecular Microbiology, 26(4), 665– 674. https://doi.org/10.1046/j.1365-2958.1997.5881952.x

Bhullar, K. S., Lagarón, N. O., McGowan, E. M., Parmar, I., Jha, A., Hubbard,

B. P., & Rupasinghe, H. P. V. (2018). Kinase-targeted cancer therapies: Progress, challenges and future directions. Molecular Cancer, 17(1), 1–20. https://doi.org/10.1186/s12943-018-0804-2

Biology, C., Sokolova, O., Vieth, M., Gnad, T., Bozko, P. M., & Naumann,

M. (2014). The International Journal of Biochemistry *Helicobacter pylori* promotes eukaryotic protein translation by activating phosphatidylinositol 3 kinase / mTOR.

International Journal of Biochemistry and Cell Biology, 55, 157–163. https://doi.org/10.1016/j.biocel.2014.08.023

Blanchard, T. G., & Nedrud, J. G. (2012). Laboratory Maintenance of Helicobacter Species. Current Protocols in Microbiology, 24(1). https://doi.org/10.1002/9780471729259.mc08b01s24

Bodger, K., & Crabtree, J. E. (1998). Helicobacter pyloriand gastric inflammation. British Medical Bulletin, 54(1), 139–150. https://doi.org/10.1093/oxfordjournals.bmb.a011664

Boudreault, S., Armero, V. E. S., Scott, M. S., Perreault, J.-P., & Bisaillon, M. (2019). The Epstein-Barr virus EBNA1 protein modulates the alternative splicing of cellular genes. Virology Journal, 16(1), 29. https://doi.org/10.1186/s12985-019-1137-5

Bouhaddou, M., Memon, D., Meyer, B., White, K. M., Rezelj, V. V., Correa Marrero, M., Krogan, N. J. (2020). The Global Phosphorylation Landscape of SARS-CoV-2 Infection. Cell, 182(3), 685-712.e19. https://doi.org/10.1016/j.cell.2020.06.034

Brandt, S., Shafikhani, S., Balachandran, P., Jin, S., Hartig, R., König, W., Backert, S. (2007). Use of a novel coinfection system reveals a role for Rac1, H-Ras, and CrkII phosphorylation in Helicobacter pylori-induced host cell actin cytoskeletal rearrangements. FEMS Immunology and Medical Microbiology, 50(2), 190–205. https://doi.org/10.1111/j.1574- 695X.2007.00234.x

Bravo, D., Hoare, A., Soto, C., Valenzuela, M. A., & Quest, A. F. (2018). *Helicobacter pylori* in human health and disease: Mechanisms for local gastric and systemic effects. World Journal of Gastroenterology, 24(28), 3071–3089. https://doi.org/10.3748/wjg.v24.i28.3071

Byrd, J. C., Furman, R. R., Coutre, S. E., Flinn, I. W., Burger, J. A., Blum, K. A., … O'Brien, S. (2013). Targeting BTK with Ibrutinib in Relapsed Chronic Lymphocytic Leukemia. New England Journal of Medicine, 369(1), 32–42. https://doi.org/10.1056/NEJMoa1215637

Byun, E., Park, B., Lim, J. W., & Kim, H. (2016). Activation of NF-κB and AP-1 Mediates Hyperproliferation by Inducing β-Catenin and c-Myc in

Helicobacter pylori-Infected Gastric Epithelial Cells. Yonsei Medical Journal, 57(3), 647–651. https://doi.org/10.3349/ymj.2016.57.3.647

Canales, J., Valenzuela, M., Bravo, J., Cerda-Opazo, P., Jorquera, C., Toledo, H., Quest, A. F. G. (2017). *Helicobacter pylori* Induced Phosphatidylinositol-3-OH Kinase/mTOR Activation Increases Hypoxia Inducible Factor-1α to Promote Loss of Cyclin D1 and G0/G1 Cell Cycle Arrest in Human Gastric Cells. Frontiers in Cellular and Infection Microbiology, 7. https://doi.org/10.3389/fcimb.2017.00092

Cárdenas-Mondragón, M. G., Carreón-Talavera, R., Camorlinga-Ponce, M., Gomez-Delgado, A., Torres, J., & Fuentes-Pananá, E. M. (2013). Epstein Barr Virus and *Helicobacter pylori* Co-Infection Are Positively Associated with Severe Gastritis in Pediatric Patients. PLoS ONE, 8(4), e62850. https://doi.org/10.1371/journal.pone.0062850

Carugo, O., & Pongor, S. (2001). A normalized root-mean-spuare distance for comparing protein three-dimensional structures. Protein Science : A Publication of the Protein Society, 10(7), 1470–1473.

Castro-Muñoz, L. J., González-Díaz, C. A., Muñoz-Escobar, A., Tovar- Ayona, B. J., Aguilar-Anguiano, L. M., Vargas-Olmos, R., & Sánchez- Monroy, V. (2017). Prevalence of *Helicobacter pylori* from the oral cavity of Mexican asymptomatic

children under 5 years of age through PCR. Archives of Oral Biology, 73, 55–59. https://doi.org/10.1016/j.archoralbio.2016.09.007

Chan, G., Nogalski, M. T., & Yurochko, A. D. (2009). Activation of EGFR on monocytes is required for human cytomegalovirus entry and mediates cellular motility. Proceedings of the National Academy of Sciences, 106(52), 22369–22374. https://doi.org/10.1073/pnas.0908787106

Chandra, J., Samali, A., & Orrenius, S. (2000). Triggering and modulation of apoptosis by oxidative stress. Free Radical Biology and Medicine, 29(3–4), 323–333. https://doi.org/10.1016/S0891-5849 (00)00302-6

Chaudhary, A., Singh, V., Varadwaj, P. K., & Mani, A. (2020). Screening natural inhibitors against upregulated G-protein coupled receptors as potential therapeutics of Alzheimer's disease. Journal of Biomolecular Structure and Dynamics, 1–12. https://doi.org/10.1080/07391102.2020.1817784

Chen, J., Malone, B., Llewellyn, E., Grasso, M., Shelton, P. M. M., Olinares,

P. D. B., Campbell, E. A. (2020). Structural Basis for Helicase-Polymerase Coupling in the SARS-CoV-2 Replication-Transcription Complex. Cell, 182(6), 1560-1573.e13. https://doi.org/10.1016/j.cell.2020.07.033

Chen, S.-Y., Zhang, R.-G., & Duan, G.-C. (2016). Pathogenic mechanisms of the oncoprotein CagA in *H. pylori*-induced gastric cancer (Review). Oncology Reports, 36(6), 3087–3094. https://doi.org/10.3892/or.2016.5145

Chen, W., Lin, K., Zhang, L., Guo, G., Sun, X., Chen, J.,Xue, X. (2015). The cytomegalovirus protein UL138 induces apoptosis of gastric cancer cells by binding to heat shock protein 70. Oncotarget, 7(5), 5630–5645. https://doi.org/10.18632/oncotarget.6800

Chen, Y., Wang, Y., Li, J., Xu, W., & Zhang, Y. (2006). H pylori stimulates proliferation of gastric cancer cells through activating mitogen-activated protein kinase cascade. 12(37), 5972–5977.

Cheung, K. S., Hung, I. F., Chan, P. P., Lung, K. C., Tso, E., Liu, R., … Leung, W. K. (2020). Gastrointestinal Manifestations of SARS-CoV-2 Infection and Virus Load in Fecal Samples from the Hong Kong Cohort and Systematic Review and Meta-analysis. Gastroenterology, 0(0). https://doi.org/10.1053/j.gastro.2020.03.065

Chichirau, B. E., Diechler, S., Posselt, G., & Wessler, S. (2019). Tyrosine Kinases in *Helicobacter pylori* Infections and Gastric Cancer. Toxins, 11(10). https://doi.org/10.3390/toxins11100591

Chmiela, M., Karwowska, Z., Gonciarz, W., Allushi, B., & Stączek, P. (2017). Host pathogen interactions in *Helicobacter pylori* related gastric cancer. World Journal of Gastroenterology, 23(9), 1521–1540. https://doi.org/10.3748/wjg.v23.i9.1521

Choi, I. J., Kim, J. S., Kim, J. M., Jung, H. C., & Song, I. S. (2003). Effect of inhibition of extracellular signal-regulated kinase 1 and 2 pathway on apoptosis and bcl-2 expression in Helicobacter pylori-infected AGS cells. Infection and Immunity, 71(2), 830–837. https://doi.org/10.1128/IAI.71.2.830-837.2003

Chugh, T. D. (2008). Emerging and re-emerging bacterial diseases in India.

Journal of Biosciences, 33(4), 549–555. https://doi.org/10.1007/s12038-008-0073-0

Cicenas, J., Zalyte, E., Bairoch, A., & Gaudet, P. (2018). Kinases and Cancer.

Cancers, 10(3). https://doi.org/10.3390/cancers10030063

Ciufo, D. M., Cannon, J. S., Poole, L. J., Wu, F. Y., Murray, P., Ambinder, R. F., & Hayward, G. S. (2001). Spindle Cell Conversion by Kaposi's Sarcoma-Associated Herpesvirus: Formation of Colonies and Plaques with Mixed Lytic and Latent Gene Expression in Infected Primary Dermal Microvascular Endothelial Cell Cultures. Journal of Virology, 75(12), 5614–5626. https://doi.org/10.1128/jvi.75.12.5614-5626.2001

Clinical, T., Significance, B., Kinases, T., & Cancer, G. (n.d.). The Clinical and Biological Significance of Tyrosine Kinases in Gastric Cancer. https://doi.org/10.1007/978-981-13-1486-5

C-Met Inhibitor AMG 337, Oxaliplatin, Leucovorin Calcium, and Fluorouracil in Treating Patients With Advanced Stomach or Esophageal Cancer—Full Text View—ClinicalTrials.gov. (n.d.). Retrieved October 8, 2020, from https://clinicaltrials.gov/ct2/show/NCT02344810

Coleman, C. B., Wohlford, E. M., Smith, N. A., King, C. A., Ritchie, J. A., Baresel, P. C., Rochford, R. (2015). Epstein-Barr Virus Type 2 Latently Infects T Cells, Inducing an Atypical Activation Characterized by Expression of Lymphotactic Cytokines. Journal of Virology, 89(4), 2301–2312. https://doi.org/10.1128/JVI.03001-14

Correa, P., & Piazuelo, M. B. (2011). *Helicobacter pylori* Infection and Gastric Adenocarcinoma. US Gastroenterology & Hepatology Review, 7(1), 59.

Costela-Ruiz, V. J., Illescas-Montes, R., Puerta-Puerta, J. M., Ruiz, C., & Melguizo-Rodríguez, L. (2020). SARS-CoV-2 infection: The role of cytokines in

COVID-19 disease. Cytokine & Growth Factor Reviews, S135961012030109X. https://doi.org/10.1016/j.cytogfr.2020.06.001

Cover, T. L. (2016). *Helicobacter pylori* Diversity and Gastric Cancer Risk GASTRIC CANCER. 7(1), 1–9. https://doi.org/10.1128/mBio.01869-15.Copyright

Cover, T. L., & Blanke, S. R. (2005). *Helicobacter pylori* VacA, a paradigm for toxin multifunctionality. Nature Reviews Microbiology, 3(4), 320–332. https://doi.org/10.1038/nrmicro1095

Crew, K. D., & Neugut, A. I. (2006). Epidemiology of gastric cancer. World Journal of Gastroenterology : WJG, 12(3), 354–362. https://doi.org/10.3748/wjg.v12.i3.354

Croxtall, J. D., & McKeage, K. (2010). Trastuzumab: In HER2-Positive Metastatic Gastric Cancer. Drugs, 70(17), 2259–2267. https://doi.org/10.2165/11205900-000000000-00000

Cui, Y., Yu, S., Zhu, M., Cheng, X., Yu, Y., Tang, Z., … Liu, T. (2020).

Identifying Predictive Factors of Recurrence after Radical Resection in Gastric Cancer by RNA Immune-oncology Panel. Journal of Cancer, 11(3), 638–647. https://doi.org/10.7150/jca.38536

Datta, S., Chattopadhyay, S., Patra, R., De, R., Ramamurthy, T., Hembram, J., Mukhopadhyay, A. K. (2005). Most *Helicobacter pylori* strains of Kolkata in India are resistant to metronidazole but susceptible to other drugs commonly used for eradication and ulcer therapy. Alimentary Pharmacology & Therapeutics, 22(1), 51–57. https://doi.org/10.1111/j.1365- 2036.2005.02533.x

Dávila-Collado, R., Jarquín-Durán, O., Dong, L. T., & Espinoza, J. L. (2020). Epstein–Barr Virus and *Helicobacter pylori* Co-Infection in Non-Malignant Gastroduodenal Disorders. Pathogens, 9(2). https://doi.org/10.3390/pathogens9020104

Almeida Carvalho, L. M., de Oliveira Sapori Avelar, S., Haslam, A., Gill, J., & Prasad, V. (2019). Estimation of Percentage of Patients With Fibroblast Growth Factor Receptor Alterations Eligible for Off-label Use of Erdafitinib. JAMA Network Open, 2(11). https://doi.org/10.1001/jamanetworkopen.2019.16091

Del Moral-Hernández, O., Castañón-Sánchez, C. A., Reyes-Navarrete, S., Martínez-Carrillo, D. N., Betancourt-Linares, R., Jiménez-Wences, H., …Fernández-Tilapa, G. (2019). Multiple infections by EBV, HCMV and *Helicobacter pylori* are highly frequent in patients with chronic gastritis and gastric cancer from Southwest Mexico: An observational study. Medicine, 98(3), e14124. https://doi.org/10.1097/MD.0000000000014124

Deng, N., Goh, L. K., Wang, H., Das, K., Tao, J., Tan, I. B., … Tan, P. (2012).

A comprehensive survey of genomic alterations in gastric cancer reveals systematic patterns of molecular exclusivity and co-occurrence among distinct therapeutic targets. Gut, 61(5), 673–684. https://doi.org/10.1136/gutjnl-2011-301839

Díaz, P., Valenzuela Valderrama, M., Bravo, J., & Quest, A. F. G. (2018). *Helicobacter pylori* and Gastric Cancer: Adaptive Cellular Mechanisms Involved in Disease Progression. Frontiers in Microbiology, 9, 5. https://doi.org/10.3389/fmicb.2018.00005

Dong, Z., & Cui, H. (2019). Epigenetic modulation of metabolism in glioblastoma.

Seminars in Cancer Biology, 57(2), 45–51. https://doi.org/10.1016/j.semcancer.2018.09.002

Du, G., Wang, J., Zhang, T., Ding, Q., Jia, X., Zhao, X., Lu, Y. (2020). Targeting Src family kinase member Fyn by Saracatinib attenuated liver fibrosis in vitro and in vivo. Cell Death & Disease, 11(2), 1–12. https://doi.org/10.1038/s41419-020-2229-2

Dubovsky, J. A., Beckwith, K. A., Natarajan, G., Woyach, J. A., Jaglowski, S., Zhong, Y., …Byrd, J. C. (2013). Ibrutinib is an irreversible molecular inhibitor of ITK driving a Th1-selective pressure in T lymphocytes. Blood, 122(15), 2539–2549. https://doi.org/10.1182/blood-2013-06-507947

Dwivedy, A., Mariadasse, R., Ahmad, M., Kar, D., Jeyakanthan, J., & Biswal, B. K. (2020). In silico characterization of the NiRAN domain of RNA- dependent RNA polymerase provides insights into a potential therapeutic target against SARS-CoV2. https://doi.org/10.31219/osf.io/wd6zu Eichelberg, M. R., Welch, R., Guidry, J. T., Ali, A., Ohashi, M., Makielski, K. R., Johannsen, E. (2019). Epstein-Barr Virus Infection Promotes Epithelial Cell Growth by Attenuating Differentiation-Dependent Exit from the Cell Cycle. MBio, 10(4). https://doi.org/10.1128/mBio.01332-19

Endeman, H., van der Zee, P., van Genderen, M. E., van den Akker, J. P. C., & Gommers, D. (2020). Progressive respiratory failure in COVID-19: A hypothesis. The Lancet Infectious Diseases, S1473309920303662. https://doi.org/10.1016/S1473-3099(20)30366-2 Sivachandran, N., Cao, J. Y., & Frappier, L. (2010). Epstein-Barr virus nuclear antigen 1 hijacks the host kinase CK2 to disrupt PML nuclear bodies. Journal of virology, 84(21), 11113-11123.

Esau, D. (2017). Viral Causes of Lymphoma: The History of Epstein-Barr Virus and Human T-Lymphotropic Virus 1. Virology: Research and Treatment, 8,

1178122X17731772.
https://doi.org/10.1177/1178122X17731772

Falush, D. (2003). Traces of Human Migrations in *Helicobacter pylori* Populations. Science, 299(5612), 1582–1585.
https://doi.org/10.1126/science.1080857

Fan, E., Beitler, J. R., Brochard, L., Calfee, C. S., Ferguson, N. D., Slutsky, A. S., & Brodie, D. (2020). COVID-19-associated acute respiratory distress syndrome: Is a different approach to management warranted? The Lancet Respiratory Medicine, 8(8), 816–821. https://doi.org/10.1016/S2213- 2600(20)30304-0

Fattahi, S., Kosari-Monfared, M., Ghadami, E., Golpour, M., Khodadadi, P., Ghasemiyan, M., & Akhavan-Niaki, H. (2018). Infection-associated epigenetic alterations in gastric cancer: New insight in cancer therapy. Journal of Cellular Physiology, 233(12), 9261–9270.
https://doi.org/10.1002/jcp.27030

Fattahi, S., Nikbakhsh, N., Taheri, H., Ghadami, E., Kosari-Monfared, M., Amirbozorgi, G., Akhavan-Niaki, H. (2018). Prevalence of multiple infections and the risk of gastric adenocarcinoma development at earlier age. Diagnostic Microbiology and Infectious Disease, 92(1), 62–68. https://doi.org/10.1016/j.diagmicrobio.2018.04.015

Foegeding, N. J., Caston, R. R., McClain, M. S., Ohi, M. D., & Cover, T. L. (2016). An Overview of *Helicobacter pylori* VacA Toxin Biology. Toxins, 8(6), 173. https://doi.org/10.3390/toxins8060173

Foglieni, C., Scabini, S., Belloni, D., Broccolo, F., Lusso, P., Malnati, M. S., & Ferrero, E. (2005). Productive infection of HUVEC by HHV-8 is associated with changes compatible with angiogenic transformations. European Journal of

Histochemistry : EJH, 49(3), 273–284. https://doi.org/10.4081/954

Fontana, E., & Smyth, E. C. (2016). Novel targets in the treatment of advanced gastric cancer: A perspective review. Therapeutic Advances in Medical Oncology, 8(2), 113–125. https://doi.org/10.1177/1758834015616935 Jha, H. C., Pei, Y., & Robertson, E. S. (2016). Epstein–Barr virus: diseases linked to infection and transformation. Frontiers in microbiology, 7, 1602. https://doi.org/10.3389/fmicb.2016.01602

Fukayama, M. (2010). Epstein-Barr virus and gastric carcinoma. Pathology International, 60(5), 337–350. https://doi.org/10.1111/j.1440- 1827.2010.02533.x

Fukuda, M., & Longnecker, R. (2004). Latent Membrane Protein 2A Inhibits Transforming Growth Factor-β1-Induced Apoptosis through the Phosphatidylinositol 3-Kinase/Akt Pathway. Journal of Virology, 78(4), 1697–1705. https://doi.org/10.1128/JVI.78.4.1697-1705.2004

Fukuda, M., & Longnecker, R. (2007). Epstein-Barr Virus Latent Membrane Protein 2A Mediates Transformation through Constitutive Activation of the Ras/PI3-K/Akt Pathway. Journal of Virology, 81(17), 9299–9306. https://doi.org/10.1128/JVI.00537-07

Gadina, M., Schwartz, D. M., & O'Shea, J. J. (2016). Decernotinib: A Next-Generation Jakinib. Arthritis & Rheumatology (Hoboken, N.J.), 68(1), 31–34. https://doi.org/10.1002/art.39463

Gao, C., Ma, T., Pang, L., & Xie, R. (2014). Activation of P21-activated protein kinase 2 is an independent prognostic predictor for patients with gastric cancer. Diagnostic Pathology, 9(1), 1–6. https://doi.org/10.1186/1746- 1596-9-55

Gao, Y., Yan, L., Huang, Y., Liu, F., Zhao, Y., Cao, L., Rao, Z. (2020). Structure

of the RNA-dependent RNA polymerase from COVID-19 virus. Science, 368(6492), 779–782. https://doi.org/10.1126/science.abb7498.

Gautam, S. S., & Gautam, R. S. (2018). A case of ARF after chromopertubation with povidone iodine. International Journal of Reproduction, Contraception, Obstetrics and Gynecology, 7(7), 2982–2984. https://doi.org/10.18203/2320-1770.ijrcog20182923

Gebara, E. C. E., Faria, C. M., Pannuti, C., Chehter, L., Mayer, M. P. A., & Lima, L. A. P. A. (2006). Persistence of *Helicobacter pylori* in the oral cavity after systemic eradication therapy. Journal of Clinical Periodontology, 33(5), 329–333. https://doi.org/10.1111/j.1600-051X.2006.00915.x

Gebert, B., Fischer, W., Weiss, E., Hoffmann, R., & Haas, R. (2003). *Helicobacter pylori* vacuolating cytotoxin inhibits T lymphocyte activation. Science, 301(5636), 1099–1102. https://doi.org/10.1126/science.1086871

Geddert, H., Hausen, A. zur, Gabbert, H. E., & Sarbia, M. (2010). EBV- Infection in Cardiac and Non-Cardiac Gastric Adenocarcinomas is Associated with Promoter Methylation of p16, p14 and APC, but not hMLH1. https://doi.org/10.3233/ACP-CLO-2010-0540

Genovese, M. C., Vollenhoven, R. F. van, Pacheco-Tena, C., Zhang, Y., & Kinnman, N. (2016). VX-509 (Decernotinib), an Oral Selective JAK-3 Inhibitor, in Combination With Methotrexate in Patients With Rheumatoid Arthritis. Arthritis & Rheumatology, 68(1), 46–55. https://doi.org/10.1002/art.39473

Gerstenberger, B. S., Ambler, C., Arnold, E. P., Banker, M.-E., Brown, M. F., Clark, J. D., Wright, S. W. (2020). Discovery of Tyrosine Kinase 2 (TYK2) Inhibitor (PF-06826647) for the Treatment of Autoimmune Diseases. Journal of Medicinal Chemistry, acs.jmedchem.0c00948.

https://doi.org/10.1021/acs.jmedchem.0c00948

Ghoshal, U. C., Tiwari, S., Dhingra, S., Pandey, R., Ghoshal, U., Tripathi, S., Ayyagari, A. (2008). Frequency of *Helicobacter pylori* and CagA Antibody in Patients with Gastric Neoplasms and Controls: The Indian Enigma. Digestive Diseases and Sciences, 53(5), 1215–1222. https://doi.org/10.1007/s10620-008-0229-7

Goodwin, R. J. A., Bunch, J., & McGinnity, D. F. (2017). Mass Spectrometry Imaging in Oncology Drug Discovery. In Advances in Cancer Research (Vol. 134, pp. 133–171). Elsevier. https://doi.org/10.1016/bs.acr.2016.11.005

Gozgit, J. M., Wong, M. J., Moran, L., Wardwell, S., Mohemmad, Q. K., Narasimhan, N. I., Rivera, V. M. (2012). Ponatinib (AP24534), a Multitargeted Pan-FGFR Inhibitor with Activity in Multiple FGFR-Amplified or Mutated Cancer Models. Molecular Cancer Therapeutics, 11(3), 690–699. https://doi.org/10.1158/1535-7163.MCT-11-0450

GRAHAM, D. Y., LU, H., & YAMAOKA, Y. (2009). African, Asian or Indian enigma, the East Asian Helicobacter pylori: Facts or medical myths. Journal of Digestive Diseases, 10(2), 77–84. https://doi.org/10.1111/j.1751-2980.2009.00368.x

Grimes, J. M., & Grimes, K. V. (2020). p38 MAPK inhibition: A promising therapeutic approach for COVID-19. Journal of Molecular and Cellular Cardiology, 144, 63–65. https://doi.org/10.1016/j.yjmcc.2020.05.007

Gryko, M., Pryczynicz, A., Zareba, K., Kędra, B., Kemona, A., & Guzińska-Ustymowicz, K. (2014, February 19). The Expression of Bcl-2 and BID in Gastric Cancer Cells [Clinical Study]. https://doi.org/10.1155/2014/953203

Guo, J. qiang, Li, S. jie, & Guo, G. xiao. (2017). Long Noncoding RNA AFAP1-AS1 Promotes Cell Proliferation and Apoptosis of Gastric Cancer Cells via PTEN/p-AKT Pathway. Digestive Diseases and Sciences, 62(8), 2004–2010. https://doi.org/10.1007/s10620-017-4584-0

Guo, X., Ma, N., Wang, J., Song, J., Bu, X., Cheng, Y., Wei, L. (2008). Increased p38-MAPK is responsible for chemotherapy resistance in human gastric cancer cells. BMC Cancer, 8(1), 375. https://doi.org/10.1186/1471- 2407-8-375

Gupta, S., Singh, V., Varadwaj, P. K., Chakravartty, N., Katta, A. V. S. K. M., Lekkala, S. P., … Reddy Lachagari, V. B. (2020). Secondary metabolites from spice and herbs as potential multitarget inhibitors of SARS-CoV-2 proteins. Journal of Biomolecular Structure and Dynamics, 1–20. https://doi.org/10.1080/07391102.2020.1837679

H, N., S, N., S, I., H, O., M, M., S, H., & T, A. (2005). Clinical significance of nuclear expression of spleen tyrosine kinase (Syk) in gastric cancer. Cancer Letters, 236(1), 89–94. https://doi.org/10.1016/j.canlet.2005.05.022

Halder, S., Murakami, M., Verma, S. C., Kumar, P., Yi, F., & Robertson, E. S. (2009). Early Events Associated with Infection of Epstein-Barr Virus Infection of Primary B-Cells. PLoS ONE, 4(9). https://doi.org/10.1371/journal.pone.0007214

Halgren, T. A., Murphy, R. B., Friesner, R. A., Beard, H. S., Frye, L. L., Pollard, W. T., & Banks, J. L. (2004). Glide: A new approach for rapid, accurate docking and scoring. 2. Enrichment factors in database screening.

Journal of Medicinal Chemistry, 47(7), 1750–1759. https://doi.org/10.1021/jm030644s Hatakeyama, M. (2009). *Helicobacter pylori* and gastric carcinogenesis.

Journal of Gastroenterology, 44(4), 239–248. https://doi.org/10.1007/s00535- 009-0014-1 Heawchaiyaphum, C., Iizasa, H., Ekalaksananan, T., Burassakarn, A., Kiyono, T., Kanehiro, Y., Pientong, C. (2020). Epstein-Barr Virus Infection of Oral Squamous Cells. Microorganisms, 8(3). https://doi.org/10.3390/microorganisms8030419

Hecht, J. R., Bang, Y.-J., Qin, S. K., Chung, H. C., Xu, J. M., Park, J. O. Slamon, D. (2016). Lapatinib in Combination With Capecitabine Plus Oxaliplatin in Human Epidermal Growth Factor Receptor 2–Positive Advanced or Metastatic Gastric, Esophageal, or Gastroesophageal Adenocarcinoma: TRIO-013/LOGiC—A Randomized Phase III Trial. Journal of Clinical Oncology, 34(5), 443–451. https://doi.org/10.1200/JCO.2015.62.6598

Heijde, D. van der, Song, I.-H., Pangan, A. L., Deodhar, A., Bosch, F. van den, Maksymowych, W. P., … Sieper, J. (2019). Efficacy and safety of upadacitinib in patients with active ankylosing spondylitis (SELECT-AXIS 1): A multicentre, randomised, double-blind, placebo-controlled, phase 2/3 trial. The Lancet, 394(10214), 2108–2117. https://doi.org/10.1016/S0140-6736(19)32534-6

Hill, R. J., Dabbagh, K., Phippard, D., Li, C., Suttmann, R. T., Welch, M., Wong, B. R. (2008). Pamapimod, a novel p38 mitogen-activated protein kinase inhibitor: Preclinical analysis of efficacy and selectivity. The Journal of Pharmacology and Experimental Therapeutics, 327(3), 610–619. https://doi.org/10.1124/jpet.108.139006

Hillen, H. S., Kokic, G., Farnung, L., Dienemann, C., Tegunov, D., & Cramer,

P. (2020). Structure of replicating SARS-CoV-2 polymerase. Nature, 584(7819), 154–156. https://doi.org/10.1038/s41586-020-2368-8

Hino, R., Uozaki, H., Inoue, Y., Shintani, Y., Ushiku, T., Sakatani, T., Fukayama, M. (2008). Survival Advantage of EBV-Associated Gastric Carcinoma: Survivin Up-regulation by Viral Latent Membrane Protein 2A. Cancer Research, 68(5), 1427–1435. https://doi.org/10.1158/0008-5472.CAN-07-3027

Hirata, Y., Maeda, S., Mitsuno, Y., Akanuma, M., Yamaji, Y., Ogura, K., Omata, M. (2001). *Helicobacter pylori* Activates the Cyclin D1 Gene through Mitogen-Activated Protein Kinase Pathway in Gastric Cancer Cells. Infection and Immunity, 69(6), 3965–3971. https://doi.org/10.1128/IAI.69.6.3965-3971.2001

Hooi, J. K. Y., Lai, W. Y., Ng, W. K., Suen, M. M. Y., Underwood, F. E., Tanyingoh, D., … Ng, S. C. (2017). Global Prevalence of *Helicobacter pylori* Infection: Systematic Review and Meta-Analysis. Gastroenterology, 153(2), 420–429. https://doi.org/10.1053/j.gastro.2017.04.022

Hu, D., Li, X., Sreenivasan, P. K., & DeVizio, W. (2009). A randomized, double-blind clinical study to assess the antimicrobial effects of a cetylpyridinium chloride mouth rinse on dental plaque bacteria. Clinical Therapeutics, 31(11), 2540–2548. https://doi.org/10.1016/j.clinthera.2009.11.004

Hu, Y., He, C., Liu, J.-P., Li, N.-S., Peng, C., Yang-Ou, Y.-B., Zhu, Y. (2018). Analysis of key genes and signaling pathways involved in Helicobacter pylori-associated gastric cancer based on The Cancer Genome Atlas database and RNA sequencing data. Helicobacter, 23(5), e12530. https://doi.org/10.1111/hel.12530

Huang, T., Liu, D., Wang, Y., Li, P., Sun, L., Xiong, H., Qiu, H. (2018). FGFR2 Promotes Gastric Cancer Progression by Inhibiting the Expression of Thrombospondin4 via PI3K-Akt-Mtor Pathway. Cellular Physiology and

Biochemistry, 50(4), 1332–1345. https://doi.org/10.1159/000494590

Huang, Y.-C., Lin, S.-J., Lin, K.-M., Chou, Y.-C., Lin, C.-W., Yu, S.-C.,Tsai, C.-H. (2016). Regulation of EBV LMP1-triggered EphA4 downregulation in EBV-associated B lymphoma and its impact on patients' survival. Blood, 128(12), 1578–1589. https://doi.org/10.1182/blood-2016-02-
702530

Iizasa, H., Nanbo, A., Nishikawa, J., Jinushi, M., & Yoshiyama, H. (2012). Epstein-Barr Virus (EBV)-associated Gastric Carcinoma. Viruses, 4(12), 3420–3439. https://doi.org/10.3390/v4123420

Ilver, D., Arnqvist, A., Ögren, J., Frick, I.-M., Kersulyte, D., Incecik, E. T., … Borén, T. (1998). *Helicobacter pylori* Adhesin Binding Fucosylated Histo- Blood Group Antigens Revealed by Retagging. Science, 279(5349), 373–377. https://doi.org/10.1126/science.279.5349.373

Indari, O., Jakhmola, S., Manivannan, E., & Jha, H. C. (2021). An Update on Antiviral Therapy Against SARS-CoV-2: How Far Have We Come? Frontiers in Pharmacology, 12. https://doi.org/10.3389/fphar.2021.632677

Ishihara, K., Miura, T., Kimizuka, R., Ebihara, Y., Mizuno, Y., & Okuda, K. (2006). Oral bacteria inhibit *Helicobacter pylori* growth. FEMS Microbiology Letters, 152(2), 355–361. https://doi.org/10.1111/j.1574-6968.1997.tb10452.x

Jakhmola, S., Indari, O., Baral, B., Kashyap, D., Varshney, N., Das, A.,Jha, H. C. (2020). Comorbidity Assessment Is Essential During COVID-19 Treatment. Frontiers in Physiology, 11, 984. https://doi.org/10.3389/fphys.2020.00984

Jakhmola, S., Indari, O., Kashyap, D., Varshney, N., Rani, A., Sonkar, C.,Jha, H.

C. (2020). Recent updates on COVID-19: A holistic review. Heliyon, 6(12), e05706. https://doi.org/10.1016/j.heliyon.2020.e05706

Jha, Hem C., Yang, K., El-Naccache, D. W., Sun, Z., & Robertson, E. S. (2015). EBNA3C regulates p53 through induction of Aurora kinase B. Oncotarget, 6(8), 5788–5803. https://doi.org/10.18632/oncotarget.3310

Jha, Hem Chandra, Lu, J., Saha, A., Cai, Q., Banerjee, S., Prasad, M. A. J., & Robertson, E. S. (2013). EBNA3C-mediated regulation of aurora kinase B contributes to Epstein-Barr virus-induced B-cell proliferation through modulation of the activities of the retinoblastoma protein and apoptotic caspases. Journal of Virology, 87(22), 12121–12138. https://doi.org/10.1128/JVI.02379-13

Jia, C.-Y., Li, J.-Y., Hao, G.-F., & Yang, G.-F. (2020). A drug-likeness toolbox facilitates ADMET study in drug discovery. Drug Discovery Today, 25(1), 248–258. https://doi.org/10.1016/j.drudis.2019.10.014

Jin, Z., Du, X., Xu, Y., Deng, Y., Liu, M., Zhao, Y., Yang, H. (2020). Structure of Mpro from SARS-CoV-2 and discovery of its inhibitors. Nature. https://doi.org/10.1038/s41586-020-2223-y

Judd, L. M., Menheniott, T. R., Ling, H., Jackson, C. B., Howlett, M., Kalantzis, A., Giraud, A. S. (2014). Inhibition of the JAK2/STAT3 Pathway Reduces Gastric Cancer Growth In Vitro and In Vivo. PLOS ONE, 9(5), e95993. https://doi.org/10.1371/journal.pone.0095993

Kable, M. E., Hansen, L. M., Styer, C. M., Deck, S. L., Rakhimova, O., Shevtsova, A., Solnick, J. V. (2017). Host Determinants of Expression of the *Helicobacter pylori* BabA Adhesin. Scientific Reports, 7(1), 46499. https://doi.org/10.1038/srep46499

Kale, J., Osterlund, E. J., & Andrews, D. W. (2018). BCL-2 family proteins: Changing partners in the dance towards death. Cell Death and Differentiation, 25(1), 65–80. https://doi.org/10.1038/cdd.2017.186

Kamran, M., Long, Z.-J., Xu, D., Lv, S.-S., Liu, B., Wang, C.-L., Liu, Q. (2017). Aurora kinase A regulates Survivin stability through targeting FBXL7 in gastric cancer drug resistance and prognosis. Oncogenesis, 6(2), e298–e298. https://doi.org/10.1038/oncsis.2016.80

Kang, B. W., Baek, D. W., Kang, H., Baek, J. H., & Kim, J. G. (2019). Novel Therapeutic Approaches for Epstein-Barr Virus Associated Gastric Cancer. Anticancer Research, 39(8), 4003–4010. https://doi.org/10.21873/anticanres.13555

Kashyap, D., Baral, B., Verma, T. P., Sonkar, C., Chatterji, D., Jain, A. K., & Jha, H. C. (2020). Oral rinses in growth inhibition and treatment of *Helicobacter pylori* infection. BMC Microbiology, 20(1), 45. https://doi.org/10.1186/s12866-020-01728-4

Katoh, M. (2016). FGFR inhibitors: Effects on cancer cells, tumor microenvironment and whole-body homeostasis (Review). International Journal of Molecular Medicine, 38(1), 3–15. https://doi.org/10.3892/ijmm.2016.2620

Kauser, F., Hussain, M. A., Ahmed, I., Ahmad, N., Habeeb, A., Khan, A. A., & Ahmed, N. (2005). Comparing Genomes of *Helicobacter pylori* Strains from the High-Altitude Desert of Ladakh, India. Journal of Clinical Microbiology, 43(4), 1538–1545. https://doi.org/10.1128/JCM.43.4.1538-1545.2005

Khanna, P., Chua, P. J., Bay, B. H., & Baeg, G. H. (2015). The JAK/STAT

signaling cascade in gastric carcinoma (Review). International Journal of Oncology, 47(5), 1617–1626. https://doi.org/10.3892/ijo.2015.3160

Kim, G., Kim, T.-H., Kang, M.-J., Choi, J.-A., Pack, D.-Y., Lee, I.-R., Park, J.-H. (2016). Inhibitory effect of withaferin A on Helicobacter pylori-induced IL-8 production and NF-κB activation in gastric epithelial cells. Molecular Medicine Reports, 13(1), 967–972. https://doi.org/10.3892/mmr.2015.4602

Kim, N., Weeks, D. L., Shin, J. M., Scott, D. R., Young, M. K., & Sachs, G. (2002). Proteins Released by *Helicobacter pylori* In Vitro. Journal of Bacteriology, 184(22), 6155–6162. https://doi.org/10.1128/JB.184.22.6155-6162.2002

King, C. C., & Obonyo, M. (2015). *Helicobacter pylori* modulates host cell survival regulation through the serine-threonine kinase, 3-phosphoinositide dependent kinase 1 (PDK-1). BMC Microbiology, 15. https://doi.org/10.1186/s12866-015-0543-0

Kirchdoerfer, R. N., & Ward, A. B. (2019). Structure of the SARS-CoV nsp12 polymerase bound to nsp7 and nsp8 co-factors. Nature Communications, 10(1), 2342. https://doi.org/10.1038/s41467-019-10280-3

Koc, E. C., Miller-Lee, J. L., & Koc, H. (2017). Fyn kinase regulates translation in mammalian mitochondria. Biochimica et Biophysica Acta (BBA) General Subjects, 1861(3), 533–540. https://doi.org/10.1016/j.bbagen.2016.12.004

Kosaka, Y., Felices, M., & Berg, L. J. (2006). Itk and Th2 responses: Action but no reaction. Trends in Immunology, 27(10), 453–460. https://doi.org/10.1016/j.it.2006.08.006

Kosari-Monfared, M., Nikbakhsh, N., Fattahi, S., Ghadami, E., Ranaei, M., Taheri, H.,Akhavan-Niaki, H. (2019). CTNNBIP1 downregulation is associated with tumor grade and viral infections in gastric adenocarcinoma. Journal of Cellular Physiology, 234(3), 2895–2904. https://doi.org/10.1002/jcp.27106.

Krogan, N. (n.d.). Coronavirus and cancer hijack the same parts in human cells to spread – and our team identified existing cancer drugs that could fight COVID-19. Retrieved September 19, 2020, from The Conversation website: http://theconversation.com/coronavirus-and-cancer-hijack-the-same-parts-in-human-cells-to-spread-and-our-team-identified-existing-cancer-drugs-that- could-fight-covid-19-139955

Kwok, T., Backert, S., Schwarz, H., Berger, J., & Meyer, T. F. (2002). Specific entry of *Helicobacter pylori* into cultured gastric epithelial cells via a zipper-like mechanism. Infection and Immunity, 70(4), 2108–2120. https://doi.org/10.1128/IAI.70.4.2108-2120.2002

Kyttaris, V. C. (2012). Kinase inhibitors: A new class of antirheumatic drugs. Drug Design, Development and Therapy, 6, 245–250. https://doi.org/10.2147/DDDT.S25426

Laha, S., Chakraborty, J., Das, S., Manna, S. K., Biswas, S., & Chatterjee, R. (2020). Characterizations of SARS-CoV-2 mutational profile, spike protein stability and viral transmission. Infection, Genetics and Evolution, 85, 104445.

Lahner, E., Carabotti, M., & Annibale, B. (2018). Treatment of *Helicobacter pylori* infection in atrophic gastritis. World Journal of Gastroenterology, 24(22), 2373–2380. https://doi.org/10.3748/wjg.v24.i22.2373

Lang, S. A., Gaumann, A., Koehl, G. E., Seidel, U., Bataille, F., Klein, D., Stoeltzing, O. (2007). Mammalian target of rapamycin is activated in human gastric

cancer and serves as a target for therapy in an experimental model. International Journal of Cancer, 120(8), 1803–1810. https://doi.org/10.1002/ijc.22442

Lay, M.-L. J., Lucas, R. M., Ratnamohan, M., Taylor, J., Ponsonby, A.-L., Dwyer, D. E., & Ausimmune Investigator Group (AIG). (2010). Measurement of Epstein-Barr virus DNA load using a novel quantification standard containing two EBV DNA targets and SYBR Green I dye. Virology Journal, 7, 252. https://doi.org/10.1186/1743-422X-7-252

Lee, G. H., Yoo, K. C., An, Y., Lee, H. J., Lee, M., Uddin, N., Lee, S. J. (2018). FYN promotes mesenchymal phenotypes of basal type breast cancer cells through STAT5/NOTCH2 signaling node. Oncogene, 37(14), 1857– 1868. https://doi.org/10.1038/s41388-017-0114-y

Lehmann, K. C., Gulyaeva, A., Zevenhoven-Dobbe, J. C., Janssen, G. M. C., Ruben, M., Overkleeft, H. S., Gorbalenya, A. E. (2015). Discovery of an essential nucleotidylating activity associated with a newly delineated conserved domain in the RNA polymerase-containing protein of all nidoviruses. Nucleic Acids Research, 43(17), 8416–8434. https://doi.org/10.1093/nar/gkv838

Li, S., Du, H., Wang, Z., Zhou, L., Zhao, X., & Zeng, Y. (2010). Meta- analysis of the relationship between Epstein-Barr virus infection and clinicopathological features of patients with gastric carcinoma. Science China Life Sciences, 53(4), 524–530. https://doi.org/10.1007/s11427-010-0082-8

Liersch-Löhn, B., Slavova, N., Buhr, H. J., & Bennani-Baiti, I. M. (2016). Differential protein expression and oncogenic gene network link tyrosine kinase ephrin B4 receptor to aggressive gastric and gastroesophageal junction cancers: EPHB4 associates to aggressive gastroesophageal cancers. International Journal of Cancer, 138(5), 1220–1231. https://doi.org/10.1002/ijc.29865

Lin, W., Kao, H., Robinson, D., Kung, H., Wu, C., & Chen, H. (2000a). Tyrosine kinases and gastric cancer. 5680–5689.

Lin, W., Kao, H.-W., Robinson, D., Kung, H.-J., Wu, C.-W., & Chen, H.-C. (2000b). Tyrosine kinases and gastric cancer. Oncogene, 19(49), 5680–5689. https://doi.org/10.1038/sj.onc.1203924

Lipinski, C. A. (2004). Lead- and drug-like compounds: The rule-of-five revolution. Drug Discovery Today: Technologies, 1(4), 337–341. https://doi.org/10.1016/j.ddtec.2004.11.007

Liu, D., Ma, X., Yang, F., Xiao, D., Jia, Y., & Wang, Y. (2020). Discovery and validation of methylated-differentially expressed genes in Helicobacter pylori-induced gastric cancer. Cancer Gene Therapy, 27(6), 473–485. https://doi.org/10.1038/s41417-019-0125-7

Liu, J., Xu, B., Xu, G., Zhang, X., Yang, X., & Wang, J. (2017). Reduced EphB6 protein in gastric carcinoma and associated lymph nodes suggests EphB6 as a gastric tumor and metastasis inhibitor. 19, 241–248. https://doi.org/10.3233/CBM-160256

Liu, N., Zhou, N., Chai, N., Liu, X., Jiang, H., Wu, Q., & Li, Q. (2016). *Helicobacter pylori* promotes angiogenesis depending on Wnt/beta-catenin-mediated vascular endothelial growth factor via the cyclooxygenase-2 pathway in gastric cancer. BMC Cancer, 16(1), 321. https://doi.org/10.1186/s12885-016-2351-9

Liu, Xuan, Ji, Q., Zhang, C., Liu, X., Liu, Y., Liu, N., Li, Q. (2017). MiR- 30a acts as a tumor suppressor by double-targeting COX-2 and BCL9 in *H. pylori* gastric cancer models. Scientific Reports, 7(1), 7113. https://doi.org/10.1038/s41598-017-07193-w

Liu, XueQiao, & Cohen, J. I. (2016). Epstein-Barr Virus (EBV) Tegument Protein BGLF2 Promotes EBV Reactivation through Activation of the p38 Mitogen-Activated Protein Kinase. Journal of Virology, 90(2), 1129–1138. https://doi.org/10.1128/JVI.01410-15

Liu, Y., Wang, X., Deng, L., Ping, L., Shi, Y., Zheng, W., Zhu, J. (2019). ITK inhibition induced in vitro and in vivo anti-tumor activity through downregulating TCR signaling pathway in malignant T cell lymphoma. Cancer Cell International, 19(1), 32. https://doi.org/10.1186/s12935-019-0754-9

Lodish, H., Berk, A., Zipursky, S. L., Matsudaira, P., Baltimore, D., & Darnell, J. (2000). Proto-Oncogenes and Tumor-Suppressor Genes. Molecular Cell Biology. 4th Edition. Retrieved from https://www.ncbi.nlm.nih.gov/books/NBK21662/

Luo, W., Li, Y.-X., Jiang, L.-J., Chen, Q., Wang, T., & Ye, D.-W. (2020). Targeting JAK-STAT Signaling to Control Cytokine Release Syndrome in COVID-19. Trends in Pharmacological Sciences, 41(8), 531–543. https://doi.org/10.1016/j.tips.2020.06.007

Magnelli, L., Schiavone, N., Staderini, F., Biagioni, A., & Papucci, L. (2020). MAP Kinases Pathways in Gastric Cancer. International Journal of Molecular Sciences, 21(8), 2893. https://doi.org/10.3390/ijms21082893

Mahajan, S., Hogan, J. K., Shlyakhter, D., Oh, L., Salituro, F. G., Farmer, L., & Hoock, T. C. (2015). VX-509 (Decernotinib) Is a Potent and Selective Janus Kinase 3 Inhibitor That Attenuates Inflammation in Animal Models of Autoimmune Disease. Journal of Pharmacology and Experimental Therapeutics, 353(2), 405–414. https://doi.org/10.1124/jpet.114.221176

Mahameed, M., Wilhelm, T., Darawshi, O., Obiedat, A., Tommy, W.-S., Chintha, C., Tirosh, B. (2019). The unfolded protein response modulators GSK2606414 and KIRA6 are potent KIT inhibitors. Cell Death & Disease, 10(4), 1–12. https://doi.org/10.1038/s41419-019-1523-3

Mao, R., Qiu, Y., He, J.-S., Tan, J.-Y., Li, X.-H., Liang, J., Chen, M.-H. (2020). Manifestations and prognosis of gastrointestinal and liver involvement in patients with COVID-19: A systematic review and meta-analysis. The Lancet Gastroenterology & Hepatology, 0(0). https://doi.org/10.1016/S2468-1253(20)30126-6

Marchetti, E., Mummolo, S., Di Mattia, J., Casalena, F., Di Martino, S., Mattei, A., & Marzo, G. (2011). Efficacy of essential oil mouthwash with and without alcohol: A 3-Day plaque accumulation model. Trials, 12, 262. https://doi.org/10.1186/1745-6215-12-262

Marsh, P. D. (2010). Controlling the oral biofilm with antimicrobials. Journal of Dentistry, 38, S11–S15. https://doi.org/10.1016/S0300-5712(10)70005-1

Mathur, S., Mathur, T., Srivastava, R., & Khatri, R. (2011). Chlorhexidine: The Gold Standard in Chemical Plaque Control. National Journal of Physiology, Pharmacy and Pharmacology, 1.

Matsusaka, K., Funata, S., Fukayama, M., & Kaneda, A. (2014). DNA methylation in gastric cancer, related to *Helicobacter pylori* and Epstein-Barr virus. World Journal of Gastroenterology : WJG, 20(14), 3916–3926. https://doi.org/10.3748/wjg.v20.i14.3916

Matsusaka, K., Kaneda, A., Nagae, G., Ushiku, T., Kikuchi, Y., Hino, R., … Fukayama, M. (2011). Classification of Epstein-Barr virus-positive gastric cancers

by definition of DNA methylation epigenotypes. Cancer Research, 71(23), 7187–7197. https://doi.org/10.1158/0008-5472.CAN-11-1349

Mazurek, A. M., Wygoda, A., Rutkowski, T., Olbryt, M., Pietrowska, M., Celejewska, A., Widłak, P. (2020a). Prognostic significance of Epstein- Barr virus viral load in patients with T1-T2 nasopharyngeal cancer. Journal of Medical Virology, 92(3), 348–355. https://doi.org/10.1002/jmv.25606

Mazurek, A. M., Wygoda, A., Rutkowski, T., Olbryt, M., Pietrowska, M., Celejewska, A., Widłak, P. (2020b). Prognostic significance of Epstein- Barr virus viral load in patients with T1-T2 nasopharyngeal cancer. Journal of Medical Virology, 92(3), 348–355. https://doi.org/10.1002/jmv.25606

McGaw, Wm. T., & Belch, A. (1985). Oral complications of acute leukemia: Prophylactic impact of a chlorhexidine mouth rinse regimen. Oral Surgery, Oral Medicine, Oral Pathology, 60(3), 275–280. https://doi.org/10.1016/0030-4220(85)90311-1

McGee, M. C., August, A., & Huang, W. (n.d.). BTK/ITK dual inhibitors: Modulating immunopathology and lymphopenia for COVID-19 therapy. Journal of Leukocyte Biology, n/a(n/a). https://doi.org/10.1002/JLB.5COVR0620-306R

Meng, L., Ding, L., Yu, Y., & Li, W. (2020, October 6). JAK3 and TYK2 Serve as Prognostic Biomarkers and Are Associated with Immune Infiltration in Stomach Adenocarcinoma [Research Article]. https://doi.org/10.1155/2020/7973568

Miliotis, C. N., & Slack, F. J. (2020). Multi-layered control of PD-L1 expression in Epstein-Barr virus-associated gastric cancer. Journal of Cancer Metastasis and Treatment, 6. https://doi.org/10.20517/2394-4722.2020.12

Minegishi, Y., Saito, M., Morio, T., Watanabe, K., Agematsu, K., Tsuchiya, S., Karasuyama, H. (2006). Human Tyrosine Kinase 2 Deficiency Reveals Its Requisite Roles in Multiple Cytokine Signals Involved in Innate and Acquired Immunity. Immunity, 25(5), 745–755. https://doi.org/10.1016/j.immuni.2006.09.009

Mishra, J. P., Cohen, D., Zamperone, A., Nesic, D., Muesch, A., & Stein, M. (2015). CagA of H elicobacter pylori interacts with and inhibits the serine-threonine kinase PRK2: CagA-associated host-signalling pathways. Cellular Microbiology, 17(11), 1670–1682. https://doi.org/10.1111/cmi.12464

Mishra, S. (2013). Is *Helicobacter pylori* good or bad? European Journal of Clinical Microbiology & Infectious Diseases, 32(3), 301–304. https://doi.org/10.1007/s10096-012-1773-9

Miyazaki, K., Inokuchi, M., Takagi, Y., Kato, K., Kojima, K., & Sugihara, K. (2013). EphA4 is a prognostic factor in gastric cancer. BMC clinical pathology, 13(1), 1-9. 9 http://www.biomedcentral.com/1472-6890/13/19

Mobley, H. L., Mendz, G. L., & Hazell, S. L. (Eds.). (2001). Helicobacter pylori: Physiology and Genetics. Washington (DC): ASM Press. Retrieved from http://www.ncbi.nlm.nih.gov/books/NBK2408/

Moese, S., Selbach, M., Brinkmann, V., Karlas, A., Haimovich, B., Backert, S., & Meyer, T. F. (2007). The *Helicobacter pylori* CagA protein disrupts matrix adhesion of gastric epithelial cells by dephosphorylation of vinculin. Cellular Microbiology, 9(5), 1148–1161. https://doi.org/10.1111/j.1462-5822.2006.00856.x

Mohebbi, A., Mamizadeh, Z., Bagheri, H., Sharifnezhad, F., Tabarraei, A., &

Yazdi, M. (2020). Prevalent latent human cytomegalovirus genotype b2 in biopsy samples of gastric cancer. Future Virology, 15(2), 71–78. https://doi.org/10.2217/fvl-2019-0117

Mohr, C. F., Kalmer, M., Gross, C., Mann, M. C., Sterz, K. R., Kieser, A., Kress, A. K. (2014). The tumor marker Fascin is induced by the Epstein-Barr virus-encoded oncoprotein LMP1 via NF-κB in lymphocytes and contributes to their invasive migration. Cell Communication and Signaling, 12(1), 46. https://doi.org/10.1186/s12964-014-0046-x

Montecucco, C., & Rappuoli, R. (2001). Living dangerously: How *Helicobacter pylori* survives in the human stomach. Nature Reviews Molecular Cell Biology, 2(6), 457–466. https://doi.org/10.1038/35073084

Moodley, Y., Linz, B., Bond, R. P., Nieuwoudt, M., Soodyall, H., Schlebusch, C. M., Achtman, M. (2012). Age of the Association between *Helicobacter pylori* and Man. PLoS Pathogens, 8(5). https://doi.org/10.1371/journal.ppat.1002693

Morales-Sanchez, A., & Fuentes-Panana, E. M. (2016). Epstein-Barr Virus-associated Gastric Cancer and Potential Mechanisms of Oncogenesis. Current Cancer Drug Targets, 17(6), 534–554. https://doi.org/10.2174/1568009616666160926124923

Morishita, A., Gong, J., & Masaki, T. (2014). Targeting receptor tyrosine kinases in gastric cancer. World Journal of Gastroenterology, 20(16), 4536– 4545. https://doi.org/10.3748/wjg.v20.i16.4536

Moujaess, E., Kourie, H. R., & Ghosn, M. (2020). Cancer patients and research during COVID-19 pandemic: A systematic review of current evidence. Critical Reviews in Oncology/Hematology, 150, 102972. https://doi.org/10.1016/j.critrevonc.2020.102972

Murai, Y., Zheng, H.-C., Aziz, H. O. A., Mei, H., Kutsuna, T., Nakanishi, Y., Takano, Y. (2007). High JC virus load in gastric cancer and adjacent non-cancerous mucosa. Cancer Science, 98(1), 25–31. https://doi.org/10.1111/j.1349-7006.2006.00354.x

Nakayama, A., Abe, H., Kunita, A., Saito, R., Kanda, T., Yamashita, H., Fukayama, M. (2019). Viral loads correlate with upregulation of PD-L1 and worse patient prognosis in Epstein–Barr Virus-associated gastric carcinoma. PLOS ONE, 14(1), e0211358. https://doi.org/10.1371/journal.pone.0211358

Naseem, M., Barzi, A., Brezden-Masley, C., Puccini, A., Berger, M. D., Tokunaga, R., Lenz, H.-J. (2018). Outlooks on Epstein-Barr virus associated gastric cancer. Cancer Treatment Reviews, 66, 15–22. https://doi.org/10.1016/j.ctrv.2018.03.006

Nelson, E. A., Walker, S. R., Kepich, A., Gashin, L. B., Hideshima, T., Ikeda, H., Frank, D. A. (2008). Nifuroxazide inhibits survival of multiple myeloma cells by directly inhibiting STAT3. Blood, 112(13), 5095–5102. https://doi.org/10.1182/blood-2007-12-129718

Neogi, U., Hill, K. J., Ambikan, A. T., Heng, X., Quinn, T. P., Byrareddy, S. N., Singh, K. (2020). Feasibility of Known RNA Polymerase Inhibitors as Anti-SARS-CoV-2 Drugs. Pathogens, 9(5), 320. https://doi.org/10.3390/pathogens9050320

Nilsson, J. S., Forslund, O., Andersson, F. C., Lindstedt, M., & Greiff, L. (2019). Intralesional EBV-DNA load as marker of prognosis for nasopharyngeal cancer. Scientific Reports, 9(1), 15432. https://doi.org/10.1038/s41598-019-51767-9

Nishikawa, J., Iizasa, H., Yoshiyama, H., Shimokuri, K., Kobayashi, Y., Sasaki, S.,

Sakaida, I. (2018). Clinical Importance of Epstein–Barr Virus- Associated Gastric Cancer. Cancers, 10(6). https://doi.org/10.3390/cancers10060167

Niwa, T., Tsukamoto, T., Toyoda, T., Mori, A., Tanaka, H., Maekita, T., … Ushijima, T. (n.d.). Inflammatory Processes Triggered by *Helicobacter pylori* Infection Cause Aberrant DNA Methylation in Gastric Epithelial Cells. Cancer Research, 12.

Nogueira, M., Puig, L., & Torres, T. (2020). JAK Inhibitors for Treatment of Psoriasis: Focus on Selective TYK2 Inhibitors. Drugs, 80(4), 341–352. https://doi.org/10.1007/s40265-020-01261-8

Nomura, A., Stemmermann, G. N., Chyou, P.-H., Kato, I., Perez-Perez, G. I., & Blaser, M. J. (1991). *Helicobacter pylori* Infection and Gastric Carcinoma among Japanese Americans in Hawaii. New England Journal of Medicine, 325(16), 1132–1136. https://doi.org/10.1056/NEJM199110173251604

Novartis Pharmaceuticals. (2020). A Phase IB, Multicenter, Open-label Dose Escalation Study of the PI3K Inhibitor BYL719 in Combination With the HSP90 Inhibitor AUY922 in Patients With Advanced or Metastatic Gastric Cancer Carrying a Molecular Alteration of PIK3CA or an Amplification of HER2 (Clinical Trial Registration No. NCT01613950). clinicaltrials.gov. Retrieved from clinicaltrials.gov website: https://clinicaltrials.gov/ct2/show/NCT01613950

Ogden, S. R., Noto, J. M., Allen, S. S., Patel, D. A., Romero-Gallo, J., Washington, M. K.,Peek, R. M. (2010). Matrix metalloproteinase-7 and premalignant host responses in Helicobacter pylori-infected mice. Cancer Research, 70(1), 30–35. https://doi.org/10.1158/0008-5472.CAN-09-2899

Oki, M., Yamamoto, H., Taniguchi, H., Adachi, Y., Imai, K., & Shinomura, Y.

(2008). Overexpression of the receptor tyrosine kinase EphA4 in human gastric cancers. World Journal of Gastroenterology : WJG, 14(37), 5650– 5656. https://doi.org/10.3748/wjg.14.5650

Oleastro, M., & Ménard, A. (2013). The Role of *Helicobacter pylori* Outer Membrane Proteins in Adherence and Pathogenesis. Biology, 2(3), 1110– 1134. https://doi.org/10.3390/biology2031110 Page, K. M., Suarez-Farinas, M., Suprun, M., Zhang, W., Garcet, S., Fuentes- Duculan, J., Peeva, E. (2020). Molecular and Cellular Responses to the TYK2/JAK1 Inhibitor PF-06700841 Reveal Reduction of Skin Inflammation in Plaque Psoriasis. Journal of Investigative Dermatology, 140(8), 1546- 1555.e4. https://doi.org/10.1016/j.jid.2019.11.027

Pandey, S., Jha, H. C., Shukla, S. K., Shirley, M. K., & Robertson, E. S. (2018a). Epigenetic Regulation of Tumor Suppressors by *Helicobacter pylori* Enhances EBV-Induced Proliferation of Gastric Epithelial Cells. MBio, 9(2). https://doi.org/10.1128/mBio.00649-18

Pandey, S., Jha, H. C., Shukla, S. K., Shirley, M. K., & Robertson, E. S. (2018b). Epigenetic Regulation of Tumor Suppressors by *Helicobacter pylori* Enhances EBV-Induced Proliferation of Gastric Epithelial Cells. MBio, 9(2). https://doi.org/10.1128/mBio.00649-18

Pandeya, K. B., Ganeshpurkar, A., & Mishra, M. K. (2020). Natural RNA dependent RNA polymerase inhibitors: Molecular docking studies of some biologically active alkaloids of Argemone mexicana. Medical Hypotheses, 144, 109905. https://doi.org/10.1016/j.mehy.2020.109905

Patel, R., Gallagher, J., & Chapple, I. (2018). Question from practice: How to select the right mouthwash. J Cereb Circ, 13, 57.

Pathogenesis of *Helicobacter pylori* Infection | Clinical Microbiology Reviews.

(n.d.). Retrieved April 8, 2021, from https://cmr.asm.org/content/19/3/449

Patwardhan, G. A., Beverly, L. J., & Siskind, L. J. (2016). Sphingolipids and mitochondrial apoptosis. Journal of Bioenergetics and Biomembranes, 48(2), 153–168. https://doi.org/10.1007/s10863-015-9602-3

Peek, R. M., & Blaser, M. J. (2002). *Helicobacter pylori* and gastrointestinal tract adenocarcinomas. Nature Reviews Cancer, 2(1), 28–37. https://doi.org/10.1038/nrc703

Pena-Ponce, M. G. dela, Jimenez, M. T., Hansen, L. M., Solnick, J. V., & Miller, L. A. (2017). The *Helicobacter pylori* type IV secretion system promotes IL-8 synthesis in a model of pediatric airway epithelium via p38 MAP kinase. PLOS ONE, 12(8), e0183324. https://doi.org/10.1371/journal.pone.0183324

Peng, Q., Peng, R., Yuan, B., Zhao, J., Wang, M., Wang, X., Shi, Y. (2020). Structural and Biochemical Characterization of the nsp12-nsp7-nsp8 Core Polymerase Complex from SARS-CoV-2. Cell Reports, 31(11), 107774. https://doi.org/10.1016/j.celrep.2020.107774

Perez-Villar, J. J., O'Day, K., Hewgill, D. H., Nadler, S. G., & Kanner, S. B. (2001). Nuclear localization of the tyrosine kinase Itk and interaction of its SH3 domain with karyopherin α (Rch1α). International Immunology, 13(10), 1265–1274. https://doi.org/10.1093/intimm/13.10.1265

Porras-Hurtado, L., Ruiz, Y., Santos, C., Phillips, C., Carracedo, Á., & Lareu, M. (2013). An overview of STRUCTURE: Applications, parameter settings, and supporting software. Frontiers in Genetics, 4. https://doi.org/10.3389/fgene.2013.00098

Pottier, C., Fresnais, M., Gilon, M., Jérusalem, G., Longuespée, R., & Sounni, N.

E. (2020). Tyrosine Kinase Inhibitors in Cancer: Breakthrough and Challenges of Targeted Therapy. Cancers, 12(3), 731. https://doi.org/10.3390/cancers12030731

Pourhoseingholi, M. A., Vahedi, M., & Baghestani, A. R. (2015). Burden of gastrointestinal cancer in Asia; an overview. Gastroenterology and Hepatology From Bed to Bench, 8(1), 19–27.

Prabhu, S. R., Amrapurkar, A. D., & Amrapurkar, D. N. (1995). Role of *Helicobacter pylori* in gastric carcinoma. 8(2), 58–60.

Praveen, D., Chowdary, P. R., & Aanandhi, M. V. (2020). Baricitinib - a januase kinase inhibitor - not an ideal option for management of covid 19. International Journal of Antimicrobial Agents, 105967-105967https://doi.org/10.1016/j.ijantimicag.2020.105967

Pritchard, J. K., Stephens, M., Rosenberg, N. A., & Donnelly, P. (2000). Association Mapping in Structured Populations. American Journal of Human Genetics, 67(1), 170–181. https://doi.org/10.1086/302959

Qi, Y.-F., Liu, M., Zhang, Y., Liu, W., Xiao, H., & Luo, B. (2019). EBV down-regulates COX-2 expression via TRAF2 and ERK signal pathway in EBV-associated gastric cancer. Virus Research, 272, 197735. https://doi.org/10.1016/j.virusres.2019.197735

Ragab, D., Salah Eldin, H., Taeimah, M., Khattab, R., & Salem, R. (2020). The COVID-19 Cytokine Storm; What We Know So Far. Frontiers in Immunology, 11. https://doi.org/10.3389/fimmu.2020.01446

Raimondi, C., & Falasca, M. (2011). Targeting PDK1 in cancer. Current medicinal chemistry, 18(18), 2763-2769.

Ramakrishna, B. S. (2006). *Helicobacter pylori* infection in India: The case against eradication. Indian Journal of Gastroenterology: Official Journal of the Indian Society of Gastroenterology, 25(1), 25–28.

Rath, S. K., & Singh, M. (2013). Comparative clinical and microbiological efficacy of mouthwashes containing 0.2% and 0.12% chlorhexidine. Dental Research Journal, 10(3), 364–369.

Reisfield, G. M., Goldberger, B. A., Pesce, A. J., Crews, B. O., Wilson, G. R., Teitelbaum, S. A., & Bertholf, R. L. (2011). Ethyl Glucuronide, Ethyl Sulfate, and Ethanol in Urine after Intensive Exposure to High Ethanol Content Mouthwash. Journal of Analytical Toxicology, 35(5), 264–268. https://doi.org/10.1093/anatox/35.5.264

Research, A. A. for C. (2013). Ibrutinib Also Inhibits ITK. Cancer Discovery, 3(9), 967–967. https://doi.org/10.1158/2159-8290.CD-RW2013-168

Ribble, D., Goldstein, N. B., Norris, D. A., & Shellman, Y. G. (2005). A simple technique for quantifying apoptosis in 96-well plates. BMC Biotechnology, 5, 12. https://doi.org/10.1186/1472-6750-5-12

Richardson, C. J., Gao, Q., Mitsopoulous, C., Zvelebil, M., Pearl, L. H., & Pearl, F. M. G. (2009). MoKCa database—Mutations of kinases in cancer. Nucleic Acids Research, 37(suppl_1), D824–D831. https://doi.org/10.1093/nar/gkn832

Romano, M., Ruggiero, A., Squeglia, F., Maga, G., & Berisio, R. (2020). A Structural View of SARS-CoV-2 RNA Replication Machinery: RNA Synthesis, Proofreading and Final Capping. Cells, 9(5). https://doi.org/10.3390/cells9051267

Roopashri, G., Jayanthi, K., & Guruprasad, R. (2011). Efficacy of benzydamine hydrochloride, chlorhexidine, and povidone iodine in the treatment of oral mucositis among patients undergoing radiotherapy in head and neck malignancies: A drug trail. Contemporary Clinical Dentistry, 2(1), 8–12. https://doi.org/10.4103/0976-237X.79292

Roose, J., Polevoy, G. A., Clevers, H., & Embo, J. (1998). Letters To Nature. Nature, 395(October), 521–525.

Safari, F., & Jodeiry Zaer, S. (2017). Evaluation of Cell- Morphological Changes by *Helicobacter pylori* CagA and Pragmin in AGS Human Gastric Carcinoma Cells. Gene, Cell and Tissue, 4(2), 0–3. https://doi.org/10.5812/gct.12598

Saju, P., Murata-Kamiya, N., Hayashi, T., Senda, Y., Nagase, L., Noda, S., Hatakeyama, M. (2016). Host SHP1 phosphatase antagonizes *Helicobacter pylori* CagA and can be downregulated by Epstein–Barr virus. Nature Microbiology, 1(4), 1–8. https://doi.org/10.1038/nmicrobiol.2016.26

Salles, N., & Mégraud, F. (2007). Current management of *Helicobacter pylori* infections in the elderly. Expert Review of Anti-Infective Therapy, 5(5), 845– 856. https://doi.org/10.1586/14787210.5.5.845

Sankaranarayanan, R., Ramadas, K., & Qiao, Y. (2014). Managing the changing burden of cancer in Asia. BMC Medicine, 12(1), 3. https://doi.org/10.1186/1741-7015-12-3

Sankaran-Walters, S., Ransibrahmanakul, K., Grishina, I., Hung, J., Martinez, E., Prindiville, T., & Dandekar, S. (2011). Epstein–Barr virus replication linked to B cell proliferation in inflamed areas of colonic mucosa of patients with inflammatory bowel disease. Journal of Clinical Virology, 50(1), 31–36. https://doi.org/10.1016/j.jcv.2010.09.011

Sanpui, P., Chattopadhyay, A., & Ghosh, S. S. (2011). Induction of Apoptosis in Cancer Cells at Low Silver Nanoparticle Concentrations using Chitosan Nanocarrier. ACS Applied Materials & Interfaces, 3(2), 218–228. https://doi.org/10.1021/am100840c

Sasaki, S., Nishikawa, J., Sakai, K., Iizasa, H., Yoshiyama, H., Yanagihara, M., Sakaida, I. (2019). EBV-associated gastric cancer evades T-cell immunity by PD-1/PD-L1 interactions. Gastric Cancer, 22(3), 486–496. https://doi.org/10.1007/s10120-018-0880-4

Sato, T., Yuki, H., Ogura, K., & Honma, T. (2018). Construction of an integrated database for hERG blocking small molecules. PLOS ONE, 13(7), e0199348. https://doi.org/10.1371/journal.pone.0199348

Schönrich, G., & Raftery, M. J. (2019). The PD-1/PD-L1 Axis and Virus Infections: A Delicate Balance. Frontiers in Cellular and Infection Microbiology, 9, 207. https://doi.org/10.3389/fcimb.2019.00207

Schwab, M., & Gale (Firm), T. (2009). Encyclopedia of cancer. Springer. Retrieved from http://gen.lib.rus.ec/book/index.php?md5=284a9a745981e5ec0c948f715ee270 d5

Sefton, B. M. (1985). Oncogenes encoding protein kinases. Trends in Genetics, 1, 306–308. https://doi.org/10.1016/0168-9525(85)90120-9

Selbach, M., Moese, S., Backert, S., Jungblut, P. R., & Meyer, T. F. (2004). The *Helicobacter pylori* CagA protein induces tyrosine dephosphorylation of ezrin. Proteomics, 4(10), 2961–2968. https://doi.org/10.1002/pmic.200400915

Selbach, M., Moese, S., Hurwitz, R., Hauck, C. R., Meyer, T. F., & Backert, S.

(2003). The *Helicobacter pylori* CagA protein induces cortactin dephosphorylation and actin rearrangement by c-Src inactivation. EMBO Journal, 22(3), 515–528. https://doi.org/10.1093/emboj/cdg050

Servetas, S. L., Bridge, D. R., & Merrell, D. S. (2016). Molecular mechanisms of gastric cancer initiation and progression by Helicobacter pylori: Current Opinion in Infectious Diseases, 29(3), 304–310. https://doi.org/10.1097/QCO.0000000000000248

Shan, Y., Klepeis, J. L., Eastwood, M. P., Dror, R. O., & Shaw, D. E. (2005). Gaussian split Ewald: A fast Ewald mesh method for molecular simulation. The Journal of Chemical Physics, 122(5), 54101. https://doi.org/10.1063/1.1839571

Shannon-Lowe, C., Adland, E., Bell, A. I., Delecluse, H.-J., Rickinson, A. B., & Rowe, M. (2009). Features Distinguishing Epstein-Barr Virus Infections of Epithelial Cells and B Cells: Viral Genome Expression, Genome Maintenance, and Genome Amplification. Journal of Virology, 83(15), 7749–7760. https://doi.org/10.1128/JVI.00108-09

Sharma, A., & Radhakrishnan, V. (2011). Gastric cancer in India. Indian Journal of Medical and Paediatric Oncology : Official Journal of Indian Society of Medical & Paediatric Oncology, 32(1), 12–16. https://doi.org/10.4103/0971-5851.81884

Shen, X., Xue, Y., Si, Y., Wang, Q., Wang, Z., Yuan, J., & Zhang, X. (2015). The unfolded protein response potentiates epithelial-to-mesenchymal transition (EMT) of gastric cancer cells under severe hypoxic conditions. Medical Oncology, 32(1), 447. https://doi.org/10.1007/s12032-014-0447-0

Shenoy, A. T., & Orihuela, C. J. (2016). Anatomical site-specific contributions of pneumococcal virulence determinants. Pneumonia, 8.

https://doi.org/10.1186/s41479-016-0007-9

Shi, L., Fan, B., Chen, D., Guo, C., Xiang, H., Nie, Y., Shi, X. (2020). Human cytomegalovirus protein UL136 activates the IL-6/STAT3 signal through MiR-138 and MiR-34c in gastric cancer cells. International Journal of Clinical Oncology. https://doi.org/10.1007/s10147-020-01749-z

Shinozaki-Ushiku, A., Kunita, A., & Fukayama, M. (2015). Update on epstein-barr virus and gastric cancer (review). International Journal of Oncology, 46(4), 1421–1434. https://doi.org/10.3892/ijo.2015.2856

Shirin, H., & Moss, S. F. (1998). *Helicobacter pylori* induced apoptosis. Gut, 43(5), 592–594. https://doi.org/10.1136/gut.43.5.592

Shukla, S. K., Jha, H. C., El-Naccache, D. W., & Robertson, E. S. (2016). An EBV recombinant deleted for residues 130-159 in EBNA3C can deregulate p53/Mdm2 and Cyclin D1/CDK6 which results in apoptosis and reduced cell proliferation. Oncotarget, 7(14), 18116–18134. https://doi.org/10.18632/oncotarget.7502

Sinclair, J. (2008). Human cytomegalovirus: Latency and reactivation in the myeloid lineage. Journal of Clinical Virology: The Official Publication of the Pan American Society for Clinical Virology, 41(3), 180–185. https://doi.org/10.1016/j.jcv.2007.11.014

Singh, K., & Ghoshal, U. C. (2006). Causal role of *Helicobacter pylori* infection in gastric cancer: An Asian enigma. World Journal of Gastroenterology : WJG, 12(9), 1346–1351. https://doi.org/10.3748/wjg.v12.i9.1346

Singh, S., & Jha, H. C. (2017, March 21). Status of Epstein-Barr Virus Coinfection with *Helicobacter pylori* in Gastric Cancer [Review Article].

https://doi.org/10.1155/2017/3456264

Sitarz, R., Skierucha, M., Mielko, J., Offerhaus, G. J. A., Maciejewski, R., & Polkowski, W. P. (2018). Gastric cancer: Epidemiology, prevention, classification, and treatment. Cancer Management and Research, 10, 239– 248. https://doi.org/10.2147/CMAR.S149619

Slanina, H., Madhugiri, R., Bylapudi, G., Schultheiß, K., Karl, N., Gulyaeva, A., Ziebuhr, J. (2021). Coronavirus replication–transcription complex: Vital and selective NMPylation of a conserved site in nsp9 by the NiRAN- RdRp subunit. Proceedings of the National Academy of Sciences, 118(6). https://doi.org/10.1073/pnas.2022310118

Slavova, N., Buhr, H. J., & Bennani-Baiti, I. M. (2016). Differential protein expression and oncogenic gene network link tyrosine kinase ephrin B4 receptor to aggressive gastric and gastroesophageal junction cancers. International journal of cancer, 138(5), 1220-1231. https://doi.org/10.1002/ijc.29865

Slobedman, B., Cao, J. Z., Avdic, S., Webster, B., McAllery, S., Cheung, A. K., Abendroth, A. (2010). Human cytomegalovirus latent infection and associated viral gene expression. Future Microbiology, 5(6), 883–900. https://doi.org/10.2217/fmb.10.58

Snijder, E. J., Decroly, E., & Ziebuhr, J. (2016). The Nonstructural Proteins Directing Coronavirus RNA Synthesis and Processing. In Advances in Virus Research (Vol. 96, pp. 59–126). Elsevier. https://doi.org/10.1016/bs.aivir.2016.08.008

Sonkar, C., Kashyap, D., Varshney, N., Baral, B., & Jha, H. C. (2020). Impact of Gastrointestinal Symptoms in COVID-19: A Molecular Approach. SN Comprehensive Clinical Medicine. https://doi.org/10.1007/s42399-020-00619- z

Sonkar, C., Verma, T., Chatterji, D., Jain, A. K., & Jha, H. C. (2020). Status of kinases in Epstein-Barr virus and *Helicobacter pylori* Coinfection in gastric Cancer cells. BMC Cancer, 20(1), 925. https://doi.org/10.1186/s12885-020- 07377-0

Soroceanu, L., & Cobbs, C. S. (2011). Is HCMV a tumor promoter? Virus Research, 157(2), 193–203. https://doi.org/10.1016/j.virusres.2010.10.026

Sousa, H., Pinto-Correia, A. L., Medeiros, R., & Dinis-Ribeiro, M. (2008). Epstein-Barr virus is associated with gastric carcinoma: The question is what is the significance? World Journal of Gastroenterology, 14(27), 4347–4351. https://doi.org/10.3748/wjg.14.4347

Stebbing, J., Phelan, A., Griffin, I., Tucker, C., Oechsle, O., Smith, D., & Richardson, P. (2020). COVID-19: Combining antiviral and anti-inflammatory treatments. The Lancet Infectious Diseases, 20(4), 400–402. https://doi.org/10.1016/S1473-3099(20)30132-8

Stein, M., Bagnoli, F., Halenbeck, R., Rappuoli, R., Fantl, W. J., & Covacci, A. (2002). C-Src/Lyn kinases activate *Helicobacter pylori* CagA through tyrosine phosphorylation of the EPIYA motifs. Molecular Microbiology, 43(4), 971–980. https://doi.org/10.1046/j.1365-2958.2002.02781.x

Šterbenc, A., Jarc, E., Poljak, M., & Homan, M. (2019). *Helicobacter pylori* virulence genes. World Journal of Gastroenterology, 25(33), 4870–4884. https://doi.org/10.3748/wjg.v25.i33.4870

Subissi, L., Imbert, I., Ferron, F., Collet, A., Coutard, B., Decroly, E., & Canard, B. (2014). SARS-CoV ORF1b-encoded nonstructural proteins 12–16: Replicative enzymes as antiviral targets. Antiviral Research, 101, 122–130. https://doi.org/10.1016/j.antiviral.2013.11.006

Subissi, L., Posthuma, C. C., Collet, A., Zevenhoven-Dobbe, J. C., Gorbalenya, A. E., Decroly, E., … Imbert, I. (2014). One severe acute respiratory syndrome coronavirus protein complex integrates processive RNA polymerase and exonuclease activities. Proceedings of the National Academy of Sciences, 111(37), E3900–E3909. https://doi.org/10.1073/pnas.1323705111

Sunakawa, Y., & Lenz, H.-J. (2015). Molecular Classification of Gastric Adenocarcinoma: Translating New Insights from The Cancer Genome Atlas Research Network. Current Treatment Options in Oncology, 16(4), 17. https://doi.org/10.1007/s11864-015-0331-y

Takada, K. (2000). Epstein-Barr virus and gastric carcinoma. Molecular Pathology, 53(5), 255–261. https://doi.org/10.1136/mp.53.5.255

Teo, W. H., Chen, H.-P., Huang, J. C., & Chan, Y.-J. (2017). Human cytomegalovirus infection enhances cell proliferation, migration and upregulation of EMT markers in colorectal cancer-derived stem cell-like cells. International Journal of Oncology, 51(5), 1415–1426. https://doi.org/10.3892/ijo.2017.4135

Thrift, A. P., & El-Serag, H. B. (2020). Burden of Gastric Cancer. Clinical Gastroenterology and Hepatology, 18(3), 534–542. https://doi.org/10.1016/j.cgh.2019.07.045

Thyagarajan, S., Ray, P., Das, B. K., Ayyagari, A., Khan, A. A., Dharmalingam, S., Habibullah, C. (2003). Geographical difference in antimicrobial resistance pattern of *Helicobacter pylori* clinical isolates from Indian patients: Multicentric study. Journal of Gastroenterology and Hepatology, 18(12), 1373–1378. https://doi.org/10.1046/j.1440- 1746.2003.03174.x

Tian, W., Chen, C., Lei, X., Zhao, J., & Liang, J. (2018). CASTp 3.0: Computed

atlas of surface topography of proteins. Nucleic Acids Research, 46(Web Server issue), W363–W367. https://doi.org/10.1093/nar/gky473

Toh, J. W. T., & Wilson, R. B. (2020). Pathways of Gastric Carcinogenesis, *Helicobacter pylori* Virulence and Interactions with Antioxidant Systems, Vitamin C and Phytochemicals. International Journal of Molecular Sciences, 21(17), 6451. https://doi.org/10.3390/ijms21176451

Tomb, J. F., White, O., Kerlavage, A. R., Clayton, R. A., Sutton, G. G., Flelschmann, R. D., … Venter, J. C. (1997). Erratum: The complete genome sequence of the gastric pathogen *Helicobacter pylori* (Nature (1997) 388 (539-547)). Nature, 389(6649), 412. https://doi.org/10.1038/38792

Tomb, J.-F., White, O., Kerlavage, A. R., Clayton, R. A., Sutton, G. G., Fleischmann, R. D., … Venter, J. C. (1997). Erratum: The complete genome sequence of the gastric pathogen Helicobacter pylori. Nature, 389(6649), 412– 412. https://doi.org/10.1038/38792

Tsintarakis, A., & Zafiropoulos, A. (2017). Oncogenic Kinases in Cancer. In ELS (pp. 1–7). American Cancer Society. https://doi.org/10.1002/9780470015902.a0006051.pub3

Van Cutsem, E., Sagaert, X., Topal, B., Haustermans, K., & Prenen, H. (2016). Gastric cancer. The Lancet, 388(10060), 2654–2664. https://doi.org/10.1016/S0140-6736(16)30354-3

van der Heijde, D., Baraliakos, X., Gensler, L. S., Maksymowych, W. P., Tseluyko, V., Nadashkevich, O., … Landewé, R. (2018). Efficacy and safety of filgotinib, a selective Janus kinase 1 inhibitor, in patients with active ankylosing spondylitis (TORTUGA): Results from a randomised, placebo- controlled, phase 2 trial. The Lancet, 392(10162), 2378–2387. https://doi.org/10.1016/S0140-6736 (18)32463-2

Vanhoutte, F., Mazur, M., Voloshyn, O., Stanislavchuk, M., Aa, A. V. der, Namour, F., Klooster, G. van ’t. (2017). Efficacy, Safety, Pharmacokinetics, and Pharmacodynamics of Filgotinib, a Selective JAK-1 Inhibitor, After Short-Term Treatment of Rheumatoid Arthritis: Results of Two Randomized Phase IIa Trials. Arthritis & Rheumatology, 69(10), 1949– 1959. https://doi.org/10.1002/art.40186

Vennepureddy, A., Singh, P., Rastogi, R., Atallah, J., & Terjanian, T. (2017). Evolution of ramucirumab in the treatment of cancer – A review of literature. Journal of Oncology Pharmacy Practice, 23(7), 525–539. https://doi.org/10.1177/1078155216655474

Waltuch, T., Gill, P., Zinns, L. E., Whitney, R., Tokarski, J., Tsung, J. W., & Sanders, J. E. (2020). Features of COVID-19 post-infectious cytokine release syndrome in children presenting to the emergency department. The American Journal of Emergency Medicine. https://doi.org/10.1016/j.ajem.2020.05.058

Wang, F., Meng, W., Wang, B., & Qiao, L. (2014). Helicobacter pylori- induced gastric inflammation and gastric cancer. Cancer Letters. https://doi.org/10.1016/j.canlet.2013.08.016

Wang, J. D., Chen, X. Y., Ji, K. W., & Tao, F. (2016). Targeting Btk with ibrutinib inhibit gastric carcinoma cells growth. American Journal of Translational Research, 8(7), 3003–3012.

Wang, S. Q., Wang, C., Chang, L. M., Zhou, K. R., Wang, J. W., Ke, Y., ... & Liu, H. M. (2016). Geridonin and paclitaxel act synergistically to inhibit the proliferation of gastric cancer cells through ROS-mediated regulation of the PTEN/PI3K/Akt pathway. Oncotarget, 7(45), 72990.

Wang, Shui, Ding, Y.-B., Chen, G.-Y., Xia, J.-G., & Wu, Z.-Y. (2004).

Hypermethylation of Syk gene in promoter region associated with oncogenesis and metastasis of gastric carcinoma. World Journal of Gastroenterology : WJG, 10(12), 1815–1818. https://doi.org/10.3748/wjg.v10.i12.1815

Wang, X., Zhang, Y., Jiang, L., Zhou, F., Zhai, H., Zhang, M., & Wang, J. (2016). Interpreting the distinct and shared genetic characteristics between Epstein–Barr virus associated and non-associated gastric carcinoma. Gene, 576(2), 798–806. https://doi.org/10.1016/j.gene.2015.11.010

Wehbe, Z., Hammoud, S., Soudani, N., Zaraket, H., El-Yazbi, A., & Eid, A. H. (2020). Molecular Insights Into SARS COV-2 Interaction With Cardiovascular Disease: Role of RAAS and MAPK Signaling. Frontiers in Pharmacology, 11. https://doi.org/10.3389/fphar.2020.00836

Wei, L., Surma, M., Shi, S., Lambert-Cheatham, N., & Shi, J. (2016). Novel Insights into the Roles of Rho Kinase in Cancer. Archivum Immunologiae et Therapiae Experimentalis, 64(4), 259–278. https://doi.org/10.1007/s00005-015-0382-6

Weisberg, E., Parent, A., Yang, P. L., Sattler, M., Liu, Q., Liu, Q., Griffin, J. D. (2020). Repurposing of Kinase Inhibitors for Treatment of COVID-19. Pharmaceutical Research, 37(9). https://doi.org/10.1007/s11095-020-02851-7

Wen, W., Chen, W. (Sting), Xiao, N., Bender, R., Ghazalpour, A., Tan, Z., … Press, M. F. (2015). Mutations in the Kinase Domain of the HER2/ERBB2 Gene Identified in a Wide Variety of Human Cancers. The Journal of Molecular Diagnostics, 17(5), 487–495. https://doi.org/10.1016/j.jmoldx.2015.04.003

Westhovens, R., Taylor, P. C., Alten, R., Pavlova, D., Enríquez-Sosa, F., Mazur, M., Harrison, P. (2017). Filgotinib (GLPG0634/GS-6034), an oral JAK1 selective

inhibitor, is effective in combination with methotrexate (MTX) in patients with active rheumatoid arthritis and insufficient response to MTX: Results from a randomised, dose-finding study (DARWIN 1). Annals of the Rheumatic Diseases, 76(6), 998–1008. https://doi.org/10.1136/annrheumdis- 2016-210104 WHO Coronavirus Disease (COVID-19) Dashboard. (n.d.). Retrieved September 17, 2020, from https://covid19.who.int

William, B. M., An, W., Feng, D., Nadeau, S., Mohapatra, B. C., Storck, M. A., Band, H. (2016). Fasudil, a clinically-safe ROCK Inhibitor, Decreases Disease Burden in a Cbl/Cbl-b Deficiency-Driven Murine Model of Myeloproliferative Disorders. Hematology (Amsterdam, Netherlands), 21(4), 218–224. https://doi.org/10.1179/1607845415Y.0000000031

Wilson, N. S., Dixit, V., & Ashkenazi, A. (2009). Death receptor signal transducers: Nodes of coordination in immune signaling networks. Nature Immunology, 10(4), 348–355. https://doi.org/10.1038/ni.1714

Wöss, K., Simonović, N., Strobl, B., Macho-Maschler, S., & Müller, M. (2019). TYK2: An Upstream Kinase of STATs in Cancer. Cancers, 11(11), 1728. https://doi.org/10.3390/cancers11111728

Wu, C., Li, A. F., Chi, C., Huang, C. L., Shen, K., Liu, W., & Lin, W. (2007). Human Gastric Cancer Kinase Profile and Prognostic Significance of MKK4 Kinase. The American Journal of Pathology, 156(6), 2007–2015. https://doi.org/10.1016/S0002-9440 (10)65073-0

Wu, Y., Prager, A., Boos, S., Resch, M., Brizic, I., Mach, M., … Adler, B. (2017). Human cytomegalovirus glycoprotein complex gH/gL/gO uses PDGFR-α as a key for entry. PLOS Pathogens, 13(4), e1006281. https://doi.org/10.1371/journal.ppat.1006281

Xie, L., Su, X., Zhang, L., Yin, X., Tang, L., Zhang, X., Ji, Q. (2013). FGFR2 Gene Amplification in Gastric Cancer Predicts Sensitivity to the Selective FGFR Inhibitor AZD4547. Clinical Cancer Research, 19(9), 2572– 2583. https://doi.org/10.1158/1078-0432.CCR-12-3898

Xie, Y. G., Yu, Y., Hou, L. K., Wang, X., Zhang, B., & Cao, X. C. (2016). FYN promotes breast cancer progression through epithelial-mesenchymal transition. Oncology Reports, 36(2), 1000–1006. https://doi.org/10.3892/or.2016.4894

Xu, J., Gong, L., Qian, Z., Song, G., & Liu, J. (2018). ERBB4 promotes the proliferation of gastric cancer cells via the PI3K / Akt signaling pathway. 2892–2898. https://doi.org/10.3892/or.2018.6343

Yamaoka, Y. (2008). Roles of *Helicobacter pylori* BabA in gastroduodenal pathogenesis. World Journal of Gastroenterology, 14(27), 4265–4272. https://doi.org/10.3748/wjg.14.4265

Yamaoka, Y. (2010). Mechanisms of disease: *Helicobacter pylori* virulence factors. Nature Reviews. Gastroenterology & Hepatology, 7(11), 629–641. https://doi.org/10.1038/nrgastro.2010.154

Yan, L., Du, Q., Yao, J., & Liu, R. (2016). ROR2 inhibits the proliferation of gastric carcinoma cells via activation of non - canonical Wnt signaling. (June 2013), 4128–4134. https://doi.org/10.3892/etm.2016.3883

Yap, T. A., Bjerke, L., Clarke, P. A., & Workman, P. (2015). Drugging PI3K in cancer: Refining targets and therapeutic strategies. Current Opinion in Pharmacology, 23, 98–107. https://doi.org/10.1016/j.coph.2015.05.016

Yau, T. O., Tang, C.-M., & Yu, J. (2014). Epigenetic dysregulation in Epstein- Barr virus-associated gastric carcinoma: Disease and treatments. World Journal of Gastroenterology, 20(21),6448–6456. https://doi.org/10.3748/wjg.v20.i21.6448

Ye, Y., Jiang, D., Li, J., Wang, M., Han, C., Zhang, X., & Kan, Q. (2016). Silencing of FGFR4 could influence the biological features of gastric cancer cells and its therapeutic value in gastric cancer. Tumor Biology, 37(3), 3185- 3195. https://doi.org/10.1007/s13277-015-4100-0

Yee, J. K. (2016). *Helicobacter pylori* colonization of the oral cavity: A milestone discovery. World Journal of Gastroenterology, 22(2), 641–648. https://doi.org/10.3748/wjg.v22.i2.641

Yılmaz, N., & Koruk Özer, M. (2019, June 13). The Prevalence of *Helicobacter pylori* babA, homB, aspA, and sabA Genes and Its Relationship with Clinical Outcomes in Turkey [Research Article]. https://doi.org/10.1155/2019/1271872

Youle, R. J., & Strasser, A. (2008). The BCL-2 protein family: Opposing activities that mediate cell death. Nature Reviews Molecular Cell Biology, 9(1), 47–59. https://doi.org/10.1038/nrm2308

Young, L. S., Arrand, J. R., & Murray, P. G. (2007). EBV gene expression and regulation. In A. Arvin, G. Campadelli-Fiume, E. Mocarski, P. S. Moore, B. Roizman, R. Whitley, & K. Yamanishi (Eds.), Human Herpesviruses: Biology, Therapy, and Immunoprophylaxis. Cambridge: Cambridge University Press. Retrieved from http://www.ncbi.nlm.nih.gov/books/NBK47431/

Yu, B., Xu, L., Chen, L., Wang, Y., Jiang, H., Wang, Y., Zhai, Z. (2020). FYN is required for ARHGEF16 to promote proliferation and migration in colon cancer

cells. Cell Death & Disease, 11(8). https://doi.org/10.1038/s41419-020-02830-1

Yu, J., Liang, Q., Wang, J., Wang, K., Gao, J., Zhang, J., Sung, J. J. Y. (2017). REC8 functions as a tumor suppressor and is epigenetically downregulated in gastric cancer, especially in EBV-positive subtype. Oncogene, 36(2), 182–193. https://doi.org/10.1038/onc.2016.187

Yu, Jie, Zhou, Z., Wei, Z., Wu, J., OuYang, J., Huang, W., Zhang, C. (2020). FYN promotes gastric cancer metastasis by activating STAT3- mediated epithelial-mesenchymal transition. Translational Oncology, 13(11), 100841. https://doi.org/10.1016/j.tranon.2020.100841

Zali, H., Rezaei-Tavirani, M., & Azodi, M. (2011). Gastric cancer: Prevention, risk factors and treatment. Gastroenterology and Hepatology From Bed to Bench, 4(4), 175–185.

Zarić, S., Bojić, B., Janković, Lj., Dapčević, B., Popović, B., Čakić, S., & Milašin, J. (2009). Periodontal Therapy Improves Gastric *Helicobacter pylori* Eradication. Journal of Dental Research, 88(10), 946–950. https://doi.org/10.1177/0022034509344559

Zhang, L., Zhu, F., Xie, L., Wang, C., Wang, J., Chen, R., … Zhou, M. (2020). Clinical characteristics of COVID-19-infected cancer patients: A retrospective case study in three hospitals within Wuhan, China. Annals of Oncology, 31(7), 894–901. https://doi.org/10.1016/j.annonc.2020.03.296

Zhang, Liang, Guo, G., Xu, J., Sun, X., Chen, W., Jin, J., … Xue, X. (2017). Human cytomegalovirus detection in gastric cancer and its possible association with lymphatic metastasis. Diagnostic Microbiology and Infectious Disease, 88(1), 62–68. https://doi.org/10.1016/j.diagmicrobio.2017.02.001

Zhang, R., Strong, M. J., Baddoo, M., Lin, Z., Wang, Y.-P., Flemington, E. K., & Liu, Y.-Z. (2017). Interaction of Epstein-Barr virus genes with human gastric carcinoma transcriptome. Oncotarget, 8(24), 38399–38412. https://doi.org/10.18632/oncotarget.16417

Zhang, W.-F., Stephen, P., Thériault, J.-F., Wang, R., & Lin, S.-X. (2020). Novel Coronavirus Polymerase and Nucleotidyl-Transferase Structures: Potential to Target New Outbreaks. The Journal of Physical Chemistry Letters, 11, 4430–4435. https://doi.org/10.1021/acs.jpclett.0c00571

Zhao, G., Zhu, G., Huang, Y., Zheng, W., Hua, J., Yang, S., … Ye, J. (2016). IL-6 mediates the signal pathway of JAK-STAT3-VEGF-C promoting growth, invasion and lymphangiogenesis in gastric cancer. Oncology Reports, 35(3), 1787–1795. https://doi.org/10.3892/or.2016.4544

Zhao, J., Liang, Q., Cheung, K.-F., Kang, W., Lung, R. W. M., Tong, J. H. M., Yu, J. (2013). Genome-wide identification of Epstein-Barr virus-driven promoter methylation profiles of human genes in gastric cancer cells: EBV- Driven Methylation in Gastric Cancer. Cancer, 119(2), 304–312. https://doi.org/10.1002/cncr.27724

Zhu, N., Zhang, D., Wang, W., Li, X., Yang, B., Song, J., … Lu, R. (2020). A novel coronavirus from patients with pneumonia in China, 2019. New England Journal of Medicine.

Zhu, P., Xue, J., Zhang, Z., Jia, Y., Tong, Y., Han, D., … Tang, B. (2017). *Helicobacter pylori* VacA induces autophagic cell death in gastric epithelial cells via the endoplasmic reticulum stress pathway. Cell Death & Disease, 8(12), 1–12. https://doi.org/10.1038/s41419-017-0011-x

Ziebuhr, J. (2005). The Coronavirus Replicase. In L. Enjuanes (Ed.), Coronavirus

Replication and Reverse Genetics (pp. 57–94). Berlin, Heidelberg: Springer Berlin Heidelberg. https://doi.org/10.1007/3-540-26765- 4_3